UNIVERSITÉ DU QUÉBEC À MONTRÉAL

STRUCTURE AND FUNCTION STUDIES ON THE HERG POTASSIUM CHANNEL INCLUDING THE DEVELOPMENT AND CHARACTERIZATION OF MEMBRANE MIMETICS

DISSERTATION

PRESENTED

AS PARTIAL REQUIREMENT

OF THE DOCTORATE OF BIOCHEMISTRY

BY

MAÏWENN BEAUGRAND

OCTOBER 2015

UNIVERSITÉ DU QUÉBEC À MONTRÉAL

ÉTUDE STRUCTURALE ET FONCTIONNELLE DU CANAL POTASSIQUE HERG, INCLUANT LE DÉVELOPPEMENT ET LA CARACTÉRISATION DE MEMBRANES MODÈLES

THÈSE

PRÉSENTÉE

COMME EXIGENCE PARTIELLE

DU DOCTORAT EN BIOCHIMIE

PAR

MAÏWENN BEAUGRAND

OCTOBRE 2015

DEDICATION

Je dédicace cette thèse à Erwan Beaugrand

J'espère que tu aurais été fier de ta petite sœur

"The greatest mistake you can make in life is to be continually fearing you will make one" - Elbert Hubbard (1859-1915)

ACKNOWLEDGEMENTS

Throughout my doctoral studies I have received support from family, friends and co-workers. This acknowledgement section conveys them my full gratitude.

Je tiens tout d'abord à remercier ma directrice de recherche, Professeure Isabelle Marcotte (Université du Québec à Montréal, Canada) pour m'avoir fait confiance et accueillie dans son laboratoire ainsi que pour son soutien tout au long de mon parcours. Merci pour tous tes enseignements ainsi que de m'avoir donné tant d'opportunités d'échanges, congrès, formations et enseignements ici et autour du monde. C'est une superviseure en or et passionnée.

I am lucky to have been co-supervised by Professor Philip T. F. Williamson (University of Southampton, UK). Thank you for welcoming me in your laboratory so many times (from my Master's studies to my PhD, such as a 'boomerang') and for all your support and advice. You are always available to explain, discuss and think about science and it helps a lot. Many thanks for your patience and careness.

La réalisation de ces projets de doctorat a requis l'expertise en résonance magnétique nucléaire du Docteur Alexandre A. Arnold. C'est grâce à tes enseignements que j'ai pu devenir indépendante sur notre capricieux spectromètre RMN 600 MHz et sa version 'relookée', ainsi que sur le 400 MHz. Je te remercie pour tous tes conseils et de répondre présent à ma liste interminable de questions.

Dans cette lignée, je souhaite remercier les professeurs, employés, collègues et amis de l'Université du Québec à Montréal (UQAM) qui m'ont offert de leur temps, de leur savoir et de leur bonne humeur. Tout d'abord, un grand merci à mes collègues,

passés et présents, du laboratoire de résonance magnétique nucléaire des systèmes biologiques complexes: Andrée Gravel, Souryvanh Nirasay, Frédéric Byette, Marc-Olivier Seguin Heine, Delphine Harel, Aline Gambaro, Marwa Laadhari, David Vernon Youmssi, André-Luiz dos Anjos Gomes da Silva, Zeineb Bouhlel, Bertrand Gérard, Antoine Juneau, Abdallah Oukaroum et Catherine Tardy-Laporte. Nous en avons passé des heures ensemble à nous torturer les méninges mais cela aurait été beaucoup plus difficile sans vous. Merci aussi à de formidables étudiants, post-doctorants et employés de cette université: aux biochimistes, Dahmane Ouazia, Audrey Glory, Carole-Anne De Carufel, Germain Lacoste et Mathieu Laporte Wolwertz; aux chimistes, Ngoc Duc Trinh, Danny Chhin, Mathieu Saulnier, Basile Commarieu, Aurore Castets, Chiche Shiao, Jean-Christophe Daigle, David Lepage, Gaëtan Maertens, Melissa Barrera Tomas, André Leblanc, Christian and Sabine Kuss, Sylvain Rocheleau, Marc-André Desjardins, Julien Martel et Elham Akbariromani. Il y a aussi ces professeurs, qui ont pris de leur temps pour m'aider et me conseiller, Professeurs Steve Bourgault, Marc Lussier et Jérome Claverie. Sans oublier, les conseils et clarifications administratives des deux directrices successives du programme des études graduées de Biochimie, les professeures Joanne Paquin et Louise Brissette. Merci aussi à l'équipe du personnel de soutien et plus particulièrement: Sonia Lachance, Odette Desrosiers, Mathieu Maurin-Soucy, Luc Arsenault, Chantal Soucy, Sophie Chen, Jacqueline Tieu Hue, Isabelle Rheault, Marie-Josée Crevier, Sylvie Lemieux et Louise Martin-Falstrault. Merci enfin à toute l'équipe du réseau étudiant des cycles supérieurs du secteur des sciences (RECSSS), on faisait une belle brochette: Marie Line Gentes, Sophie Carpentier, Alexandre Terrasa, Anthony François, Dominic Matte et Pierre-Marc Godbout. Je conserverai de bons souvenirs de mon passage entre les murs de l'UQAM grâce à vous tous.

I will also forever be in debt to my colleagues and collaborators at the University of Southampton: James Jarvis, Garrick Foster Taylor, Phedra Marius, Christopher D. Johnson, Neville Wright, Mark S. Friddin, Sumit Kalsi, Rafeel Gomes, Luke S.

Evans, Professors Maurits R. R. De Planque, Morgan Hywel and Declan A. Doyle. I also want to thank Halina Bainbridge, Kelly Hooper, Louise Bolton, John Butler, Nicolas Dalls, Ben Mulcahy, James Beggs, Matt Rodrigues, Professors Stuart Findlow, Marina Carravetta and Anthony Lee. All those hours of studying and experimenting in the laboratory would have been unbearable without you all.

Additionnaly, I was very fortunate to have had internship supervisors that I would like to thank for their guidance, Professor Jason C. Young (McGill University, Canada) and Professor Ansgar B. Siemer (University of Southern California, USA). Each Biochemistry laboratory has its own tips and tricks and I was glad to learn from them. Many thanks to professor Young for his help with the hERG expression project and to professor Siemer for all his advice during my PhD.

I would also like to thank the group of Professor Young: Michael Wong, Imad Baaklini, Patrick Kim Chiaw and Yogita Patel, and the people in the biochemistry department at McGill University: Kristjan Bloudoff, Shane Caldwell and Asparouh Lilov. Un merci tout particulier à Fabien Bergeret qui est devenu très rapidement un très bon ami et m'a aussi donné de précieux conseils et motivation pendant la phase d'écriture. Thanks to all them, I enjoyed my internship there.

I want to express my sincere thanks to members at University Southern California and their warm welcoming: Thalia Bajakian, Rachel Service, Ninad Agashe, Silvia Cervantes, Maria Contrad and Sandy Falk, and also to scientists I was lucky to met there: Mario Isas, Mark Ambroso, Alan Okada, Nathalie C. Kegulian, Thomas Schmidt and Professor Ralf Langen.

Je tiens à remercier Michèle Auger (Université de Laval, Canada) pour m'avoir donné accès à son laboratoire pour préparer mes échantillons d'infrarouge, ainsi que Jean-François Rioux-Dubé et François Paquet-Mercier pour leur aide technique sur

leur spectromètre infrarouge. J'en profite aussi pour souligner le merveilleux accueil de Mathieu Fillion (même si virtuel), Kim Potvin-Fournier et Thierry Lefevre.

Ces projets ont été rendus possibles grâce à la collaboration de nombreux scientifiques et je tiens donc à remercier pour leur aide deux collaborateurs non mentionnés antérieurement, les Professeurs Dror E. Warschawski et Jérôme Hénin (Université Paris-Diderot, France).

Un grand merci également à ces enseignants qui ont eu une grande influence pendant ma scolarité: l'équipe enseignante de l'école primaire de Trémuson et particulièrement, Mme Brigault et Mr Chapelet; Mlle Le Carroux (lycée Eugène Freyssinet), Mme Guillaume et le Professeur Henri Wroblewski (Université Rennes 1).

Un remerciement tout spécial à ma famille. Merci à mes parents, Jean-Claude et Marie-Christine Beaugrand pour leur soutien moral sans faille. Merci à mon frère aîné, Gaël Beaugrand, qui a dans mon enfance été mon modèle, qui a toujours cru en moi et m'a donné le goût des mathématiques durant mes premières années de scolarité ainsi qu'à mon frère cadet, Goulwen Beaugrand, avec qui j'ai partagé les jeux d'enfance. J'en profite pour citer les membres étendus de ma famille qui m'ont soutenue durant ces années doctorales: Mikaël Potrat, Pierre, Marie-France et Cécile Chaudot, Nathalie, Pascal, Rémi et Théo Véra, Elizabeth Salou, Dany Léo, Catherine, Jean-Luc et Stéphane Coquio. La présence de ma famille ainsi que leurs encouragements dans les moments difficiles auront été source de réconfort et de motivation inestimable. Je me considère extrêmement chanceuse de vous avoir et merci de ne pas m'en vouloir d'avoir mis un océan entre nous. Je tiens aussi à rendre hommage à Suzanne Salou, ma grand-mère et Jean-Pierre Salou, mon oncle, pour qui je n'ai pu être présente dans leurs derniers instants.

Un profond merci à mes amis, et notamment ceux qui malgré la distance et l'absence sont restés à mes côtés. Tout d'abord mes amis d'enfance: Delphine Calvez, Karen Salmon, Clément Houzé et Guillaume Roussel. Merci à ma partenaire de danse privilégiée, Mushu Le Dragon (alias Aurélie), pour toutes ces années insolites. Merci à Geneviève Martin pour notre amitié. J'aimerais aussi remercier les personnes formidables que j'ai rencontrées à Rennes et avec lesquelles j'ai pu conserver contact: Elisa Marivin, Valentine Genet, Céline Camus, Sophie Rouanet, Phuhai Nguyen, Alexis Saintilan, Eniss Hedhli, Angélique Faramus, Mathieu Le Rouzic, Arnaud le Febvrier, Loïc Cara, Wennaël Deslandes et Audrey Bachatera.

Merci aussi au soutien que j'ai eu pendant cette rude première année de doctorat où j'ai passé près du rapatriement. J'en profite pour remercier ma médecin de famille, la Docteure Janik Le Corveller qui m'a conseillée judicieusement et évité un arrêt d'études non nécessaire. A big thank you to my friends met at Southampton, especially Stefania Fabbri, Vanesa Martinez, Joe Kakande, Asad Ali, Asim Munir et Priyanth Mehta. Gracias a mi mejor amigo, Joaquin Matres Abril por ayudarme a abrir los ojos en momentos importantes de mi doctorado que permitieron volverme a centrar en mi trabajo. I want to thank my friends from INRS: Romain Dugas, Ivan Cito, Mernusc Azodi, Gastón C. Jimenez and Sami Tomoyo. Un agradecimiento para Orlando Trejo por motivarme mientras acababa de escribir esta tesis y, en paralelo, ayudarme a encontrar posiciones post-doctorales. Merci aussi à des personnes formidables rencontrées à Montréal: Christopher Wardell, Sébastien Guerry, Manuel Labridy et Jorge Juárez. Un énorme merci à Huynh Van Du Tran pour son soutien et son aide pour tous les petits tracas technologiques et quotidiens, pour croire en moi ainsi que pour avoir sauvé mes données et phases d'écriture de ce manuscrit face à d'énièmes guignes informatiques. *Cám ơn nhiều, tim của em.* Sans oublier mes animaux à 4 pattes, Picolo, Wolvie et Ayla, qui méritent également une place dans ma reconnaissance par leur présence, leur affection et tous leurs ronrons réconfortants.

Je tiens à remercier les membres du jury de projet de thèse: Professeurs Richard Desrosiers, Jean Danyluk (UQAM) et Yves Aubin (Carleton University, Canada), ainsi que les membres de mon comité de thèse pour leur temps à lire, évaluer et corriger ce travail de longue haleine: Professeur Joanne Paquin, Marc Lussier (UQAM) et Natalie Goto (University of Ottawa, Canada).

Finally, I want to thank several organizations for their financial supports during my PhD studies, laboratory exchanges and conferences: le département de chimie de l'UQAM, le programme des études graduées de Biochimie de l'UQAM, la fondation de l'UQAM, les Fonds à l'accessibilité et à la réussite des études (FARE) de l'UQAM, le syndicat des professeurs et professeures de l'UQAM (SPUQ), le programme de reconnaissance de l'implication étudiante de l'UQAM, le ministère de l'éducation, des loisirs et du sport du Québec (MELS), the McGill University Chemical Biology Training Program (ChemBIO) and their coordinator, professor John R. Silvius, the Create Training Program in Bionanomachines (Bionano) and their coordinators, Christopher von Roretz and Anne Noronha, le Groupe de Recherche Axé sur la Structure des Protéine (GRASP) et leur coordinatrice, Annick Guyot, le Centre Québécois des Matériaux Fonctionnels (CQMF) et leur coordinatrice Patricia Basque, the organization committee of South West Structural Biology Consortium (SWSBC) 2012, the organization committee of EUROMAR 2013, the Biophysical Society and the Education Committee for the annual meeting of the Biophysical Society in 2014. This also gave me the opportunity to meet great scientists during meetings, journal clubs and workshops which enlarged my network.

AVANT-PROPOS

Par égard pour le fait que ce diplôme de Doctorat en Biochimie a été réalisé dans une université francophone, une traduction en français de chaque résumé ainsi que de cet avant-propos peut être trouvée avant la version en anglais.

Cette thèse se concentre sur l'application de la spectroscopie de résonance magnétique nucléaire pour obtenir de l'information sur les systèmes membranaires, telles que les membranes modèles et les protéines membranaires. Le Chapitre I est l'introduction. Le Chapitre II fournit une description théorique des principales techniques utilisées. Les Chapitres III et IV sont des études détaillées sur des membrane modèles, les bicelles. Le but du Chapitre III est une caractérisation en profondeur des bicelles diluées constituées de dimyristoylphosphatidylcholine (DMPC ou D14PC) et dihexanoyl-phosphatidylcholine (DHPC ou D6PC). Le Chapitre IV décrit et caractérise des bicelles formées à partir de détergent de la famille des monoalkylphosphocholines (MAPCHO). Deux études sur le canal potassique eucaryote *human ether-à-go-go related gene* (hERG) sont traitées dans les Chapitres V et VI. Le Chapitre V est une étude comparative des hélices du pore de hERG et de Kv1.5 dans des bicelles formées à partir de détergent MAPCHO. Le Chapitre VI dépeint un protocole d'expression et de purification du domaine du pore fonctionnel de hERG. Finalement, le Chapitre VII regroupe les conclusions et perspectives. Les sections résultats sont présentées sous forme de manuscrits d'articles. Les références sont rassemblées ensemble en une section à la fin de cette thèse.

Les travaux présentés dans les Chapitres III, IV et V ont été faits dans le laboratoire de la Professeure Marcotte (Département de Chimie, Université du Québec à Montréal – UQAM, Canada), alors que ceux du Chapitre VI ont été réalisés dans le laboratoire du Professeur Williamson (Centre pour les Sciences Biologiques, *University of Southampton*, Angleterre).

Publications supplémentaires:

- Friddin, M. S., Smithers, N. P., Beaugrand, M., Marcotte, I., Williamson, P. T. F., Morgan, H., & de Planque, M. R. R. (2013). Single-channel electrophysiology of cell-free expressed ion channels by direct incorporation in lipid bilayers. *Analyst*, *138*, 7294–7298.

- Warschawski, D. E., Arnold, A. A., Beaugrand, M., Gravel, A., Chartrand, É., & Marcotte, I. (2011). Choosing membrane mimetics for NMR structural studies of transmembrane proteins. *Biochimica et Biophysica Acta*, *1808*, 1957–1974.

PREFACE

In respect to achieving this Doctor of Philosophy degree in Biochemistry in a francophone university, a French translation of each abstract and this preface are found prior to the English version.

This dissertation focuses on the application of nuclear magnetic resonance spectroscopy to obtain information on membrane systems, such as model membranes and membrane proteins. Chapter I is the introduction. Chapter II provides a theoretical description of the main techniques used. Chapters III and IV are detailed studies on model membranes, the bicelles. The purpose of Chapter III is a deeper characterization of diluted dimyristoylphosphatidylcholine (DMPC or D14PC) / dihexanoylphosphatidylcholine (DHPC or D6PC) bicelles. Chapter IV describes and characterizes monoalkylphosphocholine (MAPCHO) detergent - based bicelles. Two studies on the eukaryotic potassium channel human ether-à-go-go related gene (hERG) are covered in Chapters V and VI. Chapter V is a comparative study of hERG and Kv1.5 pore helices in MAPCHO-based bicelles. Chapter VI depicts the expression and purification protocol of a functional hERG pore domain. Finally, Chapter VII presents the concluding remarks and future perspectives. Results are presented in form of publication manuscripts. References are gathered together into one section at the end of this dissertation.

The work presented in Chapters III, IV and V has been carried out in the laboratory of Professor Marcotte (Chemistry department, *Université du Québec à Montréal* – UQAM, Canada) while the one in Chapter VI was achieved in the laboratory of

Professor Williamson (Centre for Biological Sciences, University of Southampton, UK).

Additionnal Publications:

- Friddin, M. S., Smithers, N. P., Beaugrand, M., Marcotte, I., Williamson, P. T. F., Morgan, H., & de Planque, M. R. R. (2013). Single-channel electrophysiology of cell-free expressed ion channels by direct incorporation in lipid bilayers. *Analyst*, *138*, 7294–7298.

- Warschawski, D. E., Arnold, A. A., Beaugrand, M., Gravel, A., Chartrand, É., & Marcotte, I. (2011). Choosing membrane mimetics for NMR structural studies of transmembrane proteins. *Biochimica et Biophysica Acta*, *1808*, 1957–1974.

TABLE OF CONTENTS

LIST OF FIGURES

LIST OF TABLES

RÉSUMÉ

Les protéines membranaires, notamment eucaryotes, sont connues pour représenter un défi à étudier. Dans cette thèse, des méthodes ont été développées pour aider dans le domaine de recherche des protéines membranaires. Plus précisément, le but de cette thèse était de permettre l'étude de la structure et de la fonction des canaux potassiques voltage-dépendants par résonance magnétique nucléaire.

Des membranes modèles pour l'analyse des protéines membranaires ont été développées et caractérisées. Deux types de bicelles ont été étudiés: les bicelles faites avec des phospholipides à courtes chaînes et celles constituées de détergents monoalkylphosphocholines (MAPCHO). Les bicelles couramment utilisées formées de dimyristoyl-phosphatidylcholine (DMPC ou D14PC) et de dihexanoyl-PC (DHPC ou D6PC) ont été étudiées afin de déterminer leur morphologie et leur miscibilité dans des conditions diluées. Les résultats indiquent les concentrations seuils de formation de ces agrégats, la frontière de rapport molaire DMPC / DHPC (q) entre bicelle et micelle mixte ainsi que les meilleures concentrations à utiliser.

Afin d'améliorer la solubilisation des protéines membranaires et permettre leur étude en systèmes bicellaires, le DHPC a été remplacé par les détergents de la famille MAPCHO, dont la dodécylphosphocholine (DPC ou DPC12) est connue pour sa capacité à solubiliser les protéines membranaires. Par l'ajout progressif de phospholipides à des mélanges de tensioactifs et de protéines membranaires, la protéine membranaire pourrait être reconstituée dans un environnement bicellaire. Une étude systématique a été menée en variant la longueur de chaîne du phospholipide (C12 à C20) ainsi que du détergent (C12 à C16). Les résultats ont indiqué qu'il était possible de former des systèmes orientés magnétiquement pour six des douze mélanges binaires testés avec différentes épaisseurs de bicouche, à différents rapports molaires lipides / détergents (q) et différentes températures. La qualité de l'alignement, la miscibilité, les concentrations seuils de formation de ces agrégats ainsi que l'effet de l'ajout des ions lanthanides ou des lipides anioniques ont également été étudiés. Une tentative d'établir un critère empirique qui pourrait prédire si une paire donnée de tensioactif et de phospholipide formerait des bicelles a été discutée.

Pour évaluer le potentiel de ces membrane modèles comme système de reconstitution directe, des peptides de canaux potassiques ont été solubilisés dans des micelles de

DPC, suivi par l'addition de DMPC. Ce projet a permis d'obtenir des données intéressantes sur la structure et les interactions avec les membranes des hélices du pore de Kv1.5 et du *human ether-a-go-go related gene* (hERG).

Un obstacle majeur dans la détermination de structure des protéines membranaires est l'absence de stratégie d'expression et de purification appropriée. La protéine hERG a été sélectionnée pour son implication dans une cardiopathie associée avec d'importants effets hors-cible de médicaments. Un protocole d'expression et de purification efficace du domaine du pore du hERG a été développé. Cela a permis d'obtenir des caractérisations biophysiques et des mesures électrophysiologiques préliminaires.

Ces résultats fournissent des méthodes pour solubiliser les protéines membranaires afin de pouvoir les étudier, ainsi que pour réaliser l'expression et la purification du domaine du pore d'un important canal potassique eucaryote: le hERG, qui ouvre la voie à l'obtention de sa structure.

Mots clés: Protéine membranaire, Canal potassique hERG, Membrane modèle, Bicelle, Détergent monoalkylphosphocholine et Résonance magnétique nucléaire.

ABSTRACT

The study of membrane proteins, especially eukaryotic, is known to be challenging. In this PhD thesis, methods were developed to aid the membrane protein research area. More specifically, the aim of this thesis was to allow the study of the structure and function of voltage-gated potassium channels using nuclear magnetic resonance.

First, model membranes for the analysis of membrane proteins were developped and characterized. Two types of bicelles were investigated; the short-chain phospholipid-based and the monoalkylphosphocholine (MAPCHO)-based bicelles. The popular dimyristoylphosphatidylcholine (DMPC or D14PC) / dihexanoyl-PC (DHPC or D6PC) bicelles were studied to determine their morphology and miscibility in diluted conditions. The results provide the concentration thresholds of the formation of the aggregates, the DMPC-to-DHPC molar ratio (q) boundary between bicelle and mixed micelle as well as the recommended concentrations to use.

To improve the solubilization of membrane proteins and their study in bicellar systems, DHPC was replaced by detergents from the MAPCHO family of which dodecylphosphocholine (DPC or DPC12) is known for its ability to solubilize membrane proteins. By progressively adding phospholipids to the surfactant-membrane protein mixture, the membrane protein could be safely reconstituted in a bicelle bilayer environment. A systematic study was carried out by varying the length of the phospholipid (C12 to C20) as well as one of the detergents (C12 to C16). The results indicated a possibility to form magnetically-aligned systems with six binary mixtures on the twelve tested with different thicknesses of the bilayer, at several lipid-to-detergent molar ratios (q) and temperatures. The quality of the alignement, the miscibility, the concentration thresholds of the formation of the aggregates, as well as the effect of the addition of lanthanide ions or anionic lipids were also investigated. An attempt to establish an empirical criterion which could predict whether a given surfactant-phospholipid pair will form bicelles is discussed.

To assess the potential of this system as a direct model membrane for reconstitution, membrane peptides from potassium channels were solubilized into DPC micelles, followed by the addition of DMPC. This project presented interesting data on the structure of the pore helices of Kv1.5 and the human ether-a-go-go related gene (hERG) and their interaction with membranes.

A major hurdle when determining the structure of membrane proteins is the absence of a suitable expression and purification strategy. The protein hERG was selected for its involvement in a cardiopathy associated with important off-target effects of drugs. An effective protocol for the expression and purification of the hERG pore domain was developped. This formed the basis of preliminary biophysical characterization and electrophysiological measurements.

The results in this thesis provide methods to solubilize membrane proteins, allowing detailed study, as well as to express and purify the pore domain of an important eukaryotic potassium channel: the hERG, paving the way to obtain its structure.

Keywords: Membrane protein, Potassium channel hERG, Model membrane, Bicelle, Monoalkylphosphocholine detergent and Nuclear magnetic resonance.

CHAPTER I

INTRODUCTION

In this section, the following elements are introduced: the biological membrane and its components, the potassium channels, the voltage-gated potassium channels and lastly, the different model membranes and expression systems to study membrane proteins. The objectives of this thesis are highlighted at the end of this chapter.

1.1 Biological Membrane

Biological membranes encompass the cells and their compartments. The plasma membrane is the boundary between the cytoplasm and the extracellular medium. It maintains the homeostasis of the cell and regulates the passage of both information and materials in and out of the cell. As the ultimate protection from the environment, this barrier is also the target for viruses, bacteria, or drugs. This section will give an overview of the organisation of the membrane, the lipids and the membrane proteins.

1.1.1 Organisation of the Membrane

Cell membranes are composed of a lipid bilayer to which proteins and carbohydrates (glycolipids and glycoproteins) are associated. The proportion of these three

components in membranes are dependant on the type of organism, cell and organelle (Table 1.1).

Table 1.1 Composition (percent of their dry weight) of lipid, protein and carbohydrate of membrane from different sources.

Species	Membrane	Lipid (%)	Protein (%)	Carbohydrate (%)
Homo sapiens	Central nervous system myelin[a]	79	20	1.0
	Erythrocyte	40	60	-
Bos taurus	Peripheral nervous system myelin[a]	76	23	1.0
Rattus norvegicus	Muscle skeletal[a]	35	65	0.0
	Liver[a]	40	60	0.0
	Liver mitochondria[a]	27-29	70	1.3
Pisum sativum	Thylakoid[b]	35-37	63-65	-
Acanthamoeba castallanii	Plasma membrane[c]	27	37	37[d]

[a] (Sastry & Tomer, 2008)
[b] (Chapman *et al.*, 1983)
[c] (E. D. Korn & Wright, 1973)
[d] Phosphoglycan

The membrane structure proposed in 1972 by Singer & Nicolson is composed of a fluid bilayer (at physiological temperatures) of phospholipids with intercalated membrane proteins and glycoproteins, this so-called fluid-mosaic model membrane (FMMM). The view of the membrane as a homogeneous mixture of lipids and proteins has been questioned. The revised version of the FMMM takes into consideration the constraints of distribution and mobility of some (if not all) integral globular membrane proteins and lipids. These phenomena are due to interactions with membrane components, such as other membrane proteins and lipids as well as with the complex network of cytoskeleton and/or carbohydrates (Nicolson, 2014) (Figure 1.1). This mobility limitation of certain molecules in a sea of fluid molecules leads to specialized nano-, micro- or macro-domains of lipids, proteins and mixture of both, such as lipid rafts (Nicolson, 2014).

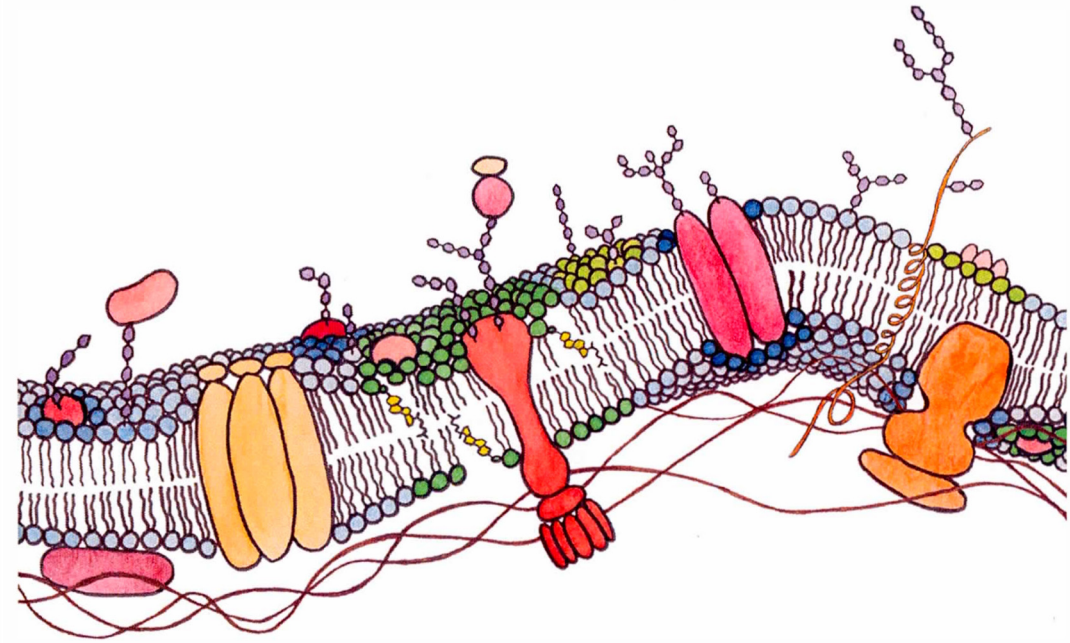

Figure 1.1 Fluid (non random) mosaic model membrane with representation of lipid-protein domains in different colors. Lipids are in green and blue while proteins are colored in pink, red and orange. Extramembrane components, such as cytoskeleton and carbohydrates are represented by brown and purple, respectively.

1.1.2 Membrane Lipids

In humans, membranes are about 4 nm thick and cover a total surface *circa* 100 km^2 (Mouritsen, 2005). They are composed of thousands of different types of lipids (Han & Gross, 2005). Nevertheless, a given cell is limited in its lipid composition, allowing a specificity of membrane function, structure and dynamics (Bagatolli *et al.*, 2010; Cullis & De Kruijff, 1979).

1.1.2.1 Types of Membrane Lipids

The fundamental building blocks of the bilayer are phospholipids. Phospholipids are amphiphilic (or amphipathic) molecules, with a hydrophilic "head" and a hydrophobic "tail" groups. Phospholipids are composed of a backbone to which fatty acids are esterified at one or two sites with a headgroup link to the third site via phosphodiester bond (Figure 1.2).

According to the backbone, two main types of phospholipids can be described – the glycerophospholipids (or phosphoglycerides) and the sphingophospholipids. In glycerophospholipids, the backbone is a glycerol, esterified by a phosphate in position 'stereospecifically numbered' (sn)-3 and by two fatty acids in position sn-1 and sn-2 (Figure 1.2A). In sphingo-phospholipids, the backbone is a sphingosine, a long aliphatic amino alcohol N-linked to a fatty acid and O-linked to a polar group (Figure 1.2A). The structure composed of the sphingosine and the fatty acid is called a ceramide.

Depending on the polar head group associated with the backbone, there are different classes of phospholipids, such as phosphatidylcholine (PC), phosphatidyl-ethanolamine (PE), phosphatidylserine (PS) and phosphatidylinositol (PI) for the glycerophospholipids (Figure 1.2B). The addition of a choline polar group to ceramide leads to sphingomyelin (SM). Different polar head groups confer different sizes and charges to the phospholipid (Figure 1.2B).

In membranes, it is possible to find alkyl chains with an even number of carbons from 14 to 24 with or without unsaturation (Cullis *et al.*, 1996; Marsh, 2013; Schechter, 1990). The length of the alkyl chains determines the thickness of the bilayer with an increase in the length, giving rise to an increase of the bilayer thickness. The number of carbon atoms and unsaturation of the alkyl chains affects the fluidity of the membrane. Increasing the degree of unsaturation and reducing the alkyl chain length

of the fatty acid will reduce the melting temperature (T_m) of the lipid. Palmitic acid (16:0) and oleic acid (18:1) are the most abundant fatty acids found in human cell membranes (Watkins, 2005) (Figure 1.2C).

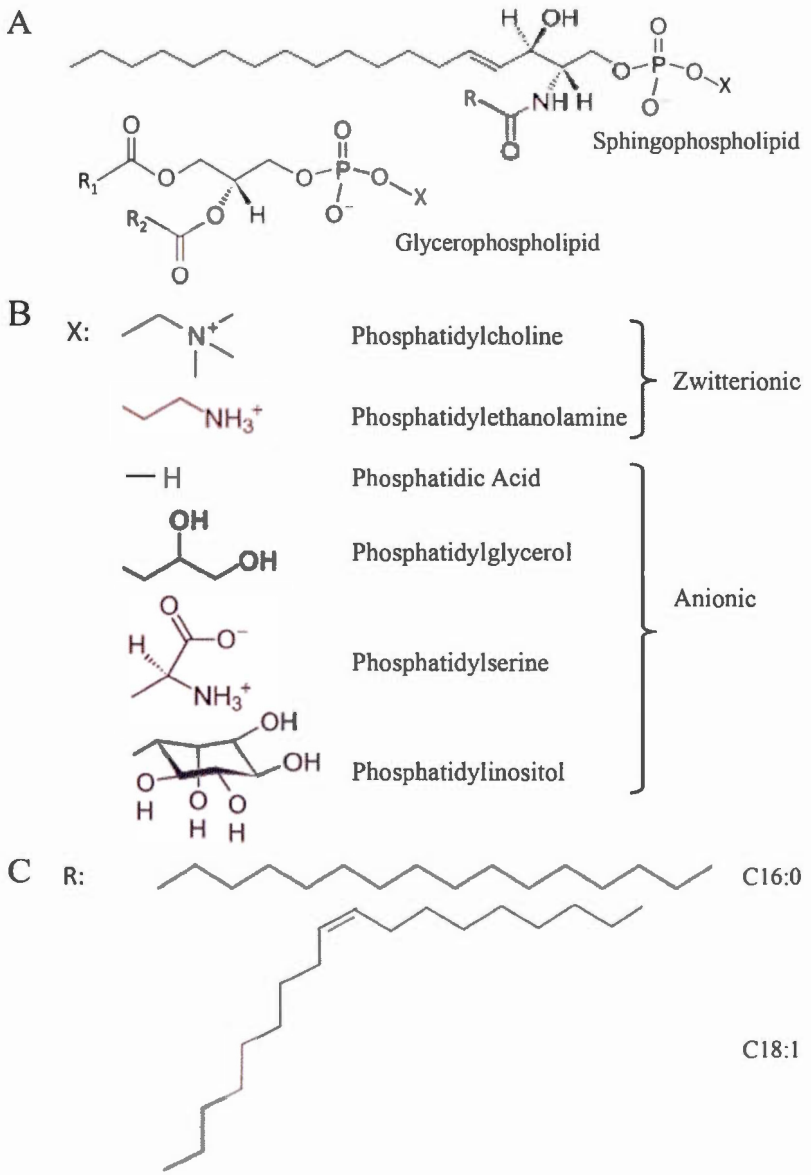

Figure 1.2 Representation of phospholipid structures. (A) Phospholipid backbone with X, the headgroup and R, the alkyl chain(s). (B) Hydrophilic headgroups with the associated glycerophospholipid name. (C) Examples of saturated (16:0) and unsaturated (18:1) alkyl chains.

Another essential lipid found in animal membranes but not present in bacteria and plants is cholesterol. Its structure is based on four rings with a hydrocarbon tail and a polar hydroxyl group (Figure 1.3).

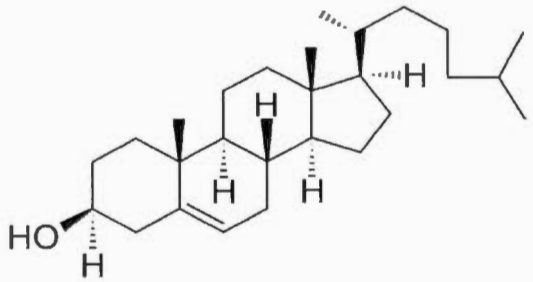

Figure 1.3 Representation of cholesterol structure.

It is found in membranes with similar molar amounts relative to phospholipids (Cooper, 2000; Post *et al.*, 1995). This lipid also has an effect on membrane fluidity. Due to its rigid steroid ring structure cholesterol maintains membrane fluidity by preventing close interaction between alkyl chains at low temperatures while at higher temperature, it decreases the fluidity by restricting the motion of the alkyl chains (Cooper, 2000; Post *et al.*, 1995).

The most abundant phospholipids in eukaryotic membranes are PC (Warschawski *et al.*, 2011). For example, sarcolemma (plasma membrane of the myocardium cell) are composed of 40-52% PC, 25-36% PE, 6-13% PS and PI, 4-18% SM and a cholesterol/phospholipid molar ratio from 0.33 to 0.59 for mammals (Post *et al.*, 1995). The distribution of phospholipids within the cellular membranes is asymmetric. The choline-based phospholipids PC and SM are located on the external (luminal) leaflet of the bilayer while the amine-based PE and the anionic phospholipids PS, PI and phosphatidic acid (PA) are found on the cytoplasmic side (Daleke, 2003). This phenomenon is initiated and maintained by lipid transporters (Daleke, 2003; Nicolson, 2014). The asymmetry is physiologically important as demonstrated by the energy consumption spent by eukaryotic cells to generate it and

diseases associated with disruption of this process, such as cardiopathy and diabetes (Bengt & Ding, 2009; Daleke, 2003).

1.1.2.2 Lipid Motions in the Bilayer

The membrane is dynamic. Five lipid movements can be described in the bilayer (Blume, 1993; Smith & Magid, 1984): (a) axial rotation where lipids will rotate along their longitudinal axis; (b) oscillation in a cone around this axis; (c) pendulum movement of the alkyl chains due to their flexibility; (d) lateral diffusion; and (e) flip-flop when a lipid switches to another leaflet (Figure 1.4).

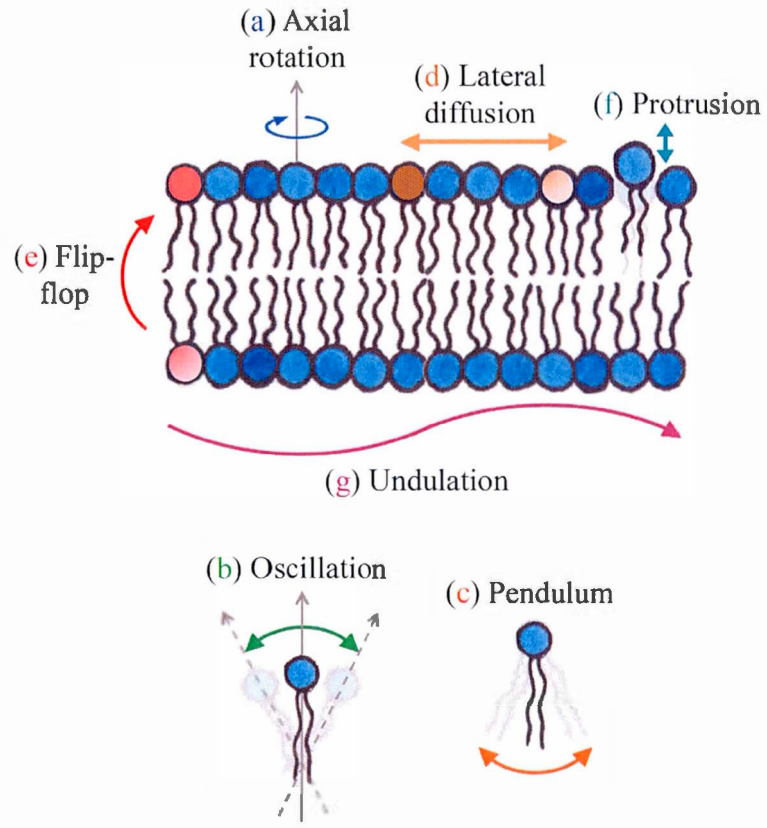

Figure 1.4 Representation of the lipid motions in the membranes.

A lipid might (f) exchange between membranes (or protrusion) according to the curvature of the bilayer (Israelachvili, 2011; Jahnig, 1984) (Figure 1.4). Additionally, the membrane can undergo (g) collaborative lipid motions in a wave-like movement (or undulation) (Brown *et al.*, 1983; Israelachvili, 2011) (Figure 1.4). All these movements are enabled by the membrane fluidity.

The free rotation about the carbon-carbon bonds in the fatty acid chains allows different "phases" of the bilayer according to the temperature. In the gel phase, the lipids are in the all-trans conformation (i.e. extended). The alkyl chains are close and parallel (structure L_{β}) or inclined (structure $L_{\beta'}$) with respect to the bilayer normal (Figure 1.5). This phase occurs at low temperature when thermal motion is restricted. In the liquid-crystalline fluid phase, the lipids adopt the trans/gauche conformation (i.e. disordered or melted). The alkyl chains are free to change direction around their carbon-carbon bonds, thus they are more disordered and less compact (structure L_{α}) (Figure 1.5). This phase occurs at temperatures above the main transition temperature of the lipid, the so-called melting temperature (T_m) where the thermal motion is greater.

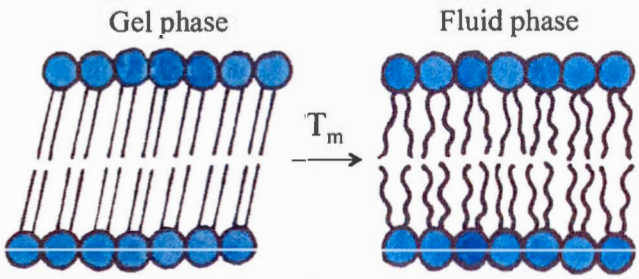

Figure 1.5 Gel phase (left) conformation of lipids versus liquid crystalline phase (right).

1.1.2.3 Organization of Lipids

At low concentration in an aqueous solution, lipids exist as monomers. Above a characteristic concentration, the so-called "critical micelle concentration" (CMC), these amphiphilic molecules will be driven together into a bilayer organization by the hydrophobic effect and numerous van der Waals interactions. This phenomenon minimizes the contact of the tails with water. The self-assembled bilayer is maintained and thus stabilized by the ability of the hydrophilic head groups to interact with the aqueous environment and one another.

The Hydrophobic Effect

In liquid water, each water molecule can form up to four hydrogen bonds, giving rise to a dynamic network. The addition of amphiphilic compounds in an aqueous medium destabilizes this network since hydrogen bonds can no longer be formed between water molecules and the lipid alkyl chains. Thus, the solvent forms a cage around the hydrophobic region, giving rise to a reduction of the entropy since the motions of water molecules are restricted. When many lipids are in solution, the hydrophobic tails are driven together to limit their contact with the aqueous medium while the hydrophilic head groups are exposed to the solvent. The water molecules can form hydrogen bonds with the polar groups and are free to move. The association of many lipid molecules gives rise to spontaneous formation of supramolecular aggregates.

Lipid Phases

The overall organization of cell membranes is a lipid bilayer (or lamellar phase). However, some membrane lipids when studied in water do not form a bilayer. The lipid shape is the main factor in determining the organization of the aggregates. Many phospholipids have a cylindrical shape, i.e. the cross-section of the headgroup is similar to that of the alkyl chains (Figure 1.6). These lipids tend to organize in bilayers. For example, PC and PS are bilayer-prone lipids (Gruner *et al.*, 1985).

In contrast, nonbilayer-prone lipids have different cross-sectional areas between the head and the tails. They are differentiated into two types. The first one has an inverted conical shape with a larger headgroup in comparison to the alkyl chains (Figure 1.6). These lipids generate a positive spontaneous curvature. They form micelles at low concentrations while they adopt a normal hexagonal H_I phase at higher concentrations. In H_I phase, lipids form cylinders with the hydrophobic tails towards the center of the cylinder. These cylinders are organized into hexagons. For example, lysoPC (one alkyl chain) is an inverted conical shaped lipid, which forms micelles in solution (Gruner *et al.*, 1985).

The second nonbilayer-prone lipid type exhibits a conical shape with a smaller headgroup in comparison to the alkyl chains (Figure 1.6), such as PE (Gruner *et al.*, 1985). They induce a negative spontaneous curvature and adopt a reverse hexagonal H_{II} phase. In this phase, lipids are organized in hexagonally arranged cylinders with the hydrophobic tails towards the outside of the cylinder.

The cubic phases are more complex organizations of lipids. It is a bicontinuous phase with a three dimensional symmetry, since the water regions are separated by the bilayer. This bilayer has positive and negative curvatures (Mouritsen, 2005) (Figure 1.6).

The cell membranes contain bilayer- and nonbilayer-prone lipids. By modulating the ratio between the different lipid types, membrane curvatures can be induced. This membrane phenomenon can influence cellular processes, such as membrane fusion and fission as well as the activity of membrane proteins (Carsten & Unger, 2012).

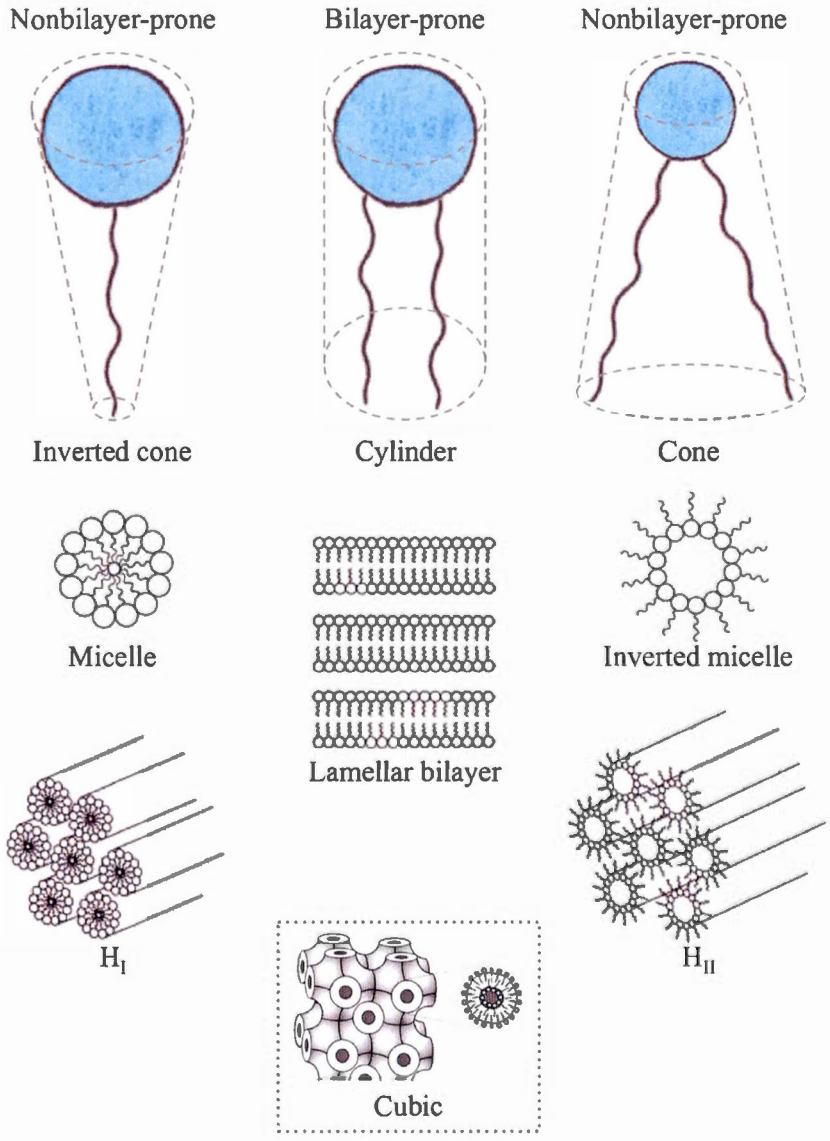

Figure 1.6 The different shape of lipids associated with their organization in aqueous medium. A representation of the complex cubic phase is in an inset. This figure is adapted from (Landau & Rosenbusch, 1996; Lasic, 1998).

1.1.3 Membrane Proteins

The lipid bilayers of cell membranes are embedded with intrinsic (or integral) and extrinsic (or peripheral) proteins (Figure 1.1). These proteins have roles in cell-to-cell communications or interactions and molecular transport. For example, ion channels allow the flow of ions through the membranes. Membrane proteins are the components giving the specificity of a cell (Koolman & Roehm, 2013). They are essential drug targets to treat many pathologies, such as cystic fibrosis and cancer (Clunes & Boucher, 2007; Prevarskaya *et al.*, 2007). About 20 to 30% of the genome is predicted to encode for membrane proteins (Stevens & Arkin, 2000; Wallin & von Heijne, 1998).

1.1.3.1 Classification of Membrane Proteins

Membrane proteins can be defined in three classes according to their process of extraction and their interactions with the components of the membranes (Figures 1.1 and 1.7).

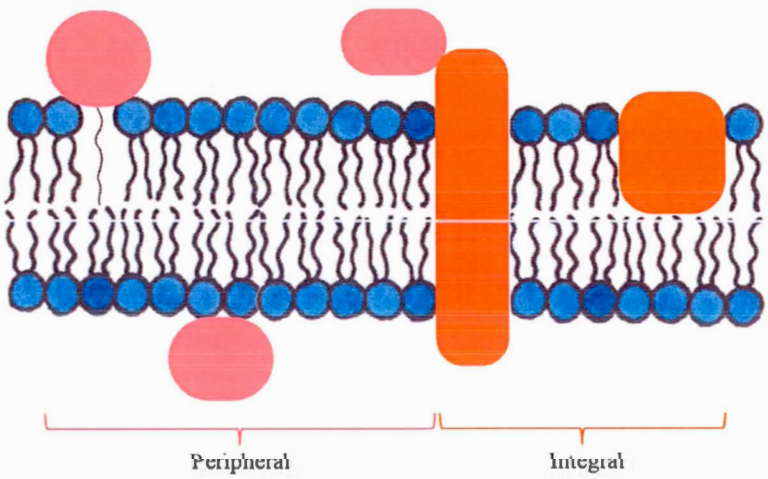

Figure 1.7 Representation of integral (orange) and peripheral (light red) membrane protein classes. Membrane-associated proteins are not represented.

Peripheral Membrane Proteins and Membrane-Associated Proteins

The first class of membrane proteins comprises extrinsic (or peripheral) membrane proteins that are localized at the surface/hydrophilic part of the membrane (Figure 1.7). Their adhesion to the membrane can be via electrostatic or ionic interactions with integral membrane protein(s) or with the headgroup of lipid(s). Some peripheral membrane proteins are linked to a hydrophobic motif, a fatty acid or a lipid (e.g. glycophosphatidylinositol anchored proteins). Their structures are mainly extended β-sheet (Nicolson, 2014).

The second class of membrane proteins are the membrane-associated proteins which do not have direct interactions with the membrane (Nicolson, 2014). They can have interactions with peripheral protein(s), the cytoskeleton or the carbohydrates (Figure 1.1).

These two classes of membrane proteins are mainly soluble in aqueous environment and removable from a cell membrane without affecting its bilayer structure (Cooper, 2000; Nicolson, 2014). An exception to this extraction "rule" can happen with proteins anchored to the membrane by their hydrophobic motif, fatty acid or lipid covalently linked. Their purification process is closer of the one of integral membrane proteins.

Integral Membrane Proteins

The third class of membrane proteins are the intrinsic (or integral) membrane proteins and they are embedded into the hydrophobic part of the phospholipid bilayer (Figure 1.7). They interact with both the polar heads and the apolar tails of the lipids. Most of them consist of one or several transmembrane domains and are called transmembrane

proteins. To extract integral membrane proteins from the membrane, it is necessary to disrupt the bilayer by using surfactants, also called detergents (Figure 1.8, Section 1.4.1).

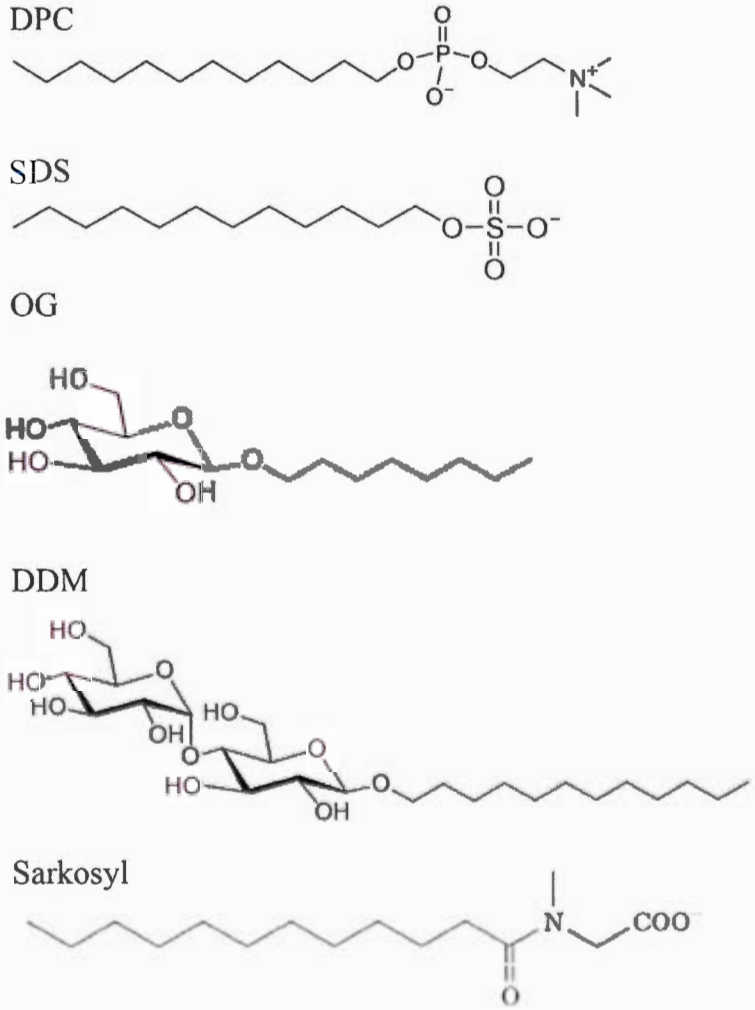

Figure 1.8 Representation of detergent structures. SDS, DPC, OG, DDM are sodium dodecyl sulfate, dodecylphosphocholine, octylglucoside and dodecylmaltoside, respectively.

Most of the transmembrane proteins have their transmembrane domains made of α-helical segments and organized in helix bundle (von Heijne, 1999). To cross the

membrane, the α-helix portion needs to be 20-25 amino-acid long (Cooper, 2000; Koolman & Roehm, 2013). These proteins with α-helical segment(s) can be subdivided into five types according to their orientation and the number of segment(s) as detailed in Figure 1.9. An exception is the porin family, which structure consists in a β-barrel (Benz, 1994). These integral membrane proteins are found in bacteria and in the mitochondria (Benz, 1994).

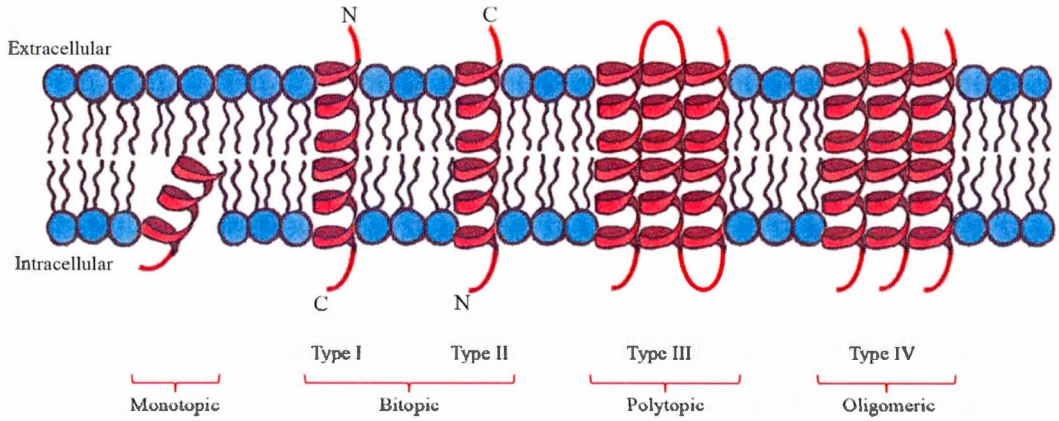

Figure 1.9 Representation of the different types of transmembrane proteins with α-helical segment(s). N and C are for the NH_2- and COOH-terminus, respectively.

1.1.3.2 Major Families of Integral Membrane Proteins

In 2006, it has been estimated that about 4075 transmembrane protein families exist with at least two transmembrane domains (Oberai *et al.*, 2006). The top ten of the largest membrane protein families is listed in Table 1.2 and comprises proteins such as G-protein-coupled receptors (GPCR), ATP-binding cassette (ABC) transporters and cytochrome b (Oberai *et al.*, 2006). Potassium channels, which two members were studied in this thesis (Chapters V and VI), are ranked sixth with 1153 members (Table 1.2).

Table 1.2 List of the top ten largest membrane protein families with at least two transmembrane segments (Oberai *et al.*, 2006).

Family	Number of members
1. GPCR #1 (Rhodopsin-like)	5520
2. Major facilitator	3680
3. ABC transporter #1 (amino acid, phosphate, ferric, nitrate, nickel, taurine, sugar)	2469
4. GPCR #2 (serpentine)	1311
5. ABC transporter #2 (multidrug resistance)	1179
6. Potassium channel	1153
7. Receptor protein kinase	1150
8. Transporter #1 (cationic acid, aromatic amino acid, choline, K^+ uptake)	1082
9. Cytochrome b#1 (N-terminal part)	1030
10. Cytochrome b#2 (C-terminal part)	942

1.2 Potassium Channels

A major objective of this thesis was to understand the function of potassium channels. These channels are ubiquitous and highly specialized for the selective conduction of potassium ions down their electrochemical gradient. Potassium channels are well known for their role in excitable cells (i.e. neurons and cardiomyocytes). They shape the action potential and regulate the membrane potential. This section will give an overview of the structure, the ion selectivity, the gating and the subgroups of the potassium channels.

1.2.1 Structure

Despite significant differences in K^+ channels, they consist of a well-conserved pore domain with four subunits (identical or different). Each subunit consists of two α-

helical transmembrane domains linked by a loop (Figure 1.10A-B). This P-loop is composed of (i) an extracellular loop connecting S5 to the pore helix also called the turret of S5P-linker, (ii) a short pore helix, (iii) a selectivity filter and a (iv) post-selectivity filter loop (Capener *et al.*, 2002; Doyle *et al.*, 1998) (Figures 1.10 and 1.11). The K^+ channel signature sequence TXTTVGYG contains the highly conserved motif of the selectivity filter. In a tetramer, this sequence has a crucial role in the permeation and the selectivity mechanism of the K^+ channel (Capener *et al.*, 2002).

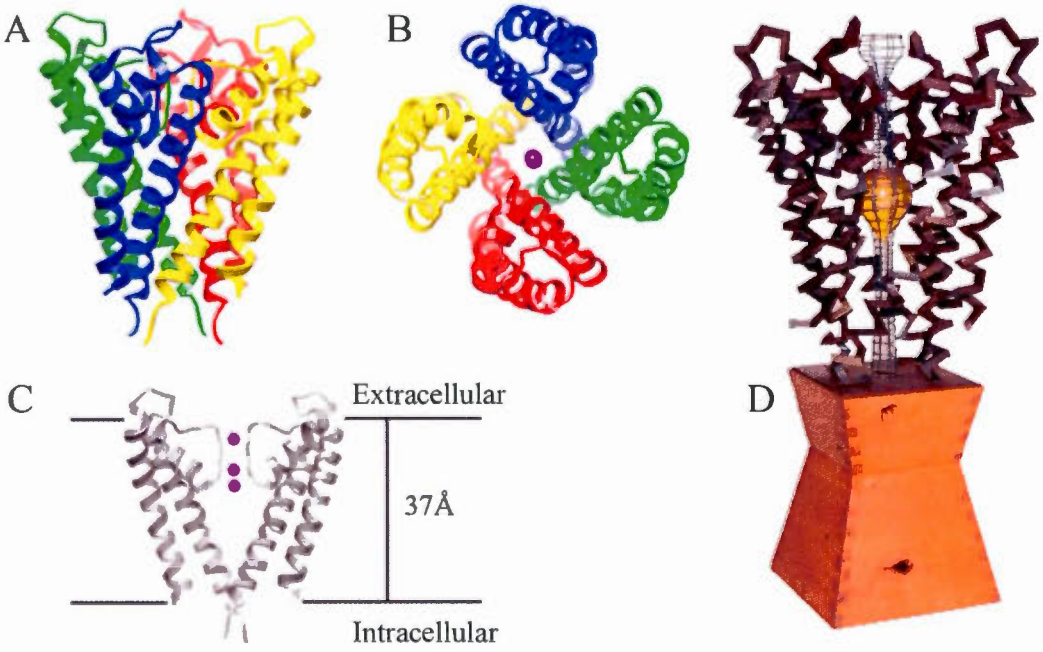

Figure 1.10 Structure of the bacterial KcsA potassium channel which constitute a pore model. (A-C) Ribbon representation of the KcsA channel based on the KcsA crystal structure (PDB number: 2QTO). (A) Side view and (B) above view with each subunit highlighted in a different color. (C) Side view with only two of the four subunits are displayed for the sake of clarity. The horizontal lines show the probable limits between the hydrophobic and hydropholic parts of the phospholipids. Potassium ions are represented in purple. Representations (A-C) are generated with UCSF Chimera software. (D) Sculpture of the KcsA channel where the internal pore and the aqueous cavity are highlighted with an iron and yellow glass structure, respectively (http://julianvossandreae.com/works/protein-sculptures-indoor-works/).

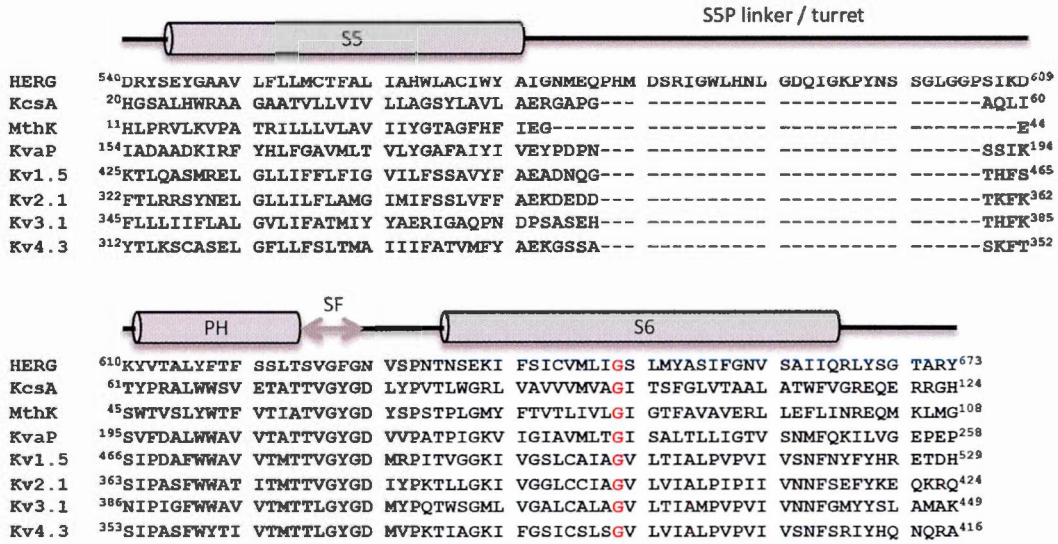

Figure 1.11 Sequence alignment of the hERG pore domain (UniProt Accession Number: Q12809) with KcsA (P0A334), MthK (O27564), KvAP (Q9YDF8), Kv1.5 (P22460), Kv2.1 (Q14721), Kv3.1 (P48547) and Kv4.3 (Q9UK17). Transmembrane helices (S5-S6) and pore helix (PH) are represented with grey cylinders while the selectivity filter (SF) sequence is shown by an arrow. The well-conserved glycine hinge is in red.

The first and second transmembrane helices of the pore domain are termed outer and inner helix, respectively. They are localized on the exterior and the inside side of the pore, respectively. Both stabilize the orientation of the pore helix and the selectivity filter. All together, they are organized in a cone shape (Doyle *et al.*, 1998) (Figure 1.10C).

From this base core topology, some helical transmembrane segments, non-membrane domains and subunits that control their gating can be added (Capener *et al.*, 2002). Three types of subunits can be defined; (i) the primary (α) subunits forming the pore, (ii) accessory (β) subunits which might associate with the α-subunits regulating the activity of the channel and (iii) silent α-subunits, which form altered heterotetramers

with the α-subunits. These silent α-subunits are not functional on their own and can also have regulating activity (Korn & Trapani, 2005).

1.2.2 Ion Selectivity

A cation is stabilised in the large central cavity by the negative end of the dipole formed by the pore helices. This aqueous cavity is maintained by the hydrophobic gate formed by the inner helices (Doyle *et al.*, 1998) (Figure 1.10C-D).

The permeability for K^+ 1,000 times greater than Na^+ (MacKinnon, 2003a). The channels can discriminate these two ions since the distance between the carbonyl oxygen atoms of the selectivity filter corresponds to the hydration shell of K^+ ions (atomic radius of 1.33 Å) but is too large for smaller Na^+ ions (atomic radius of 0.95 Å) (Doyle *et al.*, 1998; Hille, 2001; Shrivastava *et al.*, 2002). The selectivity for monovalent ions follows generally: $Tl^+ >> K^+ > Rb^+ > NH_4^+ >> Cs^+ > Na^+ \approx Li^+$ (Cuello *et al.*, 1998; Hille, 2001). Thallium ions have a higher selectivity than potassium ions but they are not found free in the nature.

Several ions can accumulate in a single line inside the long and narrow conduction pathway of potassium channels (Doyle *et al.*, 1998) (Figure 1.10C). The conductance of potassium channel is 10^7 and 10^8 ions per second (MacKinnon, 2003b).

1.2.3 Gating

The ion conduction through a channel is highly regulated and associated with structural changes of the proteins. There are the opening (activation) and closure (deactivation) of the potassium channels. The channel can prevent the membrane

crossing of ions through it whilst it is still open (inactivation) and recover from this situation (reactivation) (Figure 1.12).

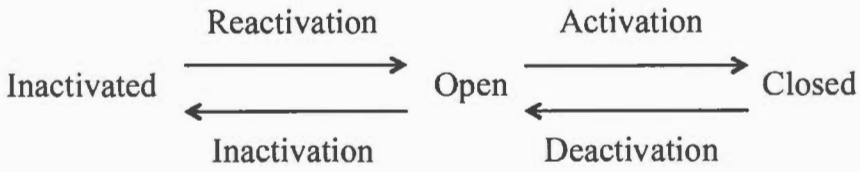

Figure 1.12 Activation, deactivation, inactivation and reactivation of ion channels.

The inner helices obstruct the pore at the intracellular entrance in the closed state and unblock it in the opened state (MacKinnon, 2003a) (Figure 1.13). A highly conserved glycine residue in the middle of the inner helix might be involved as a hinge in this process (MacKinnon, 2003a) (Figures 1.11 and 1.13). Most of mechanisms of activation and deactivation required a stimulus, such as voltage, pH or ligand binding.

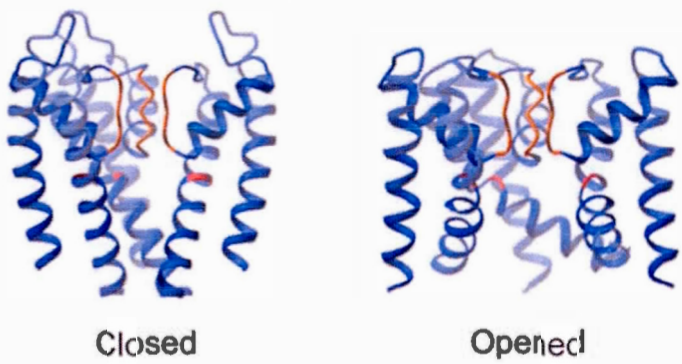

Figure 1.13 Different activity states of a potassium channel. The selectivity filter is in orange and the glycine hinge in red (MacKinnon, 2003a).

There are several types of inactivation process for K^+ channels. The N-type inactivation is also called "ball and chain" model. At least one intracellular N-terminal domain of the protein organizes and enters in the permeation pathway to

block the channel (Hoshi *et al.*, 1990; Mackinnon *et al.*, 1993). This domain is constituted of about 10 conserved residues and a sequence of several positive residues (Murrell-Lagnado & Aldrich, 1993a, 1993b). The N-type inactivation process is quicker than the C-type inactivation and thus termed fast inactivation.

The C-type inactivation is slower (Hoshi *et al.*, 1990). It is believed to involve the C-terminal domain but it seems to be associated with changes of structure around the selectivity filter. A partial collapse of the filter is suggested (Yellen, 2002).

1.2.4 Subgroups of Potassium Channels

Potassium channels are classified into four main structural and functional subgroups according to their mode of activation and their number of transmembrane segments (Capener *et al.*, 2002; Wulff *et al.*, 2010). (i) Inwardly rectifying K^+ channels (K_{ir}) have two transmembrane domains. They are active at negative membrane potentials and maintain the resting potential. (ii) Two-pore K^+ channels (K_{2P}) have four spanning segments. They are also called "leak" channels since it was believed they were continually open. Their role is unclear. (iii) Calcium-activated K^+ channels (K_{Ca}) are constituted of six or seven transmembrane domains. They are activated by the intracellular concentration of Ca^{2+} and some are also sensitive to the membrane depolarization. They could have a role in terminating active and intense period of action potentials. Finally (iv) the voltage-gated K^+ channels (K_V) have six transmembrane domains. They are activated by the depolarization of the membrane and are responsible for the shape, duration of action potentials as well as their frequency of occurrence, also called firing frequency (Capener *et al.*, 2002; Wulff *et al.*, 2010).

1.3 Voltage-Gated Potassium Channels

In this thesis, we focused on the voltage-gated potassium (K_V) channels. They are expressed in variety of tissues but it is their role in the heart and brain that is of great interest. The membrane potential is important since its perturbation will lead to heart and neurological dysfunctions. In this section, an overview of voltage-gated potassium channels will be described, followed by a section on their subfamilies as well as a presentation of the two Kv channels studied in this thesis.

1.3.1 Overview of K_V channels

K_V channels are regulated by regulators of the membrane potential. They adopt an open position upon depolarization. The K^+ ions leave the cell through these channels which play a crucial role in the hyperpolarisation. This phenomenon helps to bring the membrane potential to the resting values, and the K_V channels adopt a closed position.

In addition to the two transmembrane segments forming the pore domain (S5 and S6), K_v channels have four α-helical transmembrane segments (S1 to S4) which form the voltage-sensor domain (Wulff *et al.*, 2010). The S4 segment has positive charges at every three residues and is sensitive to the membrane potential. The voltage changes will induce conformational changes initiated by the motion of the S4 segment in the membrane. These conformational changes will lead to the open state of the channel.

1.3.2 Subfamilies of K_V channels

The K_V channel subfamilies are divided mainly according to their sequence similarity. For example, the first potassium gene, *Shaker*, was cloned in 1987 from *Drosophila melanogaster* (Tempel *et al.*, 1987) and lead to channels named K_V1.x, since they belong to the mammalian Shaker-family (Wulff *et al.*, 2010). Seven other α-subunits subfamilies have been identified K_V2.x (Shab), K_V3.x (Shaw), K_V4.x (Shal), K_V7.x (KCNQ), K_V10.x (KCNH-EAG), K_V11.x (KCNH-ERG) and K_V12.x (KCNH-ELK) as well as four silent α-subunits subfamilies K_V5.x (KCNF), K_V6.x (KCNG), K_V8.x (KCNV) and K_V9.x (KCNS) (www.uniprot.org). Although expressed in other tissues, the functional expression of K_V1.5 and K_V11.1 in the heart is of great interest for pharmaceutical companies.

1.3.3 K_V1.5 and hERG

The study of human ether-à-go-go related gene (hERG) was an important part of this thesis, since its involvement in side effects of drugs. Figure 1.11 presents a multi-alignment of hERG and several K^+ channels, such as K_V1.5.

1.3.3.1 K_V1.5, a representative of K_V channels

The K_V1.5 is encoded by the gene KCNA5. Each subunit is composed of six helical-transmembrane domains (Figure 1.14). Its structure has not been determined experimentally and is based on molecular homology from crystallographic structure of other channels. In *Homo sapiens*, this K_V channel is 613 amino acid residues (Wulff *et al.*, 2010).

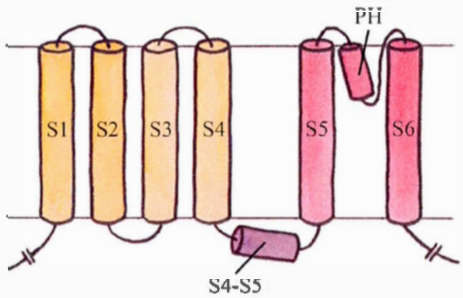

Figure 1.14 Predicted topology of Kv1.5 channel. The voltage sensor (S1-S4) is in orange and the pore region (S5-S6) in pink. S4-S5 linker helix (S4-S5) and pore helix (PH). The horizontal lines represent the membrane.

The $K_V1.5$ channel is the primary molecular component of the ultra rapid delayed rectifier current (I_{Kur}) (Figure 1.15) which plays a role in the early phase of the human atrial action potential repolarization (Wulff *et al.*, 2010). Mutations in the $K_V1.5$ protein are involved in a familial form of atrial fibrillation, a cardiac rhythm disturbance that can result in congestive heart failure (Olson *et al.*, 2006) (Figure 1.16).

Atrial fibrillation is a major problem and identified as the most common cardiac arrhythmia that physicians have to overcome (Ford & Milnes, 2008). It affects 0.4 to 1% of people (Tamargo *et al.*, 2009) and that could increase to 12% for those older than 85 years with a cost of $3,600 USD per patient per year (Ford & Milnes, 2008). People with atrial fibrillation are five times more likely to suffer from a stroke (Ford & Milnes, 2008). The importance for pharmaceutical companies could be felt by the submission of more that 50 patent applications to inhibit $K_V1.5$ for the prevention of atrial fibrillation (Ford & Milnes, 2008; Wulff *et al.*, 2010). This protein is also involved in the glioma cancer (Arvind *et al.*, 2012; Preußat *et al.*, 2003).

$K_V1.5$ was selected for its representative pore helix sequence of K_V channels (Figure 5.1) which allows a comparative study with the one of hERG.

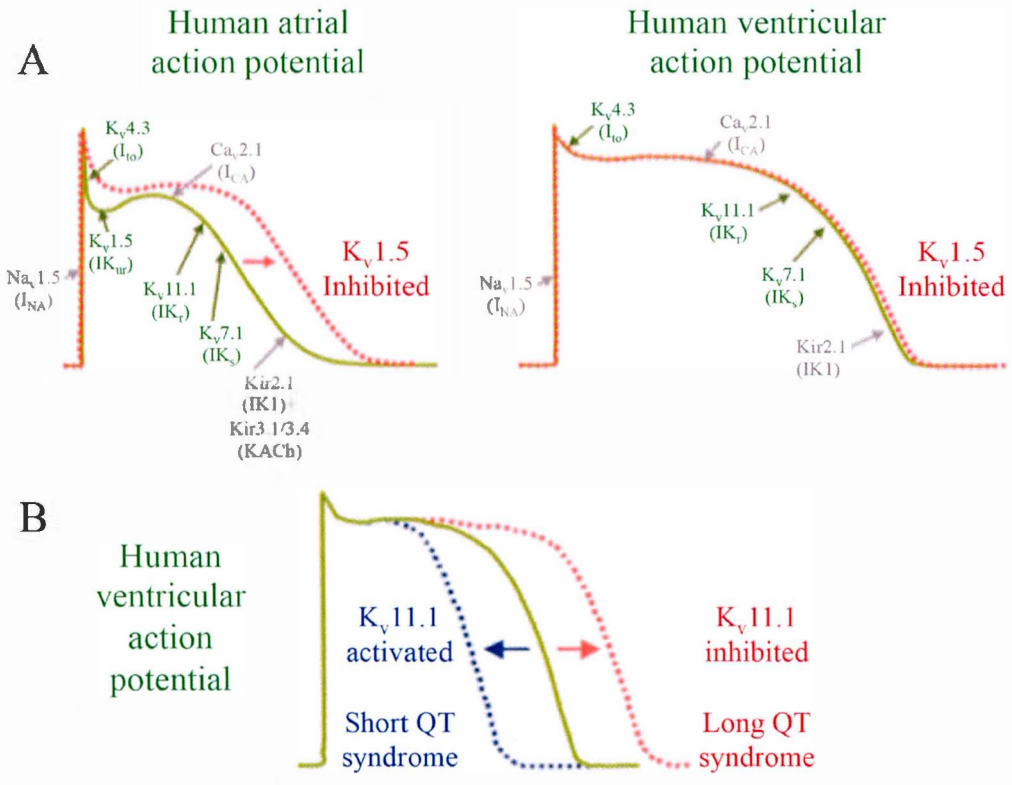

Figure 1.15 Human atrial and ventricular action potential illustrated with indication of ionic currents and ion proteins involved (Wulff *et al.*, 2010). The action potential curve can be seen in green, with the blockade of (A) $K_V1.5$ and (B) hERG ($K_V11.1$) curves in red. The (B) activation of hERG is shown with a blue curve.

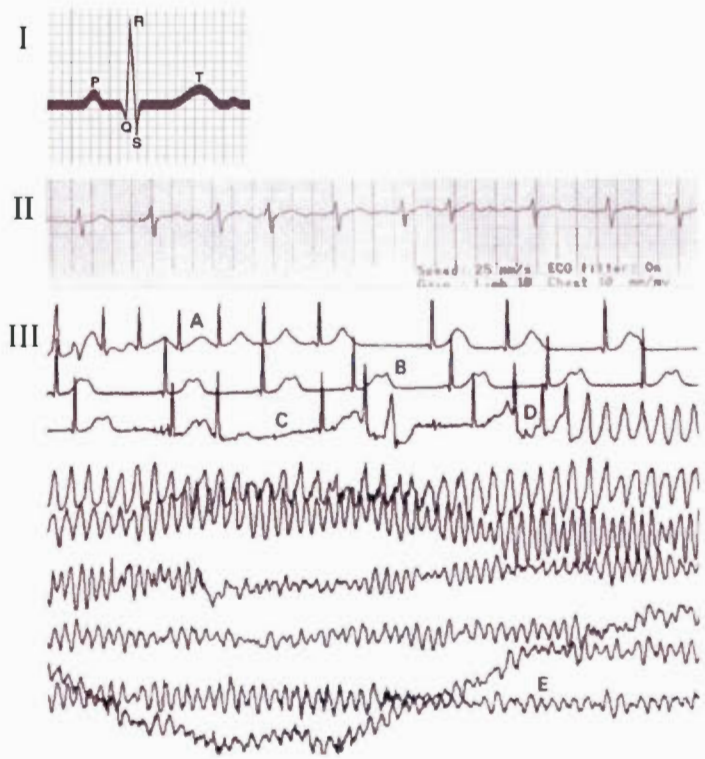

Figure 1.16 (I) Electrocardiogram representation for an healthy person is about 0.8 sec with P wave, the atrial depolarization, QRS, the ventricular depolarization and T wave, the ventricular repolarization (Martin, 2007). (II) Electrocardiogram of a 35-year-old patient with $K_V1.5$ mutations (Olson *et al.*, 2006). The rapid oscillations between ventricular beats are characteristic of the atrial fibrillation. (III) Electrocardiogram of a 25-year-old woman with congenital long QT syndorme (LQTS) recorded during her sleep during a 'bad dream' (Benhorin & Medina, 1997). (A) Prolongation of the QT interval, (B) bifid or notched T-wave (the double 'hills'), (C-D) the arrhytmia episode is initiated by premature beats and (E) ventricular fibrillation.

1.3.3.2 hERG

The hERG is also termed $K_V11.1$ and is encoded by the KCNH2 gene (Vandenberg *et al.*, 2012). This name comes from the analogy of this human protein with the one from *Drosophila melanogaster* ether-a-go-go (EAG) that describes the movement of

the legs of a mutant fruit fly when anaesthetized by ether, similarly to a dance popular at the Whisky a Go-Go nightclub in West Hollywood, California (Kaplan & Trout, 1969; Swain, 2007).

The hERG is involved in a cardiac dysfunction, the long QT syndrome (LQTS), characterized by a prolongation of the QT wave on the electrocardiogram that could lead to sudden death (Figure 1.16) (Curran *et al.*, 1995; Sanguinetti *et al.*, 1995). The LQTS could result from genetic mutations (inherited) or as a side effect of some prescription drugs (acquired). The hERG-associated LQTS is called long QT syndrome 2 (LQT2), accounting for 35-40% of mutation cases (Bhuiyan, 2009). In 2005, it was estimated that 2-3% of all prescription drugs could lead to the disease and the main blockade is on the hERG protein, especially the pore domain (Recanatini *et al.*, 2005). A list of the numerous drugs leading to QT prolongation from different chemical classes and therapeutic areas is available on the independent non-profit organization CredibleMeds® Worldwide website (https://crediblemeds.org/new-drug-list/). The US Food and Drug Administration requires to perform *in vitro* testing for hERG-blocking potential for all new interesting chemical compounds (Food and Drug Administration guidelines, 2005). The hERG is also over-expressed in several tumor cells, such as leukaemia and gastric cancer (Camacho, 2006).

The native hERG channel is most likely a 1a/1b heterotetramer (Vandenberg *et al.*, 2012). The hERG-1a subunit is composed of 1159 residues while in hERG-1b the first 373 amino acids at the N-terminus are replaced by a sequence of 36 residues. As for $K_V1.5$ its structure of hERG is not available and based on homology (Figure 1.17). Its primary structure suggests that its internal cavity is wider than other K_v channels (Mitcheson *et al.*, 2005; Sanguinetti & Mitcheson, 2005). Moreover, the loop between S5 and S6 helices is unique to the hERG channel with a longer extracellular loop connecting S5 to the pore helix (S5P linker) which has 43 residues (possibly

with a little helix, the turret-helix) compared to ~12 for other K_V channels (Pardo-Lopez *et al.*, 2002) (Figures 1.11 and 1.17).

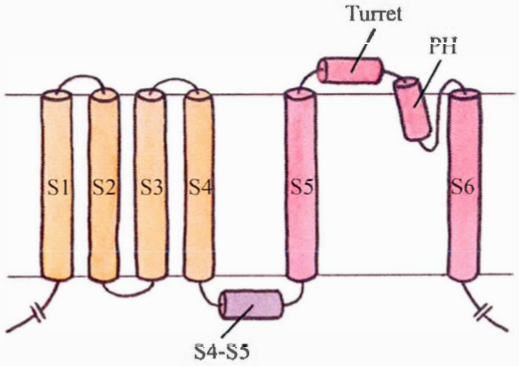

Figure 1.17 Predicted topology of hERG channel. The transmembrane region is composed of six transmembrane domains (S1-S6) with the voltage sensor in orange and the pore region in pink. S4-S5 linker helix (S4-S5), S5P linker with the turret helix and the pore helix (PH) are also represented. The horizontal lines show the probable limits between the hydrophobic and hydrophilic parts of the phospholipids.

Furthermore, the sequence of the selectivity filter is SVGFG compared to the conserved TVGYG (Figure 1.11). Finally, tryptophan residues are absent in the pore helix (Figure 1.11). The open conformation of the K_V channel is stabilized by H-bonds between the Y of the selectivity filter and tryptophan in the pore helix that are missing for hERG. In view of these significant differences that can modulate the conformation and therefore the function of $K_V11.1$, it is important to determine its structure.

Two post-translational modifications have been reported; namely an N-glycosylation on residue 598 (Gong *et al.*, 2002) and numerous phosphorylations (Vandenberg *et al.*, 2012). N-glycosylation does not seem to be necessary for the function and the trafficking of the hERG channel while it has an effect on its stability at the plasma membrane (Gong *et al.*, 2002). Phosphorylations are located preferentially at N- and C-termini and allow regulation processes, such as protein synthesis and gating (Vandenberg *et al.*, 2012).

$K_V11.1$ is responsible for the rapid component of the delayed rectifier current (I_{Kr}) (Figure 1.15). The electrophysiology of this channel is atypical with slow activation and deactivation processes and fast voltage-dependent inactivation (Vandenberg *et al.*, 2012). Therefore, during the depolarization step, the channel will go slowly from a closed to an open conformation, and will then quickly adopt an inactivated state (Vandenberg *et al.*, 2012). Then, during the repolarization, the hERG channel opens again for a longer time before adopting a closed conformation (Vandenberg *et al.*, 2012).

This protein was selected to develop an expression protocol and study its function (Chapters V and VI) for its involvement in the important side effect of drugs.

1.4 Studying the Membrane Proteins

The structural research field on membrane proteins is challenging as proved by the under-representation of the number of their structures available compared to the ones of water-soluble proteins (http://blanco.biomol.uci.edu/mpstruc/ and http://www.wwpdb.org/). This could be correlated with problems of expression, purification, reconstitution, labelling and cristallisation. In this section, two elements to overcome the issues that concern this thesis will be described; (i) the selection of an appropriate membrane system to study the membrane proteins, since membrane proteins are insoluble in aqueous media and (ii) obtaining sufficient amounts of proteins for structural determination.

1.4.1 Model Membrane Systems

Since the cell membranes are complex the use of membrane mimetic systems or model membranes allow the studies of membrane proteins. A model membrane must reproduce the native environment, in the sense that the structure and function adopted by the protein of interest in it should be similar to the ones in a biological membrane. However, the system should also be usable with the appropriate technique to get the information that is searched for. An appropriate choice of model membranes is thus essential to study membrane proteins. Conformations and functions of integral membrane proteins are sensitive to membrane shape and composition (Cady *et al.*, 2010; Foo *et al.*, 2014; Hu *et al.*, 2011; Koehler *et al.*, 2010; Lee, 2004; Marius *et al.*, 2012; Schnell & Chou, 2008).

In addition to the lipids described in Section 1.1.2 detergent molecules are often used in model membranes to solubilise membrane proteins. Similarly to lipids, they are amphiphilic molecules with a hydrophobic hydrocarbon part and a hydrophilic headgroup. Detergents are diverse in their structure (Figure 1.8) (Helenius & Simons, 1975; Lichtenberg *et al.*, 1983; Linke, 2009; Tulumello & Deber, 2012). They can be classified according to their headgroup types: nonionic, anionic, cationic and zwitterionic detergents. The choice of a detergent suitable for a given membrane protein solubilisation can be challenging and typically, it requires a trial and error approach. Nevertheless, there is some guidelines to help determining the detergents most amenable to stabilize the membrane protein of interest, such as the matching between the size of the transmembrane domain of the protein and the thickness of the hydrophobic core of the detergent micelle (Columbus *et al.*, 2009) with a preference for chain lengths of 12 carbons (Vinogradova *et al.*, 1998) as well as zwitterionic headgroups giving rise to high water solubility and monodispersity to the micelles (Sanders & Sönnichsen, 2006). Moreover, some detergents can maintain the activity

of a membrane protein such as lysophospholipid and tetradecylphosphocholine (TPC14) micelles in the case of diacylglycerol kinase (Koehler *et al.*, 2010).

Model membranes can be as small as micelles (~5 nm diameter) and as big as multilamellar vesicles (MLVs) (~1000 nm diameter). Bilayered micelles of bicelles (10-100 nm) are in between micelles and MLVs (Figure 1.18). The morphology of the model membranes is sensitive to the medium conditions, such as temperature, concentration, pH and salts. However, this aspect will not be discussed in this section.

In this thesis, micelles (Chapters V and VI), bicelles (Chapters III, IV and V) and liposomes (Chapter V) were used and will be more detailed in this section. A thorough review describing the different model membranes to study transmembrane proteins with NMR, is found in Warschawski *et al.*, 2011.

1.4.1.1 Micelles

Micelles are made of inverted cone shape amphiphilic molecules, such as detergents, lysolipids or short-chain phospholipids. The size, morphology and charge of these aggregates will depend of the molecules used. Table 1.3 provides information on micelles made with the DPC, SDS and DHPC detergents, which are commonly used in structural studies.

Table 1.3 Critical micelle concentration (CMC), aggregation number, size and shape of different micelles.

Molecule	CMC (mM) [a]	Aggregation number [a]	Diameter (nm)	Shape	Charge
DPC12	1	~60	~4.7 [b]	Prolate [b]	Zwitterionic
SDS	10	~105	~4.4 [c]	Sphere/Ellipsoid [c]	Anionic
D6PC	14	~20	~3.3 [d]	Prolate [d]	Zwitterionic

[a] (Vinogradova *et al.*, 1998)
[b] (Abel *et al.*, 2012; Lauterwein *et al.*, 1979)
[c] (Pires *et al.*, 2012)
[d] (Chou *et al.*, 2004)

The use of micelles is advantageous because the sample obtained is transparent and non-viscous in solution since their size is small. They are useable with a variety of techniques, such as dynamic light scattering (DLS) or solution NMR. Moreover, they easily solubilize membrane peptides and proteins. However, micelles do not form bilayers and exhibit a high degree of curvature (Figure 1.18), giving rise to possible modulation of structure and activity of the membrane peptides or proteins (Chou *et al.*, 2002; Cross *et al.*, 2011; Epand *et al.*, 2014; Koehler *et al.*, 2010; Perozo *et al.*, 2002; Seelig *et al.*, 1985; Vold *et al.*, 1997; H. Yokoyama *et al.*, 2013).

1.4.1.2 Multilamellar Vesicles

MLVs are made of cylindrical shape lipids, such as phospholipids with longer chain compared to DHPC. They form multiple bilayers that close due to the hydrophobic effect. The structure obtained is similar to the layers of an onion (Figure 1.18). MLV samples are heterogenous suspensions with variable size in the tens to hundreds of nanometers range.

There systems are really interesting for the study of membrane peptides and proteins because they are possibly the closest to the cell membranes. However, the use of MLVs is limited to techniques where the size is not an issue, such as solid-state NMR. The large size of these vesicles leads to turbid samples, which can limit their use, especially with problems of scattering and absorption.

1.4.1.3 Bicelles

Bicelles are composed of long-chain phospholipids (cylindrical shape) and short-chain phospholipids or detergents (conical shape). The most popular ones are made

with DMPC and DHPC. This system is really attractive because (i) it has a bilayer formed by long-chain phospholipids (Sternin *et al.*, 2001; Vold & Prosser, 1996), (ii) is amenable to a variety of techniques (e.g. DLS, solution and solid-state NMR) and (iii) can orient in a magnetic field (Katsaras et al., 1997; Sanders & Landis, 1994; Sanders & Prestegard, 1990).

A small molar ratio (q) of the long-chain phospholipids to short-chain amphiphilic molecules leads to small discoid objects, usable with a variety of techniques, such as DLS and solution NMR (Andersson & Mäler, 2002; Glover *et al.*, 2001; Marcotte *et al.*, 2003; Vold *et al.*, 1997). A higher molar ratio q gives rise to bigger aggregates with the possibility of a spontaneous orientation of the bilayer normal perpendicular to the magnetic field direction when placed into a magnetic field (Marcotte & Auger, 2005) (Figure 1.18). The morphology of big bicelles depends on the temperature and q ratio and can lead to the generation of discs, perforated vesicles and vesicles (Marcotte & Auger, 2005) (Figure 1.18). The orientation of bicelles is useful for solid-state NMR and simplifies their spectra compared to the ones obtained with vesicles, as there is no orientation distribution of lipids.

The spontaneous orientation into a magnetic field (B_0) is due to the anisotropy diamagnetic susceptibility, χ, of the phospholipid alkyl chains (and carbonyl groups), which will generate a magnetic moment in B_0 (Boroske & Helfrich, 1978; Sakurai *et al.*, 1980; Seelig *et al.*, 1985). It is called diamagnetic due to the negative sign of the magnetic anisotropy, and will induce an orientation of the magnetic moment perpendicular to B_0, which is the orientation with the lower energy. This spontaneous orientation occurs when the total diamagnetic anisotropy in a bilayer can overcome the Brownian motion. This orientation can be flipped with the normal of the bilayer parallel to B_0 by, for example, adding paramagnetic salts, such as lanthanides with a large positive $\Delta\chi$ (Katsaras, 1998; Katsaras *et al.*, 1997; Prosser *et al.*, 1996).

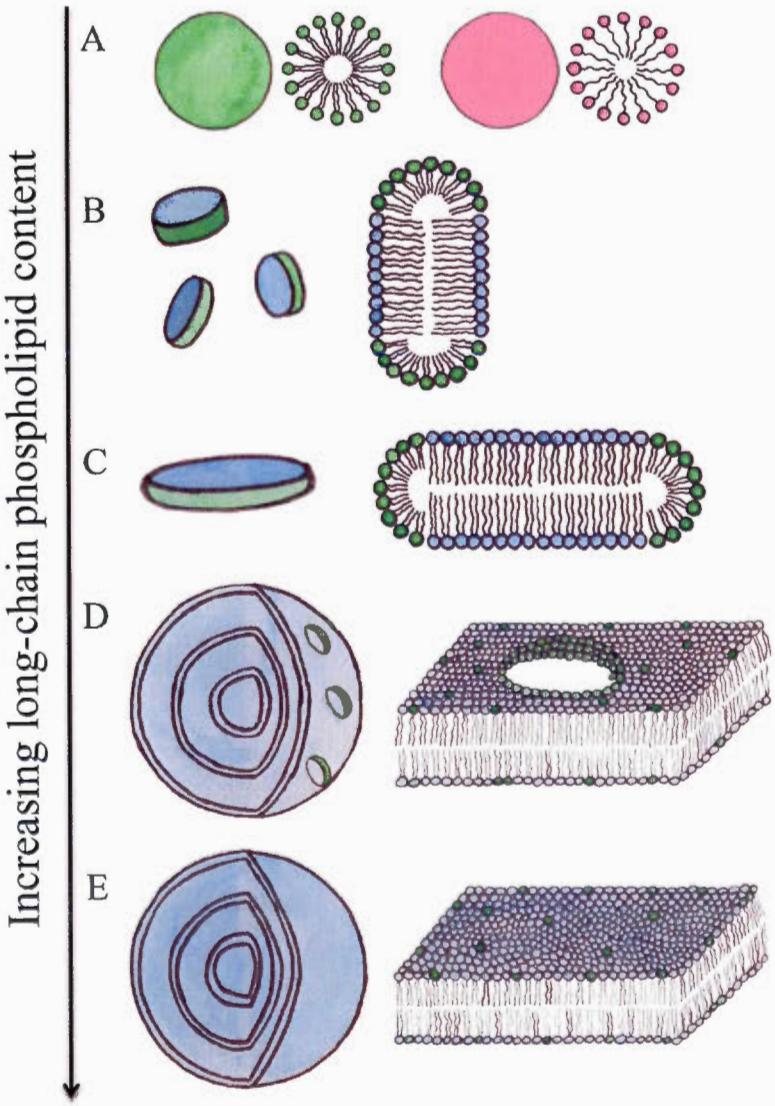

Figure 1.18 Representations depicting several membrane mimetics with a representation of the aggregate (left) and a focus on the organisation of molecule (right). Detergent, short-chain and long-chain phospholipids are represented in pink, green and blue, respectively. (A) Short-chain phospholipid (left) and detergent (right) micelle. (B) Isotropic disk-like aggregate. (C) Magnetically-aligned disk-like aggregate. (D) Perforated multilamellar vesicle. (E) Multilamellar vesicle.

1.4.2 Production of Membrane Proteins

A limitation in the study of membrane proteins and especially tertiary and quaternary structure determination is the requirement of a huge amount of protein (on the order of milligrams). Moreover, for NMR spectroscopy, uniform and specific isotopic labelling may be necessary. Among the structures obtained for eukaryotic membrane proteins, four were expressed in *Escherichia coli*, 20 in yeast, 35 in insect cells and 3 in mammalian cells (He *et al.*, 2014).

There are many different vectors and hosts available for the expression of membrane proteins. However, the major problem with this class of protein is their hydrophobicity and toxicity. If the membrane protein of interest from an organism is expressed in another host, especially from another kingdom, there is a possible absence of the appropriate membrane protein insertion machinery or of extensive intracellular membranes to aid expression. Indeed, no universal expression system exists for proteins. Therefore, it is necessary to use a trial and error approach. Additionally, to achieve the correct folding and expression of the protein, post-translational modifications such as glycosylation and disulfide bonds, lipid composition close to that of the host membrane, molecular chaperones, possibly ligands, co-factors or partner proteins could be necessary.

1.4.2.1 Bacteria - *Escherichia coli*

If post-translational modifications are not needed, *E. coli* remains a preferred choice with the possibility of large yields and the flexibility of specific or complete labelling. Advantages of this host are numerous: (i) low production cost due to the inexpensive components necessary to make the media, even in the case of labelled compounds, compared to production in other systems (ii) fast growth with a division about every

20 min in a rich medium (Sezonov *et al.*, 2007), (iii) high density cell culture, (iv) fast transformation which is possible in 5 min, (v) many vectors such as pET or pQE vectors, and (vi) availability of many strains with different features, such as DH5α selected for high DNA production and BL21 for high expression (Rosano & Ceccarelli, 2014).

However, over-expression of recombinant membrane proteins in this host often results in the accumulation of insoluble aggregates, known as inclusion bodies. Fortunately, this process allows pre-purification of the protein of interest and is expected to be reversible for more that 40% of proteins (Singh & Panda, 2005). An efficient solubilization of the inclusion bodies and the subsequent refolding into a native and functional conformation of the protein is dependent on the type of aggregate (Burgess, 2009). An example of effective solubilizing agent is sarkosyl, which is a strong anionic detergent that seems to lead to higher protein concentration than the common denaturing molecules, i.e. 8 M urea and 6 M guanidine hydrochloride (Burgess, 1996, 2009).

1.4.2.2 Yeast – *Pichia pastoris*

Besides bacteria, yeasts are unicellular eukaryotic hosts capable of processing proteins alike higher eukaryotes. A promising yeast system to overexpress membrane proteins is the methylotrophic *Pichia pastoris* which can reduce one-carbon compounds such as methane and multi-carbon molecules without carbon-carbon bonds, such as dimethylamine. As for *E. coli*, this yeast (i) has low production cost and possibility of uniform labelling (Fan *et al.*, 2011; Pickford & O'Leary, 2004) and also specific labelling (even if limited) of membrane proteins (Nietlispach & Gautier, 2011; Whittaker, 2007), (ii) is still fast growth with a duplication time of 90 min in a rich liquid medium (Cregg *et al.*, 2009), (iii) has several strains, and (iv) vectors

available (Pickford & O'Leary, 2004). Moreover, it allows (v) certain post-translational modifications like glycosylation and disulfide-bond formation (Nietlispach & Gautier, 2011; Pickford & O'Leary, 2004).

This host demonstrates advantages compared to the well-known yeast *Saccharomyces cerevisiae*. *Pichia pastoris* promotes an aerobic rather than anaerobic growth for *Saccharomyces cerevisiae* thus avoiding the problem of toxic level of ethanol and acetic acid that limits the yeast culture (Pickford & O'Leary, 2004). Moreover, the glycosylation process of *Pichia pastoris* is similar to higher eukaryotes with 8-14 mannose residues per chain (Pickford & O'Leary, 2004). Finally, *Pichia pastoris* confers higher protein-expression yields (Pickford & O'Leary, 2004).

1.4.2.3 Other systems

It is possible to perform the expression of integral membrane proteins with high eukaryotes, i.e. insect or mammalian cell lines. *Spodoptera frugiperda* infected by baculovirus is usually used with insect cell systems while chinese hamster ovary (CHO) and human embryo kidney (HEK) cells are employed as mammalian cell lines. However, the production of proteins in these systems is expensive with complex culture media. The labelling process with these rich media is challenging.

An alternative to cell-based and possibly the most promising future expression system for integral membrane proteins is the cell-free expression system (Maslennikov *et al.*, 2010; Sobhanifar *et al.*, 2010). Despite its high cost, this system provides high yields of proteins and enables uniform and selective isotopic labelling (Etezady-Esfarjani *et al.*, 2007; Sobhanifar *et al.*, 2010; J. Yokoyama *et al.*, 2011). Interestingly, it is possible to directly reconstitute the cell-free expressed membrane proteins into liposomes (Friddin *et al.*, 2013).

An alternative or combinatory option for small peptides (inferior to 50-100 amino acids according to the sequence) is to use chemical synthesis.

1.4.2.4 Fusion Tag and Optimization of the Expression

After the choice of an appropriate host system, a specific protein sequence can be added in the gene of interest. Combination of the recombinant membrane proteins with a fusion partner, such as His-tag or maltose-binding protein (MBP), can help in solubilisation, purification process or membrane targetting. These tags are especially convenient when a small segment of membrane protein is studied. Indeed, if the peptide is about 5 kDa or smaller, it is almost impossible to purify it. Some little amino-acid tags rich in Lys could be also added in the sequence to boost the expression (Cunningham & Deber, 2007). If interference with structure or function of protein of interest occurred, tags could be eliminated before further studies.

Finally, it is possible to optimize the expression conditions, for example by trying different media, temperatures or induction regimes to tune the appropriate environment to lead the best yields of the protein of interest.

In this thesis, the potassium channel hERG has been chosen to develop an expression system in *E. coli* for its importance in drug-induced cardiopathy, the long QT syndrome (LQTS) (see section 1.3.3.2). The bacterial system was selected for its low cost and its convenience with labelling process.

1.5 Objectives

The aim of the studies presented in this thesis is to be able to study the structure and function of hERG channels using nuclear magnetic resonance (NMR). As described in the introduction, membrane protein studies require suitable membrane systems and high yields of the protein of interest. Bicelles have been shown to form a bilayer and are usable with solution and solid-state NMR. They are also interesting with their property of alignment in a magnetic field. The first objective was to better characterize the well-known D14PC/D6PC bicelles and their limits (Chapter III). To improve the solubilisation process, bicelles with detergents known to well solubilize membrane proteins were developed and characterized, i.e. the family of monoalkylphosphocholine (MAPCHO) bicelles (Chapter IV). The investigation of how pore helices of hERG and Kv1.5 channels interactions with membranes was performed in vesicles and MAPCHO bicelles (Chapter V). This Chapter V allowed also testing the MAPCHO systems. To address the second issue requiring sufficient materials for structural studies, an expression and purification protocol for the hERG pore domain was developed in bacteria (Chapter VI).

CHAPTER II

THEORICAL ASPECTS OF BIOPHYSICAL TECHNIQUES

This section describes the main techniques used in this thesis, with emphasis on NMR. Many concepts introduced in the following section are inspired from the book written by Malcolm H Levitt (2001). Then a brief description of circular dichroism and Fourier transform infrared spectroscopy will follow.

2.1 Nuclear Magnetic Resonance

NMR spectroscopy is a powerful non-invasive method to obtain information on molecular structure and dynamics of biological systems such as membranes and proteins (Baldus, 2006; Renault *et al.*, 2012; Watts *et al.*, 1998; Wüthrich, 1987).

In this section, basic concepts on the nuclear spin and the Larmor frequency, and the free induction decay of magnetization will be introduced. A description of the nuclear spin Hamiltonian will follow. Finally, ^{31}P- and ^{2}H-NMR of membrane systems will be described.

A NMR spectrometer is equipped with a large magnet to probe the intrinsic spin of nuclei, a quantum mechanical property which has no classical analog. The measurement of the spin interaction with the magnetic field provides information on the spin's environment. Wolfgang Pauli (University of Hamburg) in 1924 proposed

the concept of the spin with two possible values, 'up' and 'down'. Later, in 1946, Edward Mills Purcell, Robert Pound and Henry Torrey of Harvard University along with Felix Bloch, William Webster Hansen and Martin E. Packard of Stanford University (Bloch, 1946) discovered that magnetic nuclei were able to absorb the radiofrequency after the splitting of energy levels induced by a magnetic field. Bloch and Purcell shared the Nobel Prize in Physics in 1952 for the first NMR experiment performed. In 1949, Knight (Knight, 1949) described the chemical shift effect. The application of the Fourier transform for NMR (Ernst & Anderson, 1966) and the introduction of two-dimensional NMR spectroscopy (Jeener, 1971) paved the way for the NMR we know nowadays. Richard R. Ernst was awarded the Nobel Prize of Chemistry in 1991 for his development of techniques for high resolution NMR spectroscopy.

2.1.1 Nuclear Spin and Larmor Frequency

The spin is a form of angular momentum ($\vec{I}$). It is an intrinsic property of the nucleus, as are mass, magnetism and electric charge. Table 2.1 lists the nuclei used in this project.

Table 2.1 Properties of different isotopes (Malcom H Levitt, 2005).

Isotope	Spin Quantum Number I	Natural Abundance (%)	Gyromagnetic Ratio γ (10^6.rad.s^{-1}.T^{-1})	Larmor Frequency at 14.1 T (MHz)	Larmor Frequency at 9.4 T (MHz)
^{1}H	1/2	~100	267.5	600	400
^{2}H	1	0.015	41.1	92	61
^{31}P	1/2	~100	108.4	243	162

The spin can be visualized as a vector pointing in the axis about which it rotates (Figure 2.1). Since the particle is not in real rotation, the spin is an abstract concept, difficult to grasp due to the lack of a macroscopic counterpart. The direction of the spin angular momentum is called the spin polarization axis.

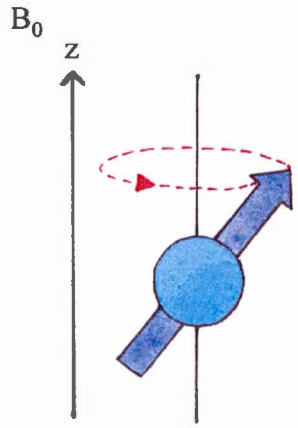

Figure 2.1 Spin angular momentum (dark blue) of a nucleus (light blue) and motion of precession of the spin (red).

A nucleus ($I \neq 0$) has a magnetic moment ($\vec{\mu}$) since it is composed of charged particles. The spin angular momentum ($\vec{I}$) and the magnetic moment ($\vec{\mu}$) are linked by the gyromagnetic ratio γ, which is characteristic of each nucleus:

$$\vec{\mu} = \gamma \vec{I} \tag{2.1}$$

Similar to a compass needle in the earth's field, the magnetic moment aligns with the external magnetic field B_0. For particles with a positive value of γ (most nuclei), the magnetic moment is parallel to the angular momentum. For particles with a negative value of γ, the magnetic moment is in opposite direction to the angular momentum (Figure 2.2).

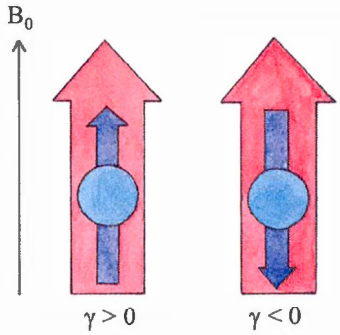

Figure 2.2 Directions of spin angular momentum (dark blue) and magnetic moment (pink) according to the sign of the gyromagnetic ratio.

In the presence of an external magnetic field B_0, the combination of the magnetic moment and the angular momentum leads to the precession motion (Figure 2.1), also called Larmor Frequency:

$$\omega = -\gamma B_0 \tag{2.2}$$

where ω is the angular frequency of precession in radian per second and B_0, the strength of the magnetic field. The Larmor frequency ν_0 in Hz can be calculated by:

$$\nu_0 = -\frac{\gamma B_0}{2\pi} \tag{2.3}$$

This equation allows the calculation of the Larmor frequency for each nucleus (Table 2.1). Since γ is specific to each nucleus, so is ν_0. This allows the selective excitation of nuclei with a specific radio frequency.

2.1.2 Free Induction Decay

Nuclei in a magnetic field go from a degenerate state (one energy level) to a split in $2I + 1$ sublevels (i.e., 2 for $I = 1/2$) with different energy values from $+I$ to $-I$ (i.e., +1/2 and -1/2 for $I = 1/2$). The Boltzmann distribution causes the lower energy state to be more populated by spins than the higher energy level. Consequently, the

resulting magnetization is in the +z direction (in case of a positive value of γ) (Figure 2.2).

The NMR signal is linked to the difference of spin population between energy levels and the transitions between neighbouring energy levels that are induced by electromagnetic radiation. To disrupt the magnetization, an oscillating magnetic field (B_{ν_0}) at resonance frequency (ν_0), called the pulse, is applied for a determined time to a coil placed in the transverse plane (xy). The magnetization is therefore rotated in the xy plane and continues to precess at or close to the Larmor Frequency. This induces a current in the coil which decreases as the spins return to equilibrium and gives rise to the free induction decay (FID) (Figure 2.3).

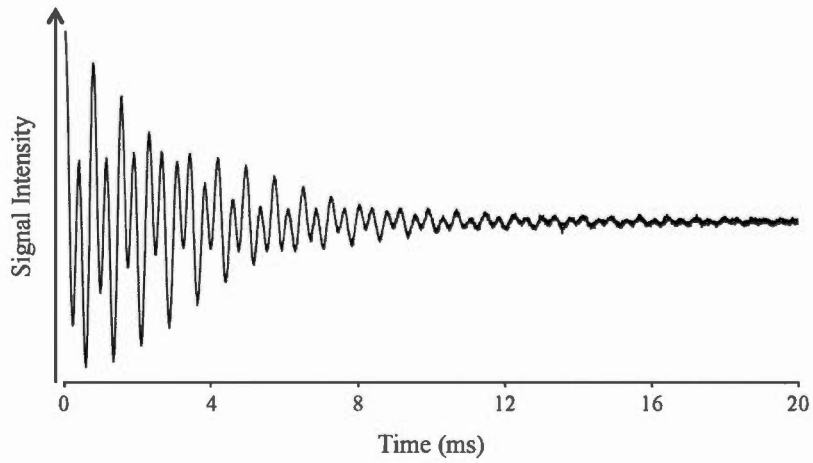

Figure 2.3 Example of free induction decay (FID) of a binary mixture of phospholipid and MAPCHO detergent (q = 2).

The current of the FID decreases with time due to the phenomenon of relaxation. A Fourier transform is applied to obtain a frequency spectrum.

2.1.3 Nuclear Spin Hamiltonian

The nuclear spin Hamiltonian is a quantum mechanical operator which describes the interactions of a nucleus spin with its environment (i.e. the magnetic field and the particles around, other nuclei and electrons). These interactions are responsible of the position and shape of the NMR signal of a nucleus on the spectrum. A brief summary of the Hamiltonian describing a nuclear spin k in a magnetic field follows.

2.1.3.1 The Zeeman Interaction

The Zeeman interaction ($\widehat{H}_Z$) (Figure 2.4) is the strongest one and it is the interaction of the spins with the static magnetic field:

$$\widehat{H}_Z = \gamma \hat{I}_{kz} B_0 \tag{2.4}$$

where $\hat{I}_k$ is the spin angular momentum operator. This interaction leads to 2I+1 energy levels (E), each of which is separated by:

$$\Delta E = h\nu_0 = \hbar\gamma B_0 \tag{2.5}$$

where ν_0 is the frequency of the electromagnetic radiation, also called the resonance frequency, and $\hbar$ is Planck's constant (h) divided by 2π. This discovery led to a Nobel Prize in Physics for Pieter Zeeman and Hendrik Antoon Lorentz in 1902. The stronger the magnetic field or the gyromagnetic ratio, the higher the difference of energy, which leads to improved sensitivity due to a large population difference.

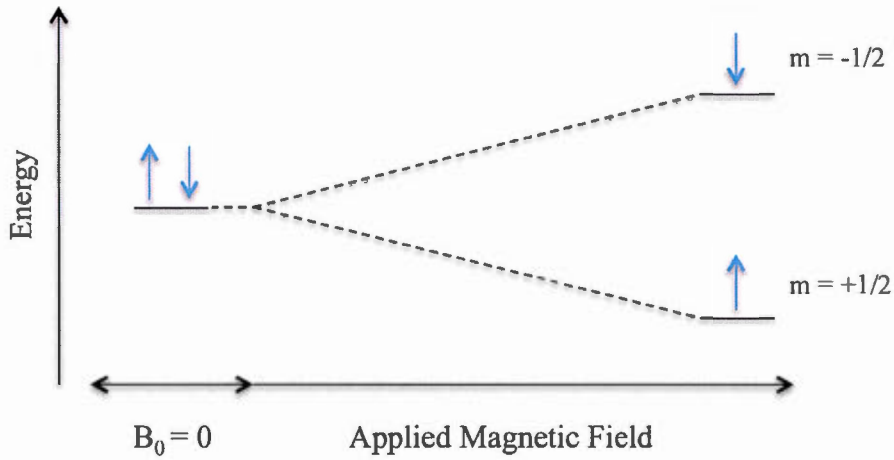

Figure 2.4 Representation of the Zeeman effect with energy levels in the presence of a magnetic field for a hydrogen nucleus (I=1/2), m is the magnetic quantum number.

2.1.3.2 The Chemical Shift Interaction

The chemical shift interaction ($\widehat{H}_{CS}$) describes the change of the local magnetic field due to the presence of electrons around the corresponding nucleus:

$$\widehat{H}_{CS} = \gamma \hat{I}_{kz} B_0 \left[\sigma_{iso} + \bar{\sigma}\left(\frac{3\cos^2\theta - 1}{2} - \eta \frac{\sin^2\theta \cos 2\alpha}{2}\right)\right] \quad (2.6)$$

where θ and α describes the orientation of the principal axis of the chemical shift anisotropy tensor with respect to the magnetic field and η is the asymmetry parameter (Equation 2.9). The isotropic asymmetry parameter (chemical shift σ_{iso} is defined by:

$$\sigma_{iso} = \frac{1}{3}(\sigma_{xx} + \sigma_{yy} + \sigma_{zz}) \quad (2.7)$$

with σ_{xx}, σ_{yy} and σ_{zz} the principle axis components of the chemical shielding tensor. The anisotropy ($\bar{\sigma}$) is:

$$\bar{\sigma} = \sigma_{zz} - \sigma_{iso} \quad (2.8)$$

and the asymmetry parameter (η) is:

$$\eta = \frac{\sigma_{yy} - \sigma_{xx}}{\bar{\sigma}} \tag{2.9}$$

Equation 2.6 shows the orientational dependence of the chemical-shift interaction.

The motion of the electron cloud around the nucleus creates an induced magnetic field (B_i) which can increase (shield) or decrease (deshield) the local strength of B_0. Therefore, the magnetic field sensed by a nucleus (B_S) is:

$$B_S = B_0 + B_i \tag{2.10}$$

The resonance frequency for a specific nucleus (ν_S) is influenced by the shielding constant (σ) created by the electrons:

$$\nu_S = \frac{\gamma B_0 (1-\sigma)}{2\pi} \tag{2.11}$$

This phenomenon provides information on the nucleus environment and depends on the orientation since the electron cloud is non-uniform. Chemical shifts (δ) are expressed in parts per million (ppm):

$$\delta = \frac{\nu - \nu_{ref}}{\nu_{ref}} 10^6 \tag{2.12}$$

where ν is the frequency of the signal of interest and ν_{ref} the frequency of the reference standard (i.e. tetramethylsilane and H_3PO_4).

2.1.3.3 The Scalar Interaction

The *J*-coupling (also called scalar coupling or indirect dipole dipole coupling) interaction ($\widehat{H}_J$) is the coupling between two spins mediated through the electrons of chemical bonds. This leads to multiple lines on the spectrum. Homo- (k and k') and

hetero-nuclear (k and l) coupling distinguish interactions between identical and different nuclei, respectively.

$$\widehat{H}_J^{Homo} = 2\pi J_{kk'} \hat{I}_{kz} \hat{I}_{k'z} \tag{2.13}$$

$$\widehat{H}_J^{Hetero} = 2\pi J_{kl} \hat{I}_{kz} \hat{I}_{lz} \tag{2.14}$$

where $J_{kk'}$ and J_{kl} are J-coupling constants.

2.1.3.4 The Dipolar Interaction

The dipolar interaction ($\widehat{H}_D$) is the coupling between two spins through space. In the same manner as $\widehat{H}_J$, it is possible to distinguish homo- and hetero-nuclear dipolar-coupling.

$$\widehat{H}_D^{Homo} = -\frac{\mu_0}{4\pi} \frac{\hbar \gamma_k \gamma_{k'}}{2r_{kk'}^3} \left(\frac{3\cos^2\theta - 1}{2}\right) \left[3\hat{I}_{kz}\, \hat{I}_{k'z} - \left(\hat{I}_k \hat{I}_{k'}\right)\right] \tag{2.15}$$

$$\widehat{H}_D^{Hetero} = -\frac{\mu_0}{4\pi} \frac{\hbar \gamma_k \gamma_l}{2r_{kl}^3} \left(\frac{3\cos^2\theta - 1}{2}\right) 2\hat{I}_{kz} \hat{I}_{lz} \tag{2.16}$$

where μ_0 is the vacuum permeability and r the distance between the spins involved. There is an orientation dependence involved due to the anisotropic contribution.

2.1.3.5 The Quadrupolar Interaction

The quadrupolar interaction ($\widehat{H}_Q$) affects only nuclei with a spin equal or superior to 1. The charge distribution of these nuclei is non-uniform and leads to an electric

quadrupole moment which interacts with electric field gradients of the nucleus environment:

$$\widehat{H}_Q = \frac{eQ}{4I(2I-1)\hbar}\left(\frac{3\cos^2\Theta-1}{2} - \eta\frac{\sin^2\Theta\cos 2\varphi}{2}\right)\left[3(\hat{I}_{kz})^2 - I(I+1)\right] \quad (2.17)$$

where Θ and φ describes the orientation of the principal axis of the electric field gradient tensor (located along the carbon-deuterium bond) versus the magnetic field while eQ is the quadrupolar moment of the nucleus k.

The Zeeman interaction alone leads to two transitions with equal energy gap and therefore to one peak on the spectrum (Equation 2.4) (Figure 2.5). With a spin of 1, the quadrupolar interaction perturbs them leading to transition with different energy gap and the spectrum displays two symmetric peaks (Figure 2.5). The interaction of the quadrupolar moment with electric gradients causes different energy transitions:

$$\Delta E = h\nu_0 \pm \frac{\Delta\nu_Q}{2} \quad (2.18)$$

where $\Delta\nu_Q$ is the quadrupolar splitting and defined as:

$$\Delta\nu_Q = \frac{3e^2qQ}{4h}\left[(3\cos^2\Theta - 1) + (\eta\sin^2\Theta\cos 2\varphi)\right] \quad (2.19)$$

where $\frac{e^2qQ}{h}$ is the nuclear quadrupolar coupling constant.

Since the electric gradients tensor is symmetric for a spherical distribution of nuclei (Figure 2.6) the asymmetric parameter, $\eta = 0$. Thus, the quadrupolar splitting can be simplified:

$$\Delta\nu_Q = \frac{3e^2qQ}{4h}(3cos^2\Theta - 1) \quad (2.20)$$

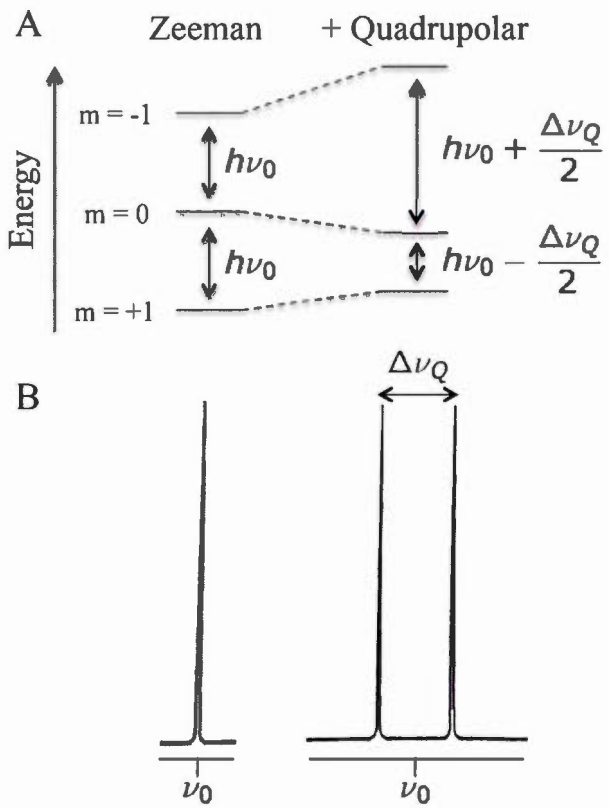

Figure 2.5 Illustration of (A) energy levels for a spin I=1 and (B) ^{2}H-NMR spectra with Zeeman interaction (left) and with both Zeeman and quadrupolar interactions (right). Spectra were obtained from Marcotte, 2003.

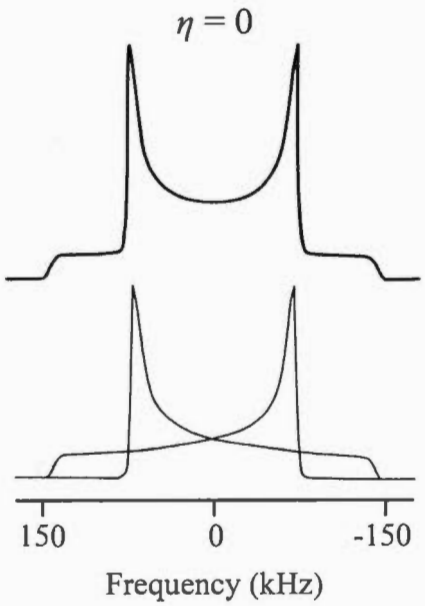

Figure 2.6 ^{2}H-NMR (spin=1) spectrum (top) and individual transitions (bottom) in a spheric symmetric distribution of nuclei. Spectra were obtained from Vega, 2000.

2.1.3.1 The Hamiltonian in Solution and in « Solid » States

In solution NMR, macromolecules in a solvent are tumbling, leading to the average of all anisotropic interactions, such as dipolar and quadrupolar couplings as well as chemical shift interactions. The Hamiltonian describing a nuclear spin system in solution ($\widehat{H}_{Solution}$) is:

$$\widehat{H}_{Solution} = \widehat{H}_Z + \widehat{H}_{CSI} + \widehat{H}_J \tag{2.21}$$

where $\widehat{H}_{CSI}$ is the isotropic chemical shift, which is not orientation-dependent.

In solid-state NMR, the sample is in 'solid' form such as a powder, gel or crystal. The molecular motions are slow, hence molecules will stay longer in a given orientation.

The anisotropic interactions will not be averaged and the Hamiltonian describing a nuclear spin system in solid ($\widehat{H}_{Solid}$) is:

$$\widehat{H}_{Solid} = \widehat{H}_Z + \widehat{H}_{CSA} + \widehat{H}_J + \widehat{H}_D + \widehat{H}_Q \quad (2.22)$$

where $\widehat{H}_{CSA}$ is the chemical shift anisotropy, which is orientation-dependent.

2.1.4 NMR Study of Membrane Systems

The use of ^{31}P solution NMR gives information on the headgroup of the phospholipid molecule. The use of static solid-state NMR with ^{31}P and ^{2}H provides information on the organization of membrane phospholipids and also on the dynamics of the polar headgroup and alkyl chains. This section describes the study of membrane system by phosphorus and deuterium NMR.

2.1.4.1 Phosphorus NMR of Lipid Membranes

Phosphorus NMR is a crucial method in the study of membranes. Indeed, phospholipids are the main component of eukaryotic membranes and each one contains only one phosphate group. Moreover, its natural abundance is 100%, the gyromagnetic ratio is high and it possesses a spin of $\frac{1}{2}$ (Table 2.1). Therefore, this allows the study by NMR of the phospholipid headgroup without labelling.

Asymmetry of the electron cloud surrounding the phosphorus nucleus induces chemical shifts that are orientation-dependent. Therefore, the chemical shift anisotropy can be defined by the second-rank tensor describing the shielding anisotropy ($\bar{\sigma}$) (Gorenstein, 1984).

In the situation of slow-tumbling non-oriented objects, the phosphorus spectrum gives a powder pattern (Figure 2.7A-C). A static phosphodiester, such as the one found in phospholipid, will give an anisotropic spectrum with σ_{xx} and σ_{zz} defining the right and left edge, respectively while σ_{yy} leads to a peak (Figure 2.7A) (Smith & Magid, 1984). The shielding (or chemical shift) tensor is axially asymmetric.

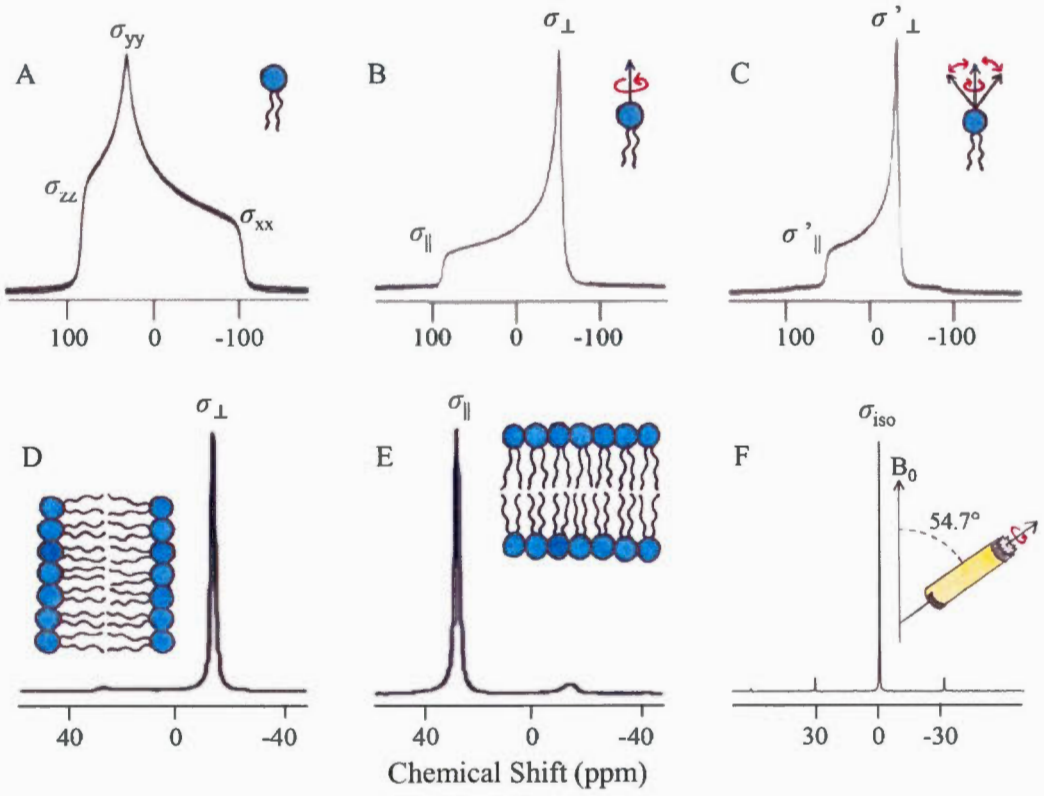

Figure 2.7 Representation of the chemical shift anisotropy effect on ^{31}P-NMR spectra of phospholipids. (A) No movement, (B) rapid axial rotation of the lipid, (C) rapid rotation into a cone along the axis of the lipid for a phosphodiester in membrane lipid. Spectra A-C are from Smith & Magid, 1984. (D) A bilayer of POPC with its normal (longitudinal axis of the lipids) oriented perpendicular or (E) parallel at the magnetic field. Spectra D and E are taken from van der Wel *et al.*, 2002. (F) Sample of DMPC subjected to magic angle spinning (MAS).

From the spectrum it is therefore possible to determine the values of the three component of the shielding tensor (Figure 2.8).

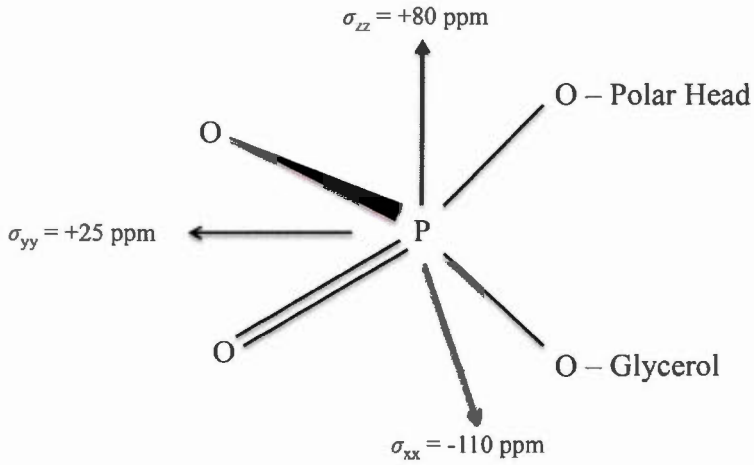

Figure 2.8 Components of the chemical shift anisotropy tensor and their values (Smith & Magid, 1984) for the phosphorus nucleus of a lipid.

For axial symmetry shielding tensor, with axial rotation of membrane lipids along z, σ_{xx} and σ_{yy} are averaged into $\sigma_{\perp}$ (perpendicular component):

$$\sigma_{\perp} = \frac{\sigma_{xx}+\sigma_{yy}}{2} \tag{2.23}$$

while σ_{zz} is called $\sigma_{\parallel}$ (parallel component) (Smith & Magid, 1984) (Figure 2.7B):

$$\sigma_{\parallel} = \sigma_{zz} \tag{2.24}$$

$\sigma_{\perp}$ represents the chemical shift when the magnetic field is perpendicular to this axis and $\sigma_{\parallel}$, corresponds to the chemical shift expected when the magnetic field is parallel to this axis.

The CSA ($\Delta\sigma$) represented on the spectrum and the tensor anisotropy ($\bar{\sigma}$) are respectively defined as:

$$\Delta\sigma = \sigma_{\parallel} - \sigma_{\perp} \tag{2.25}$$

and:

$$\bar{\sigma} = \frac{2}{3}\Delta\sigma \tag{2.26}$$

All anisotropic frequencies (ν_θ) are dependent on the orientation (θ) of the phosphorus nucleus in the magnetic field and can be connected to the CSA by:

$$\nu_\theta = \frac{2}{3}\Delta\sigma\frac{(3cos^2\theta-1)}{2} \tag{2.27}$$

The phosphorus powder pattern is the result of these different orientations (Figures 2.7A-C and 2.9).

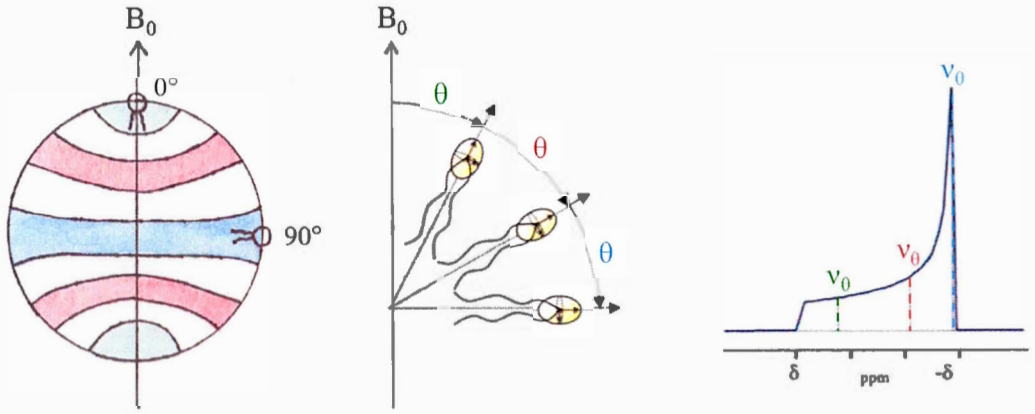

Figure 2.9 Illustration of the distribution of lipids in a multilamellar vesicle (right), example of three different lipid orientations $\boldsymbol{\theta}$ (middle) and the intensity of the corresponding signal with their resonance frequencies on ^{31}P-NMR spectrum (left). Adapted from a figure of Alexandre A. Arnold, UQAM.

For visualisation, the phosphorus powder pattern spectrum of a multilamellar vesicle can be decomposed into many narrow peaks with different frequencies due to different lipid orientations (Figure 2.9).

As the lipid exhibits rapid fluctuations about the bilayer direction, $\sigma_\perp$ and $\sigma_\parallel$ undergo partial averaging that lead to smaller values, called $\sigma'_\perp$ and $\sigma'_\parallel$ (Figure 2.7C). The shielding tensor is still axially symmetric. The CSA observed on the spectrum is

reduced proportionally to the amplitude of the motion. The bilayer normal can undergo motional deviation and an order parameter can be described:

$$S_{bilayer} = \langle \frac{3\cos^2\phi - 1}{2} \rangle \quad (2.28)$$

where ϕ is the angle between the bilayer normal with respect to the magnetic field and the brackets mean time average.

The extreme frequencies of oriented systems for phosphorus nuclei are from an orientation of ϕ equal 90° (Figure 2.7D) to ϕ equal 0° (Figure 2.7E). The orientation can be obtained mechanically from lipid bilayers between glass plates, where the tilt can be controlled externally, or spontaneously in the magnetic field with bicelles. The use of non-mechanically oriented systems is advantageous since the signal-to-noise is greatly enhanced.

Another technique to improve the spectrum is the magic angle spinning (MAS) of the sample. From section 2.1.3 on nuclear spin Hamiltonian, it is possible to observe that chemical shift, dipolar and quadrupolar interactions have an angular dependence with respect to the magnetic field $(3cos^2\theta - 1)$ (Equations 2.6, 2.15, 2.16 and 2.17). The rapid mechanical rotation of the whole sample at the magic angle (54.74°) allows an averaging of the three principal components of the chemical-shift tensor and as a consequence the cancellation of the orientational dependence of the interactions. MAS leads to peak(s) with σ_{iso} value and sidebands appear at multiple frequencies of the spinning speed (Figure 2.7F). This technique allows an increase in both sensitivity and resolution by recreating the isotropic conditions in solid-samples.

In the case of isotropic systems with fast tumbling, the shielding constant is averaged (Equation 2.7) and the phosphorus spectrum gives a narrow peak. The isotropic values for lipids vary slightly according the lipid type as well as the buffer conditions and are ± 5 ppm (Smith & Magid, 1984).

The rapid exchange of a molecule between two environments, such as monomeric form and aggregate lead to an average of the chemical shift between the respective phosphorus chemical-shifts of the amphiphilic molecule in the two conditions (Dennis & Plückthun, 1984; Glover *et al.*, 2001).

Information on the type of lipid-assembly and the bilayer orientation can be directly and quickly extracted from the shape of the solid phosphorus NMR spectrum. As a consequence, it is possible to have a representation of the effect of a peptide interaction with the membrane polar region. Phosphorus NMR allows the identification of oriented bilayer and can be used to judge the quality of this orientation. This technique was used in Chapters IV and V. Chapter III used the averaging chemical shift of one compound between two environments to extract a minimal concentration required to form the lipid aggregate.

2.1.4.2 Deuterium NMR of Deuterated Lipid Membranes

To obtain deeper information on the membrane and protein as well as the interact between them, ^{2}H NMR experiments can be used to see the effect in the hydrophobic region of the membrane. It is also possible to see which region of the alkyl chain is most affected by comparing the quadrupolar splitting with and without peptide.

The natural abundance of deuterium is low (0.015%) hence ^{2}H NMR requires deuterated phospholipids commercially available. ^{2}H has a spin of 1 (Table 2.1).

Since, the quadrupolar interaction is dependent on the orientation (Equation 2.17), the quadrupolar splitting ($\Delta\nu_Q$) is correlated with the molecular movements of the membrane lipids and can be defined as:

$$\Delta\nu_Q = \frac{3e^2qQ}{2h}\left\langle\frac{3cos^2\phi-1}{2}\right\rangle\left\langle\frac{3cos^2\psi-1}{2}\right\rangle\left\langle\frac{3cos^2\kappa-1}{2}\right\rangle \quad (2.29)$$

where ϕ is the angle between the bilayer normal and the magnetic field, ψ is the angle between the carbon-deuterium bond and the lipid axis and κ is the angle between the lipid axis and the bilayer normal (Figure 2.10).

On the spectrum, the motion (axial rotation and movement into a cone along the lipid longitudinal axis) of a lipid with one deuteron (C-D) will have an effect (Figure 2.11A-C) and the bigger the lipid motion, the lower the quadrupolar splitting will be.

The quadrupolar splitting for a carbon-deuterium bond in a lipid bilayer system with axial symmetry is correlated with the orientational order parameter for the deuterium bond vector (S_{CD}) as:

$$\Delta\nu_Q = \frac{3e^2qQ}{2h} S_{CD} \tag{2.30}$$

with for an aliphatic carbon-deuterium (C-D) bond, $\frac{e^2qQ}{h} \approx 170$ kHz (Jones *et al.*, 1997).

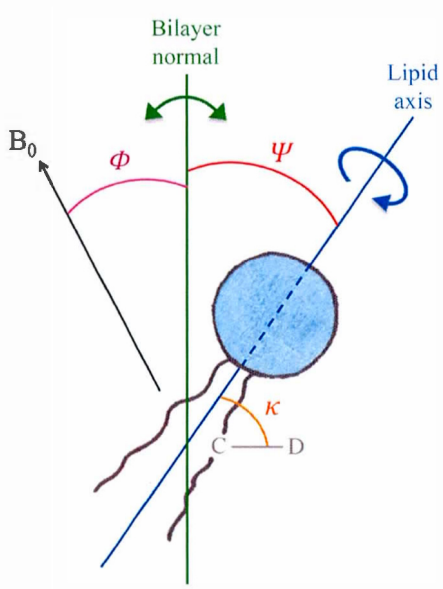

Figure 2.10 Representation of the membrane lipid motions with axial symmetry in a fluid phase.

In the case of lipids in fluid phase with completely deuterated alkyl chains, multiple quadrupolar splittings appear. Figure 2.11D displays an example of a vesicle. In the case of a bilayer mechanically oriented between glass plates or spontaneously in a magnetic field (bicelles), the spectrum will improve in resolution (Figure 2.11E-F). This improvement of the spectra in oriented samples is the result of only one angular orientation of lipids. As the degree of movement differs along the alkyl chain, there is a $\Delta\nu_Q$ for each deuterium.

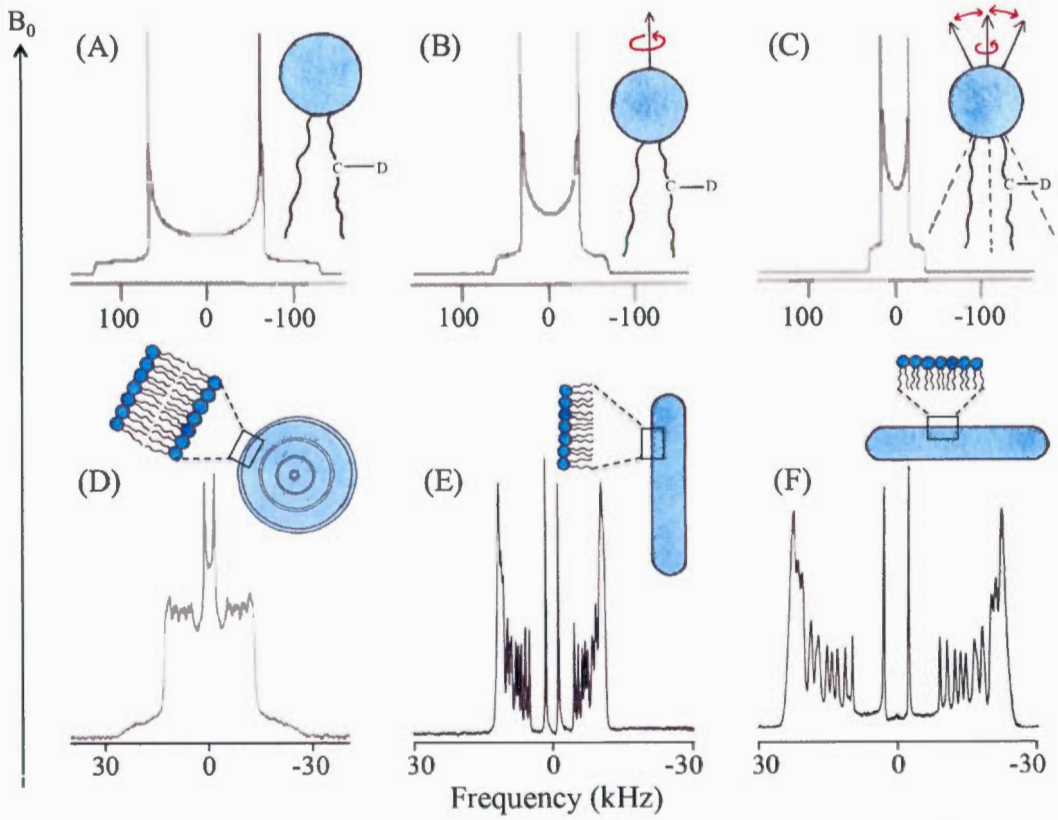

Figure 2.11 Representation of the chemical shift anisotropy effect on ^{2}H-NMR spectra of phospholipids. Spectra A-C correspond to lipids with one deuterium and D-F are lipid fully deuterated. (A) No movement, (B) rapid axial rotation of the lipid, (C) rapid rotation into a cone along the axis of the lipid for a phosphodiester in membrane lipid. (D) Multilamellar vesicle of DMPC. Spectra A-D are from Ouellet, 2007. A bicelle (E) with its normal (thus the longitudinal axis of the lipids) spontaneously oriented perpendicular at the magnetic field, or (F) parallel induced by lanthanide ion Ytterbium. Spectra E and F are from Lorigan, 2006.

The CD_2 position closer to the headgroup, due to restricted molecular movements, will display a higher $\Delta\nu_Q$ compared to the lowest one for CD_3 which has the biggest range of motion (Figure 2.12). Thus, the well-resolved ^2H spectrum is the result of the different motional properties of the CD_2 and CD_3 from DMPC-d_{54} with the normal of the bilayer oriented perpendicular (Figures 2.11E and 2.12A) or parallel (Figures 2.11F and 2.12B) to the magnetic field B_0.

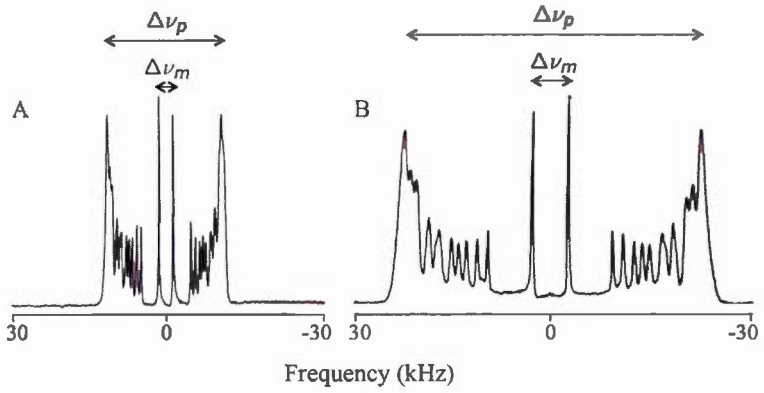

Figure 2.12 ^2H-NMR spectra of a bicelle (A) with its normal (thus the longitudinal axis of the lipids) spontaneously oriented perpendicular at the magnetic field, or (B) parallel due to lanthanide ion Ytterbium. Spectra are from Lorigan, 2006.

As for phosphorus nuclei, information on dynamic and orientation of the bilayer can be extracted from the ^2H-NMR spectrum. Since the deuterium quadrupolar splitting of the lipid' terminal methyl and plateau (carbon-deuterium bonds near the headgroup) (Figure 2.12) can be differentiated, it is possible to study the effect of a peptide at different depths into the hydrophobic core of the membrane.

Since the use of phospholipids with fully deuterated alkyl chains is expensive, deuterium experiments were only performed to see the interaction with the pore helix peptides in Chapter V and verify the alignment of one of the binary system in Chapter IV.

2.2 Circular Dichroism - Study of Peptide and Protein Secondary Structures

Circular dichroism spectroscopy allows the rapid and easy distinction, in a non-destructive way and without isotopic labelling, of peptide and protein structures. Typically, 0.1 to 1 mL with 0.2 to 1 $mg.mL^{-1}$ of pure protein is needed (Kelly & Price, 2000). It is possible from the region 190-260 nm to study the secondary structures, while the region 260-320 nm provides information on the tertiary structure.

The measure of circular dichroism is based on a difference in absorption of the left (counter-clockwise) versus right (clockwise) circularly polarized light with a chiral molecule. Amino acid residues are examples of these optically active molecules. The light source from xenon or xenon/mercury lamp is decomposed in left and right circular polarized light. A signal (called elliptical polarization) will be obtained only if a difference of absorption can be measured (Figure 2.13).

François Jean Dominique Arago first observed the optical activity in 1811. Then, Louis Pasteur revealed molecular chirality in 1848.

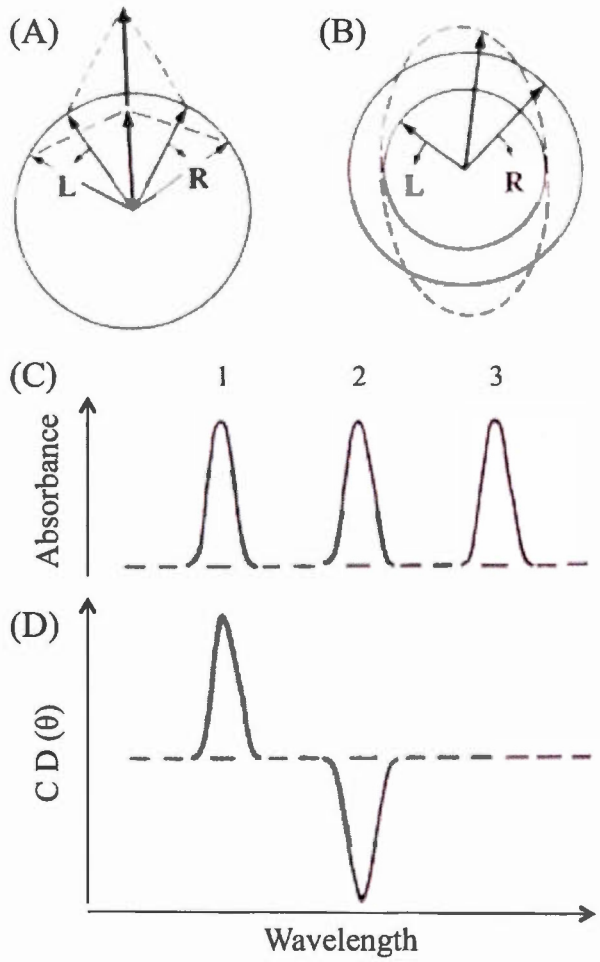

Figure 2.13 Representation of the origin of the CD signal (Kelly *et al.*, 2005). (A) The left (L) circularly polarised light have the same amplitude as the right (R) component and the resultant is a plane polarised radiation. (B) R and L do not have the same magnitude and this generates an elliptically polarised radiation (dashed line). (C) and (D) are the absorption and CD spectra, respectively. Case 1 displays a positive CD spectrum with R less absorbed than L, case 2, a negative CD spectrum and case 3, a group that is not chiral.

The different chromophores that can be absorbed in proteins are peptide bonds (below 240 nm), aromatic amino acid side chains (260-320 nm) and disulphide bonds (around 260 nm) (Kelly *et al.*, 2005). As a consequence, the characteristic CD spectra for secondary structures (190-260 nm) are mainly due to the peptide bond, but

aromatic side chains can also contribute at these signals in the far-ultraviolet (UV) range (Kelly *et al.*, 2005). There is an intense $\pi \rightarrow \pi^*$ transition due to the partial double bond (no rotation allowed around that bond) between the α-carbon and the amine nitrogen at around 190 nm and a weak $n \rightarrow \pi^*$ transition from carbonyls at around 210-220 nm (Kelly *et al.*, 2005; Kelly & Price, 2000). The $n \rightarrow \pi^*$ transitions are weaker because they are symmetry forbidden (Atkins & de Paula, 2010). For example, α-helical proteins have two minima at 208 and 222 nm and a maximum at 193 nm (Holzwarth & Doty, 1965), anti-parallel β-sheets have a large negative band around 218 nm and a positive band at 195 nm (Greenfield, 1969) and disordered proteins have a minimum at 195 nm and low negative ellipticity above 210 nm (Venyaminov *et al.*, 1993) (Figure 2.14).

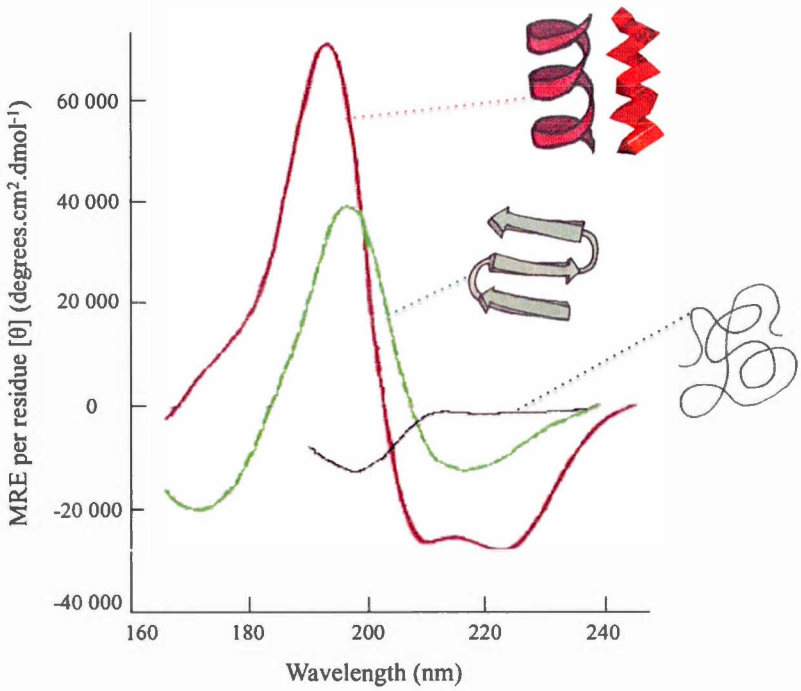

Figure 2.14 Representation of far-UV CD spectra for characteristic secondary structures with random coil in black, α-helix in dark red (on the right, it is a sculpture representation of an α-helix from the Linus Pauling Center for Science, Peace and Health, Portland, OR, USA) and β-sheet in green. This figure is adapted from Kelly *et al.*, 2005.

A major drawback with circular dichroism is that the signal obtained is an average of the different elements involved. Therefore, it is not possible to distinguish different domains or the source of the main signal. Amino acid segment deletion or study of a specific sequence can enable differentiation of the signal's origin. However, this process might change the interactions in the protein and as a consequence the secondary or tertiary conformations.

Circular dichroism rapidly provides information on the secondary structure of a protein, a peptide, or even membrane proteins by subtraction of the model membrane background signal. This technique was used in this thesis for the studies in Chapters V and VI.

2.3 Fourier Transform Infrared Spectroscopy – Study of Miscibility Between Lipids

Fourier transform infrared (FTIR) spectroscopy is a non-invasive method to obtain information on structure and dynamics of molecules due to their vibrational properties. The amount of sample needed is low: 0.1-1 mg of solid, 10-50 µL for a solution (or suspension) with 1-5% by weight (Mendelsohn & Mantsch, 1986).

FTIR is equipped with an optical device, which contains the 'heart' of the FTIR: the interferometer. The interferogram obtained, which gives the light intensity versus the optical path difference, is converted with the fast Fourier transform algorithm into the intensity light measured for each wavelength, which is the spectrum (Figure 2.15A-B).

The discovery of infrared began in 1800 and was directed by Sir Frederick William Herschel. Then, Albert Abraham Michelson designed the first interferometer in 1880s. He received the Nobel Prize in Physics in 1907 for his research. Atom

vibrations of an organic molecule can be probed by infrared electromagnetic radiation, which has wavelengths from 1 to 1000 μm (Atkins & de Paula, 2010). The absorbance frequency is linked with the atom identity (mass and geometry) as well as the conformation of a chemical bond, whereas the bandwidth is due to the molecular dynamics.

The mid-infrared, covered in the wavelength range from 2.5 to 25 μm (4000-400 cm^{-1}), is the spectral area that gives the most information on structure and dynamics of biological systems, such as lipids and proteins (Lee & Chapman, 1986). To overcome the difficulty with biological samples with the strong absorption of water, high concentrations, low pathlength cells and/or deuterium oxide solvent can be used (Lee & Chapman, 1986). The limited absorption bands at 2450-2540 cm^{-1} and 1215-1555 cm^{-1} of deuterated water are outside the infrared bands of interest for biological membranes. FTIR spectroscopy allows the simultaneous study of several constituents of lipids through the analysis of their spectra, giving functional groups specific frequencies. In the case of PLs with choline headgroups (Figure 2.15), the frequencies are listed in Table 2.2 (Mendelsohn & Mantsch, 1986). An example of an infrared spectrum is given in Figure 2.15B, where each functional group of the lipid has a characteristic band frequency, intensity and width. Figures 2.15C-D are enlargement of the CH_2 and CD_2 stretching vibration bands.

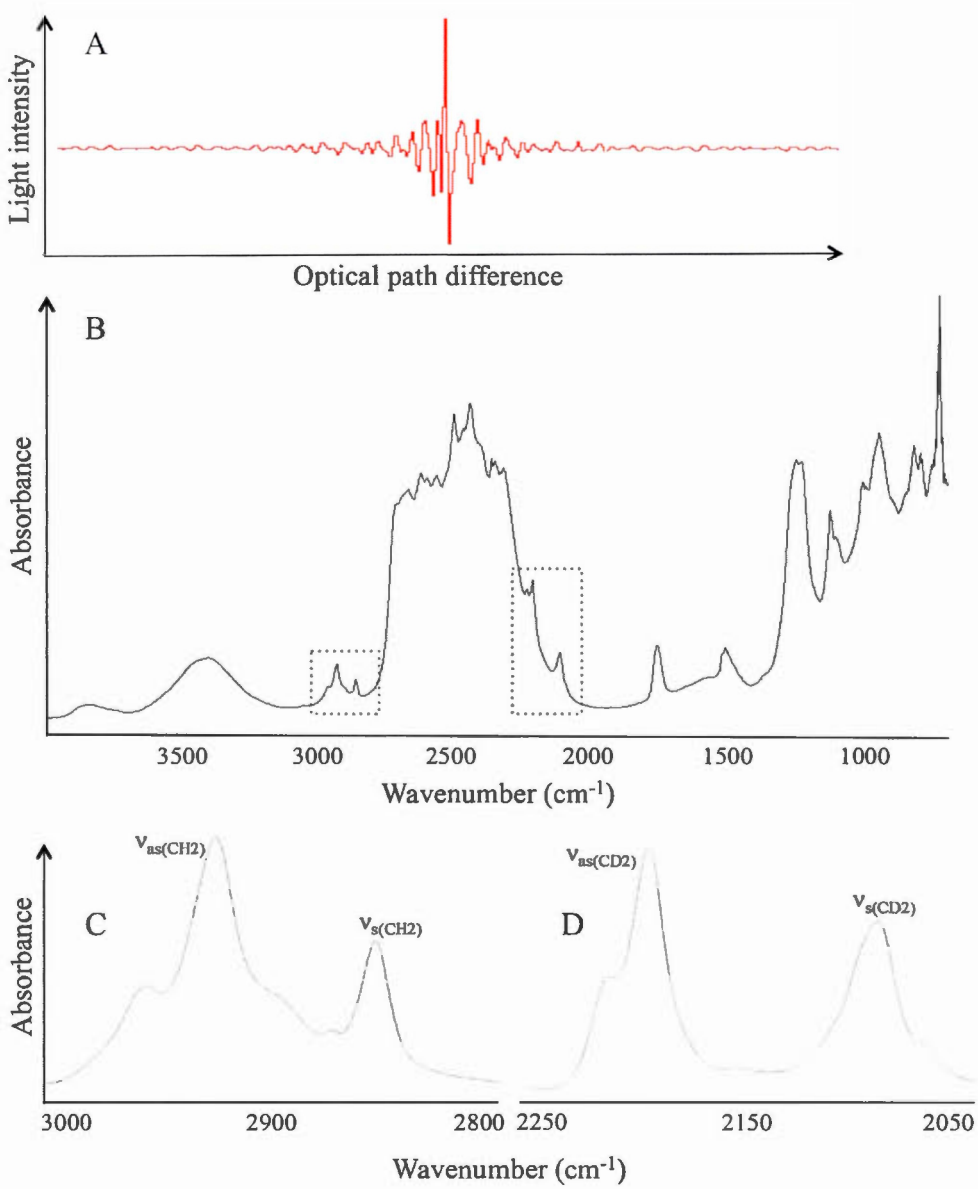

Figure 2.15 (A) Interferogram of a mixture of DPPC-d_{62} lipid and TPC detergent at molar ratio q of 2, and its corresponding (B) infrared spectrum with framing of interest bands used in this study. Enlargement and application of the quartic function on the (C) CH_2 symmetric ($\nu_{s(CH_2)}$) and antisymmetric ($\nu_{as(CH_2)}$) as well as (D) CD_2 symmetric ($\nu_{s(CD_2)}$) and antisymmetric ($\nu_{as(CD_2)}$) stretching vibration bands.

Table 2.2 Frequencies of different functional groups of a choline phospholipid (deuterated acyl chains) with symmetric (ν_s) and antisymmetric (ν_{as}) stretching vibration bands (Mendelsohn & Mantsch, 1986)

Part of the lipid	Functional group	Frequency (cm^{-1})
Choline	$\nu_{as(CH_3)_3N^+}$	3038
Polar head	$\nu_{as(PO_2^-)}$	1228
Interfacial region	$\nu_{(CO)}$	1735
Hydrophobic region	$\nu_{as(CH_2)}$	2920
	$\nu_{s(CH_2)}$	2850
	$\nu_{as(CD_2)}$	2195
	$\nu_{s(CD_2)}$	2090

Infrared is a powerful tool for the study of phase transition between gel (or rigid and ordered) and fluid (or disordered liquid-crystal) phases of lipids (Lewis & McElhaney, 1998; Mendelsohn & Mantsch, 1986). This change of phases is induced by the temperature and result in a conformational modification of alkyl chain that can be measured by analyzing the stretching frequencies of CH_2 or CD_2 groups (Mantsch & McElhaney, 1991). As a consequence, the frequencies of asymmetric and symmetric stretching bands of CH_2 or CD_2 increase by 2-5 cm^{-1} with the temperature. The curve obtained is called the thermotropism curve (Figure 2.16). Thereby, lipid alkyl chains are mainly in an all-trans conformation ($L_{\beta'}$) below the transition temperature (T_m) while above T_m, gauche conformations are induced (L_α) (Figure 1.5). It is however not possible to determine the contribution of each CD bond in infrared because it is an average effect.

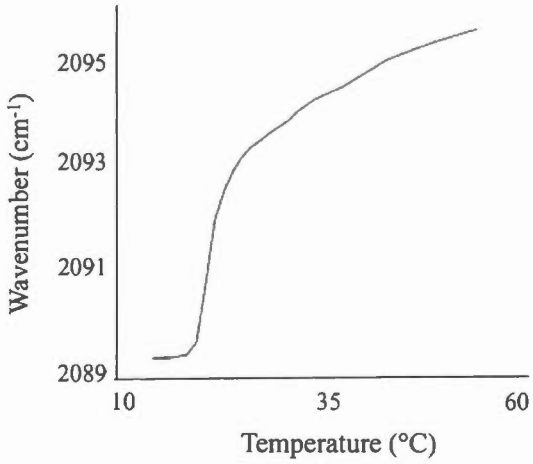

Figure 2.16 Thermotropism curve of a binary mixture of DPPC-d_{62} lipid and TPC detergent at molar ratio q of 2. The inflection point corresponds to the gel-fluid melting temperature (T_m).

The study of transition phases to obtain information on miscibility of long- and short-chain phospholipid (or detergent) in bicelles was used in Chapters III and IV.

CHAPTER III

LIPID CONCENTRATION AND MOLAR RATIO BOUNDARIES FOR THE USE OF ISOTROPIC BICELLES

Langmuir 2014, 30, 6162-6170, DOI: 10.1021/la5004353

Received: February 3, 2014
Revised: May 2, 2014
Published: May 5, 2014

Maïwenn Beaugrand[†], Alexandre A. Arnold[†], Jérôme Hénin[‡], Dror E. Warschawski[§], Philip T. F. Williamson[∥] and Isabelle Marcotte[†]

†Department of Chemistry, Université du Québec à Montréal and Centre Québécois sur les Matériaux Fonctionnels, P.O. Box 8888, Downtown Station, Montreal, H3C 3P8, Canada

‡Laboratoire de Biochimie Théorique, CNRS, Université Paris Diderot and Institut de Biologie Physico-Chimique, 13 rue Pierre et Marie-Curie, 75005 Paris, France

§Laboratoire de Biologie Physico-Chimique des Protéines Membranaires, CNRS, Université Paris Diderot and Institut de Biologie Physico-Chimique, 13 rue Pierre et Marie-Curie, 75005 Paris, France

∥School of Biological Sciences, Highfield Campus, University of Southampton, Southampton, SO17 1BJ, United Kingdom

Foreword

Maïwenn Beaugrand carried out the majority of the experiments and analyzed the results. Professor Jérôme Hénin was responsible of the molecular dynamics simulations. Maïwenn Beaugrand conducted the literature research and wrote the manuscript with the help of Doctor Alexandre A. Arnold and Professors Jérôme Hénin, Dror E. Warschawski, Philip T. F. Williamson and Isabelle Marcotte.

Résumé

Les bicelles sont des membranes modèles généralement faites des lipides à longues chaînes dimyristoylphosphatidylcholine (DMPC) et courtes chaînes dihexanoyl-PC (DHPC). Elles sont largement utilisées dans l'étude des interactions membranaires et la détermination structurale des peptides membranaires, étant donné leur composition et leur morphologie imitant les membranes eucaryotes riches en PC. À faibles rapports molaires DMPC/DHPC (q), les bicelles se réorientent rapidement sur elles-mêmes. La bicouche de DMPC est stabilisée par des molécules de DHPC sur les bords qui sont fortement courbés. Les contraintes expérimentales imposées par des techniques telles que le dichroïsme circulaire, la diffusion dynamique de la lumière ou la microscopie peut nécessiter l'utilisation de bicelle à haute dilution. Des études ont montré que de telles conditions induisent la formation de petits agrégats et altèrent le rapport lipide/détergent des systèmes bicellaires. Les objectifs de ce travail étaient de déterminer la composition exacte des bicelles isotropes DMPC/DHPC et d'étudier la miscibilité des lipides. Ceci a été réalisé en utilisant la résonance magnétique nucléaire (RMN) du phosphore et en explorant une large gamme de concentrations lipidiques (2-400 mM) et de rapports molaires q (0.15-2). Nos données démontrent comment la dilution modifie le rapport molaire DMPC/DHPC

dans les bicelles. Une attention spéciale doit être prise pour les échantillons avec une concentration lipidique totale ≤ 250 mM. Et ce notamment avec $q \sim 1.5-2$, car des dilutions modérées peuvent amener à la formation de grosses structures lipidiques se réorientant lentement et pouvant affecter l'utilisation de techniques comme la RMN en solution, le dichroïsme circulaire et la diffusion dynamique de la lumière. Nos résultats, soutenus par la spectroscopie infrarouge ainsi que les simulations moléculaires dynamiques, ont aussi montré que les phospholipides dans les bicelles sont majoritairement ségrégés seulement quand $q > 1$. Les frontières sont présentées pour les bicelles où il est possible de contrôler le rapport molaire q. Ce travail tente donc de guider le choix de rapport molaire q et de concentration totale de phospholipides à utiliser pour obtenir des bicelles isotropes.

Abstract

Bicelles are model membranes generally made of long-chain dimyristoylphosphatidylcholine (DMPC) and short-chain dihexanoyl-PC (DHPC). They are extensively used in the study of membrane interactions and structure determination of membrane-associated peptides, since their composition and morphology mimic the widespread PC-rich natural eukaryotic membranes. At low DMPC/DHPC (q) molar ratios, fast-tumbling bicelles are formed in which the DMPC bilayer is stabilized by DHPC molecules in the high-curvature rim region. Experimental constraints imposed by techniques such as circular dichroism, dynamic light scattering, or microscopy may require the use of bicelles at high dilutions. Studies have shown that such conditions induce the formation of small aggregates and alter the lipid-to-detergent ratio of the bicelle assemblies. The objectives of this work were to determine the exact composition of those DMPC/DHPC isotropic bicelles and study the lipid miscibility. This was done using ^{31}P nuclear magnetic

resonance (NMR) and exploring a wide range of lipid concentrations (2–400 mM) and q ratios (0.15–2). Our data demonstrate how dilution modifies the actual DMPC/DHPC molar ratio in the bicelles. Care must be taken for samples with a total lipid concentration ≤ 250 mM and especially at q ~ 1.5–2, since moderate dilutions could lead to the formation of large and slow-tumbling lipid structures that could hinder the use of solution NMR methods, circular dichroism or dynamic light scattering studies. Our results, supported by infrared spectroscopy and molecular dynamics simulations, also show that phospholipids in bicelles are largely segregated only when q > 1. Boundaries are presented within which control of the bicelles' q ratio is possible. This work, thus, intends to guide the choice of q ratio and total phospholipid concentration when using isotropic bicelles.

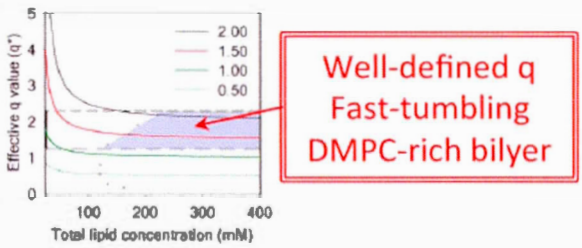

3.1 Introduction

Bilayered micelles, or so-called bicelles, were introduced in the 1990s and quickly gained in popularity due to their similarity with biological membranes (Sanders & Prestegard, 1990; Sanders & Schwonek, 1992). These membranes mimetics are most commonly composed of dimyristoylphosphatidylcholine (DMPC) which organize in a bilayer stabilized by short-chain dihexanoylphosphatidylcholines (DHPC) in high curvature regions (Chou *et al.*, 2002; Cross *et al.*, 2011; Dürr *et al.*, 2013; Marcotte & Auger, 2005; Thiyagarajan & Tiede, 1994; Warschawski *et al.*, 2011) of discs or perforated vesicles (Barbosa-Barros *et al.*, 2011; Diller *et al.*, 2009; Dürr *et al.*, 2013;

Marcotte & Auger, 2005; Ram & Prestegard, 1988; Triba *et al.*, 2005; Warschawski *et al.*, 2011). Although the morphology of bicelles is debated, the planar region made of long-chain phospholipids constitutes a favorable environment to study molecular interactions as well as the structure of membrane peptides and proteins with different biophysical techniques such as nuclear magnetic resonance (NMR), X-ray crystallography, circular dichroism (CD), and Fourier transform infrared (FTIR) spectroscopy (Diller *et al.*, 2009; Dürr *et al.*, 2013; Faham *et al.*, 2009; Macdonald *et al.*, 2013; Marcotte & Auger, 2005; Naito, 2009; Sanders & Prosser, 1998; Seddon *et al.*, 2004; Warschawski *et al.*, 2011; Yamamoto *et al.*, 2014). Most interestingly, for solid-state NMR applications, bicelles are known to spontaneously orient in a magnetic field in excess of 1 T at high DMPC/DHPC molar (q) ratios (above 2.3) and within well-defined total lipid concentrations (3–60% w/v) and temperatures (30–50°C) (Katsaras, 1998; Ottiger & Bax, 1998; Ram & Prestegard, 1988; Sanders *et al.*, 1994; Sanders & Landis, 1994; Sanders & Schwonek, 1992; Triba *et al.*, 2005; Warschawski *et al.*, 2011; Yamamoto *et al.*, 2009). This orientation is due to the negative diamagnetic susceptibility anisotropy of the phospholipids which align with their long axis perpendicular to the magnetic field direction.

When the DMPC/DHPC q ratio falls below 2.3, bicelles rapidly reorient in solution (Luchette *et al.*, 2001; Sanders & Landis, 1994; Vold *et al.*, 1997), enabling solution NMR experiments that are useful for the structural study of membrane-binding peptides such as met-enkephalin (Marcotte *et al.*, 2004), motilin (Andersson & Mäler, 2002), antimicrobial peptides (Haney *et al.*, 2009), as well as the assessment of membrane association of peptides and small molecules (Andersson *et al.*, 2004; Chartrand *et al.*, 2010; Gravel *et al.*, 2013; Marcotte *et al.*, 2004). The use of low q ratio $\leq$0.5 allows improving the resolution of the NMR (Son *et al.*, 2012; Vold *et al.*, 1997) and CD (Biverståhl *et al.*, 2009; Bocharov *et al.*, 2008; Mineev *et al.*, 2011; Surya *et al.*, 2013; Vold *et al.*, 1997) spectra. These so-called isotropic bicelles are also employed in others studies such as dynamic light scattering (DLS) (Bocharov *et*

al., 2008; Mineev *et al.*, 2011), FTIR spectroscopy (Surya *et al.*, 2013), fluorescence (Biverståhl *et al.*, 2009; Glover *et al.*, 2001) and electron paramagnetic resonance (EPR) (Andersson & Mäler, 2005). The morphology of isotropic bicelles is generally considered to be disc-shaped with DMPC molecules on the planar section segregated from the DHPC molecules in the rim, and a diameter which increases with q ratio (Glover *et al.*, 2001; Luchette *et al.*, 2001). The presence of transmembrane proteins in low q bicelles may however lead to a change in the size of the aggregates, as shown for micelles, and possibly to a reorganization of the lipids and detergents (Kang & Li, 2011; le Maire *et al.*, 2000).

Bicelles samples with a total lipid concentration lower than 150 mM are required with techniques using a laser light source to avoid light scattering effects when performing CD (Bocharov *et al.*, 2008; Chartrand *et al.*, 2010; Mineev *et al.*, 2011; Surya *et al.*, 2013; Vold *et al.*, 1997) or DLS (Bocharov *et al.*, 2008; Mineev *et al.*, 2011) but are also employed in other techniques such as NMR (Bocharov *et al.*, 2008; Gravel *et al.*, 2013; Mineev *et al.*, 2011; Surya *et al.*, 2013), FTIR spectroscopy (Surya *et al.*, 2013) and crystallography (Faham *et al.*, 2009). A thorough study of D14PC/D6PC bicelles in such conditions with q ratios from 0.5 to 5 was carried out by van Dam and co-workers (van Dam *et al.*, 2004) using cryo-transmission electron microscopy (TEM), DLS, and fluorescence spectroscopy. At q ratios below 1 and for strong dilutions, small aggregates were observed. This work also provided strong indications that the formed aggregates are more complex than the ideal bicelle model in which the DMPC and DHPC molecules are fully segregated. In addition, as was originally evidenced by Glover *et al.* (Glover *et al.*, 2001), the authors noted that dilution alters the actual composition of the aggregates. Indeed, the individual constituents of bicelles have specific critical micelle concentrations (CMCs) that can range from the nanomolar for the phospholipids, to the millimolar for the detergents. As a consequence, in samples prepared with concentrations in the millimolar range, a significant proportion of free surfactants in solution will be present in equilibrium

with the phospholipid aggregate. The importance of this effect has recently been considered by the group of Sanders who has proposed alternative bicelles composed of surfactants with higher CMCs (Lu *et al.*, 2012). The widespread use of DMPC/DHPC bicelles prompted us to carry out a systematic study of the effect of dilution on this system.

The objective of this work is thus to study the effect of dilution on the exact composition of the widely utilized DMPC/DHPC bicelles and the miscibility of its constituents. Using ^{31}P NMR, q ratios ranging from 0.15 to 2 and concentrations from 2 to 400 mM are investigated. The work is carried without the use of paramagnetic shift reagents. The NMR results indicate changes in miscibility between short-and long-chain phospholipids and these are further supported by FTIR spectroscopy and molecular dynamics simulations. We thus provide data which will guide the choice of q ratio and total phospholipid concentration to enable the study of membranes and membrane-related processes using isotropic bicelles.

3.2 Materials and Methods

3.2.1 Materials

1,2-Myristoyl-1-sn-glycero-3-phosphocholine (DMPC) and 1,2-hexanoyl-1-sn-glycero-3-phosphocholine (DHPC) were obtained from Avanti Polar Lipids (Alabaster, AL, USA) and used without further purification. DHPC, which is highly hygroscopic, was freeze-dried prior to weighing. Deuterium oxide (D_2O) was purchased from CDN Isotopes (Pointe-Claire, QC, Canada).

3.2.2 Sample Preparation

Bicelle samples with the highest concentration (400 mM) and at q ratios ranging between 0.25 and 2 were prepared by suspending the appropriate weight of DMPC and DHPC in a 100 mM KCl solution made with D_2O. The sample was then submitted to 10 cycles of freeze (liquid N2)/thaw (60 °C) and vortex shaking, resulting in a uniform transparent nonviscous solution. Serial dilutions were then performed from 400 to 2 mM before NMR spectrum acquisition.

3.2.3 ^{31}P Solution NMR Experiments

All spectra were recorded on a Varian Inova Unity 600 (Agilent, Santa Clara, CA) spectrometer operating at a frequency of 246.86 MHz for ^{31}P and equipped with a 5 mm double-resonance probe. A single-pulse experiment was employed with a $\pi/2$ pulse of 13.3 μs, a recycle delay of 5 s, and an acquisition time of 1 s with broadband proton continuous wave decoupling at a field strength of 5 kHz. A preacquisition delay of 15 min was used before each experiment to ensure sample thermal equilibration. Spectra were acquired at least in triplicate with 32 to 512 scans at 25 °C unless otherwise specified. They were referenced internally using a sealed capillary containing phosphate ions at pH = 11 in D_2O which was previously referenced with respect to 85% H3PO4 at 3.38 ppm. All spectra were processed using MNova software (Mestrelab Research, Santiago de Compostela, Spain).

3.2.4 FTIR Experiments

Infrared spectra were recorded with a Nicolet Magna-560 Fourier transform spectrometer (Thermo Scientific, Madison, WI, USA) equipped with a narrow-band

mercury-cadmium-telluride (MCT) detector and a germanium-coated KBr beamsplitter. A volume of 30 µL of the 400 mM bicelle sample was placed between CaF2 Biocell windows (Biotools Inc., Jupiter, FL, USA) manufactured with a calibrated path length of 50 µm. The windows were placed in a homemade heating cell using a Peltier element as a heating/cooling device. To prevent solvent evaporation during the course of long-term measurements, the sealing surface of the cell was lubricated with mineral oil. A total of 128 interferograms were acquired with a resolution of 2 cm^{-1} apodized with a Happ-Genzel function in the spectral range of 4000-650 cm^{-1} at various temperatures ranging from 5 to 70 °C. Spectra were corrected for water vapor and CaF2 contributions by substraction of a reference spectrum. Data were processed with the software Grams/AI 8.0 (Galactic Industries Corporation, Salem, NH, USA). The spectral regions corresponding to the carbon-hydrogen stretching vibrations were baseline-corrected using a quartic function. The methylene symmetric stretching frequency was obtained from the center of gravity calculated at the top 10% of the band.

3.2.5 Molecular Dynamics Simulations

Three sets of MD simulations were performed at 310 K, namely, a self-assembly of DMPC/DHPC at q of 0.25 (350 ns), the relaxation of an ideal DMPC/DHPC bicelle at q of 0.25 (450 ns), and the self-assembly of pure DMPC in water (60 ns), aimed at validating the DHPC model. Each simulation box contained 200 lipid molecules (200 DHPC or 160 DHPC + 40 DMPC) in a volume of about 850 nm^3, yielding a total lipid concentration of 400 mM, and 130 mM NaCl. Each simulation system contained about 80 000 atoms. Lipids were described by the CHARMM36 force field (Klauda *et al.*, 2010), in our modified version with united-atom acyl chains (Hénin *et al.*, 2008); the water model was TIP3P. Both the all-atom force field and its united-atom modification are extensively validated against experimental data; the united-atom

version enhances the relaxation kinetics of the lipids while reducing computational cost, leading to improved sampling. All simulations were run using the NAMD 2.9 software package (Phillips *et al.*, 2005) on the SGI Altix supercomputer Jade at CINES (Montpellier, France). Self-assembly simulations were started from randomly distributed solutes prepared with the GROMACS tool genbox (Pronk *et al.*, 2013). The ideal bicelle system was prepared by cutting a disc out of a pre-equilibrated DMPC bilayer, and inserting it in a water environment with randomly placed DHPC molecules. The DMPC bilayer structure was preserved by positional restraints applied to the DMPC headgroups. After 30 ns of simulation, the restraints were lifted to let the overall structure relax.

DMPC/DHPC aggregation was analyzed using a customized version of the g_clustsize tool from GROMACS 4.5.5 (Pronk *et al.*, 2013). Hydrophobic clusters were detected by restricting the analysis to united-atom particles forming the acyl chains of the lipid and detergent. A cutoff distance of 4.1 Å was chosen in order to include all contact peaks of the interparticle radial distribution function, while minimizing the contribution of short-lived contacts, detected in the form of high-frequency noise in the cluster size dependence as a function of time. Chain order in DMPC was quantified by measuring the distribution of torsional angles between neighboring acyl chains (with centers less than 10 Å away). The direction of each myristoyl chain was computed as the principal axis of inertia with the lowest eigenvalue; the analysis was implemented within the LOOS framework (Romo & Grossfield, 2009).

3.3 Results and Discussion

3.3.1 Exact Composition of Bicelles under Dilution: ^{31}P NMR

The long and short-chain phosphatidylcholines constituting the bicelles comprise a single phosphorus atom in their polar headgroup. The high gyromagnetic ratio of the ^{31}P isotope as well as its 100% natural abundance leads to an easily detectable NMR signal which is dominated by the chemical shift anisotropy (CSA). The resulting spectra are characteristic of the lipid phases present in the sample (Seelig, 1978). However, the CSA is averaged by the fast tumbling of bicelles at low q ratios, resulting in an isotropic resonance for each lipid which can be exploited to obtain information on their environment and dynamics.

^{31}P NMR spectra of DMPC/DHPC bicelles were recorded for q ratios ranging between 0 (pure DHPC) and 2 in water. An example is given in Figure 3.1 for spectra obtained at q = 1 and concentrations decreasing from 400 to 2 mM. For concentrated solutions at a magnetic field of 14.1 T, two resonances can be resolved. The broader upfield signal at ca. -0.50 ppm is assigned to the long-chain DMPC, whereas the narrow downfield signal is ascribed to DHPC (Sanders & Schwonek, 1992). As the sample is diluted, DMPC's resonance gradually broadens until it completely disappears at 8 mM, while its chemical shift slightly decreases from -0.51 to -0.58 ppm. For concentrations above 25 mM the DMPC/DHPC molar ratio calculated from the integrals of the two lipid resonances on the ^{31}P NMR spectra is in agreement with the q value. DMPC molecules appear to be part of rapidly reorienting aggregates as suggested by the relative resolution of the peak compared to the one obtained with DMPC vesicles. Interestingly, sample turbidity could be observed at higher dilutions (<25 mM) and with q ratios ≥0.75 (Figure S3.1, Supporting Information). This phenomenon is expected if aggregates with characteristic sizes on the order of the visible wavelength are present (Lu *et al.*, 2012).

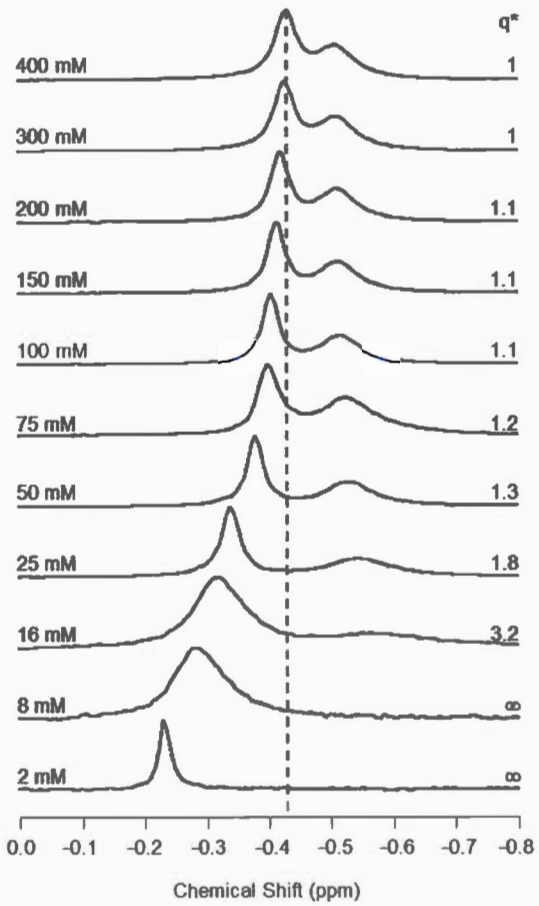

Figure 3.1 Evolution of the ^{31}P NMR spectrum of bicelles with q = 1 as a function of dilution. The calculated effective q (q*) is indicated. Data were obtained at 25 °C.

In contrast to the behavior of DMPC's resonance, the narrow DHPC signal remains sharp down to a concentration of 25 mM, then broadens with a full width at half-maximum (fwhm) of 7 to 25 Hz between 25 and 8 mM, to finally sharpen again at 2 mM (fwhm of 5 Hz). In addition, its chemical shift increases with dilution, from -0.43 ppm at 400 mM to -0.23 ppm at 2 mM, a value similar to the ^{31}P chemical shift of free DHPC molecules in solution (-0.23 ppm) (data not shown). The variation of DHPC ^{31}P chemical shift value with concentration has been previously explained as

resulting from the fast exchange between the bulk solution and the bicelles (Glover *et al.*, 2001). As a consequence, the chemical shift value observed on the spectrum (δ_{obs}) is a weighted average of the chemical shifts of the free (δ_{free}) and bicelle-bound (δ_{bic}) DHPC molecules:

$$\delta_{obs} = \chi_{free}\delta_{free} + \chi_{bic}\delta_{bic} \quad (3.1)$$

where χ_i corresponds to the molar fractions of DHPC molecules in solution and in the bicelles. Equation 3.1 can be rearranged to obtain the following expression:

$$\delta_{obs} = \frac{[DHPC]_{free}}{[DHPC]_{total}}(\delta_{free} - \delta_{bic}) + \delta_{bic} \quad (3.2)$$

Therefore, a plot of δ_{obs} as a function of the inverse of the total DHPC concentration ($[DHPC]_{total}$) should yield a straight line from which δ_{bic} can be extracted as the y-intercept and the concentration of free DHPC can be determined using the slope and a δ_{free} value of -0.23 ppm obtained for a pure DHPC solution at 2 mM. We carried out this systematic analysis for bicelles with q of 0.15 to 2 at concentrations ranging between 400 and 25 mM where DHPC molecules are in fast exchange between the bulk solution and fast-tumbling bicelles. The result is presented in Figure S3.2 in the Supporting Information for q = 1 as a representative example. In this case, δ_{bic} is equal to -0.43 ppm, the slope is equal to 1.15, and therefore the concentration of free DHPC is 5.6 mM. For all the q values studied in this work, the fast-exchange model appears to be a good approximation with correlation coefficients of the linear fits greater than 0.95. For each q value, the concentration of free DHPC which is present in bicelle samples can be referred to as a "critical bicelle concentration" (CBC), in analogy with a critical micelle concentration (CMC), and the average values obtained for triplicates are reported in Figure 3.2 as a function of all q ratios studied.

Figure 3.2 shows that the extreme case of pure DHPC (q = 0) gives an average CMC of 16.5 mM, consistent with the literature value of 16 mM reported for this detergent (Marsh, 2013). As the sample is enriched in DMPC, the CBC gradually decreases to a

value of 6.0 mM at q = 1. This result is in excellent agreement with published CBC values of 4 (at 15 and 37 °C) and 7 mM (at 25 °C) for DMPC/DHPC bicelles at q = 0.5 (Glover *et al.*, 2001; Ramirez *et al.*, 2000) or CBC values estimated to 7–10 mM (from 28 to 40 °C) for high q values (q = 2.3–3.3) (Struppe & Vold, 1998). As the system is further enriched in DMPC, the CBC is stable with possibly a slight increase up to a value of 6.7 mM at q = 2, but this increase is within the experimental error.

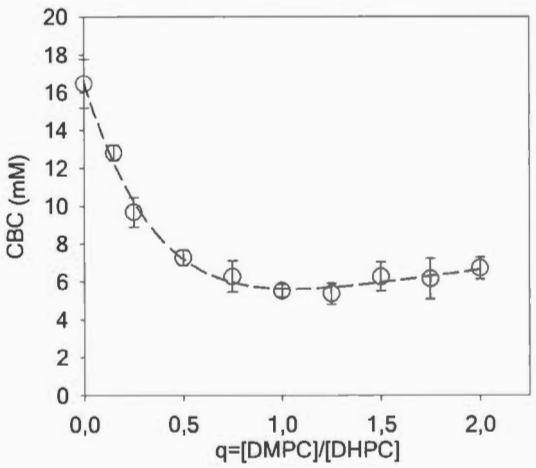

Figure 3.2 Evolution of the critical bicelle concentration (CBC) as a function of q. Average values (n = 3) determined at 25 °C with standard deviation. The dotted line is a guide to the eye. The CMC for ideally mixed bicelles (CMC_{mix}) is indistinguishable from the zero horizontal axis at the scale of this figure for all q values. Note that at q = 0, CBC = CMC_{DHPC}.

Our results were obtained at 25 °C, but they can be generalized to temperatures up to 40 °C. Indeed, it has been shown that the CMC of DHPC micelles is almost constant between 11 and 50 °C (Marsh, 2013). A similar study in bicelles at q = 0.5 also showed no difference in the concentration of free DHPC between 15 and 37 °C (Glover *et al.*, 2001). Nevertheless, we verified possible temperature effects on the CBC for q = 1 at 25, 37, and 50 °C and found similar results (data not shown), confirming that the CBC is stable in this temperature range. To take into account the presence of a non-negligible concentration of free DHPC in the bicelle mixture,

which corresponds to the CBC, the effective DMPC/DHPC molar ratio (q*) in the bicellar objects can be calculated, as proposed by Glover *et al.* (2001):

$$q^* = \frac{[DMPC]}{[DHPC]-CBC} \tag{3.3}$$

The effect of the dilution on the effective molar ratio q* for several theoretical q ratios (known from the mass of the lipid powders used during sample preparation) is presented in Figure 3.3 (top). Conversely, and in order to guide the experimentalist, the values of q* as a function of q for different total lipid concentrations are plotted in Figure 3.3 (bottom). Our results clearly show that attention must be paid when samples are prepared in diluted conditions (i.e., ≤100 mM) and especially at high q ratios (q ~ 1.5–2). Indeed under such conditions, the actual DMPC/DHPC molar ratio q* in the bicelles strongly deviates from the expected q ratio. As a result, even a moderate dilution could lead to q* ≥ 2.3, where the formation of large and slow-tumbling lipid structures that could hinder the use of solution-state NMR methods are observed. For example, for q = 1 at a total lipid concentration of 16 mM, a q* of 3.2 is found. The q* ≤ 2.3 limit is indicated as a dashed line in Figure 3.3.

By indicating q* on the ^{31}P NMR spectra in Figure 3.1, it is possible to better understand the behavior of bicelles under dilution. From 400 to 100 mM, the effective q* is very close to 1, the value expected from the sample preparation. With further dilution from 75 to 25 mM, q* increases up to 1.8, an effective q ratio at which isotropic bicelles still prevail. When reaching 16 mM, a q* of 3.2 is calculated and corresponds to large bicelles that would orient in the magnetic field if the concentration were higher (Struppe & Vold, 1998). Additional dilution of the bicelle samples led to an infinite q*, that is, DMPC vesicles are formed. Note that at such low concentrations, the broad spectra which are expected for MLVs could not be detected.

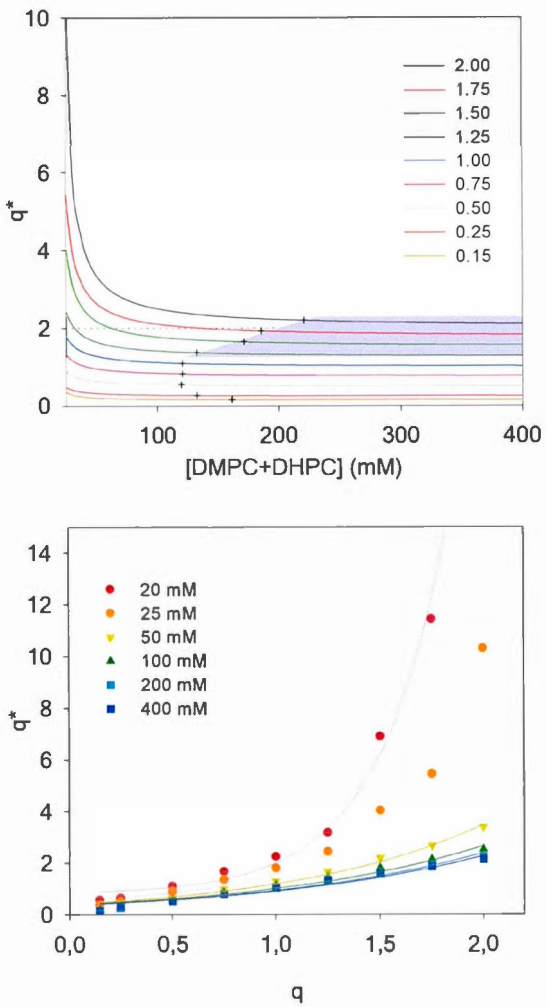

Figure 3.3 Evolution of the effective q* for DMPC/DHPC isotropic bicelles as a function of sample dilution for several q ratios determined at 25 °C (top). The gray zone is the region where bicelles are isotropic, i.e., below q* of 2.3 (limit of isotropic motion), above q* = 1 (lipid segregation between DMPC and DHPC), and q* = q + 10% (crosses). Value of q* as a function of q for different total lipid concentrations (bottom). Solid lines are a guide to the eye.

Using the effective q* and assuming bicelles are disk-shaped, it is possible to calculate the actual size of the bicelles using the following equation modified from Triba *et al.*, 2005:

$$R = \frac{r_{\perp} q^*}{4\lambda}\left[\pi + (\pi^2 + \frac{32\lambda}{3q^*})^{1/2}\right] \quad (3.4)$$

where R is the bicelle disk radius, $r_{\perp}$ is the length of a DHPC molecule (1.1 nm), and λ is the volume ratio of DHPC over DMPC (0.61 nm) (Triba *et al.*, 2005). A bicelle with q = 1 for example would have a diameter of ~65 Å. The results of the calculation (Table S3.1, Supporting Information) show an increase in the bicelle diameter for the same sample up to ~190 Å when it is diluted to a total lipid concentration of 16 mM (q* = 3.2). Variation of the concentration of free DHPC molecules at strong dilutions, and its resulting effect on bicelle size, clearly needs to be taken into account when interpreting lateral diffusion data. This is especially the case if geometrical parameters of the bicelles are inferred from diffusion data (Andersson & Mäler, 2006).

3.3.2 Lipid Concentration Threshold to Maintain the Desired q Ratio with Isotropic Bicelles.

In order to ensure that solution NMR experiments are carried out with fast- tumbling bicelles at the desired DMPC/DHPC molar ratio q, we have determined the total lipid concentration threshold that should be used. To do so, a 10% deviation from the desired q ratio was considered as acceptable. Replacing q* by 1.1 × q in equation 3.3 leads to a definition of the minimum lipid concentration threshold:

$$q^* = \frac{[DMPC]}{[DHPC] - CBC} \leq 1.1 \times q \quad (3.5)$$

which can be rearranged to define a minimal total lipid concentration for a given q ratio:

$$[DMPC + DHPC] = 11 \times CBC \times (q + 1) \quad (3.6)$$

The minimum total lipid concentration thresholds to be used at q ratios ranging from 0.15 to 2 calculated from equation 3.6 are presented in Table S3.2 in the Supporting Information and plotted in Figure 3.3 as crosses.

3.3.3 Lipid Miscibility in Bicelles: Comparing CBC and CMC

The use of bicelles to study the membrane interaction of drugs, peptides, or other molecules, or to determine the structure of membrane-associating peptides is often motivated by the presence of a flat DMPC-rich region in these aggregates. In this section, we verify lipid miscibility as a function of q. The fact that the CBC value at q $\geq$ 1 (~6 mM) is lower than the CMC of pure DHPC (16 mM) indicates that the DMPC molecules stabilize DHPC molecules into bicellar aggregates (Holland & Rubingh, 1983). It is interesting to compare the CBC determined from our analysis to the CBC that would be obtained if D14PC and DHPC would form an ideal mixed micelle (CMC_{mix}) which can be calculated as follows (Holland & Rubingh, 1983):

$$\frac{1}{CMC_{mix}} = \frac{\chi_1}{CMC_1} + \frac{1-\chi_1}{CMC_2} \tag{3.7}$$

where CMC_i is the CMC value of each pure surfactant and χ_1 is the molar fraction of surfactant 1. With CMC_{DHPC} = 16mM and CMC_{D14PC} = 6 nM (Marsh, 2013), CMC_{mix} values between 46 and 9 nM would be expected for q values between 0.15 and 2, respectively. The plot of CMC_{mix} as a function of q ratio for an ideal mixed bicelle thus becomes virtually indistinguishable from the horizontal axis in Figure 3.2. The CBCs determined from our experimental results for the same q values range between 13 and 5 mM.

The discrepancy between the experimental curve and the ideal mixing curve (Figure 3.2) shows that the partitioning of both lipids between solution and the aggregate strongly deviate from an ideal mixed micelle, suggesting that the two lipids are at

least partially segregated within the bicelle. To verify this hypothesis, FTIR experiments and molecular dynamics simulations were performed.

3.3.4 $q \geq 1$: FTIR Spectra Confirm Lipid Segregation in Isotropic Bicelles

In order to study the degree of miscibility between D14PC and D6PC in bicelles, we measured the thermotropic behavior of these lipids at different q ratios and high total lipid concentration (400 mM) by FTIR spectroscopy. This was done by using protonated D6PC and D14PC with perdeuterated acyl chains (D14PC-d_{54}), and plotting the CD_2 symmetric stretching frequency (~2090 cm^{-1}) as a function of temperature. The methylene stretching vibrations in lipid acyl chains are sensitive to changes in the trans/gauche conformer ratio and allow probing the transition between an ordered gel to more disordered liquid crystalline phase (Mendelsohn & Mantsch, 1986). In the case of an ideal homogeneous mixture, the melting temperature (T_m) can be calculated considering the respective T_m and mole fractions of the lipids (Marsh, 2013):

$$T_m^{bic} = \chi_{DHPC} T_m^{DHPC} + \chi_{DMPC} T_m^{DMPC} \tag{3.8}$$

where the T_m of D6PC and D14PC/D14PC-d_{54} are −46 (Sakuma *et al.*, 2010) and 21°C (experimental value), respectively. The thermotropic behavior of DMPC-d_{54} is shown in Figure 3.4 (top) as well as the variation of the melting temperature with DMPC-d_{54} molar fraction compared to the variation expected for an ideal mixed micelle (bottom). The experimental and ideal melting temperatures are reported in Table S3.3 in the Supporting Information. The T_m of 21 °C obtained from the infrared spectroscopy analysis is constant when q is superior to 1 and corresponds to that of pure DMPC-d_{54}. Moreover, the values of the CD_2 symmetric stretching frequencies are almost superimposable in the fluid phase, indicating that the acyl chain ordering is not affected by the presence of DHPC.

These results suggest that DMPC is largely segregated in the planar section of bicelles when q > 1. As the q ratio is decreased, the discrepancy between the experimental T_m of DMPC-d_{54} in bicelles and the calculated T_m of DMPC-d_{54} in an ideal mixed micelle diminishes, showing progressive mixing of DMPC and DHPC molecules, even though bicelles retain some level of bilayer content and anisotropy, as observed by Glover and colleagues (2001).

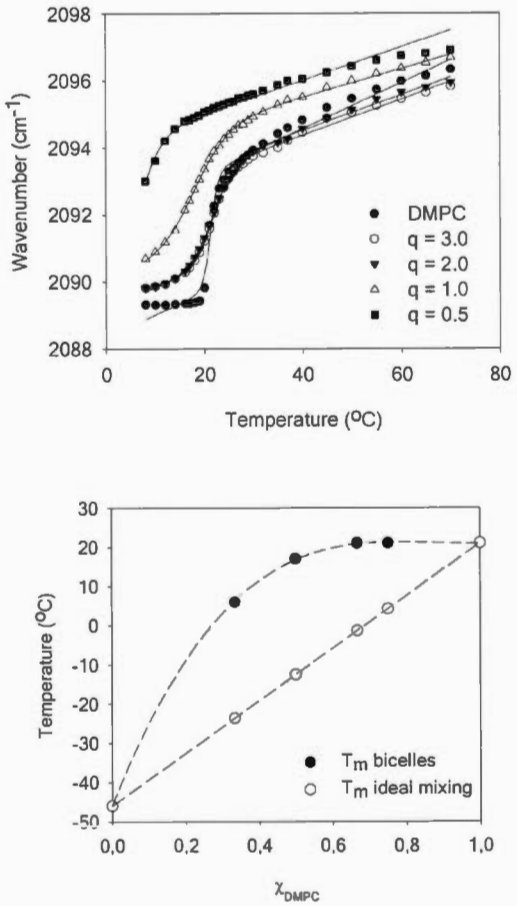

Figure 3.4 Temperature dependence of the wavenumber of the CD2 symmetric stretching vibration in bicelles with varying q ratios (top). Determined melting temperatures (T_m) for bicelles and calculated for an ideal mixture as a function of DMPC molar fraction (bottom). Dotted lines are a guide to the eye.

The CD_2 symmetric stretching frequencies augment in both the gel and fluid phases due to an increased disordering of DMPC acyl chains, probably caused by the proximity of mobile DHPC molecules. Interestingly, Andersson and Mäler (2005) have shown that the lipids' local mobility at q = 0.25 and 0.5 is more affected by the nature of the surfactant than the overall size of the bicelle. This influence is consistent with the mixing at these low q ratios found in our work. It would be of interest to study bicelles at lower q ratios; however, the melting temperatures drop below the freezing point of water and hinder such monitoring. Therefore, to study the mixing behavior of DMPC and DHPC in such conditions, molecular dynamics simulations were performed at a q of 0.25.

3.3.5 $q \leq 0.5$: Molecular Dynamics Simulations Show Lipid Mixing in Very Small Bicelles

An ideal bicelle assembly at $q^* = 0.25$, completely segregated and disc shaped, was obtained by letting DHPC molecules self-assemble around a bilayer patch of DMPC molecules with restrained positions (Figure 3.5A). The same system after 300 ns of unrestrained MD relaxation at 310 K is shown in Figure 3.5B. Our simulations give free DHPC concentrations of 34 ± 8 mM (pure DHPC/water) and 21 ± 6 mM (DMPC/DHPC self-assembly). This is higher than the experimental CMC/CBC in the same conditions, but within a factor of 2, indicating that the free energy of aggregation of the model is underestimated by less than the thermal energy RT. The atomistic model thus possesses chemical accuracy, unlike coarse-grained models that give access to much larger space and time scales, at the expense of capturing the specifics of any particular chemical system (Vácha & Frenkel, 2014).

The self-assembly simulation started with randomly distributed DMPC and DHPC molecules in solution. It showed a rapid aggregation on the nanosecond time scale,

followed by slower rearrangement and fluctuations of the aggregates that, like the one in Figure 3.5B, were not disc-shaped and did not exhibit bilayer-like regions or notable DMPC clusters. This result could also be observed for thermodynamically stable disk-like bicelles if their formation required slow ordering and segregation of the components that could not occur within the 350 ns self-assembly simulation for kinetic reasons. To test this hypothesis, we also performed a separate simulation starting from an "ideal" bicelle in which DMPC and DHPC molecules were completely segregated. In the first 30 ns, DMPC molecules were artificially restrained to preserve the bilayer arrangement, and DHPC molecules spontaneously assembled on the edges, thus forming a canonical disc-shaped bicelle as shown in Figure 3.5A. After 30 ns, DMPC restraints were lifted and a rapid mixing ensued, leading to mixed micelles (Figure 3.5B) comparable to those observed under self-assembly conditions. In general, atomistic simulations of such systems may suffer from metastability due to time scale limitations.

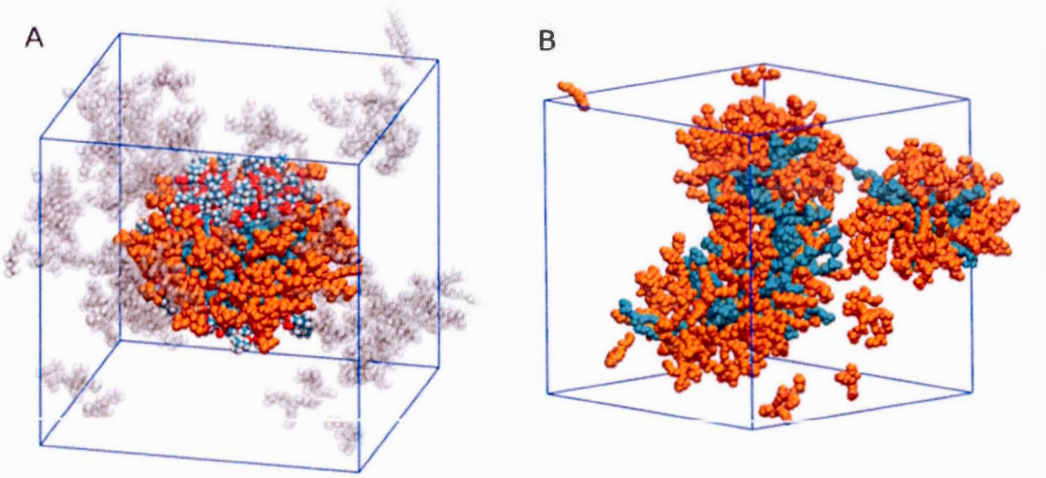

Figure 3.5 Simulation of a bicelle at q* = 0.25. (A) Ideal bicellar assembly obtained by restraining DMPC lipid positions. Cyan, DMPC (headgroup atoms colored by element); orange, bicellar DHPC; transparent, micellar and free DHPC molecules. The simulation periodic box is outlined in blue. (B) Same system after 300 ns of MD relaxation at 310 K. All DHPC molecules colored orange.

Here, we crucially obtained the same final structure starting from different states, showing that the mixed micelle is the most kinetically accessible aggregate from a random dispersion, but also that a perfectly segregated bicelle is unstable. Together, these simulations clearly predict a thermodynamic tendency of DHPC and DMPC molecules to mix and form small aggregates devoid of a bilayer-like region, at very low q ratios.

The ideal segregated bicelle prior to relaxation exhibits collective acyl chain order typical of a bilayer rearrangement, with a distribution of torsion angles between neighboring chains peaked around 0, as shown in Figure 3.6A. In sharp contrast, the DMPC/DHPC aggregates formed after relaxation show a much broader distribution of angles between the neighboring myristoyl chains. Correspondingly, the black lines in Figure 3.6B indicate a strong ordering in the ideal segregated bicelle system, where the DMPC bilayer region is indeed enriched in DMPC. In contrast, the data obtained (in red) from the aggregates formed after bicelle relaxation show very weak enrichment, denoting significant yet imperfect lipid mixing. Thus, for bicelles with $q < 1$ where infrared studies suggest some lipid segregation, our simulations predict a nonideal behavior intermediate between that of pure DMPC and an ideal homogeneous mixture of DMPC and DHPC.

Altogether, our results suggest that for studies where a bilayer-like region is required, bicelles with a $q > 1$ should be utilized. Note that in such conditions the correlation times of bicelles will be long and consequently resonances will be broadened thus potentially hindering the study of integral membrane proteins. The q ratio boundaries, where DMPC and DHPC are expected to be segregated while still forming aggregates which reorient rapidly in the magnetic field, and the lower limit of the total lipid concentration where expected and actual q ratios vary by less than 10%, define the ideal work region which is highlighted in gray in Figure 3.3.

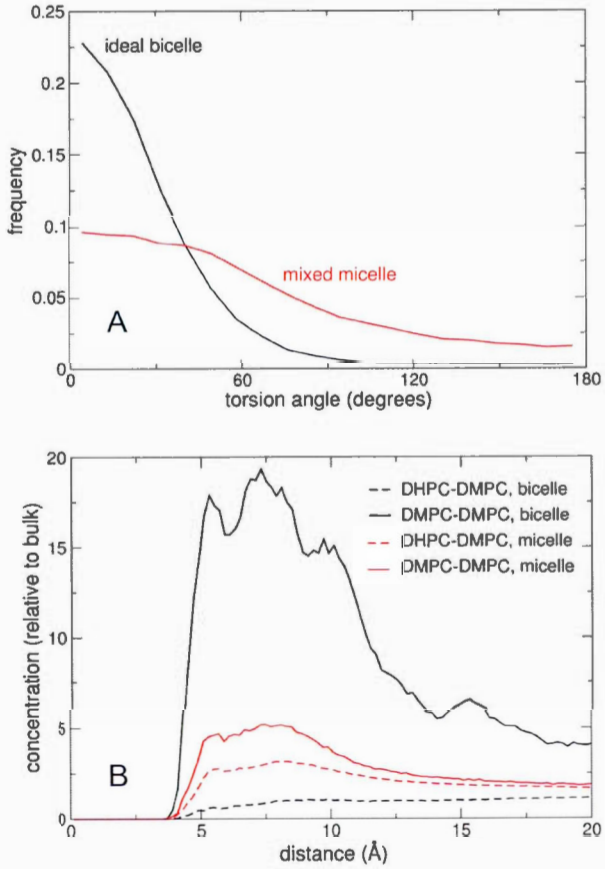

Figure 3.6 Lipid mixing and ordering in the simulated low-q* mixture. (A) Distribution of torsion angles between neighboring myristoyl chains in DMPC, in the ideal bicelle model (black) and after unrestrained relaxation (red). (B) Radial distribution functions of glycerol C2 atoms between DMPC molecules (solid lines) and between DHPC and DMPC (dashed lines), in the ideal bicelle (black) and unrestrained mixed micelle (red).

3.4 Conclusion

Low q DMPC/DHPC bicelles were studied by ^{31}P NMR, FTIR spectroscopy, and molecular dynamics. The critical bicellar concentration (CBC) was introduced as an important parameter which allows determining the exact long-to-short chain lipid ratio in the system and the diameter of the bicelle. This knowledge is necessary to

improve sample control for experiments requiring small membrane objects such as solution NMR, or diluted conditions such as CD or DLS. Finally, the word "bicelle" appears to be a misnomer for q ratios below 1 where lipid complexes would be more accurately described as mixed micelles.

Note Added in Proof

While the proofs of this article were being prepared, a publication addressing similar issues by other techniques was published by Ye *et al.* (Langmuir, DOI: 10.1021/la500231z). Overall their conclusions are in agreement with ours, although our molecular dynamics simulations point against the disc shape of mixed DMPC/DHPC micelles at low q. It should be noted that we define the critical bicelle concentration (CBC) as the free concentration of DHPC in solution at which DMPC/ DHPC aggregates are formed, in exact analogy to the critical micelle concentration (CMC). Ye *et al.* describe the CBC as the total lipid concentration at which bilayered bicelles are formed.

Acknowledgments

This work was supported by the Natural Sciences and Engineering Research Council (NSERC) of Canada. P.T.F.W. would like to acknowledge financial support from the Wellcome Trust (Grant No. 090658/Z/09/Z). M.B. wishes to thank the Université du Québec à Montréal, the Training Program in Bionanomachines (NSERC), the Canadian Institutes of Health Research Strategic Training Initiative in Chemical Biology, and the Centre Québecois sur les Matériaux Fonctionnels (CQMF) for the award of scholarships. This work was granted access to the HPC resources of CINES (Montpellier, France) under the allocation x2013077058 made by GENCI (Grand

Équipement National de Calcul Intensif). Dr. A. Grossfield is gratefully acknowledged for providing custom simulation analysis tools. I.M. is a member of the CQMF and the Groupe de Recherche Axé sur la Structure des Protéines (GRASP).

Supporting Information

Visual aspect of the bicelle samples at different lipid concentrations and molar ratios. Bicelle radius calculated for q = 1 from the effective q value (q*). Observed ^{31}P chemical shift of DHPC as a function of the inverse of DHPC concentration in DMPC/DHPC mixtures with q = 1. Minimal total phospholipid concentration recommended to conserve the desired bicelle molar ratio q. Comparison of the experimental melting temperature of DMPC-d_{54} in bicelles with values expected in ideal mixed micelles at different q ratios.

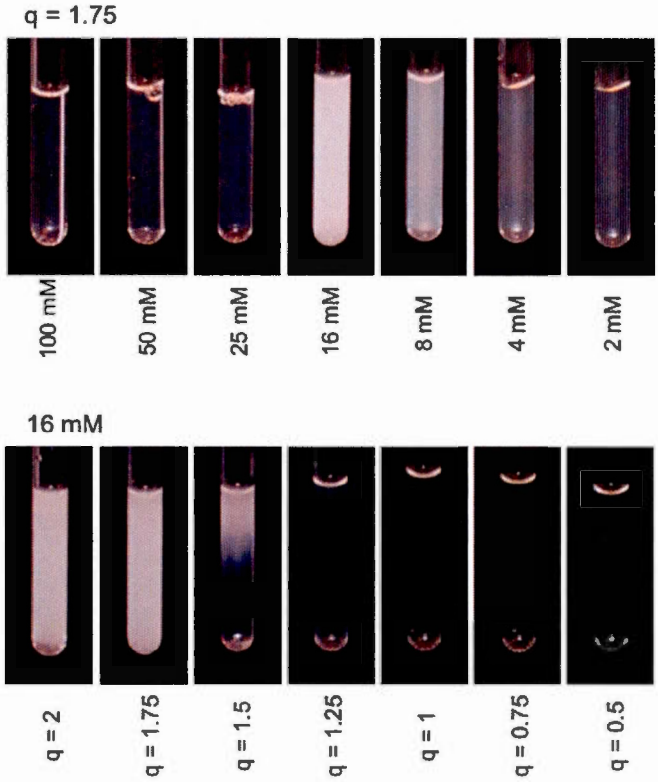

Figure S3.1 DMPC/DHPC samples with a molar ratio q of 1.75 at concentrations ranging from 100 to 2 mM (top) and a fixed concentration of 16 mM and q ratios ranging from 2 to 0.5. Data obtained at 25°C.

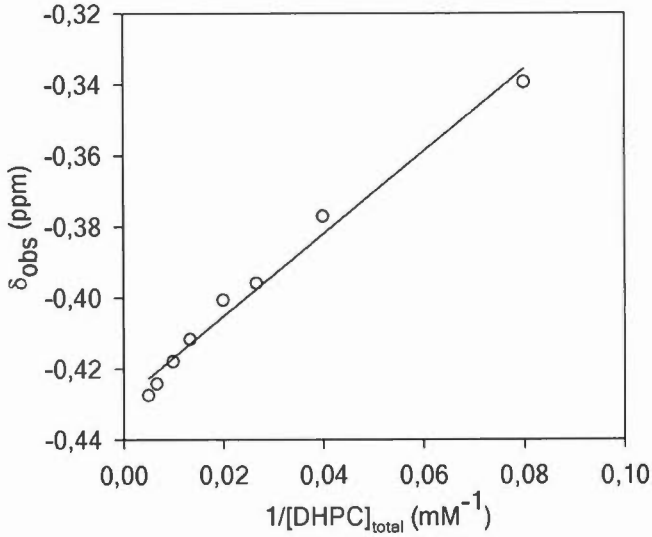

Figure S3.2 Variation of the observed ^{31}P chemical shift of DHPC as a function of the inverse of DHPC concentration in DMPC/DHPC bicelle mixtures with q =1. Data were obtained at 25°C.

Table S3.1 Bicelle disk radius calculated for q=1 according to equation 4 from the effective q value q*.

Effective q*	Bicelle radius (nm)
1	6.5
1.1	7.1
1.2	7.6
1.3	8.2
1.8	11.0
3.2	19.0

Table S3.2 Minimal total phospholipid concentration recommended to conserve the desired bicelle molar ratio q.

q	$[DMPC+DHPC]_{min}$ (mM)
0.15	162
0.25	133
0.50	120
0.75	121
1.00	121
1.25	133
1.50	172
1.75	186
2.00	221

Table S3.3 Comparison of the experimental melting temperatures (T_m) of DMPC-d_{54} in DMPC/DHPC bicelles and expected T_m for an ideal mixed micelle at different q ratios.

q [a]	Experimental bicelle T_m (°C) [a]	Calculated mixed micelle T_m (°C)
0	-	-46.0 [b]
0.5	6.0±0.3	-23.7
1	17.0±0.9	-12.5
2	21.0±0.9	-1.3
3	21.0±0.9	4.3
∞	21.0±0.3	21.0

[a] Total lipid concentration of 400 mM, therefore q = q*

[b] T_m of pure DHPC from (Sakuma *et al.*, 2010)

CHAPTER IV

MAGNETICALLY-ORIENTED MAPCHO BICELLES – VERSATILE MIMETICS FOR NMR APPLICATIONS

Maïwenn Beaugrand[†], Alexandre A. Arnold[†], Aline Balieiro Gambaro[†], Philip T. F. Williamson[‡] and Isabelle Marcotte[†]

†Department of Chemistry, Université du Québec à Montréal, P.O. Box 8888, Downtown Station, Montreal, H3C 3P8, Canada

‡Centre for Biological Sciences/Institute of Life Sciences, Highfield Campus, University of Southampton, Southampton, SO17 1BJ, United Kingdom

Foreword

Maïwenn Beaugrand carried out the majority of the experiments and analyzed the results. Aline Balieiro Gambaro performed some NMR replicas. Maïwenn Beaugrand conducted the literature research and wrote the manuscript with the help of Doctor Alexandre A. Arnold, Professors Philip T. F. Williamson and Isabelle Marcotte.

In this Chapter, lipid abbreviations are conveniently written to indicate the length of the acyl chains and thus, simplify the reading. For example, DMPC and DPC will be referred as D14PC and DPC12, respectively.

Résumé

Les bicelles (micelles en bicouche) sont des membranes modèles utilisées dans l'étude structurale de peptide et d'interactions membranaires. Elles sont traditionnellement faites de phospholipides à longues (C14) et courtes chaînes (C6), nommés dimyristoylphosphatidylcholine (D14PC) et dihexanoyl-PC (D6PC). Ce sont des mimétiques membranaires attrayants en raison de leur composition et surface planaire, similaires à l'environnement natif de la membrane. Afin d'améliorer la solubilisation des protéines membranaires et permettre leur étude dans des systèmes bicellaires, D6PC a été remplacé par les détergents de la famille monoalkylphosphocholines (MAPCHO). La dodécylphosphocholine (DPC12) est connue pour sa capacité à solubiliser les protéines membranaires. Plus spécifiquement, la DPC12, tétradecyl- (TPC14) et hexadécyl-PC (HPC16) ont été employées. Pour vérifier la possibilité de faire des bicelles avec différentes épaisseurs hydrophobes afin de mieux s'adapter aux protéines membranaires, la D14PC a été également remplacée par des phospholipides avec des longueurs de chaînes alkyles différentes: dilauroyl-PC (D12PC), dipalmitoyl-PC (D16PC), distéaroyl-PC (D18PC)

and diarachidoyl-PC (D20PC). Les résultats obtenus par RMN de l'état solide du phosphore à plusieurs rapports molaires lipide/détergent (q) et températures indiquent que des bicelles magnétiquement orientées peuvent être formées avec D12PC/DPC12 (de q=1.8 à q=3.4 et de 12 à 67°C), D14PC/DPC12 (de q=1.6 à q=3.0, de 32 à 52°C), D16PC/DPC12 (de q=1.6 à q=2.4, de 42 à 47°C), D14PC/TPC14 (de q=1.2 à 2.6, de 27 à 77°C), D16PC/TPC14 (de q=1.2 à q=2.4, de 37 à 57°C) et D18PC/HPC16 (q=1.6, 57°C). La qualité de l'alignement est similaire à celle des bicelles classiques alors que la faible concentration micellaire critique (CMC) des tensioactifs et leur miscibilité partielle avec les phospholipides sont susceptibles d'être avantageuses pour la reconstitution des protéines membranaires.

Abstract

Bicelles (bilayered micelles) are model membranes used in the study of peptide structure and membrane interactions. They are traditionally made of long- (C14) and short- (C6) chain phospholipids, namely dimyristoylphosphatidylcholine (D14PC) and dihexanoyl-PC (D6PC). They are attractive membrane mimetics because of their composition and planar surface similar to the native membrane environment. To improve the solubilisation of membrane proteins and allow their study in bicellar systems, D6PC was replaced by detergents from the monoalkylphosphocholine (MAPCHO) family of which dodecylphosphocholine (DPC12) is known for its ability to solubilize membrane proteins. More specifically DPC12, tetradecyl- (TPC14) and hexadecyl-PC (HPC16) have been employed. To verify the possibility of making bicelles with different hydrophobic thicknesses to better accommodate membrane proteins, D14PC was also replaced by phospholipids with different alkyl chain lengths: dilauroyl-PC (D12PC), dipalmitoyl-PC (D16PC), distearoyl-PC (D18PC) and diarachidoyl-PC (D20PC). Results obtained by ^{31}P solid-state NMR at several lipid-to-detergent molar ratios (q) and temperatures indicate that

magnetically-oriented bicelles can be formed with D12PC/DPC12 (from q=1.8 to q=3.4 and from 12 to 67°C), D14PC/DPC12 (from q=1.6 to q=3.0, from 32 to 52°C), D16PC/DPC12 (from q=1.6 to q=2.4, from 42 to 47°C), D14PC/TPC14 (from q=1.2 to 2.6, from 27 to 77°C), D16PC/TPC14 (from q=1.2 to q=2.4, from 37 to 57°C) and D18PC/HPC16 (q=1.6, 57°C). The quality of their alignment is similar to the one of classical bicelles while the low critical micelle concentration (CMC) of the surfactants and their partial miscibility with phospholipids are likely to be advantageous for the reconstitution of membrane proteins.

4.1 Introduction

Bilayered micelles, or so-called bicelles, were introduced in the 1990's and quickly gained in popularity due to their similarities with biological membranes (Sanders & Prestegard, 1990; Sanders & Schwonek, 1992). They are composed of long-chain phospholipids organized in a bilayer stabilized by short-chain lipids or detergents in the high curvature region of discs or perforated vesicles (Barbosa-Barros *et al.*, 2011; Diller *et al.*, 2009; Ram & Prestegard, 1988). The planar region made of long-chain phospholipids constitutes a favorable environment to study molecular interactions as well as the structure of membrane peptides and proteins with different biophysical techniques such as nuclear magnetic resonance (NMR), circular dichroism and fluorescence (De Angelis & Opella, 2007; Diller *et al.*, 2009; Dürr *et al.*, 2013; Naito, 2009; Prosser *et al.*, 2006; Raschle *et al.*, 2010; Sanders & Prosser, 1998; Whiles *et al.*, 2002). Bicelles can also be used to obtain protein crystals for X-ray crystallography (Faham & Bowie, 2002; Kimble-hill, 2013) and have potential pharmaceutical applications (Barbosa-Barros *et al.*, 2008; Lucyanna Barbosa-Barros *et al.*, 2011; Mäler & Gräslund, 2009; Rodríguez *et al.*, 2010; Rubio *et al.*, 2010).

One strength of structural studies by solid-state NMR is that they are not limited by the solubility, the size of the macromolecules or complex, or the requirement of crystals (Sun *et al.*, 2012). This enables the study of membrane peptides and proteins in a near-native membrane environment. The importance of lipid interactions to the folding, structure and functioning of membrane proteins has long been recognized (Bowie, 2004; Curran *et al.*, 1999; Lauterwein *et al.*, 1979; Perozo *et al.*, 2002; Williamson *et al.*, 2003), in particular the hydrophobic mismatch and lateral packing pressure due to the curvature of the lipids or detergents in model membranes (Bowie, 2004; Hong & Tamm, 2004; Killian, 1998; Nyholm *et al.*, 2007; Strandberg *et al.*, 2004). The insertion and folding of membrane proteins is indeed more favorable with long-chain lipids (Hong & Tamm, 2004).

To better mimick the complexity and diversity of biological membranes, different long-chain lipids with or without insaturations or net charge, and with various alkyl chain lengths have been proposed in the preparation of bicelles. The bile salt 3-(cholamidopropyl) dimethylammonio-2-hydroxyl-1-propane sulfate (CHAPSO) used with D14PC in the 1990s (Sanders & Prestegard, 1990) was quickly replaced by D6PC – more structurally similar to phospholipids (Sanders & Schwonek, 1992). Studies have been done to improve the bicelles' stability by changing the length of the detergent using dipentanoyl-PC (D5PC) and diheptanoyl-PC (D7PC), the length and unsaturation of the phospholipid using dilauroyl-PC (D12PC), dipalmitoyl-PC (D16PC) and palmitoyloleoyl-PC (POPC) (Triba *et al.*, 2006), or by using ether lipids (Aussenac *et al.*, 2005). Triton X-100 detergent demonstrated a better magnetic alignment and stability of the MPs in the bilayer (Park & Opella, 2010), while addition of cholesterol, cholesterol 3-sulfate and/or hexadecyltrimethylammonium bromide (CTAB) stabilizes the bilayer and increases the temperature range at which bicelles form (Yamamoto *et al.*, 2014). Loudet *et al.* (2007) showed that perpendicularly aligned bicelles can be formed without lanthanide addition (Prosser *et al.*, 1996, 1998) by using the modified lipid 1-tetradecanoyl-2-(4-(4-

biphenyl)butanoyl)-PC (TBBPC). To obtain bicelles at low concentrations and more suitable for solution NMR, detergents with low critical micelle concentration (CMC) were used such dodecyl-PC (DPC12) (Lu *et al.*, 2012; Nolandt *et al.*, 2012), 4-cyclohexyl-1-butyl-PC (cyclofos-4), 5-cyclohexyl-1-butyl-PC (cyclofos-5), 6-cyclohexyl-1-butyl-PC (cyclofos-6) and 7-cyclohexyl-1-butyl-PC (cyclofos-7) (Lu *et al.*, 2012). Other lipids such as the anionic phospholipid dimyristoylphosphoglycerol (D14PG) (Semchyschyn & Macdonald, 2004), cardiolipin (Parker *et al.*, 2001), and sphingomyelin (Anderluh *et al.*, 2005) can also be incorporated into bicelles to mimick a variety of biological membranes.

The objective of our work was to develop PC-based bicellar systems with various hydrophobic chain lengths to accommodate membrane proteins and peptides. We focused on phosphocholines since they are abundant in eukaryotic membrane cells (Warschawski *et al.*, 2011). Namely, a series of lipids ranging from D12PC to D20PC (diarachidonoylPC) were combined with monoalkylphosphocholine (MAPCHO) detergents (Figure 4.1 and Table 4.1).

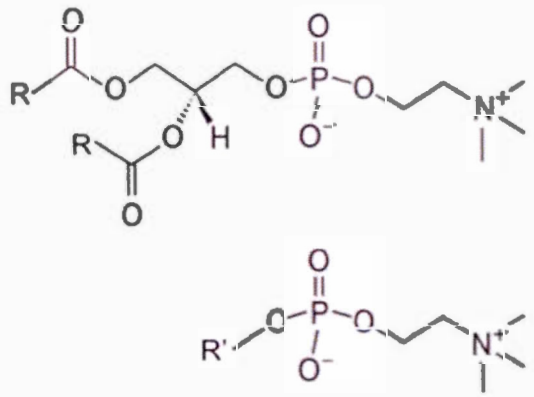

Figure 4.1 Molecular structures of phosphatidylcholines with an alkyl chain R from 12 to 20 carbones (top) and monoalkylphosphocholine detergents with an alkyl chain R' from 12 to 16 carbones (bottom) used for the preparation of bicelles.

Specifically, dodecyl- (DPC12), tetradecyl- (TPC14) and hexadecyl (HPC16) phosphocholines were employed. The detergent DPC12 is known to well solubilize membrane proteins and has previously been used with D14PC to prepare isotropic and magnetically-aligned bicelles (Arora *et al.*, 2001; Damberg *et al.*, 2001; Kallick *et al.*, 1995; Koehler *et al.*, 2010; Lu *et al.*, 2012; Nolandt *et al.*, 2012; Oxenoid *et al.*, 2002). When compared to DPC12, TPC14 micelles have shown their ability to maintain the activity of diacylglycerol kinase (DAGK) due to their better match with the hydrophobic span of the transmembrane domain of this protein (Koehler *et al.*, 2010). In this work, we present the characterization of MAPCHO bicelles using ^{31}P and ^{2}H solid-state NMR, and discuss the molar ratios and hydrophobic chain length of the phospholipids and detergents in relation to the magnetic alignment of the bicelles. Fourier transform infrared (FTIR) spectroscopy allows obtaining information on the segregation between phospholipid and detergent molecules. Finally, data on the 'critical bicellar concentration' (CBC) of the different binary systems, by analogy with the 'critical micellar concentration' (CMC), is provided using isotropic bicelles.

4.2 Materials and Methods

4.2.1 Materials

Phospholipids 1,2-dilauryl-sn-glycero-3-phosphocholine (D12PC), 1,2-dimyristoyl-sn-glycero-3-phosphocholine (D14PC), 1,2-dipalmitoyl-sn-glycero-3-phosphocholine (D16PC), 1,2-distearoyl-sn-glycero-3-phosphocholine (D18PC) and 1,2-diarachidonoyl-*sn*-glycero-3-phosphocholine (D20PC) as well as detergents n-dodecylphosphocholine (DPC12), n-tetradecylphosphocholine (TPC14) and n-hexadecylphosphocholine (HPC16) were obtained from Avanti Polar Lipids

(Alabaster, AL, USA) and used without further purification. Ytterbium(III) nitrate pentahydrate and ^{2}H-depleted water were purchased from Sigma Aldrich (Oakville, ON, Canada). Deuterium oxide (D_2O) was obtained from CDN Isotopes (Pointe-Claire, QC, Canada).

4.2.2 Sample Preparation

Samples used for solid-state NMR and infrared experiments were prepared by suspending the appropriate weight of detergent and phospholipid in nanopure water (pH 4.5) or ^{2}H-depleted water. The total concentration used was 400 mM, well above the CMC of all constituents (Table 4.1). Samples had molar ratio (q) ranging from 1 to 3.6 with 80% (w/v) hydration. Samples were then submitted to about 10 cycles of freeze (liquid N_2), thaw (60°C) and vortex shaking. The alignment of bicelles was 'flipped' with the normal of the bilayer parallel to the magnetic field by adding the lanthanide salt $YbCl_3$ at a concentration of 2.5 mM (Nolandt *et al.*, 2012; Prosser *et al.*, 1998) for the binary systems D14PC/TPC14 and D16PC/TPC14.

For solution NMR, bicelles containing DPC12 were prepared at total lipid and detergent concentration of 100 mM and q ratios of 0.5 and 1 while TPC14-based samples were made at 20 mM and a q ratio of 0.5. Samples were made using D_2O and submitted to cycles of freeze/thaw/vortex shaking. Serial dilutions were then performed.

4.2.3 Nuclear Magnetic Resonance

All solid-state NMR experiments were carried out on a hybrid solution/solid-state Varian Inova Unity 600 (Agilent, Santa-Clara, CA, USA) spectrometer operating at

frequencies of 599.95 MHz for ^{1}H, 246.86 MHz for ^{31}P and 92.125 MHz for ^{2}H, and equipped with a 4-mm broadband/^{1}H dual-frequency magic-angle-spinning (MAS) probehead. For ^{31}P NMR spectra, a phase-cycled Hahn echo pulse sequence (Rance & Byrd, 1983) was used with gated broadband proton continuous wave decoupling at a field strength of 50 kHz. A $\pi/2$ pulse of 3 µs, an interpulse delay of 33 µs, a recycle delay of 5 s, an acquisition time of 20 ms and a dwell time of 5 µs were used, and 64 to 512 scans were acquired. Spectra were externally referenced with respect to the signal of 85% phosphoric acid set to 0 ppm. ^{2}H NMR spectra were obtained using a solid echo pulse sequence (Davis *et al.*, 1976) with a $\pi/2$ pulse length of 3 µs, an interpulse delay of 45 µs and a repetition delay of 500 ms. Typically 2400 scans were acquired. For ^{31}P and ^{2}H NMR experiments, pre-acquisition delays of 10 and 15 minutes were respectively used between temperature steps. Spectra were acquired at least in duplicate at temperatures ranging from -3°C to 82°C depending on the phospholipid/detergent system. All spectra were processed using MNova software (Mestrelab Research, Santiago de Compostela, Spain).

All solution ^{31}P NMR experiments were carried out on an Avance III HD 600 MHz spectrometer (Bruker, Milton, ON, Canada) and equipped with a 5-mm double-resonance probe. A single-pulse experiment was employed with a $\pi/2$ pulse of 15 µs, a recycle delay of 5 s, and an acquisition time of 1 s with broadband proton continuous wave decoupling at a field strength of 5 kHz. A preacquisition delay of 10 min was used before each experiment to ensure thermal equilibration of the samples. Spectra were acquired at least in duplicate with 8 to 8192 scans at 37°C. They were internally referenced using a sealed capillary containing phosphate ions at pH = 11 in D_2O which was previously referenced with respect to 85% H_3PO_4 at 3.38 ppm. All spectra were processed with the Bruker TopSpin 3.2 interface.

4.2.4 Fourier Transform Infrared Spectroscopy

Infrared spectra were recorded with a Nicolet Magna-560 Fourier transform spectrometer (Thermo-Nicolet, Madison, WI, USA) equipped with a narrow-band mercury–cadmium–telluride (MCT) detector and a germanium-coated KBr beamsplitter. A volume of 30 µL of the 400 mM bicelle sample was placed between CaF_2 Biocell windows (Biotools Inc., Jupiter, FL, USA) manufactured with a calibrated path length of 45 µm. The windows were placed in a homemade heating cell using a Peltier element as a heating/cooling device. To prevent solvent evaporation during the course of long-term measurements, the sealing surface of the cell was lubricated with parafilm dissolved into chloroform. A total of 128 interferograms were acquired with a resolution of 2 cm^{-1} apodized with a Happ-Genzel function in the spectral range of 4000–650 cm^{-1} at various temperatures ranging from 13 to 70°C. Spectra were corrected for water vapor contributions using a reference spectrum. Data were processed with the software Grams/AI 8.0 (Galactic Industries Corporation, Salem, NH, USA). The spectral regions corresponding to the carbon–hydrogen stretching vibrations were baseline-corrected using a quartic function. The methylene symmetric stretching frequency was obtained from the center of gravity calculated at the top 5% of the band.

Table 4.1 Results compilation of ^{31}P solid-state NMR spectra. Black and grey squares with white font correspond to magnetically-oriented systems with a longitudinal bilayer deviation (static mosaicity) less than 5° and 10° from the magnetic field direction, respectively. Light grey squares with black font correspond to a deviation of less than 15°. Crosses are experiments done but not corresponding to an oriented system. The numbers are representative of the dynamic mosaicity when only two peaks were visible on the spectra. In parentheses next to phospholipids name, the gel-to-fluid phase transition temperature (Marsh, 2013) and next to MAPCHO detergents is the critical micelle concentration (Rakotomanga *et al.*, 2004; Sanders & Sönnichsen, 2006).

DPC (1.5 mM)	D12PC (-2.1°C)														D14PC (23.9°C)											D16PC (41.4°C)								D18PC (55.3°C)						
q \ Température (°C)	7	12	17	22	27	32	37	42	47	52	57	62	67	72	22	27	32	37	42	47	52	57	62	67	72	77	82	32	37	42	47	52	57	62	67	72	42	47	52	57	62	67	72
1,4															x	x	x	x	x	x	x	x	x	x	x	x	x	x	x	x	x	x	x	x	x	x							
1,6	x	x	x	x	x	x	x	x	x	x	x	x	x	x	x	x	24	23	22	22	22	x	x	x	x	x	x	x	x	21	21	x	x	x		x	x	x	x	x		
1,8	x	x	25	25	25	26	27	29	x	x	x	x	x	x																												
2	x	29	26	25	26	26	28	28	29	32	x	x	x	x	x	x	21	20	20	19	19	x	x	x	x	x	x	x	x	21	20	x	x	x		x	x	x	x	x	x	x
2,2																																										
2,4	x	20	19	18	18	18	18	18	19	19	19	x			x	x	x	19	19	18	18	x	x					x	x	17	x	x		x								
2,6																												x	x	x	x	x	x	x	x	x						
2,8																												x	x	x	x	x	x	x	x	x						
3	x	18	17	17	17	17	17	16	16	16	15	15	15	x	x	x	x	x	12	11	10	x	x	x	x	x		x	x	x	x	x	x	x	x	x						
3,2	x	x	17	17	17	17	16	16	15	15	14	14	14	x		x	x	x	x	x	x	x	x																			
3,4	x	x	x	16	16	16	15	15	14	13	13	x	x	x	x	x	x	x	x	x	x	x	x																			
3,6	x	x	x	x	x	x	x	x	x	x	x	x	x	x	x	x	x	x	x	x	x	x	x	x																		

TPC (0.12 mM)	D12PC (-2.1°C)														D14PC (23.9°C)											D16PC (41.4°C)								D18PC (55.3°C)						
q \ Température (°C)	7	12	17	22	27	32	37	42	47	52	57	62	67	72	22	27	32	37	42	47	52	57	62	67	72	77	82	32	37	42	47	52	57	62	67	72	42	47	52	57	62	67	72
1															x	x	x	x	x	x	x	x	x					x		x		x	x	x		x							
1,2															x	x	24	23	22	22	22	22	23	23	x	x		x	x	x	x	x	x	x	x		x	x	x	x	x	x	
1,4															x	23	22	21	21	21	21	21	21	21	x	x	x	x	x	x	22	21	20	x	x	x							
1,6																												x	x	22	21	20	x	x			x	x	x	x	x	x	
1,8																												x	x	17	16	14											
2	x	x	x	x	x	x	x	x	x	x	x	x	x	x	x	17	17	17	16	16	15	14	14	13	x			x	17	15	14	13	x	x	x	x	x	x	x	x	x	x	x
2,2																																											
2,4															x	x	x	x	14	14	12	11	10	9	9			x	x	x	14	13	x	x	x	x							
2,6															x	x	x	x	13	11	10	9	8	7	7	6	x	x	x	x	x	x	x	x									
2,8																x	x	x	x	x	x	x	x	x	x	x	x															
3															x	x	x	x	x	x	x	x	x	x	x	x	x															
3,2																																										
3,4															x	x	x	x	x	x	x	x	x	x	x																	

HPC (0.003mM)	D14PC (23.9°C)													D16PC (41.4°C)									D18PC (55.3°C)							D20PC (66.4°C)					
q \ Température (°C)	22	27	32	37	42	47	52	57	62	67	72	77	82	32	37	42	47	52	57	62	67	72	42	47	52	57	62	67	72	52	57	62	67	72	77
1																							x	x	x	x	x	x	x						
1,2															x	x	x	x	x	x			x	x	x	x	x	x	x	x	x	x	x	x	x
1,4																																			
1,6	x	x	x	x	x	x	x	x	x	x	x	x	x	x	x	x	x	x	x	x	x	x	x	x	x	11	x	x	x	x	x	x	x	x	x
1,8																																			
2	x	x	x	x	x	x	x	x	x	x	x	x	x	x	x	x	x	x	x	x	x	x	x	x	x	x	x	x	x	x	x	x	x	x	x

4.3 Results and Discussion

4.3.1 Versatile Magnetically-Oriented Bicelle with Low Free Surfactant Concentration

Several binary lipid mixtures were prepared by changing the chain length of the MAPCHO detergents (DPC12, TPC14 and HPC16) for all the phospholipids investigated, namely D12PC, D14PC, D16PC, D18PC and D20PC. Structures of the molecules are presented in Figure 4.1. All the lipid mixtures were studied by ^{31}P solid-state NMR and the experiments are summarized in Table 4.1. In this table, properties such as the melting temperature (T_m) of phospholipids and CMC of the detergents are given.

Figure 4.2 presents a characteristic example of one of the systems studied, namely D16PC/TPC14. The magnetic alignment is revealed by two well-resolved peaks on the ^{31}P solid-state NMR spectra between 42 and 52°C – similarly to classical D14PC/D6PC bicelles where the peak at *circa* -12 ppm is assigned to D14PC. This alignment is confirmed by well-resolved Pake doublets on the ^{2}H solid-state NMR spectra in the same range of temperatures.

^{31}P solid-state NMR spectra of other mixtures are presented in Figure S4.1. The molar ratios and temperatures at which MAPCHO bicelles orient are summarized in Table 4.2. Bicelles could be formed with DPC12 and phospholipids with chain lengths from 12 to 16. Our results for D14PC/DPC12 bicelles are in agreement with Nolandt *et al.* (2012) although our systems seem to orient between 37 to 52°C as compared to 36 to 47°C in their study for q = 3.2. With TPC14, bicelles could be formed with phospholipids having 14 to 16 carbon long chains. Finally, oriented bicelles containing HPC16 were only be formed with D18PC at q = 1.6 and 57°C. As shown in Figure S4.1C, the poor quality of the spectra and the limited q and

temperature range of orientation discouraged the exploration of more HPC16-based bicelles.

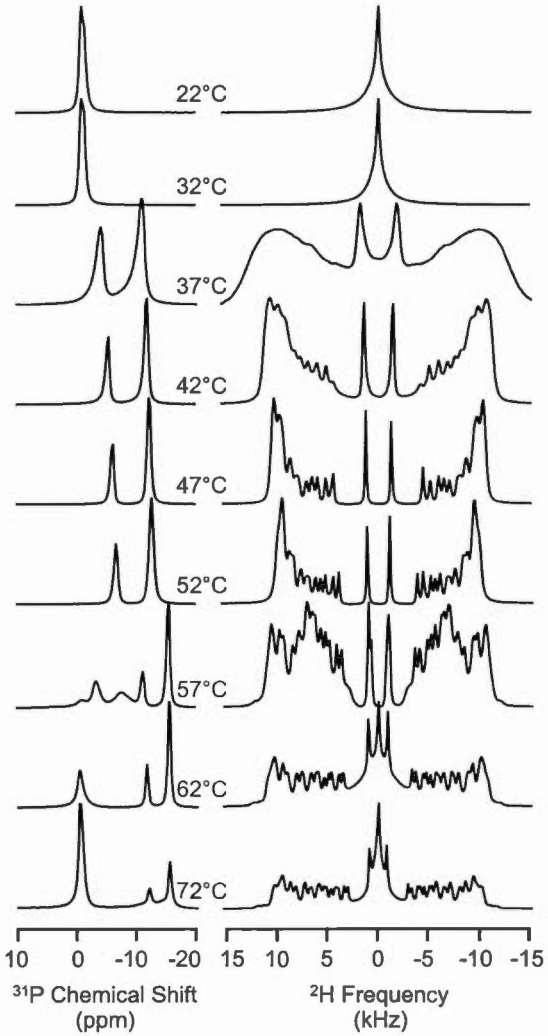

Figure 4.2 Evolution of the (A) ^{31}P and (B) ^{2}H NMR spectra of D16PC / TPC14 bicelles with q = 2 as a function of temperature

Table 4.2 Compilation of molar ratio q and temperature ranges at which magnetically-oriented systems are formed.

Lipid	Detergent	Molar ratio q	Temperature (°C)
D12PC	DPC12	1.8-3.4	12-67
D14PC	DPC12	1.6-3.0	32-52
D14PC	TPC14	1.2-2.6	27-77
D16PC	DPC12	1.6-2.4	42-47
D16PC	TPC14	1.4-2.4	37-57
D18PC	HPC16	1.6	57

In the study of transmembrane protein structure by solid-state NMR, it is interesting to orient the bilayer parallel to the magnetic field (Warschawski *et al.*, 2011). The addition of lanthanides to bicelles has been shown to flip the orientation of the bilayer plane from parallel to perpendicular to the magnetic field. Using this strategy, the flip of the alignment has been demonstrated with the system D14PC/DPC12 by ^{31}P NMR (Nolandt *et al.*, 2012). This is also possible for D16PC/TPC14 (Figure 4.3) and D16PC/DPC12 (data not shown); the possibility to flip the bicelles thus appears to be a general property of MAPCHO bicelles.

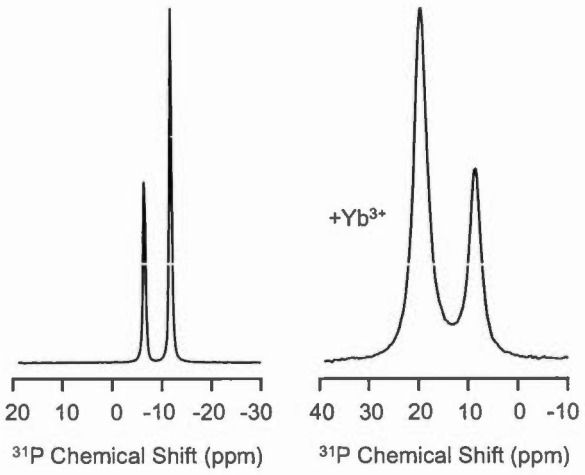

Figure 4.3 ^{31}P NMR spectra of D16PC/TPC14 bicelles (q = 2; 400 mM) at 47°C (A) without and (B) with 2.5 mM of the lanthanide ions Yb^{3+}.

One possible advantage of MAPCHO-based bicelles over classical bicelles is the very low CMCs of this type of surfactants (Table 4.1). Indeed, the presence of a significant amount of free surfactant can be a drawback in particular when samples need to be diluted (Beaugrand *et al.*, 2014). By studying the effect of dilution on ^{31}P NMR spectra, the concentration of free detergent (or critical bicellar concentration, CBC) can be determined (Beaugrand *et al.*, 2014; Glover *et al.*, 2001). The CBC values are listed in Table 4.3.

Table 4.3 Critical bicelle concentration (CBC). Free chemical shift of DPC12 at 0.125 mM and TPC14 at 0.025 mM were measured at 0.330 and 0.324 ppm, respectively.

Lipid	Detergent	Molar ratio q	CBC (mM)
D12PC			0.75±0.01
D14PC	DPC12	1	0.78±0.01
D16PC			0.82±0.01
D14PC	DPC12	0.5	0.86±0.02
	TPC14		0.07±0.01
D14PC	D6PC	0.5	7.5±0.5

For a given molar ratio q of 0.5 and long-chain phospholipid D14PC, the CBC with D6PC, DPC12 and TPC14 are 7.5 (Beaugrand *et al.*, 2014), 0.86 and 0.07 mM, respectively. The magnitude of the CBC follows the CMC of the detergents (15, 1.5 and 0.12 mM (Sanders & Sönnichsen, 2006), respectively) and it is thus clearly advantageous to use MAPCHO bicelles when diluted conditions are necessary. For a given molar ratio q of 1 and detergent DPC12, the CBC for D12PC, D14PC and D16PC are 0.75, 0.78 and 0.82 mM, respectively. By increasing the length of the phospholipid, the CBC slightly increases, possibly indicating a decrease in miscibility when the chain-length mismatch increases (Beaugrand *et al.*, 2014). For a given detergent DPC12 and phospholipid D14PC, the CBC slightly decreases from molar

ratio q of 0.5 to 1, an effect also observed for classical bicelles and attributed to a higher segregation between D14PC and D6PC as q increases (Beaugrand *et al.*, 2014).

4.3.2 Behaviour as a Function of the Temperature

As already described by Triba *et al.* (2005, 2006), it is possible to identify different characteristic transition temperatures for bicelle systems by ^{31}P solid-state NMR as a function of temperature. The best known transition for the phospholipids is the melting temperature (T_m) that corresponds to the transition between gel and liquid crystalline phases. All T_m of the lipids studied in this work are listed in Table 4.1. In bicelle systems, an important transition corresponds to the temperature at which they orient in the magnetic field (Triba *et al.*, 2005; 2006). This temperature is greater than the superior to T_m in classical bicelles.

Figures 4.2 and S4.1 displays the temperature behaviour for the molar ratio q which bicelles orient in the larger range of temperatures for the different MAPCHO systems as observed by ^{31}P solid-state NMR. Below the lipids' T_m, NMR spectra of the different MAPCHO-PC systems show a peak centered at 0 ppm indicative of fast-tumbling structures, as well as a powder pattern which is particularly intense for the systems in which the detergents and the phospholipids have the same alkyl chain length (D12PC/DPC12 and D14PC/TPC14) (Figures 4.2 and S4.1). As exemplified in Figure 4.4 with D16PC/TPC14, the sample is liquid and transparent, but was milky when a powder pattern was observed on the ^{31}P NMR spectrum. Around T_m, two broad resonances emerge from the ^{31}P NMR spectra for all the systems, as was seen for D14PC/D6PC when magnetic alignment starts (Triba *et al.*, 2005). Above the lipids' T_m, the samples are transparent and viscous (Figure 4.4) and two well-defined resonances are observable (Figures 4.2 and S4.1) and characteristic of oriented

bicelles (Sanders & Schwonek, 1992; Triba *et al.*, 2005). The low-field (higher ppm values) peak has been ascribed to the short-chain phospholipid (or the detergent in our case) mainly on the edges or holes, while the high-field (lower ppm values) resonance corresponds to the long-chain phospholipid mainly in the bilayer (Triba *et al.*, 2005). Another transition is observed at higher temperatures, when a peak appears at -15 ppm on the ^{31}P NMR spectra, which is characteristic of a 90° orientation in vesicles. This transition is described as T_V by Triba *et al.* (2005). The samples become liquid again and lose transparency (Figure 4.4). There seems to be the appearance of vesicles coexisting with other structures such as bicelles and fast-tumbling objects (Figures 4.2 and S4.1).

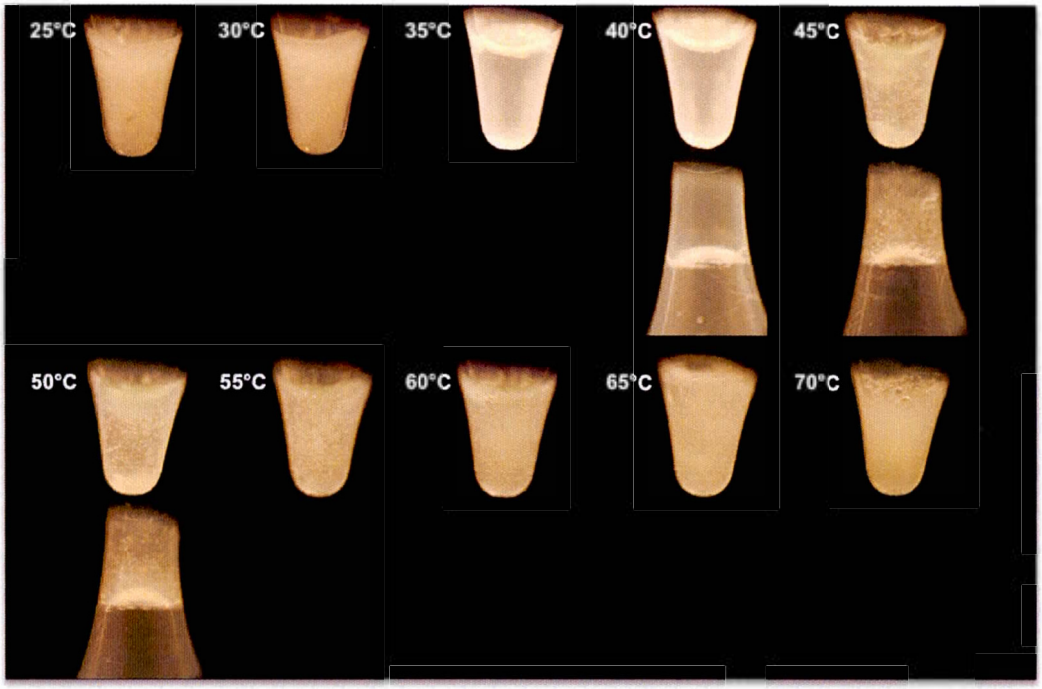

Figure 4.4 Samples of the binary system D16PC/TPC14 at a molar ratio q of 2 and a concentration of ~ 400 mM and different temperatures from 25 to 70°C. At 25°C, the sample is milky and slightly viscous, becomes less viscous at 30°C and 35°C and transparent and fluid, at 40°C, it is really viscous and transparent, at 55°C, it becomes less viscous and starts to cloud.

When compared to traditional D14PC/D6PC bicelles, the MAPCHO bicelles explored in this work displays larger temperature range of alignment. D14PC/D6PC typically orient between 30-50°C as reviewed elsewhere (Dürr *et al.*, 2013; Marcotte & Auger, 2005) while the MAPCHO systems with D14PC can orient between 27-77°C (Tables 4.1 and 4.2).

4.3.3 Behaviour as a Function of Molar Ratio q

Figures 4.5 and S4.2 show the ^{31}P NMR spectra at different q ratios at a temperature where most systems are oriented. Similarly to the temperature, it is possible to identify transitions according to the molar ratio q for systems that display aligned bicelles. Therefore, q_m describes the minimal ratio at which orientation occurs, i.e., when two resonances are observed on the ^{31}P NMR spectra. We can also define a q_v when a powder pattern starts to show on the spectra. The q_m and q_V values are displayed in Tables 4.1 and 4.2. As an example, the system D16PC/TPC14, has q_m and q_V values of 1.2 and 2.6, respectively.

When compared to traditional D14PC/D6PC bicelles, the MAPCHO bicelles explored in this work start to align at lower q molar ratios. Moreover, the q_m-q_v interval in which oriented objects are found is smaller. D16PC/D6PC typically orient for q ratios of ~2.5 and 7.5 as reviewed elsewhere (Dürr *et al.*, 2013; Marcotte & Auger, 2005). The magnetic-alignment of a bilayer is due to the anisotropy of diamagnetic susceptibility of the phospholipids. However, a sufficient number of phospholipids is required to counterbalance thermal agitation, i.e. the planar region needs to be above a certain threshold size. One might therefore infer that MAPCHO bicelles at q values as low as 1.6 for DPC12 or q = 1.2 for TPC14, have already reached this threshold size for orientation which is only attained for the D14PC/D6PC system at q = 2.5.

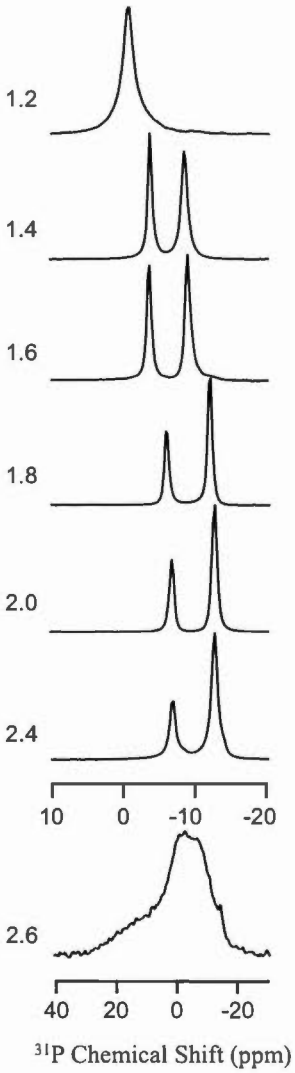

Figure 4.5 Evolution of the ^{31}P NMR spectrum of D16PC / TPC14 bicelles at 52°C as a function of the molar ratio q.

It is noteworthy that an intermediate type of oriented systems appears at low q ratios. It is characterized by two well-resolved peaks with chemical shifts, shifted to lower fields as compared to classical bicelles. In addition, the integration of the two peaks strongly deviates from the expected q values. For example, in the case of D16PC/TPC14, these type of system appears between q = 1.2 and 1.6. The observed

chemical shifts and resonance integrations would be consistent with a bicelle system in which a large proportion of phospholipids are in the high curvature area while a large proportion of surfactants are in the planar region. Therefore, if a surfactant-solubilized protein is progressively reconstituted in a bicelle by adding phospholipids (i.e. increasing q ratio), the miscibility between phospholipid and surfactant gradually diminishes and the protein is gently brought from the surfactant to the bilayer environment. The reconstitution of membrane proteins into MAPCHO bicelles would therefore be easier than in classical bicelles.

In order to better evaluate the bicelle orientation, the static (Arnold *et al.*, 2002) and dynamic (Triba *et al.*, 2005; Zandomeneghi *et al.*, 2003) mosaicities can be calculated. The static mosaic spread reports on the angle distribution of the phospholipid bilayer and the magnetic field. It can be determined from the shape of the lipid and detergent resonances in the ^{31}P solid-state NMR spectrum. Oriented bicelles can also undergo rapid oscillations around their main orientation. This dynamic mosaicity can be described with a Gaussian distribution and the width of this distribution can be extracted from the position of the long-chain phospholipid resonance on the ^{31}P solid-state NMR spectrum. Values of dynamic and static mosaic spreads for all systems are compiled in Table 4.1. Static mosaicities fall below 5° for the best oriented systems, the quality of the orientation of MAPCHO systems is therefore as good as the one of classical bicelles. The best dynamic mosaicity is of 6°, it is obtained with the D14PC/TPC14 system at 77°C.

4.3.4 Effect of Detergent-Phospholipid Chain Length Difference on MAPCHO Bicelles

Data can be analysed either by looking at the effect of varying the MAPCHO detergent on the bicelle formation with a given phospholipid, or of the phospholipid

for a given MAPCHO detergent. However, it appears that these effects can be unified by considering the difference in chain length between the phospholipid and surfactant.

As shown in Tables 4.1 and 4.2, DPC12 can form oriented bicelles with phosphatidylcholines with chain lengths ranging from 12 to 16 carbons, and TPC14 with phosphatidylcholines whose chain lengths range from 14 to 16 carbons. HPC16 can only form bicelles with D18PC. Bicelles could not be formed when the surfactant hydrophobic length was greater than the lipid bilayer (TPC14 and D12PC for example). In all cases, increasing the chain length difference resulted in a decrease of the temperature range in which bicelles could be formed. For example, D14PC/TPC14 systems orient over a temperature range of 50°C as compared to 20°C for D14PC/DPC12 bicelles. The range of q ratios at which bicelles orient is also reduced when the chain mismatch increases. For example, D12PC/DPC12 bicelles orient from q=1.8 to 3.4 while D14PC/DPC12 orient from q=1.6 to 3.0 and finally D16PC/DPC12 only orients between q=1.6 and 2.4.

Our data thus indicate that in the case of MAPCHO-based bicelles, it is ideal to use the surfactant with hydrophobic chains with the same number of carbons than the phospholipid. The maximum difference allowed is 4 carbons although it was only possible to form bicelles for DPC12 with D16PC. A certain amount of deviation from the same length rule is possible. In order to establish an empirical criterion which could predict whether a given surfactant-phospholipid pair will form bicelles, we calculated the ratio of the hydrophilic headgroup volume divided by the hydrophobic volume for both the surfactant and the phospholipid ($R = V_{Hydrophilic}/V_{Hydrophobic}$). The empirical observation is that when this ratio R is equal to the surfactant and the phospholipid (or $R_{Phospholipid}/R_{Surfactant} \approx 1$) oriented bicelles can form (Table 4.4). A similar observation can be made for bicelles made with short-chain

phospholipids instead of detergent and the phospholipid ratio however needs to be 2.5 times larger than the one of the short-chain lipid (Table 4.4).

Table 4.4 Ratio of the hydrophilic-to-hydrophobic volume ratios of the phospholipid (PL) on the detergent or short-chain phospholipid. Volumes of hydrophobic tail and hydrophilic headgroup were calculated using the average lipid component volumes from Armen *et al.* (1998). Systems that did not lead to aligned sample are in italic. The difference column is compared to the value of 1 for MAPCHO systems and 0.4 for short-chain phospholipid systems.

PL	Detergent or short-chain PL	Ratio	Difference (%)
D12PC	DPC12	0.87	-13
D14PC		1.02	+2
D16PC		1.17	+17
D18PC		*1.31*	*+31*
D12PC	TPC14	*0.77*	*-23*
D14PC		0.90	-10
D16PC		1.03	+3
D18PC		*1.16*	*+16*
D14PC	HPC16	*0.80*	*-20*
D16PC		*0.92*	*-8*
D18PC		1.03	+3
D20PC		*1.15*	*+15*
D14PC	D5PC	0.35	-12.5
D12PC	D6PC	0.49	+22.5
D14PC		0.42	+5
D16PC		0.37	-7.5
D14PC	D7PC	0.49	+22.5

4.3.5 Miscibility

Triba *et al.* (2005) have shown the importance of surfactant and phospholipid miscibility in the morphology of bicelles. In order to compare the degree of miscibility between D14PC/D6PC and MAPCHO-based bicelles, we measured the

thermotropic behaviour of these systems at a total lipid concentration of 400 mM and hydration of 80%. This was done by FTIR using protonated detergents and phospholipids with perdeuterated alkyl chains (D16PC-d_{62}). By plotting the CD_2 symmetric stretching frequency (~2090 cm^{-1}) as a function of temperature, the melting temperature of the phospholipid can be determined from the inflexion point (Figure 4.6). The values of the CD_2 symmetric stretching frequencies in the liquid-crystalline phase are almost superimposable while in the gel phase, the presence of the detergent increases the wavenumbers (Figure 4.6). This indicates that the alkyl chain ordering is affected in the gel phase but not in the fluid phase by the presence of the detergent. With MAPCHO detergent, the T_m of the phospholipid is slightly decreased compared to the systems with D6PC (-1 or -2°C) (Figure 4.6). This indicates a higher perturbation of the bilayer which is likely due to the higher miscibility of MAPCHO detergents and phospholipids compared to D14PC and D6PC in the D6PC-based bicelles.

This hypothesis is further confirmed by integrating the ^{31}P NMR peaks and comparing their ratio to the theoretical q ratio (Table 4.5). Indeed, if the surfactant and phospholipid are perfectly segregated in the high-curvature and bilayer regions respectively, the ratio of the integration of the two peaks measured on the ^{31}P NMR spectra should be equal to q. This is however not the case for MAPCHO bicelles as shown in Table 4.5. For example, in the case of the D12PC/DPC12 at 37°C, for q = 2, the ratio of the integrals of the two peaks was 1.4, while a value of 2.6 was found for q = 3. Overall, a stronger deviation from the theoretical q values is observed for MAPCHO bicelles than for the phospholipid bicelles (Table 4.5). Since the ratio of integrals is smaller than the theoretical q, phospholipids appear to be miscible in the high curvature regions.

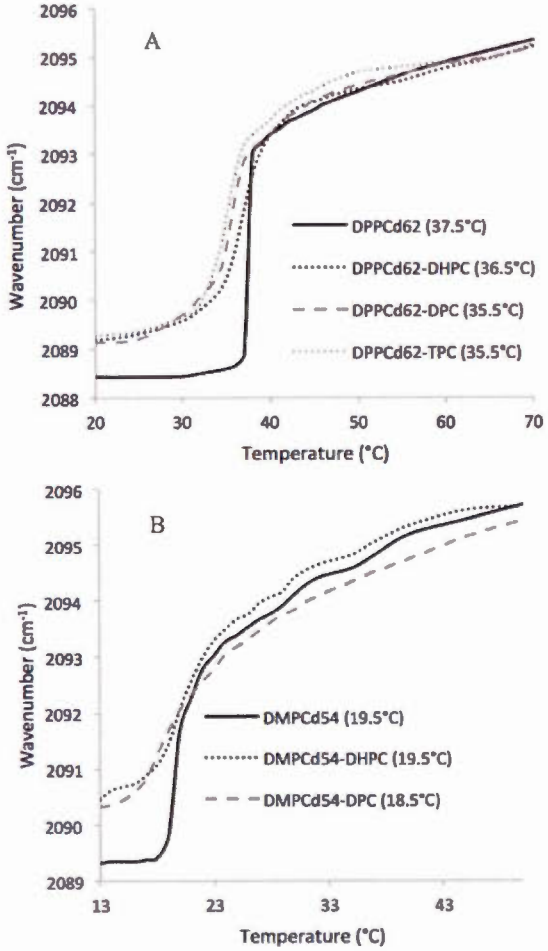

Figure 4.6 Temperature dependence of the wavenumber of the CD_2 symmetric stretching vibration in D16PC-d_{62} (A) and D14PC-d_{54} (B) vesicles and q = 2 bicelles with various detergent. Determined melting temperatures are indicated in the legend in parentheses.

Table 4.5 ^{31}P resonance integration ratio compared to the molar ratio q.

Lipid	Detergent	Temperature (°C)	Molar ratio q	Integration ratio	Difference (%)
D12PC	DPC12	37	2	1.4	-30
			3	2.6	-13.3
D14PC		37	2	1.5	-25
D16PC		47	2	1.4	-30
D14PC	TPC14	37	2	1.8	-10
D16PC		47	2	1.8	-10
D14PC	D6PC	37	2.5	2.3	-8
			3.5	3.3	-5.7

4.4 Conclusion

We have shown that mixtures of phospholipids with varying hydrophobic thicknesses (from 12 to 18 carbons) could form oriented bicelles with MAPCHO surfactants. The quality of the orientation is similar to the one obtainable with classical phospholipid-based bicelles. The orientation of the bilayer region of these bicelles could be changed from parallel to perpendicular to the magnetic field by adding lanthanides. The MAPCHO based bicelles orient in a broader temperature range than classical bicelles and offer greater stability upon dilution due to the low CMC of the surfactants. Both DPC12-d_{38} and TPC14-d_{42} are commercially available in fully perdeuterated form and are more cost-effective than the classical D6PC-d_{35}. Moreover, detergents such as DPC12 or TPC14 can be used directly in the purification process of membrane proteins. By progressively adding phospholipid to the surfactant-membrane protein mixture, and exploiting the gradual decrease in miscibility between surfactant and PL in MAPCHO bicelles, the membrane protein can be safely reconstituted in a bicelle bilayer environment (see Chapter V).

Acknowledgments

I. M. gratefully acknowledges funding from the Natural Sciences and Engineering Research Council (NSERC) of Canada and M. P. from the Engineering and Physical Sciences Research Council (EPSRC grant EP/I029036/1). M. B. wishes to thank the Faculté des Sciences of the Université du Québec à Montréal, the NSERC Bionanomachines training program, and the Canadian Institutes of Health Research Strategic Training Initiative in Chemical Biology for the award of scholarships as well as Dr. Ansgar B. Siemer. I.M. is member of the CQMF, the Bionano program and the Groupe de Recherche Axé sur la Structure des Protéines (GRASP). The authors would like to thank Dr. Dror E. Warschawski for interesting discussions.

Supporting Information

^{31}P-NMR spectra of the different systems as a function of the temperature and as a function of the molar ratio q. Determination of static mosaicity, $S_{bilayer}$ and dynamic mosaicity.

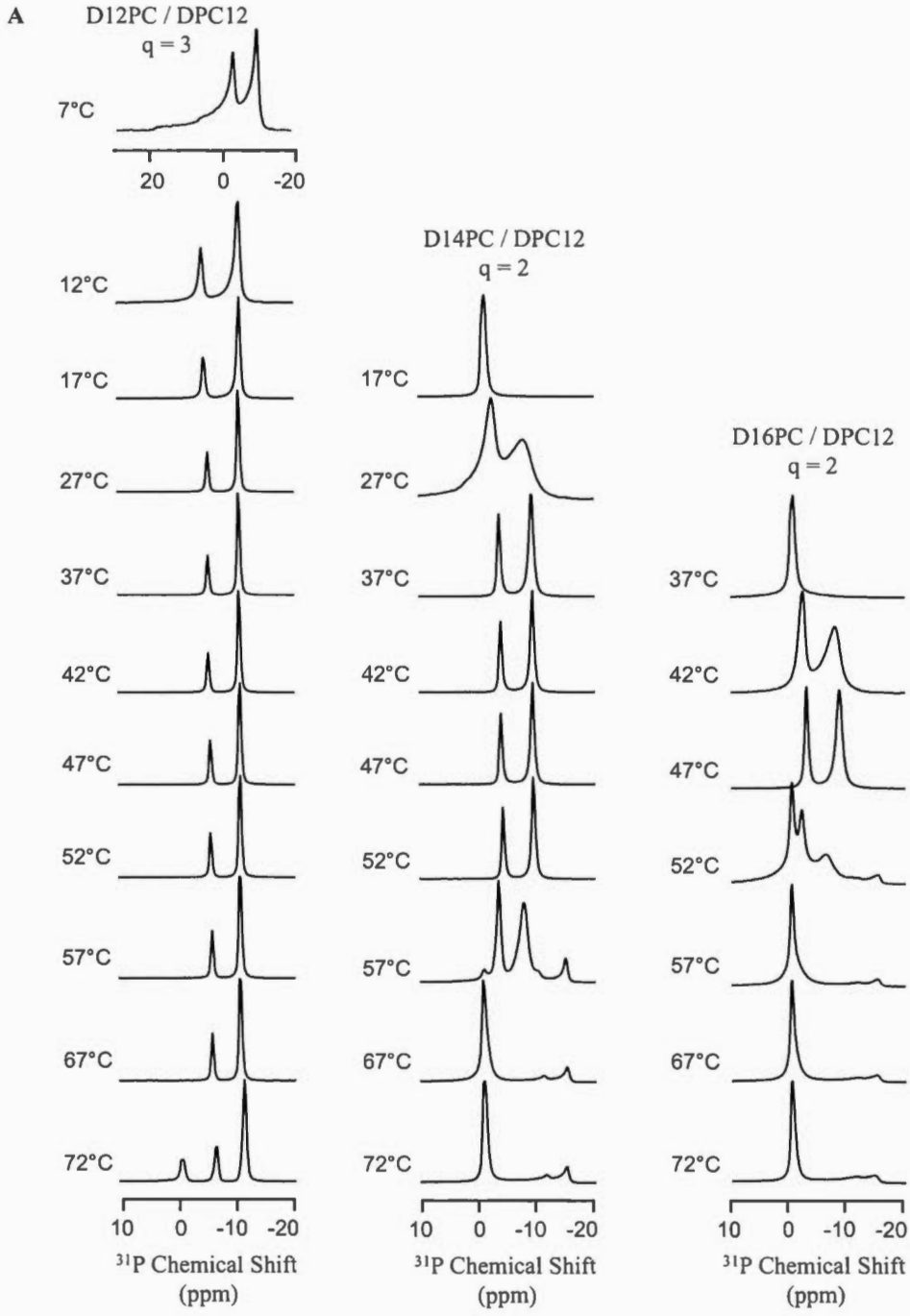
A
D12PC / DPC12
q = 3
7°C
20 0 -20
12°C
17°C
27°C
37°C
42°C
47°C
52°C
57°C
67°C
72°C
10 0 -10 -20
31P Chemical Shift
(ppm)
D14PC / DPC12
q = 2
17°C
27°C
37°C
42°C
47°C
52°C
57°C
67°C
72°C
10 0 -10 -20
31P Chemical Shift
(ppm)
D16PC / DPC12
q = 2
37°C
42°C
47°C
52°C
57°C
67°C
72°C
10 0 -10 -20
31P Chemical Shift
(ppm)

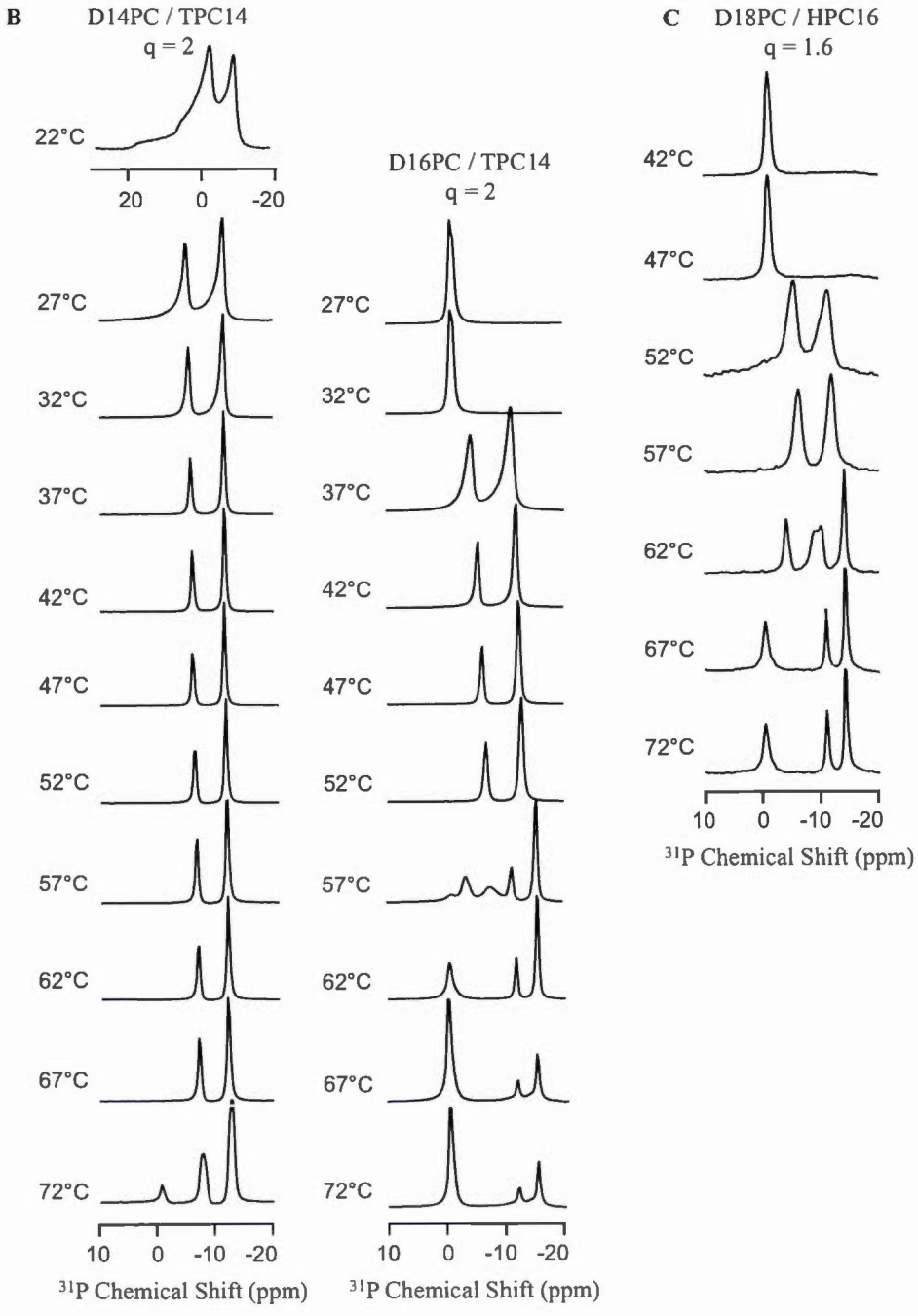

Figure S4.1 ^{31}P-NMR spectra of each oriented systems of mixtures with DPC12 (A), TPC14 (B) and HPC16 (C) at temperature between 7 and 72°C.

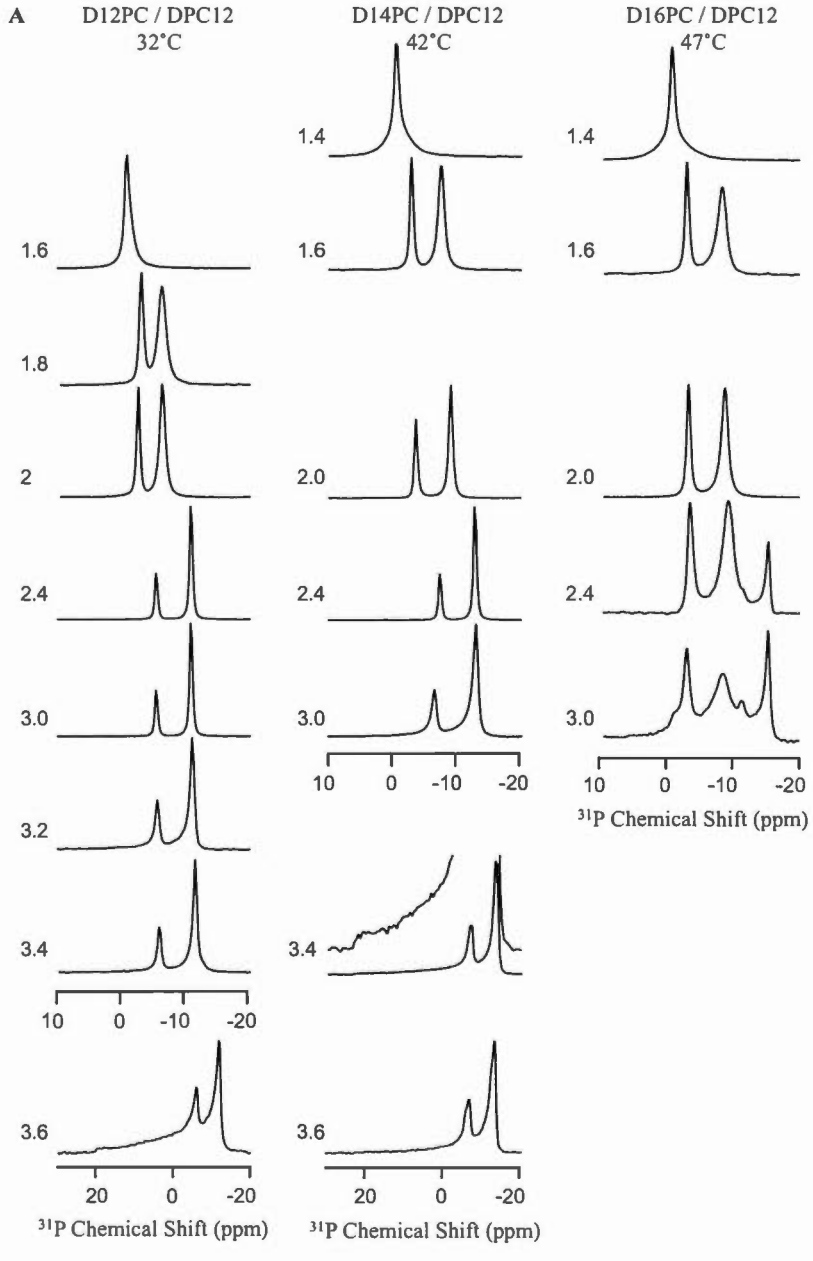
A
D12PC / DPC12
32°C
D14PC / DPC12
42°C
D16PC / DPC12
47°C
1.4
1.6
1.8
2
2.0
2.4
3.0
3.2
3.4
3.6
10
0
-10
-20
20
0
-20
31P Chemical Shift (ppm)

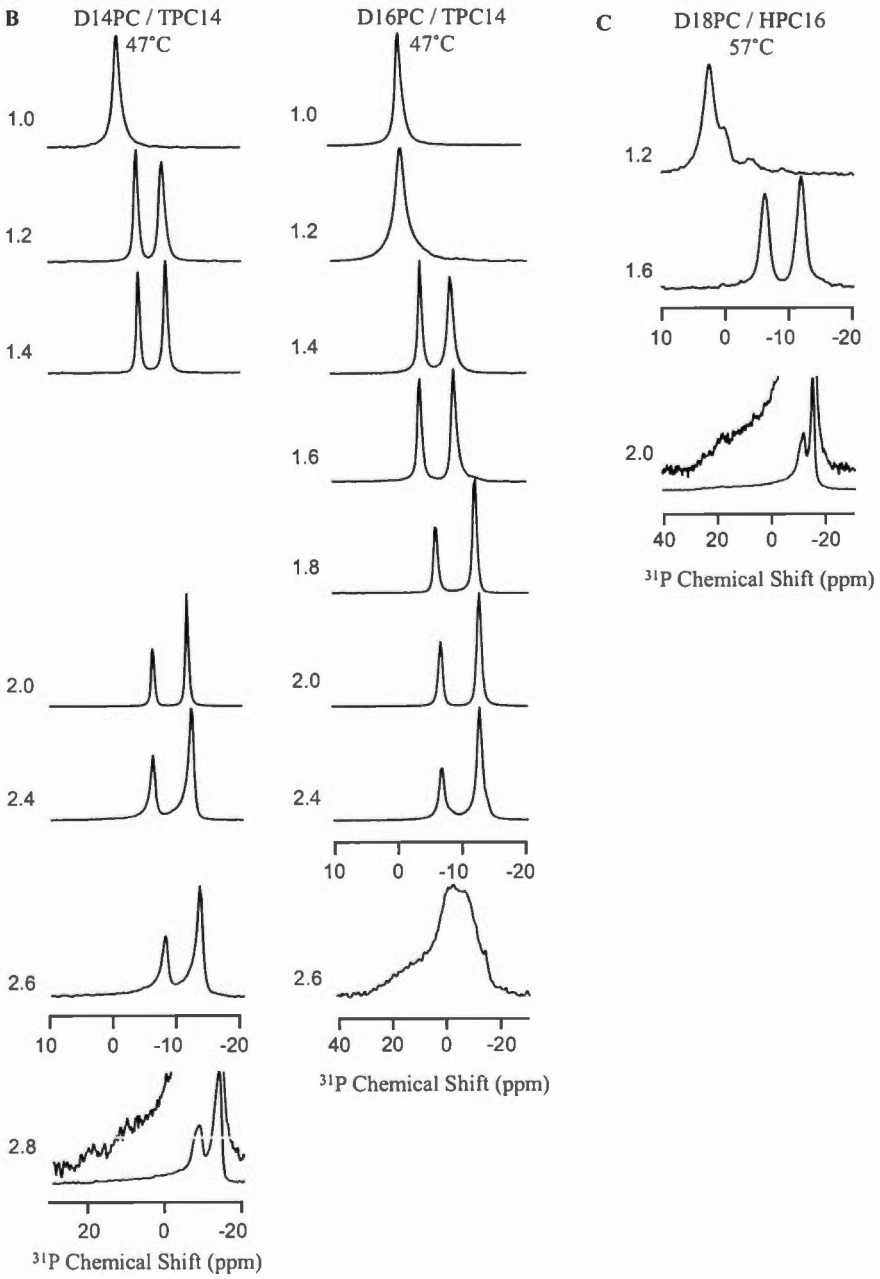

Figure S4.2 ^{31}P-NMR spectra of each oriented systems of mixtures with DPC12 (A), TPC14 (B) and HPC16 (C) at different [phospholipid] / [detergent] molar ratio q between 1 and 2.8. Enlarged spectra above the figures were added when necessary to define the orientation of the system.

Static mosaicity

The shape of the ^{31}P resonance spectrum allowed us to estimate the mosaic static spread (ζ), which is the standard deviation of the gaussian distribution of the bicelle orientation angle (β) from the main orientation at 90° (β_0). The probability to find bicelles whose normals are at an angle β with respect to the magnetic field is thus given by (Arnold *et al.*, 2002; Zandomeneghi *et al.*, 2003):

$$p(\beta) = \frac{1}{\zeta\sqrt{2\pi}} e^{-\frac{(\beta-\beta_0)^2}{2\zeta^2}} \quad \text{(S4.1)}$$

$S_{bilayer}$ and dynamic mosaicity

The ^{31}P resonance frequency (δ_{obs}) of phospholipid in bicelles (Triba *et al.*, 2005; Zandomeneghi *et al.*, 2003) is given by:

$$\delta_{obs} = \delta_{iso} + \frac{1}{2}(3cos^2\theta - 1)\bar{\sigma}\times S_{bil} \quad \text{(S4.2)}$$

where δ_{iso} is the isotropic chemical shift, θ is the angle between the bilayer normal and the magnetic field direction, $\bar{\sigma}$ is the anisotropy and S_{bil} is the order parameter describing the motions of the bilayer normal compared to its average orientation.
In a magnetic field B_0, bicelles have their bilayer normal perpendicular to the direction of B_0 (i.e. $\theta = 90$), thus:

$$\delta_{obs} = \delta_{iso} + \frac{1}{2}\bar{\sigma}\times S_{bil} \quad \text{(S4.3)}$$

Since bicelles undergo rapid fluctuations, $S_{bilayer}$ would be unequal to 1. The deviation of the angle of the Gaussian distribution (ε) is called mosaic dynamic spread and can be estimated, as it is dependent of the $S_{bilayer}$:

$$S_{bil} = \frac{\int_0^{90°} e^{\frac{sin^2\theta}{2\varepsilon^2}} \times \frac{1}{2}(3cos^2\theta - 1) \times sin\theta \times d\theta}{\int_0^{90°} e^{\frac{sin^2\theta}{2\varepsilon^2}} \times sin\theta \times d\theta} \quad \text{(S4.4)}$$

This Gaussian distribution can be represented graphically (adapted from Schmidt-Rohr & Spiess, 1994) by:

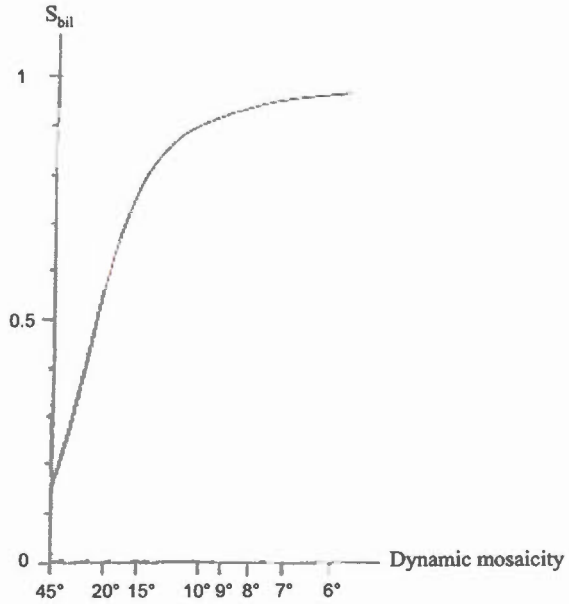

CHAPTER V

A COMPARATIVE STUDY OF THE STRUCTURE AND INTERACTION OF THE PORE HELICES OF THE HERG AND KV1.5 POTASSIUM CHANNELS IN MODEL MEMBRANES

Maïwenn Beaugrand[†], Alexandre A. Arnold[†], Steve Bourgault[†§], Philip T. F. Williamson[‡], and Isabelle Marcotte[†]

†Department of Chemistry, Université du Québec à Montréal, P.O. Box 8888, Downtown Station, Montreal, H3C 3P8, Canada

‡Centre for Biological Sciences/Institute of Life Sciences, Highfield Campus, University of Southampton, Southampton, SO17 1BJ, United Kingdom

§Quebec Network for Research on Protein Function, Structure, and Engineering, PROTEO

Foreword

Maïwenn Beaugrand carried out the experiments, analyzed the results, conducted the literature research and wrote the manuscript with the help of Doctor Alexandre A. Arnold and Professors Philip T. F. Williamson and Isabelle Marcotte.

Résumé

Le syndrome du QT long (SQTL) est un dysfonctionnement cardiaque qui prolonge l'intervalle de repolarisation du cœur, pouvant amener à des arythmies cardiaques et à la mort subite. Cette pathologie est induite par des mutations ou acquise par la liaison hors cible de médicaments bloquant les canaux potassiques du *human ether-a-go-go related gene* (hERG). Pour réduire les risques du SQTL acquis, les autorités réglementaires requièrent des tests *in vitro* pour tous les nouveaux médicaments vérifiant leur potentiel à bloquer les canaux hERG. De nombreuses mutations associées au SQTL et les sites de liaison de médicament présumés qui conduisent au blocage du canal ont été repérés sur l'hélice du pore, suggérant qu'il joue un rôle clé dans cette pathologie. De plus, il est connu que la présence de lipides spécifiques a un rôle potentiel dans la régulation du processus d'ouverture et de fermeture du pore des canaux potassiques. Pour approfondir notre compréhension moléculaire de cette pathologie, nous avons étudié le comportement de l'hélice du pore dans des membranes zwitterioniques et anioniques utilisant une approche combinée avec dichroïsme circulaire et RMN de l'état solide. Tout d'abord nous avons étudié la structure secondaire par dichroïsme circulaire de l'hélice du pore du hERG, en la comparant à celle d'un autre canal potassique typique, $K_v1.5$, dans différents milieux (tampon, micelles et bicelles). Dans les membranes modèles, les hélices du pore étaient principalement en structure α-hélicoïdale. Dans un deuxième temps, les interactions des hélices du pore de hERG ou de $K_v1.5$ ont été étudiées par RMN de

l'état solide du phosphore et du deutérium. L'hélice du pore du hERG a une plus forte affinité avec la bicouche anionique. Ensemble, ces résultats suggèrent un rôle potentiel des lipides anioniques sur la fonction de l'hélice du pore du hERG.

Abstract

Long QT syndrome (LQTS) is a cardiac dysfunction that prolongs the heart repolarization interval, leading to cardiac arrhythmia or failure. This pathology can be induced by mutations or acquired through the off-target binding of drugs that block the human ether-a-go-go related gene (hERG) potassium channels. To reduce the risks of acquired LQTS, regulatory authorities demand *in vitro* testing of all new drug entities for hERG-blocking potential. Many of the mutations associated with LQTS and putative drug binding sites that lead to channel block have been mapped to the pore helix, suggesting that it plays a key role in defining the pathology. Moreover, the presence of specific lipids have potential role in the regulation of the gating process on several potassium channels. To further our molecular understanding of this pathology we have investigated the pore-helix in both zwitterionic and anionic model membranes using a combined circular dichroism and solid-state NMR approach. Firstly, we have studied the secondary structure of the hERG pore-helix by circular dichroism, comparing it to that of another typical potassium channel - Kv1.5 - in different environments (buffer, micelles and bicelles). In both model membranes the pore-helices were predominantly α-helical in structure. Secondly, interactions of the hERG or Kv1.5 pore-helices with the membrane were investigated using ^{31}P and ^{2}H solid-state NMR. The hERG pore-helix has a stronger affinity with anionic bilayers. Together, these results suggest a potential role of anionic lipids on the hERG pore-helix function.

5.1 Introduction

The human ether-a-go-go related gene (hERG) voltage-gated potassium channels are located in the myocardium cell membranes and responsible for the I_{Kr} current (Tamargo *et al.*, 2004; Wulff *et al.*, 2010) essential for the repolarization following the cardiac action potential (Pearlstein *et al.*, 2003; Sanguinetti *et al.*, 1995; Wulff *et al.*, 2010). Inhibition of the hERG channel, through mutation (inherited) or the binding of channel blockers (acquired), prolongs the heart repolarization interval, resulting in long QT syndrome (LQTS) - a condition that may lead to cardiac arrhythmia or failure (Kamiya *et al.*, 2006; Pearlstein *et al.*, 2003; Vandenberg *et al.*, 2012). This pathology is of particular importance in drug development as many compounds have been shown to bind off-target to the hERG channel resulting in enhanced risk of acquired LQTS. Indeed, acquired LQTS has led to the withdrawal of several blockbuster medications (Aronov, 2005; Pearlstein *et al.*, 2003), such that regulatory authorities now demand *in vitro* testing of all new drug entities for hERG-blocking potential (Roden & Temple, 2005; Shah, 2008).

The hERG channel is composed of four monomers containing six transmembrane helices each (Sanguinetti *et al.*, 1995). The current structure of this membrane protein is predicted by homology with other voltage-gated K^+ channels (Kutteh *et al.*, 2007; Stansfeld *et al.*, 2007; Subbiah *et al.*, 2004; Tseng *et al.*, 2007) and its structure has never been determined experimentally. The first four helices (S1 to S4) constitute the voltage sensor domain and the last two helices (S5 and S6) compose the pore domain. A longer S5P linker as well as a pore-helix and a K^+ selectivity filter with unique amino acid sequences as compared to other potassium channels are found on the extracellular loop that links S5 to S6 (Vandenberg *et al.*, 2012). Despite the paucity of structural information, mutations in patients with inherited LQTS suggest that inhibition of the channel by drug binding may result from interactions with the pore

helix and thus a clear understanding of its structure and potential interactions with drugs may help reduce these off-target effects.

From homology studies, residues Y_{611} to S_{621} are believed to form an α-helical pore helix within the hERG channel (Figure 5.1A). The most extensive structural studies conducted on the pore helix to date have been done by solution NMR studies with the peptide solubilised into detergent micelles. Interestingly, the pore helix of the hERG channel was extended by three residues on the N-terminal side (K_{608}-S_{621}) in both zwitterionic dodecylphosphocholine (DPC) and anionic sodium dodecylsulfate (SDS) micelles (Pages *et al.*, 2009). This three-residue extension of the pore helix results in the inclusion of three charged residues (K_{608}, D_{609} and K_{610}) that lie at the membrane interface (Pages *et al.*, 2009).

These three residues are absent in a number of other potassium channels (Figure 5.1B-E), many of which are used as templates for the generation of hERG homology models, yet the inclusion of these residues may clearly influence both the structure of the pore helix and its interaction with the bilayer influencing its role in determining channel function. A notable differences between the pore helix in hERG and other K_v channels is the absence of the double W motif (Figure 5.1C) that is thought to contribute to the stability of the selectivity filter in other K^+ channels (Doyle *et al.*, 1998) and are close to the anionic lipid binding site important in regulating channel gating (Alvis *et al.*, 2003; Lee, 2003, 2004; Marius *et al.*, 2008, 2012). Additionally, transmembrane helix 1 of wild-type KcsA and KcsA mutant containing the turret region of Kv1.3, in the presence of phospholipids, was shown to unwind and rewind, inducing conformational changes on the turret region and the pore helix, during the gating process (van der Cruijsen *et al.*, 2013). Moreover, other K_V channels require the presence of specific lipids for potential regulation of the gating, such as sphingomyelin with K_V2.1 (Ramu *et al.*, 2006; Swartz, 2006), anionic phosphatidylinositol 4,5-bisphosphate with K_V7.1 (Zaydman & Cui, 2014; Zaydman

et al., 2013) and anionic phosphatidic acid with $K_V1.2$ channel mutant with its helix-turn-helix segment termed the voltage sensor replaced by the one of $K_V2.1$ (Hite *et al.*, 2014).

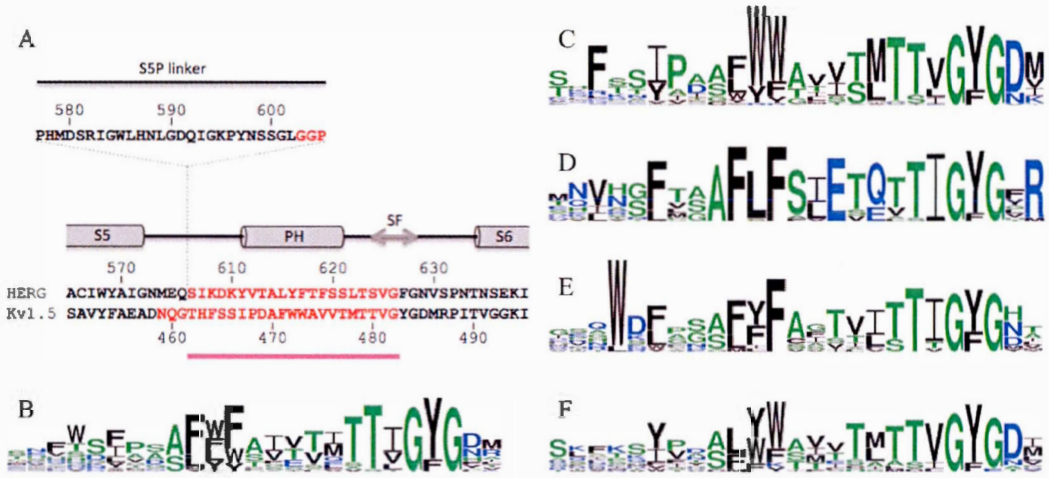

Figure 5.1 (A) Loop connecting the S5 and S6 helices of hERG and $K_V1.5$ with the 24 amino-acid residue peptides used in this study in red. (B-F) Frequency plots of residues corresponding to the purple part in A comprising the pore-helix (PH) and selectivity filter (SF). (B) 22 α subunits of human cardiac potassium channels (Tamargo *et al.*, 2004). (C) 39 human K_V channels. (D) 15 human K_{ir} channels. (E) 14 human K_{2P} channels. (F) 15 prokaryote and eukaryote channels with known structure used in the sequence homology for hERG (Kutteh *et al.*, 2007; Stansfeld *et al.*, 2007; Subbiah *et al.*, 2004; Tseng *et al.*, 2007). The height of the residues represents the frequency with which they occur. The color of the residues represents their hydrophobicity properties with neutral residues in green (S, G, H, T, A, P), hydrophilic residues in blue (R, K, D, E, N, Q) and hydrophobic residues in black (Y, V, M, C, L, F, I, W). The frequency plots were generated with WebLogo 3 (http://weblogo.threeplusone.com/). All sequences used were found on the UniProt website (http://www.uniprot.org/) and are listed in Tables S5.1-S5.5 in the Supplementary Information.

To assess how these major structural changes may influence how the hERG PH interacts with the lipid bilayer, we have undertaken a study to investigate how the hERG pore helix interacts with both zwitterionic and negatively charged lipid membranes. Dimyristoylphosphatidylcholine (DMPC) and dimyristoylphosphatidyl-

serine (DMPS) were selected, since phospholipids with PC headgroup are the most abundant in eukaryotic membrane and PS is an anionic lipid present in human membranes. To determine how the presence of the pore helix influences the polar and apolar regions of the bilayer, ^{31}P and ^{2}H solid-state NMR experiments were performed, respectively. To assess how the bilayer properties influence the structure of the pore helices comparable circular dichroism (CD) studies have been performed. Considering the particular sequence of the hERG channel pore helix, we have performed identical experiments on the pore helix from $K_V1.5$ as a 'typical' representative of the K_V channels as it possesses most of the key residues associated with this family of channels (Figure 5.1C).

5.2 Materials and Methods

5.2.1 Materials

Phospholipids 1,2-dimyristoyl-sn-glycero-3-phosphocholine non deuterated (DMPC) and deuterated (DMPC-d_{54}), 1,2-dimyristoyl-sn-glycero-3-phospho-L-serine (DMPS) as well as detergent n-dodecylphosphocholine (DPC) were purchased from Avanti Polar Lipids (Alabaster, AL, USA) or Anatrace (Maumee, OH, USA) and used without further purification. Deuterium-depleted water was obtained from Sigma Aldrich (Oakville, ON, Canada).

5.2.2 Peptide Synthesis and Purification

$K_V1.5$ (N_{459}-G_{482}) and hERG (G_{603}-G_{626}) pore helix peptides were synthetized on a Tribute peptide synthesizer (Protein Technologies, Tucson, AZ, USA) with standard

Fmoc chemistry using 2-(6-chloro-1-H-benzotriazole-1-yl)-1,1,3,3-tetramethylaminium hexafluorophosphate (HCTU) as a coupling reagent and diisopropylethylamine (DIEA) as a base. Peptides were cleaved from the resin using a mixture of TFA:ethanedithiol:phenol:water (92:2.5:3:2.5; v/v). After filtration and evaporation of the cleavage mixture, peptides were precipitated and washed with diethylether, solubilized in water and lyophilized. Crude peptides were purified by reverse-phase high performance liquid chromatography (RP-HPLC) on a preparative Luna C18 column (250 mm x 21.2 mm; 5µm, 100Å, Phenomenex) using a linear gradient of ACN in H2O/TFA (0.06% v/v). Collected fractions were analyzed by analytical RP-HPLC using an Aeris peptide XB C18 column (150 mm x 4.6 mm; 3.6µm, Phenomenex) and by ESI-TOF mass spectrometry. Fractions corresponding to the desired peptides, as confirmed by mass spectrometry, with purity higher than 95%, measured by analytical HPLC, were finally pooled and lyophilized.

5.2.3 Sample Preparation

Peptides were reconstituted into DPC-based bicelles (Nolandt *et al.*, 2012, Chapter V) as DPC has previously shown to readily solubilize a longer version of the hERG pore helix (S_{600}-I_{642}) (Pages *et al.*, 2009).

For circular dichroism (CD), the appropriate peptide at a concentration *circa* 20 µM was dissolved into 8 mM DPC micelles and Tris HCl 10 mM, pH 7.4 buffer. The sample was then subjected to multiple cycles of freeze (liquid N_2), thaw (60°C) and vortex shaking until a uniform transparent solution was obtained. The DPC concentration was thus about 7 times above the critical micelle concentration (CMC). This mixture was then added to long-chain phospholipid DMPC or DMPC with 10 mol% DMPS, and submitted to further cycles of freeze/thaw/mixing. The total concentration of phospholipid and detergent was approximately 16 mM. The

phospholipid-to-detergent molar ratio (q) was 1 while the phospholipid/peptide molar ratio was 400:1.

For solid-state NMR both bicellar and vesicular samples were studied. Bicelle samples were prepared in a similar way using nanopure water, a peptide concentration of about 5 mM, a total concentration of phospholipid and detergent of 400 mM and a 80% (w/v) hydration. The molar ratio q was 2 while the phospholipid/peptide molar ratio was 50:1. Typically, 50% of the DMPC was deuterated. Vesicles of DMPC and DMPC doped with 10 mol% DMPS at total lipid concentration of 400 mM were prepared. Both peptides and lipids at a phospholipid/peptide molar ratio of 50:1 were solubilised in nanopure water to achieve 80% (w/v) hydration and subjected to multiple cycles of freeze (liquid N_2), thaw (60°C) and vortex shaking until a homogeneous suspension was obtained.

5.2.4 Circular Dichroism Spectroscopy

Far-ultraviolet spectra were recorded using a J-815 CD-spectropolarimeter (Jasco, Easton, MD, USA). Spectra were recorded from 190 to 260 nm at 37°C using a wavelength step of 0.5 nm, scanning speed of 20 $nm.min^{-1}$, bandwidth of 1 nm and a response time of 1 s. For each sample, three scans were averaged and a background of the corresponding model membrane was subtracted. To ascertain the secondary structure contributions to the CD spectra data were analysed using protein basis 7 and the CDSSTR algorithm (Sreerama & Woody, 2000) on the DichroWeb server (Whitmore & Wallace, 2008).

5.2.5 Nuclear Magnetic Resonance (NMR)

^{31}P and ^{2}H solid-state NMR experiments were performed on an Avance III HD 400 MHz spectrometer (Bruker, Milton, ON, Canada) equipped with a 4 mm double-resonance probe. For ^{31}P NMR spectra acquired with or without magic-angle spinning (MAS), a phase cycled Hahn echo pulse sequence (Rance & Byrd, 1983) was used with broadband proton continuous wave decoupling during the acquisition at a field strength of 85 kHz. A $\pi/2$ pulse of 4 μs, an interpulse delay of 27 μs, a recycle delay of 5 s and a dwell time of 10.2 μs were used, and 256 to 2048 scans were acquired. Acquisition times of 30 and 100 ms were used for static and MAS experiments, respectively. Spectra were referenced externally with respect to the signal of 85% phosphoric acid set to 0 ppm. ^{2}H NMR spectra were obtained using a quadrupole echo pulse sequence (Davis *et al.*, 1976) with a $\pi/2$ pulse length of 3 μs, an interpulse delay of 60 μs and a recycle delay of 1 s. Typically 2400 scans were acquired. Following each temperature step the sample was allowed to equilibrate for 10 minutes at the new temperature before the spectrum was acquired. Spectra were acquired at temperatures ranging from 22°C to 62°C. All spectra were processed using MNova software (Mestrelab Research, Santiago de Compostela, Spain) and line broadening of 25 and 50 Hz were used for ^{31}P and ^{2}H spectra, respectively.

5.3 Results and Discussion

5.3.1 Secondary Structure (CD)

To assess how the structure of the pore helices of $K_V1.5$ and hERG responds to changes in lipid environment, CD spectra were recorded in membrane mimetics possessing either a zwitterionic or negative surface charge. More specifically, liposomes and DPC-based bicelles with pure DMPC (Nolandt *et al.*, 2012) and

DMPC with 10 mol% DMPS were used. The detergent DPC was selected for its ability to solubilize membrane proteins (Arora *et al.*, 2001; Damberg *et al.*, 2001; Kallick *et al.*, 1995; Koehler *et al.*, 2010; Oxenoid *et al.*, 2002; Warschawski *et al.*, 2011) and a longer version of the hERG PH (S_{600}-I_{642}) (Pages *et al.*, 2009).

In the absence of lipid membranes, the pore helices were poorly soluble and readily aggregated. In zwitterionic DPC micelles, the pore helices from both hERG and $K_V1.5$ exhibited a classical α-helical spectrum (Figures 5.2A and 5.2B, respectively) with minima at 208 nm and 222 nm and a maximum at 195 nm.

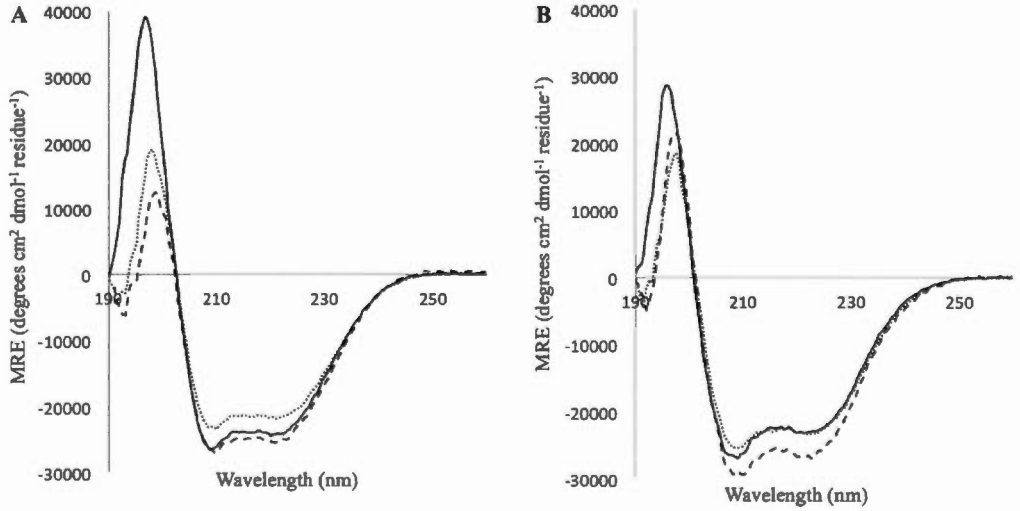

Figure 5.2 Circular dichroism far-UV spectra of the pore helices from (A) hERG and (B) $K_V1.5$ channels reconstituted into 8 mM DPC micelles (solid lines), 16 mM DMPC/DPC 2:1 bicelles (dotted lines) and 16 mM DMPC/DMPS/DPC 1.8:0.2:1 bicelles (dashed lines).

Although an accurate quantitative assessment of secondary structure remains challenging, it can provide a guide as to changes in the secondary structure in response to different environments. Deconvolution of the spectra acquired for the pore helices of the hERG and $K_V1.5$ channels in DPC exhibited 72% and 73% helicity, respectively, with the remainder arising from the contribution of β-strands, turns and random coil structures (Table 5.1).

Table 5.1 Deconvolution of secondary structure contributions to CD spectra of hERG and $K_V1.5$ pore helices in micellar and bicellar environnements of DMPC/DPC (2:1) and DMPC/DMPS/DPC (1.8/0.2/1) using dataset 7 and CDSSTR algorithms on Dichroweb server. α: α-helix, β: β-sheet, T: β-turn, R: random coil and NRMSD: normalized root mean square displacement.

Sample		α	β	T	R	NRMSD
hERG	+ DPC micelle	0.72	0.06	0.09	0.12	0.002
	+ Zwitterionic bicelle	0.67	0.12	0.07	0.15	0.002
	+ Anionic bicelle	0.61	0.18	0.04	0.17	0.002
Kv1.5	+ DPC micelle	0.73	0.09	0.06	0.11	0.003
	+ Zwitterionic bicelle	0.68	0.13	0.07	0.12	0.002
	+ Anionic bicelle	0.64	0.11	0.11	0.14	0.002

When reconstituted into zwitterionic bicelles composed of DMPC/DPC a significant drop in the maximum at 195 nm is observed for both the hERG and $K_V1.5$ with a corresponding fall in helical structure to 67% and 68%, respectively. A further decrease in helicity of about 9 and 6% compared to the zwitterionic bicelle is also observed upon reconstitution into DMPC/DMPS/DPC bicelles, respectively. These observations suggest that in both micellar and bicellar environments the helical structure extends beyond that predicted (see Figure 5.1).

5.3.2 Interaction with Membrane (Solid-State NMR)

Considering the effect of the membrane composition on the structure of the pore helices of the hERG and $K_V1.5$ channels, their interaction with model membranes was studied by solid-state NMR using liposomes and DPC-based magnetically-oriented bicelles. ^{31}P and ^{2}H solid-state NMR report on changes in organization and dynamics of the headgroup and apolar chain regions, respectively.

To determine how the pore helices influenced both the phase behaviour and the dynamics within the lipid headgroup ^{31}P solid-state NMR spectra of zwitterionic lipid bilayers were recorded of DMPC liposomes (Figure 5.3A).

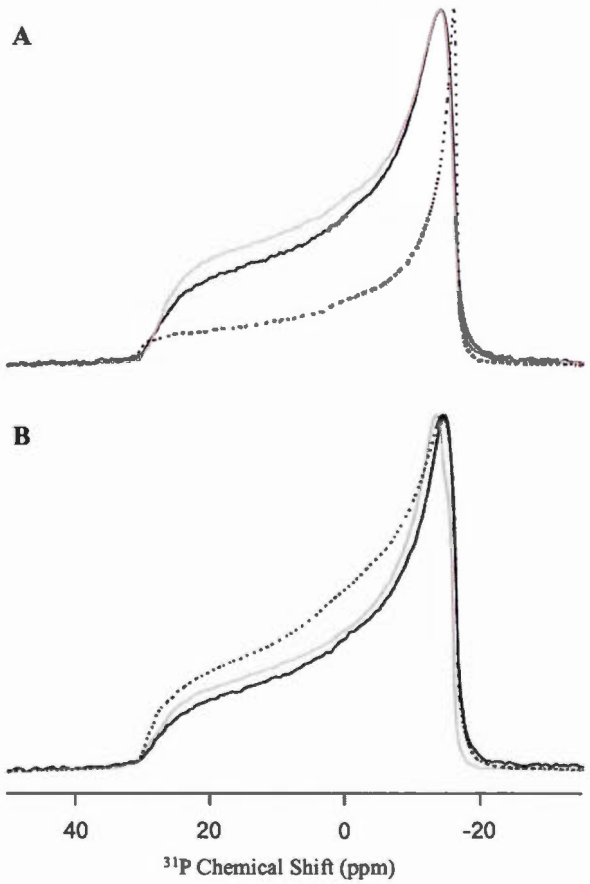

Figure 5.3 ^{31}P solid-state NMR spectra of (A) DMPC and (B) DMPC/DMPS 9:1 liposomes with pore-helix peptides were recorded at 37°C. Vesicles alone (black dotted lines), with hERG (black solid lines) and with $K_V1.5$ (grey solid lines).

The addition of the pore helices from hERG and $K_V1.5$ in DMPC liposomes resulted in a change in intensity between the 0° and 90° edges of the spectrum, with fewer lipids on the 90° edge. This can be ascribed to a change in vesicle shape or transverse relaxation (T_2) effect caused by an increase in slow motions (Dolainsky *et al.*, 1993). As shown in Table 5.2, a 10% decrease of the chemical shift anisotropy is induced by

the presence of the pore helices, indicating an increase in lipid headgroup dynamics. ^{31}P solid-state NMR experiments using MAS have been carried out to verify shielding or deshielding effect of the pore helices on the phospholipids headgroup. As shown in Table 5.2, there is no significant difference of the isotropic chemical shift of DMPC in the presence of the pore helix.

Table 5.2 Perpendicular ($\delta_\perp$) and isotropic (δ_{iso}) chemical shifts are given for liposomes of DMPC and DMPC/DMPS 9:1. The anisotropic tensor ($\bar{\sigma}$) was calculated by: $2(\delta_{iso} - \delta_\perp)$.

Sample	$\delta_\perp$ (ppm)	δ_{iso} (ppm)	$\bar{\sigma}$ (ppm)
Zwitterionic liposome	-15.8	-0.66	30.3
+hERG	-13.9	-0.67	26.5
+K_V1.5	-13.7	-0.67	26.1
Anionic liposome	-14.4	-0.66	27.5
+hERG	-14.4	-0.66	27.5
+K_V1.5	-13.8	-0.66	26.3

To assess how the pore helices interact with zwitterionic bicelles, the peptides were reconstituted into bicelles systems composed of DMPC/DPC (2:1). As expected in pure lipid systems composed of DMPC/DPC (2:1) the system adopts a magnetically aligned phase (Nolandt *et al.*, 2012) demonstrated by the two well-resolved peaks in the ^{31}P NMR spectrum and the well resolved Pake doublets in the ^{2}H NMR spectrum (Figure 5.4A) over a temperature range of 37-42°C (Table 5.3).

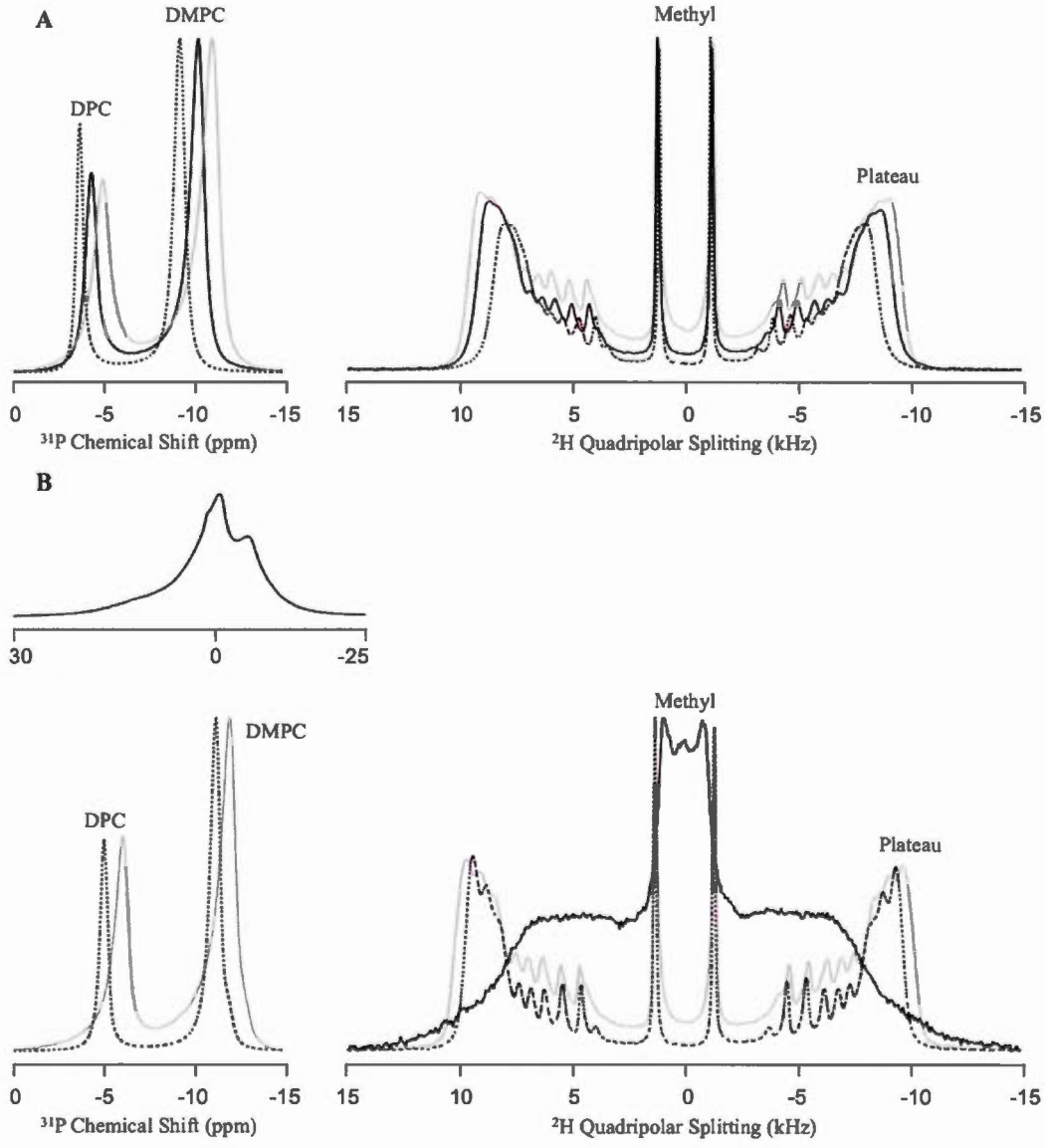

Figure 5.4 ^{31}P (left) and ^{2}H (right) solid-state NMR spectra of (A) DMPC/DPC 2:1 bicelles and (B) DMPC/DMPS/DPC 1.8:0.2:1 bicelles with and without pore-helix peptides recorded at 37°C. Pure bicelles are represented in black dotted lines, with hERG in black full lines and with $K_V1.5$ in grey full line. In panel B, the spectrum obtained in the presence of hERG's pore helix was separated since it covers a broader chemical shift range.

Table 5.3 Effect of the hERG and $K_V1.5$ pore helices on bicelles of DMPC/DPC (2:1) and DMPC/DMPS/DPC (1.8/0.2/1). The left (δ_{left}) and right (δ_{right}) peak chemical shifts, $S_{bilayer}$ (S_{bic}), static and dynamic mosaicities, as well as temperature at which oriented bicelles are observed are reported. Equations to determine the S_{bil} and mosaicities are described in the Supplementary Information, Chapter IV. The data used to calculate the S_{bil}, dynamic mosaicity are reported in Table S5.6. The static mosaicity is estimated with simulation spectra.

Sample	δ_{left} (ppm)	δ_{right} (ppm)	S_{bil}	Static mosaicity	Dynamic mosaicity	Orientation (°C)
Zwitterionic bicelle	-3.7	-9.3	0.58	4	20	37-42
+hERG	-4.4	-10.3	0.72	9	16	27-42
+$K_V1.5$	-5.0	-11.1	0.80	11	14	32-52
Anionic bicelle	-5.1	-11.3	0.77	5	16	27-42
+hERG				Not oriented		
+$K_V1.5$	-6.1	-12.0	0.82	12	13	27-42

The degree of orientation is affected by slow fluctuations around the membrane director that manifests as a distribution of resonances within the spectra and fast fluctuations about the membrane normal that lead to increased averaging of the chemical shielding anisotropy of the phosphate headgroup. The slow fluctuations can be characterised by the static (Arnold *et al.*, 2002) mosaic spread that models the distribution of lipid orientations about a membrane director as a Gaussian distribution. Similarly, the rapid fluctuations can be modelled as a dynamic mosaic spread characterised by a Gaussian distribution of the bicelle order parameter about the membrane normal (Triba *et al.*, 2005; Zandomeneghi *et al.*, 2003). In pure DMPC/DPC bicelles, this gives rise to a static mosaic spread of 4° and a dynamic mosaic spread of 20° (Table 5.3) as previously reported for pure bicellar systems (Zandomeneghi *et al.*, 2003). The addition of the pore helices from hERG and $K_V1.5$ results in an upfield shift in both the DPC and DMPC peaks in the ^{31}P NMR spectra and a broadening of the resonances. An increase in the temperature range over which the magnetically aligned phase is stable is also observed, with the pore helix of $K_V1.5$

extending the range over which a stable bicellar structure forms from 5 to 20 °C (Table 5.3). The changes in resonance position and lineshape indicate that the pore helices increase the static mosaic spread of the bicelles while the dynamic mosaicity is reduced with the most pronounced effects occurring in the case of $K_V1.5$ (Table 5.3). Therefore the interaction of the pore helices seems to slow down the bicelles

The changes in the lipid dynamics in the presence of the pore helices are not restricted to the lipid headgroup since the lipid chains exhibit a similar ordering effect. This is evidenced by the increase in quadrupolar splitting ($\Delta\nu_Q$) of DMPC-d_{54} in zwitterionic bicelles for both the methyl ($\Delta\nu_m$) and plateau ($\Delta\nu_p$) regions of the ^2H NMR spectra. The quadrupolar splitting ($\Delta\nu_Q$) for a C–D bond in a lipid bilayer system with axial symmetry reports on the variations in the lipid chain order since:

$$\Delta\upsilon_Q = \frac{3}{4}\frac{e^2qQ}{h}(3cos^2\theta - 1)S_{CD} \qquad (5.1)$$

where (e^2qQ/h) is the quadrupole coupling constant (~167 kHz), θ is the angle between the bilayer normal and the magnetic field direction, and S_{CD} is the order parameter of a deuterium bond vector. The largest quadrupolar splitting is attributed to the deuterium bonds close to the lipid headgroup (plateau) while the smallest quadrupolar splittings arise from the more mobile (methyl) deuterium atoms at the end of the alkyl chains. Table 5.4 shows an increase in $\Delta\nu_p$ of 8% and 13% for the pore helices of hERG and $K_V1.5$, respectively. The lipid chain ordering goes as far as the terminal methyl where $\Delta\nu_m$ also increases.

Table 5.4 Quadrupolar splitting of the plateau ($\Delta\nu_p$) and methyl ($\Delta\nu_m$) regions of DMPC-d54 into bicelles at 37°C of DMPC/DPC (2:1) and DMPC/DMPS/DPC (1.8/0.2/1).

Sample	$\Delta\nu_p$ (kHz)	Difference (%)	$\Delta\nu_m$ (kHz)	Difference (%)
Zwitterionic bicelle	16.1		2.3	
+hERG	17.4	+8	2.4	+4
+Kv1.5	18.2	+13	2.5	+9
Anionic bicelle	18.9		2.7	
+hERG		Not oriented		
+Kv1.5	19.5	+3	2.7	0

As the activity of a number of K^+ channels (Alvis *et al.*, 2003; Hite *et al.*, 2014; Lee, 2003, 2004; Marius *et al.*, 2008, 2012; Zaydman & Cui, 2014; Zaydman *et al.*, 2013) are known to be influenced by the presence of anionic lipids within the membrane, the pore helices were reconstituted into DMPC/DMPS (9:1) liposomes and ^{31}P NMR spectra recorded to assess how the PHs influenced the phase behaviour and dynamics of the lipid headgroups (Figure 5.3B). PC and PS are miscible (Silvius & Gagné, 1984) and the T_m of the mixture is about 25°C considering the molar fraction and T_m of DMPC (23.9°C) and DMPS (39°C) (Marsh, 2013). Therefore the negatively charged liposomes are in the fluid phase at 37°C. The spectrum shows that the presence of $K_V1.5$'s pore helix modifies the intensity distribution between the 0° and 90° edges, possibly due to a change in lipid headgroup dynamics. Also, the pore helic decreases the CSA of DMPC by about 5%. As observed with DMPC liposomes, ^{31}P NMR experiment with MAS reveals no change in the isotropic chemical shift of DMPC (DMPS could not be resolved). In contrast to the pure DMPC liposomes however, where both the hERG and $K_V1.5$ pore helices brought about a reduction in the CSA, upon the addition of DMPS to the liposomes the largest changes in CSA is with $K_V1.5$ pore helix.

To assess how the pore helix peptides interacted with DPC-based bicelles containing the anionic lipid DMPS, the pore helices were reconstituted into DMPC/DMPS/DPC bicelles (1.8:0.2:1). In the pure lipid system two peaks are resolved in the ^{31}P spectrum (Figure 5.4B), albeit upfield shifted compared to the pure DMPC/DPC system. This suggests a reduced dynamic mosaic spread in presence of DMPS, although little change in the static mosaic spread is seen. The resonance of the anionic lipid is upfield to that of DMPC, as observed by Marcotte *et al.*, 2003 with DMPC/dihexanoylPC (DHPC) bicelles containing 10 mol% DMPS, and appears as a peak shoulder. Upon the addition of the $K_V1.5$'s pore helix, all resonances move upfield and exhibit broadening, similarly to what was observed with DMPC/DPC bicelles (Figure 5.4). This again suggests a greater dynamic mosaicity but reduced dynamic mosaic spread.

Figure 5.4B shows the effect of this pore helix on the negatively-charged bicelles. Only a 3% increase of $\Delta\nu_p$ was detected (Table 5.4), suggesting that the peptide slightly orders the alkyl chain portion close and does not insert deeply in the membrane in the presence of DMPS. It is also possible that the pore helix preferentially interacts with the negatively-charged lipids, thus reducing the effects observed on DMPC, both in the bicelles and the liposomes.

In contrast to the $K_V1.5$ channel, the pore helix of hERG appears to cause significant perturbations to DMPC/DMPS/DPC bicelles. Over the temperature range studied (22-62°C), it proved impossible to identify a pure magnetically aligned phase. As seen in Figure 5.4B, the presence of the hERG pore helix results in a spectrum consistent with phase separation, with one broad resonance displaying a small shoulder downfield to the isotropic chemical shifts of the phospholipids, indicative of an isotropic phase or non-oriented bilayer under quasi-fast-tumbling. These are superimposed on an axially symmetric powder pattern indicative of a non-aligned bilayer phase. This is consistent with the ^2H NMR spectrum which is similar to that

of pure DMPC vesicles, albeit with supressed motion in the alkyl chains, superimposed with the contribution of small and slowly tumbling objects between ±2.5 kHz. These effects suggest that the presence of the anionic lipid DMPS significantly enhances the interaction of the hERG pore helix with the bilayer. The absence of any significant changes in the morphology of the DMPC/DMPS vesicles suggests that in this instance interaction between the hERG pore helix and the bicelle may be facilitated by the solubilisation by DPC.

5.4 Conclusion

Our findings demonstrate that the pore helices from both hERG and $K_V1.5$ adopt a helical conformation when reconstituted into zwitterionic and negatively charged lipid bilayer composed of DMPC/DPC and DMPC/DMPS/DPC respectively similar to that previously observed in detergent micelles (Pages *et al.*, 2009). Although the differences are slight, both peptides become less helical upon the incorporation of anionic lipids into the bilayer. Despite the peptides exhibiting similar structural changes upon the introduction of anionic lipids into the bicelles, the manner in which they interact with the bilayer differs significantly. The $K_V1.5$ pore helix interacts more strongly with zwitterionic bicelles, increasing the order within the headgroup and chain regions significantly more than the hERG pore helix. In contrast, the hERG interacts more extensively with the negatively charged lipid bilayers with significant changes in both the headgroup and chain region consistent with a reduction in lipid mobility and/or disruption of the bilayer phase. These properties can in part be explained by the amino acid sequence with $K_V1.5$ exhibiting a higher hydrophobicity (Fauchère & Pliska, 1983) and lower hydrophobic moment (Eisenberg *et al.*, 1982) than the hERG pore helix. Similarly the hERG exhibits a net positive charge

compared to the $K_V1.5$ helix that would favour its interaction with the negatively charged lipids (Table 5.5).

Table 5.5 Hydrophobicity, hydrophobic moment and net charge of the pore-helix peptides were calculated with HeliQuest website (http://heliquest.ipmc.cnrs.fr/).

Segment	Hydrophobicity	Hydrophobic moment	Net charge
hERG (Y_{611}-S_{621})	0.834	0.261	0
hERG (K_{608}-S_{621})	0.459	0.206	+1
Kv1.5 (I_{467}-T_{477})	1.033	0.203	-1

When studying fragments of the whole channel, care must be taken when extrapolating to the functional relevance of our findings to the whole channel. Based on our current structural understanding of K^+ channels the pore helices are accessible to the local bilayer, and thus the interactions of the hERG channel with the anionic lipids and the proximity of the KDK motif to the surface of the bilayer suggest that these interactions may contribute to channel regulation. Interestingly, the region corresponding to the KDK motif of hERG is located close to anionic lipid binding sites that have been identified on other K^+ channels (Alvis *et al.*, 2003; Lee, 2003, 2004; Marius *et al.*, 2008, 2012) suggesting that these residues may play a role in the regulation of the hERG channel.

Acknowledgments

This work was supported by the Natural Sciences and Engineering Research Council (NSERC) of Canada. M.B. wishes to thank the Université du Québec à Montréal, the Training Program in Bionanomachines (Bionano) (NSERC), and the Canadian Institutes of Health Research Strategic Training Initiative in Chemical Biology.

Phuong Trang Nguyen is gratefully acknowledged for the peptide synthesis and purification. I.M. and S.B. are members of the Centre Québécois sur les Matériaux Fonctionnels (CQMF), the Bionano program and the Groupe de Recherche Axé sur la Structure des Protéines (GRASP). S.B. is a member of the Quebec Network for Research on Protein Function, Structure, and Engineering, PROTEO.

Supporting Information

Lists of the pore helix sequences of the human cardiac potassium channels, prokaryotic and eukaryotic channels with known structure used in the sequence homology for hERG, human K_V channels, human K_{ir} channels and human K_{2P} channels.

Table S5.1 List of α-subunit of human cardiac potassium channels (Tamargo *et al.*, 2004) used for the frequency plot in Figure 5.1B. All sequences data are from UniProt website (http://www.uniprot.org/). AN is for accession number while start and end correspond to the position of the first and last residue of the sequence given.

Protein short name	Gene name	Uniprot AN	Sequence	Start	End
Kv1.4	KCNA4	P22459	THFQSIPDAFWWAVVTMTTVGYGDM	506	530
Kv1.5	KCNA5	P22460	THFSSIPDAFWWAVVTMTTVGYGDM	462	486
Kv1.7	KCNA7	Q96RP8	SHFTSIPESFWWAVVTMTTVGYGDM	340	364
Kv4.1	KCND1	Q9NSA2	TNFTSIPAAFWYTIVTMTTLGYGDM	354	378
Kv4.2	KCND2 / KIAA1044	Q9NZV8	SKFTSIPAAFWYTIVTMTTLGYGDM	352	376
Kv4.3	KCND3	Q9UK17	SKFTSIPASFWYTIVTMTTLGYGDM	349	373
Kv6.2	KCNG2	Q9UJ96	RDFSSVPASYWWAVISMTTVGYGDM	351	375
Kv7.1 / KvLQT1	KCNQ1 / KCNA8	P51787	VEFGSYADALWWGVVTVTTIGYGDK	294	318
Kv11.1 / hERG	KCNH2 / ERG1	Q12809	SIKDKYVTALYFTFSSLTSVGFGNV	606	630
Kir2.1 / IRK-1	KCNJ2 / IRK1	P63252	SEVNSFTAAFLFSIETQTTIGYGFR	124	148
Kir2.2 / IRK-2	KCNJ12 / IRK2	Q14500	MQVHGFMAAFLFSIETQTTIGYGLR	125	149
Kir3.1 / GIRK-1	KCNJ3 / GIRK1	P48549	ANVYNFPSAFLFFIETEATIGYGYR	125	149
Kir3.4 / GIRK-4	KCNJ5 / GIRK4	P48544	ENLSGFVSAFLFSIETETTIGYGFR	131	155
Kir6.2 / IKATP	KCNJ11	Q14654	TSIHSFSSAFLFSIEVQVTIGFGGR	112	136
K2P1.1 / TWIK-1	KCNK1 / TWIK1	O00180	NWNWDFTSALFFASTVLSTTGYGHT	99	123
K2P2.1 / TREK-1	KCNK2 / TREK1	O95069	ISHWDLGSSFFFAGTVITTIGFGNI	139	163
K2P3.1 / TASK-1	KCNK3 / TASK1	O14649	GVQWRFAGSFYFAITVITTIGYGHA	75	99
K2P5.1 / TASK-2	KCNK5 / TASK2	O95279	FNNWNWPNAMIFAATVITTIGYGNV	80	104
K2P6.1 / TWIK-2	KCNK6 / TWIK2	Q9Y257	DPAWDFASALFFASTLITTVGYGYT	88	112
K2P9.1 / TASK-3	KCNK9 / TASK3	Q9NPC2	GVQWKFAGSFYFAITVITTIGYGHA	75	99
K2P10-1 / TREK-2	KCNK10 / TREK2	P57789	SSHWDLGSAFFFAGTVITTIGYGNI	149	173
K2P13.1 / THIK-1	KCNK13	Q9HB14	IEGWSYFDSLYFCFVAFSTIGFGDL	219	243
K2P17.1 / TASK-4	KCNK17 / TASK4	Q96T54	MGRWELVGSFFFSVSTITTIGYGNL	98	122

Table S5.2 List of human Kv channels used for the frequency plot in Figure 5.1C. All sequences data are from UniProt website (http://www.uniprot.org/). AN is for accession number while start and end correspond to the position of the first and last residue of the sequence given.

Protein short name	Gene name	Uniprot AN	Sequence	Start	End
Kv1.1	KCNA1	Q09470	SHFSSIPDAFWWAVVSMTTVGYGDM	354	378
Kv1.2	KCNA2	P16389	SQFPSIPDAFWWAVVSMTTVGYGDM	356	380
Kv1.3	KCNA3	P22001	SGFSSIPDAFWWAVVTMTTVGYGDM	426	450
Kv1.4	KCNA4	P22459	THFQSIPDAFWWAVVTMTTVGYGDM	506	530
Kv1.5	KCNA5	P22460	THFSSIPDAFWWAVVTMTTVGYGDM	462	486
Kv1.6	KCNA6	P17658	SLFPSIPDAFWWAVVTMTTVGYGDM	404	428
Kv1.7	KCNA7	Q96RP8	SHFTSIPESFWWAVVTMTTVGYGDM	340	364
Kv1.8	KCNA10	Q16322	SHFSSIPDGFWWAVVTMTTVGYGDM	403	427
Kv2.1	KCNB1	Q14721	TKFKSIPASFWWATITMTTVGYGDI	359	383
Kv2.2	KCNB2	Q92953	TKFTSIPASFWWATITMTTVGYGDI	363	387
Kv3.1	KCNC1	P48547	THFKNIPIGFWWAVVTMTTLGYGDM	382	406
Kv3.2	KCNC2	Q96PR1	TQFKNIPIGFWWAVVTMTTLGYGDM	419	443
Kv3.3	KCNC3	Q14003	TYFKNIPIGFWWAVVTMTTLGYGDM	485	509
Kv3.4	KCNC4	Q03721	TDFKNIPIGFWWAVVTMTTLGYGDM	418	442
Kv4.1	KCND1	Q9NSA2	TNFTSIPAAFWYTIVTMTTLGYGDM	354	378
Kv4.2	KCND2	Q9NZV8	SKFTSIPAAFWYTIVTMTTLGYGDM	352	376
Kv4.3	KCND3	Q9UK17	SKFTSIPASFWYTIVTMTTLGYGDM	349	373
Kv5.1	KCNF1	Q9H3M0	TLFKSIPQSFWWAIITMTTVGYGDI	352	376
Kv6.1	KCNG1	Q9UIX4	PEFTSIPACYWWAVITMTTVGYGDM	406	430
Kv6.2	KCNG2	Q9UJ96	RDFSSVPASYWWAVISMTTVGYGDM	351	375
Kv6.3	KCNG3	Q8TAE7	KDFTSIPAACWWVIISMTTVGYGDM	355	379
Kv6.4	KCNG4	Q8TDN1	LEFTSIPASYWWAIISMTTVGYGDM	400	424
Kv7.1 / KvLQT1	KCNQ1	P51787	VEFGSYADALWWGVVTVTTIGYGDK	294	318
Kv7.2 / KvLQT2	KCNQ2	O43526	DHFDTYADALWWGLITLTTIGYGDK	259	283
Kv7.3 / KvLQT3	KCNQ3	O43525	EEFETYADALWWGLITLATIGYGDK	298	322
Kv7.4 / KvLQT4	KCNQ4	P56696	SDFSSYADSLWWGTITLTTIGYGDK	265	289
Kv7.5 / KvLQT5	KCNQ5	Q9NR82	KEFSTYADALWWGTITLTTIGYGDK	293	317
Kv8.1	KCNV1	Q6PIU1	TTFTSVPCAWWWATTSMTTVGYGDI	374	398
Kv8.2	KCNV2	Q8TDN2	TNFTTIPHSWWWAAVSISTVGYGDM	439	463
Kv9.1	KCNS1	Q96KK3	VGFNTIPACWWWGTVSMTTVGYGDV	403	427
Kv9.2	KCNS2	Q9ULS6	EGLATIPACWWWATVSMTTVGYGDV	356	380
Kv9.3	KCNS3	Q9BQ31	SSLTSIPICWWWATISMTTVGYGDT	352	376

Kv10.1 / hEAG1	KCNH1 / EAG1	O95259	SKNSVYISSLYFTMTSLTSVGFGNI	445	469
Kv10.2 / hEAG2	KCNH5 / EAG2	Q8NCM2	SKDSLYVSSLYFTMTSLTTIGFGNI	414	438
Kv11.1 / hERG	KCNH2 / ERG1	Q12809	SIKDKYVTALYFTFSSLTSVGFGNV	606	630
Kv11.2 / hERG2	KCNH6 / ERG2	Q9H252	SVQDKYVTALYFTFSSLTSVGFGNV	458	482
Kv11.3 / hERG-3	KCNH7	Q9NS40	SRSRESLCSIRRASSVHDIEGFGVH	261	285
Kv12.1	KCNH8	Q96L42	SIRSAYIAALYFTLSSLTSVGFGNV	416	440
Kv12.2	KCNH3	Q9ULD8	SLRSAYITSLYFALSSLTSVGFGNV	447	471
Kv12.2	KCNH3	Q9ULD8	SLRSAYITSLYFALSSLTSVGFGNV	447	471

Table S5.3 List of human Kir channels used for the frequency plot in Figure 5.1D. All sequences data are from UniProt website (http://www.uniprot.org/). AN is for accession number while start and end correspond to the position of the first and last residue of the sequence given.

Protein short name	Gene name	Uniprot AN	Sequence	Start	End
Kir1.1 / ROM-K	KCNJ1 / ROMK1	P48048	ENINGLTSAFLFSLETQVTIGYGFR	123	147
Kir1.2 / Kir4.1	KCNJ10	P78508	VQVHTLTGAFLFSLESQTTIGYGFR	110	134
Kir1.3 / Kir4.2	KCNJ15 / KCNJ14	Q99712	MKVDSLTGAFLFSLESQTTIGYGVR	109	133
Kir2.1 / IRK-1	KCNJ2 / IRK1	P63252	SEVNSFTAAFLFSIETQTTIGYGFR	124	148
Kir2.2 / IRK-2	KCNJ12 / IRK2	Q14500	MQVHGFMAAFLFSIETQTTIGYGLR	125	149
Kir2.3 / IRK-3	KCNJ4 / IRK3	P48050	MHVNGFLGAFLFSVETQTTIGYGFR	116	140
Kir2.4 / IRK-4	KCNJ14 / IRK4	Q9UNX9	SHVASFLAAFLFALETQTSIGYGVR	129	153
Kir2.6	KCNJ18	B7U540	MQVHGFMAAFLFSIETQTTIGYGLR	125	149
Kir3.1 / GIRK-1	KCNJ3 / GIRK1	P48549	ANVYNFPSAFLFFIETEATIGYGYR	125	149
Kir3.2 / GIRK-2	KCNJ6 / GIRK2	P48051	TNLNGFVSAFLFSIETETTIGYGYR	134	158
Kir3.3 / GIRK-3	KCNJ9 / GIRK3	Q92806	NNLNGFVAAFLFSIETETTIGYGHR	102	126
Kir3.4 / GIRK-4	KCNJ5 / GIRK4	P48544	ENLSGFVSAFLFSIETETTIGYGFR	131	155
Kir5.1	KCNJ16	Q9NPI9	DNVHSFTGAFLFSLETQTTIGYGYR	113	137
Kir6.1 / uKATP-1	KCNJ8	Q15842	TNVRSFTSAFLFSIEVQVTIGFGGR	122	146
Kir6.2 / IKATP	KCNJ11	Q14654	TSIHSFSSAFLFSIEVQVTIGFGGR	112	136
Kir7.1	KCNJ13	O60928	KYITSFTAAFSFSLETQLTIGYGTM	101	125

Table S5.4 List of human K2P channels used for the frequency plot in Figure 5.1E. All sequences data are from UniProt website (http://www.uniprot.org/). AN is for accession number while start and end correspond to the position of the first and last residue of the sequence given.

Protein short name	Gene name	Uniprot AN	Sequence	Start	End
K2P1.1 / TWIK-1	KCNK1 / TWIK1	O00180	NWNWDFTSALFFASTVLSTTGYGHT	99	123
K2P2.1 / TREK-1	KCNK2 / TREK1	O95069	ISHWDLGSSFFFAGTVITTIGFGNI	139	163
K2P3.1 / TASK-1	KCNK3 / TASK1	O14649	GVQWRFAGSFYFAITVITTIGYGHA	75	99
K2P4.1 / TRAAK	KCNK4 / TRAAK	Q9NYG8	HSAWDLGSAFFFSGTIITTIGYGNV	85	109
K2P5.1 / TASK-2	KCNK5 / TASK2	O95279	FNNWNWPNAMIFAATVITTIGYGNV	80	104
K2P6.1 / TWIK-2	KCNK6 / TWIK2	Q9Y257	DPAWDFASALFFASTLITTVGYGYT	88	112
K2P7.1	KCNK7	Q9Y2U2	GRTWDLPSALLFAASILTTTGYGHM	87	111
K2P9.1 / TASK-3	KCNK9 / TASK3	Q9NPC2	GVQWKFAGSFYFAITVITTIGYGHA	75	99
K2P10.1 / TREK-2	KCNK10 / TREK2	P57789	SSHWDLGSAFFFAGTVITTIGYGNI	149	173
K2P12.1 / THIK-2	KCNK12	Q9HB15	RPRWDFPGAFYFVGTVVSTIGFGMT	111	135
K2P13.1 / THIK-1	KCNK13	Q9HB14	IEGWSYFDSLYFCFVAFSTIGFGDL	219	243
K2P15.1 / TASK-5	KCNK15	Q9H427	GRQWKFPGSFYFAITVITTIGYGHA	75	99
K2P16.1 / TALK-1	KCNK16 / TALK1	Q96T55	VEGWSFSEGFYFAFITLSTIGFGDY	194	218
K2P17.1 / TASK-4	KCNK17 / TASK4	Q96T54	MGRWELVGSFFFSVSTITTIGYGNL	98	122
K2P18.1	KCNK18	Q7Z418	ETQLDFENAFYFCFVTLTTIGFGDT	305	329

Table S5.5 List of prokaryotic and eukaryotic channels with known structure used in the sequence homology for hERG (Kutteh *et al.*, 2007; Stansfeld *et al.*, 2007; Subbiah *et al.*, 2004; Tseng *et al.*, 2007) and used for the frequency plot in Figure 5.1F. All sequences data are from UniProt website (http://www.uniprot.org/). AN is for accession number while start and end correspond to the position of the first and last residue of the sequence given.

Protein short name	Uniprot AN	Organism	Sequence	Start	End
AKT1	Q38998	*Arabidopsis thaliana*	SLWMRYVTSMYWSITTLTTVGYGDL	235	259
CNG1	P29973	*Homo sapiens*	RLARKYVYSLYWSTLTLTTIG-ETP	344	367
EAG / d-eag	Q02280	*Drosophila melanogaster*	SRKSMYVTALYFTMTCMTSVGFGNV	435	459
HCN1 / BCNG-1	O60741	*Homo sapiens*	SWGKQYSYALFKAMSHMLCIGYGAQ	340	364
KcsA / KCS1	P0A334	*Streptomyces lividans*	AQLITYPRALWWSVETATTVGYGDL	57	81
KirBac1.1	P83698	*Pseudomonas pseudomallei*	QSPPGFVGAFFFSVETLATVGYGDM	92	116
Kv2.1 / h-DRK1	Q14721	*Homo sapiens*	TKFKSIPASFWWATITMTTVGYGDI	359	383
Kv4.3	Q9UK17	*Homo sapiens*	SKFTSIPASFWYTIVTMTTLGYGDM	349	373
Kv10.1 / hEAG1	O95259	*Homo sapiens*	SKNSVYISSLYFTMTSLTSVGFGNI	445	469
KvAP	Q9YDF8	*Aeropyrum pernix*	SSIKSVFDALWWAVVTATTVGYGDV	191	215
MthK	O27564	*Methanothermobacter thermautotrophicus*	---ESWTVSLYWTFVTIATVGYGDY	44	65
PAK1	Q9U001	*Paramecium tetraurelia*	DLYTKYFNSLYWITITSMTVGYGDI	301	325
rKv1.2	P63142	*Rattus norvegicus*	SQFPSIPDAFWWAVVSMTTVGYGDM	356	380
Shaker	P08510	*Drosophila melanogaster*	SFFKSIPDAFWWAVVTMTTVGYGDM	424	448
T. er	Q10V66	*Trichodesmium erythraeum*	GTRTQYINCLYWAITTLTTVGYGDI	194	218

Table S5.6 Values for the anisotropic tensor ($\bar{\delta}$) components : σ_{xx}, σ_{yy} and σ_{zz} were obtained by spectra simulation. The isotropic part (σ_{iso}) and the anisotropic tensor were defined as $\sigma_{iso} = \frac{1}{3}(\sigma_{xx} + \sigma_{yy} + \sigma_{zz})$ and $\bar{\sigma} = 2\times(\sigma_{zz} - \sigma_{iso})$, respectively.

Sample	$\sigma_{xx} = \sigma_{yy}$ (ppm)	σ_{zz} (ppm)	σ_{iso} (ppm)	$\bar{\sigma}$ (ppm)
Zwitterionic liposome	-7.45	15.40	0.17	30.46
+hERG	-6.67	13.33	0.00	26.66
+Kv1.5	-6.54	13.17	0.03	26.28
Anionic liposome	-6.73	14.56	0.37	28.38
+hERG	-6.89	14.33	0.18	28.30
+Kv1.5	-6.64	13.56	0.09	26.94

CHAPTER VI

EXPRESSION AND FUNCTIONAL CHARACTERIZATION OF THE PORE DOMAIN FROM THE EUKARYOTIC POTASSIUM CHANNEL, HERG

Maïwenn Beaugrand[†], Luke S. Evans[‡], Sumit Kalsi[§], Andrée E. Gravel[†], Christopher D. Johnson[‡], J. Neville Wright[‡], Jason C. Young[‖], Declan A. Doyle[‡], Maurits R. R. de Planque[§], Isabelle Marcotte[†] and Philip T. F. Williamson[‡]

†Department of Chemistry, Université du Québec à Montréal, P.O. Box 8888, Downtown Station, Montreal, H3C 3P8, Canada

‡Centre for Biological Sciences/Institute of Life Sciences, Highfield Campus, University of Southampton, Southampton, SO17 1BJ, United Kingdom

§Electronics and Computer Science, Highfield Campus, University of Southampton, Southampton, SO17 1BJ, United Kingdom

‖Department of Biochemistry, McGill University, Montreal, H3G 0B1, Canada

Foreword

Maïwenn Beaugrand carried out the majority of the experiments and analyzed the results. Andrée E. Gravel made the hERG pore domain plasmid under the supervision of Professor Jason C. Young. Luke S. Evans and Christopher D. Johnson collaborated in the development of the expression and purification protocol. Sumit Kalsi performed the electrophysiology measurements under the supervision of Professor Maurits R. R. de Planque. J. Neville Wright was responsible for the mass spectrometry experiment. Maïwenn Beaugrand conducted the literature research and wrote the manuscript with the help of Professors Jason C. Young, Declan A. Doyle, Maurits R. R. de Planque, Isabelle Marcotte and Philip T. F. Williamson.

Résumé

Le gène *human ether-a-go-go related* (hERG) est membre des canaux Kv et est localisé dans les membranes cellulaires du myocarde. Des mutations ou des effets secondaires de médicaments sur cette protéine peuvent induire le syndrome du QT long (SQTL). Cette maladie est un dysfonctionnement du coeur prolongeant l'intervalle de repolarisation et pouvant amener à des arythmies cardiaques et à la mort subite. Pour réduire les risques de ce SQTL acquis, les autorités réglementaires requièrent des tests *in vitro* pour tous les nouveaux médicaments pour leur potentiel à bloquer les canaux hERG. Le domaine du pore du canal hERG est une cible importante des médicaments induisant le SQTL, cependant à ce jour une compréhension moléculaire précise de ces interactions a été entravée par l'absence de données structurelles de haute résolution pour ce canal. Ce problème est en partie lié à la non obtention de haut niveau d'expression et de purification de la protéine. Dans ce papier, nous décrivons un protocole qui permet l'expression et la purification de quantités de l'ordre du milligramme du domaine du pore du canal hERG (Asp^{540}-

Tyr^{673}). L'analyse structurale préliminaire de la protéine révèle qu'avec des micelles de détergent la protéine adopte une structure cohérente avec celle proposée dans la littérature. L'enregistrement d'un seul canal révèle que la reconstitution du domaine du pore de hERG dans des bicouches montre des courants similaires à ceux observés dans la protéine entière. En dépit de l'absence de l'important domaine sensible au voltage, nous pensons que ce système fournira des indications pertinentes sur la structure et la pharmacologie du domaine du canal hERG, contribuant à la compréhension du LQTS acquis.

Abstract

The human ether-a-go-go related gene (hERG) is a member of the Kv channels and is located in the myocardium cell membranes. Mutations or off-target effects of drugs on this protein can induce the long QT syndrome (LQTS), which is a cardiac dysfunction that prolongs the heart repolarisation interval, leading to heart arrhythmia or failure. To reduce the risks of this acquired LQTS, regulatory authorities demand *in vitro* testing of all new drug entities for hERG-blocking potential. The pore domain of the hERG channel is an important target of LQTS-prone drugs, but to date a clear molecular understanding of these interactions has been hampered by the absence of high-resolution structural data pertaining to this channel, a problem which in part is due to the intractability of the protein to high-level expression and purification. In this paper we describe a protocol that permits the expression and purification of milligram quantities of the pore domain of the hERG channel (Asp^{540}-Tyr^{673}). Preliminary structural analysis of the protein reveals that with detergent micelles the protein adopts a fold consistent with its proposed structure. Single channel recording reveals that upon reconstitution into lipid bilayers the hERG pore domain exhibits similar currents to those seen in the full-length protein. Despite the absence of the important voltage-sensing domain, we believe that this system will provide valuable insights

into the structure and pharmacology of the pore-domain of the hERG channel, contributing to our understanding of acquired LQTS.

6.1 Introduction

Ion channels are key regulators of cardiac action potential, determining the rate, rhythm and contraction in response to changing demands on cardiac output. The amplitude and length of the cardiac action potential is dependent on the orchestrated flow of Na^+, Ca^{2+} and K^+ ions across the cell membrane, with potassium currents repolarizing the cell and determining the length of the refractory period (Ravens & Cerbai, 2008). Two potassium channels are largely responsible for supporting the currents responsible for cardiomyocytes repolarization hERG ($K_V11.1$/KCNH2) and K_VLQT1 ($K_V7.1$/KCNQ1). Changes in activity of these channels can significantly alter the length of the action potential delay enhancing the possibility of arrhythmia and/or cardiac arrest (Ravens & Cerbai, 2008; Vandenberg *et al.*, 2012).

The central role that the hERG channel plays in determining the rate of cardiomyocyte repolarization has led to extensive investigations into its regulation. *In vivo,* a number of cellular processes regulate hERG channel activity including secondary messengers such as cAMP and PIP_2 (Rodriguez *et al.*, 2010; Vandenberg *et al.*, 2012) as well changes in cellular environment such as oxidative stress, acidosis and hyperkalemia (Vandenberg *et al.*, 2012) all of which can influence the rate of repolarization. The inhibition of the hERG channel and the resulting prolongation of the repolarization period have stimulated great interest. This channelopathy, referred to as long-QT syndrome, can be induced through mutations within the channel or through the binding of drugs (Vandenberg *et al.*, 2012), especially within the pore domain (Aronov, 2005; Mitcheson *et al.*, 2000; Recanatini *et al.*, 2005). The inhibition by drugs resulting in acquired or drug-induced long QT syndrome is a

major concern during the development of pharmaceuticals, with products being removed from the market in the 1990's due to their off-target effects on the hERG channel (Aronov, 2005; Laverty *et al.*, 2011; Redfern *et al.*, 2003; Stummann *et al.*, 2009). Indeed, currently 27% of promising drugs fail to join the market due to off-target binding and inhibition of the hERG channel (Laverty *et al.*, 2011; Stummann *et al.*, 2009). Accordingly, a better understanding of the structural pharmacology and methods for high-throughput screening both *in vitro* and *in silico* would potentially allow such off-target effects to be identified early in the drug development pipeline and be designed out new therapies.

Despite the important role hERG plays in the regulation of the cardiac cycle and its implications in drug development, the relation between structure and function is poorly understood. On the basis of its homology with prokaryotic channels (Mitcheson *et al.*, 2000; Pearlstein *et al.*, 2003; Sanguinetti & Tristani-Firouzi, 2006), it is thought to be a tetramer with each subunit possessing six transmembrane domains (S1-S6). The first four of these (S1-S4) form the voltage-sensing domain of the channel, whilst the last two (S5-S6) form the pore domain responsible for the passage of the ions across the bilayer. To date, the best structural data for this system is a crystal structure of the PAS (acronym for the gene products of Per, Arnt and Sim) domain (amino-acid 1-135) (Adaixo *et al.*, 2013; Li *et al.*, 2010; Morais Cabral *et al.*, 1998) and the cyclic nucleotide binding domain (Haitin *et al.*, 2013). Data on the pore domain is however restricted to the analysis of small sequence fragments by NMR (Chartrand *et al.*, 2010; Gravel *et al.*, 2013; Pages *et al.*, 2009) and a number of homology models (Kutteh *et al.*, 2007; Mitcheson *et al.*, 2000; Sanguinetti & Mitcheson, 2005; Stansfeld *et al.*, 2007; Thai *et al.*, 2010; Tseng *et al.*, 2007). The hERG protein, is however unique within the voltage gated potassium channels, exhibiting unusual gating behaviour (Vandenberg *et al.*, 2012) including fast inactivation and recovery as well as characteristic sensitivities to toxins, drugs and ions (Ceccarini *et al.*, 2012; Gurrola *et al.*, 1999; Ho *et al.*, 1999; Korolkova *et al.*,

2001). These differences reflect the rather low sequence homology of the hERG channel compared to the other K^+ channels, especially with in the S5-S6 segment (Figure 6.1). Indeed, the residues that compose the SF which are highly conserved within the voltage gated potassium channel family of proteins differs (SVGFG as opposed to TVGVG) with significant differences in the supporting hydrogen-bonding network (Doyle *et al.*, 1998; Jiang *et al.*, 2005; Pardo-Lopez *et al.*, 2002). Similarly, S5P linker thought to be responsible for determining the inactivation of the channel, is some 35-38 residues longer in hERG compared to other K+ channels (Tseng *et al.*, 2007; Vandenberg *et al.*, 2012).

It is within the pore domain (S5-S6) that many of the structural determinants that result in both congenital and drug induced long-QT syndrome are thought to reside. Analysis of mutation results in LQTS Type 2 has revealed that many of the identified mutations are localised to the pore domain, with high frequencies also found within the PAS domain (Vandenberg *et al.*, 2012). Similarly, studies of compounds known to result in drug induced long-QT syndrome also indicated the existence of mutations within the channel lining (Aronov, 2005; Thai *et al.*, 2010; Zachariae *et al.*, 2009).

A detailed molecular structure of the hERG channel will clearly aid our understanding of long-QT syndrome allowing the effects of the mutations and the rather promiscuous nature with which drugs interact with this channel to be rationalised. Although extensive functional studies of the hERG channel have been conducted in Xenopus oocytes (Kiehn *et al.*, 1996; Sanguinetti *et al.*, 1995; Trudeau *et al.*, 1995; Wang *et al.*, 1997) and Chinese Hamster Ovary Cells (CHO cells) (Lu *et al.*, 2001; Torres *et al.*, 2003; Vandenberg *et al.*, 2006), structural studies have been compounded by the intractability of the hERG channel to high-level expression. Despite extensive efforts to date, the highest levels of expression were achieved with the transfer of a chimeric hERG construct in *Pichia pastoris* that resulted in the production of microgram quantities of purified protein (Dhillon *et al.*, 2014). Full-

length sodium channels have also proven difficult to express while the expression of pore-only sodium channel constructs has been a successful approach for biophsical characterization (McCusker *et al.*, 2012, 2011; Shaya *et al.*, 2011). Here we report on an expression and purification protocol of the pore-domain of the hERG channel in *E.coli* resulting in milligram quantities of protein. We demonstrate that in the absence of the PAS, the voltage sensing domain and the cyclic nucleotide-binding domain, the pore domain remains folded in detergent and upon reconstitution into lipid bilayers exhibits single channel recordings similar to those observed for the full-length channel with patch clamp electrophysiology. Although, this does not allow us to understand the molecular properties of the channel in full, the high-level expression of the pore-domain will aid in the structural characterisation of the hERG channel and will begin to allow us to rationalise its electrophysiology and pharmacology properties.

6.2 Materials and Methods

6.2.1 Plasmid Construction and Protein Expression

The hERG pore domain (Asp^{540}-Tyr^{673}) was amplified by PCR on a plasmid encoding full-length hERG obtained from Alvin Shrier (McGill University, Canada) using complementary oligonucleotides, 5'- C GGC CGG GAT CCG GAT CGC TAC TCA GAG TAC GGC GCG GC-3' and 5'-C GGG CCG CGG CCG CTA GTA GCG GGC TGT GCC CGA GT-3' (Invitrogen, Burlington, ON, Canada) as forward and reverse primers respectively. The pPROEX-HTa vector (Invitrogen, Burlington, ON, Canada) for the insertion of PCR products were both digested with BamHI and NotI restriction enzymes. The identity of the DNA sequence was confirmed by DNA sequencing (Génome Québec, QC, Canada) and corresponds to the pore domain of the hERG channel as shown in Figure 6.1.

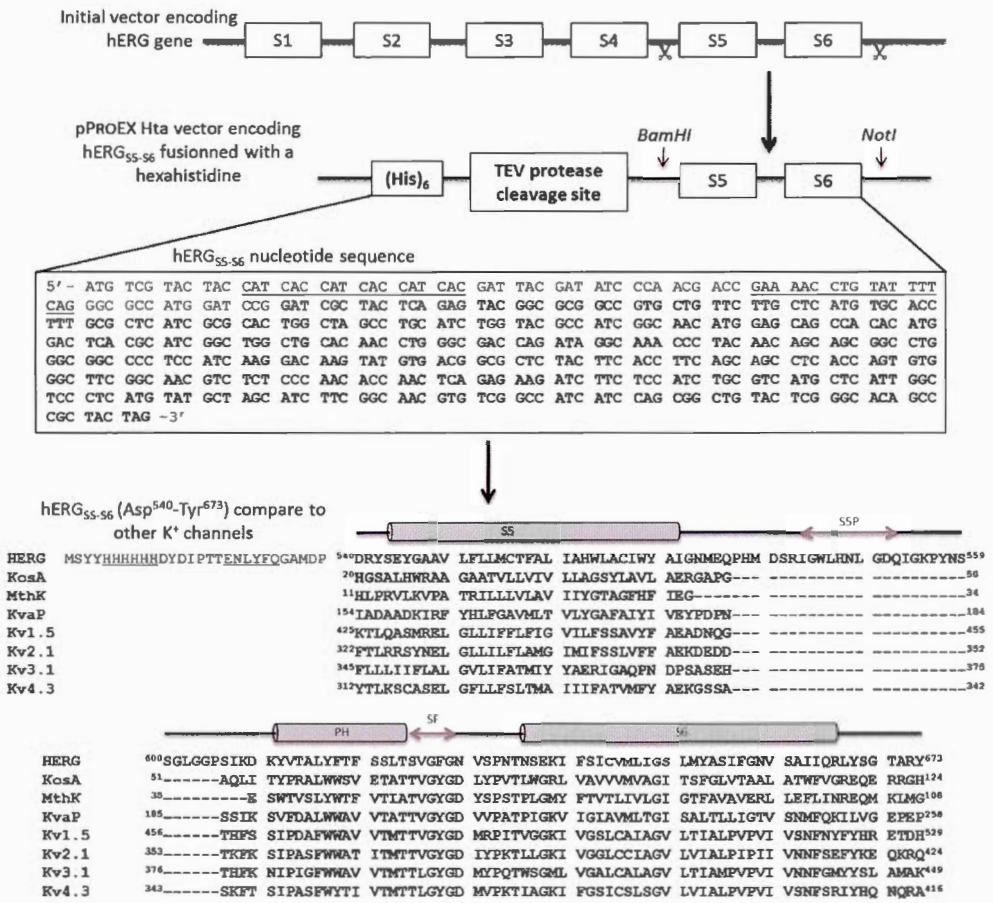

Figure 6.1 Schematic representation of the expression cassette for the His-tagged fusion of the hERG pore domain comprising the 2 transmembrane domains (S5-S6). On the nucleotide and protein sequences, the His tag and then the TEV protease cleavage site are underlined and hERG$_{S5-S6}$ is in bold. The pore domain was also multi-aligned with other K+ channels: three prokaryotic (KcsA, MthK and KvAP) and four eukaryotic (Kv1.5, Kv2.1, Kv3.1 and Kv4.3).

For protein expression, the construct was transformed into BL21 pLysS (Promega, Southampton, UK) and plated on LB agar plates supplemented with 100 $\mu g.mL^{-1}$ ampicillin. The plates were grown over night at 37°C and a single colony was picked and used to inoculate 50 mL of LB media containing 100 $\mu g.mL^{-1}$ ampicillin. The culture was left to grow overnight, and 5 mL was subsequently used to inoculate 500

mL of 2xYT media containing 100 $\mu g.mL^{-1}$ ampicillin. The culture was incubated at 37°C, shaking at 180 rpm, until an OD_{600} of 1.0 was reached. Protein expression was then induced through the addition of isopropyl-β-D-1-thiogalactopyranoside (IPTG, 1mM final concentration) and K+ ion channel activity suppressed through the addition of tetraethyl ammonium bromide (TEAB, 10 mM final concentration). After a further 4 hours the cells were harvested at 4°C by centrifugation at 6,000 g for 20 min and frozen at -20°C until use.

6.2.2 Purification

The pellet from 6 L of *E.coli* was resuspended in 40 mL of phosphate buffered saline (PBS) (140 mM NaCl, 50 mM NaH_2PO_4, 50 mM Na_2HPO_4, pH 7) supplemented with 0.2 $mg.mL^{-1}$ lysozyme, 0.02 $mg.mL^{-1}$ DNase, 1 mM PMSF and 5 mM $MgCl_2$ and incubated for 30 minutes on ice. The cells were subsequently broken by sonication on ice for 6 minutes with a 50% duty cycle. The sample was then centrifuged at 16,000 g for 30 minutes at 4°C to remove unbroken cells and other cellular debris. The supernatant was then decanted and centrifuged at 100,000 g for a further 90 minutes at 4°C resulting in a crude membrane pellet. The pellet was retained and resuspended in 50 mL of extraction buffer (PBS pH 7.4 with 20 mM imidazole, 0.9% w/v Sarkosyl) and left to stir gently in the cold room for 4h. The solubilised fraction was then passed through 0.44 μm filter and loaded onto a pre-equilibrated 1 mL HisTrap column (GE Healthcare Life Sciences, Little Chalfont, UK) on a continuous loop overnight. The column was then washed with 20 mL of wash buffer (PBS, 0.15 % w/v sarkosyl, 20 mM imidazole, pH 7.4) and eluted with elution buffer (PBS, 0.15 % w/v sarkosyl, 600 mM imidazole, pH 7.4). Protein concentration was determined by BCA assay and/or OD280 assuming an extinction coefficient of 35,935 $M^{-1}.cm^{-1}$.

The purity of the samples was ascertained on a 12 % SDS-PAGE gel. Prior to loading samples were heated to 90 °C for 5 minutes in reducing gel loading buffer. Gels were either stained with Commassie Blue and visualised on a Odyssey® Classic Infrared Imaging System (Li-Cor Biosciences Ltd., Cambridge UK) at 700 nm or transferred onto nitrocellulose membranes (1h at 100V) for Western blot analysis. The nitrocellulose membrane was probed with a monoclonal anti-polyhistidine antibody produced in mouse (Sigma-Aldrich Company Ltd., Doreset, UK), which targeted hexahistidine tag. Binding was monitored with the quick Western Kit-IRDye® 680RD and imaged on an Odyssey® Classic Infrared Imaging System at 700 nm.

6.2.3 Mass Spectrometry

The purity of the hERG pore domain was confirmed by mass spectrometry. After the purification, the sample was desalted from imidazole with SpinTrap PD-10 desalting column (GE Healthcare Life Sciences, Little Chalfont, UK) by using a buffer with 0.9 % sarkosyl in water. A volume of desalted sample corresponding to 1 mg of protein was then mixed, with 4 volumes of methanol, 1 volume of chloroform and 3 volumes of water, let on ice for 2 minutes before a 10 minute centrifugation at 8,000 g. The upper fraction was removed carefully because the proteins are at the interface. Then, 3 volumes of methanol were mixed with the lower fraction before another centrifugation of 10 minutes at 8,000 g. The protein pellet was removed from the supernatant and kept on ice before use.

Mass spectra were recorded on an LCT^{TM} (Waters, Elstree, UK) orthogonal acceleration time-of-flight mass spectrometer fitted with a nano-electospray source. The hERG pore domain in DMSO/H_2O/HCOOH (95/4/1) (20 pmol.μl^{-1}, 5 μl) was loaded into borosilicate capillaries (1.2 mm o.d. x 0.69 mm i.d.) (Clark Electromedical Instruments, Reading, UK) that had been drawn to a fine tip using a

microelectrode puller (Narishige, Tokyo, Japan) and sputter-coated with gold/palladium. Spectra were recorded in the positive ion mode between 500–2000 m/z using the following instrument settings: capillary 1200 V, sample cone 40 V, extraction cone 9 V, source temperature 80 °C. Typically, 100 spectra were combined and deconvoluted using the maximum entropy algorithm MaxEnt™ (Micromass, Altrincham, UK) to give relative molecular mass spectra over the range 10,000–50,000 Da at 1 Da resolution. Spectra were externally calibrated using myoglobin spectra recorded under identical conditions immediately after each sample.

6.2.4 Circular Dichroism Spectroscopy

Samples for circular dichroism (CD) spectroscopy were buffer exchanged into 5 mM phosphate buffer, pH 7.4 containing 0.15 % sarkosyl using a PD10 column and had a final concentration of 0.2 $mg.mL^{-1}$. Samples were transferred into a 0.01 mm path length cuvette and far-UV CD spectra recorded from 300 to 190 nm on a Jasco J720 Spectrophotometer (Jasco, Great Dunmow, UK). Spectra were acquired with a scan rate of 100 $nm.minute^{-1}$, with 1 nm step resolution and averaged over 10 accumulations.

6.2.5 Reconstitution for the Electrophysiology

The hERG pore domain was reconstituted into 100% POPG vesicles with a lipid/protein molar ratio of 2,000:1. A solution of DOPC and POPG lipids (1:1 molar ratio, 6 μmoles total lipid) in chloroform solution was dried 2-3h under high vacuum. The resulting lipid film was then hydrated with 1 mL of hydration buffer (150 mM KCl, 10 mM HEPES, pH 7.4) containing 40 mM β-D-octyl glucoside (OG) and

sonicated with a bath sonicator until a clear solution was obtained. Then, 20 μg of hERG pore domain in 0.9% of sarkosyl and PBS buffer was added to the OG-solubilized lipids to give a molar ratio of lipid/hERG tetramer of 2,000:1. Detergent molecules were then removed through the addition of two batches (80 mg each) of SM-2 Biobeads (mesh size 20-50, Bio-Rad, Hemel Hempstead, UK) with 1 hour slow mixing after each addition. The slow removal of the OG and sarkosyl by the Biobeads was associated with the formation of proteoliposomes that were subsequently decanted from the Biobeads and kept on ice until use.

6.2.6 Electrophysiology with Montal Mueller Method

Lipid bilayers were formed in a shaped aperture of ~85 μm diameter in a 50-μm thick sheet of Parylene-coated SU8 photopolymer, as described in (Kalsi *et al.*, 2014). The aperture was pretreated with 5% hexadecane in hexane solution and gently dried under a nitrogen gas flow. The sheet was clamped in between two Teflon chambers of 1.2 mL volume. After filling the chambers with buffer solution (150 mM KCl and 10 mM HEPES pH 7.4), 5 μL of POPG in chloroform solution (20 $mg.mL^{-1}$) was placed on top of the buffer solution and allowed to evaporate (20-25 minutes) to produce a lipid monolayer at the buffer-air interface. Raising and lowering of the buffer solution in both compartments produced a lipid bilayer at the aperture, which was observed as an increase in the measured capacitance. Following formation of a bilayer, 5 μL of a suspension of DOPC/POPG (1/1 molar ratio) vesicles with reconstituted hERG pore domain was added to one chamber, and the current across the membrane was monitored. If channel activity was not observed directly, the bilayer was broken and reformed, adding additional vesicles if necessary. Current and capacitance recordings were performed with Ag/AgCl wire electrodes connected to the CV-103BU headstage of an Axon Axopatch 200B amplifier and Digidata 1440A digitizer. The

bilayer current was measured at 5 kHz bandwidth and digitized at 50 kHz. Data was analyzed with Clampfit 10.4 software after applying a 50 Hz or 20 Hz low-pass 8-pole Bessel filter.

6.3 Results and Discussion

6.3.1 Expression of the hERG Pore Domain

Following transformation into BL21 pLysS, the bacteria were grown to an OD_{600} of 1.0 prior to induction. Conditions for optimal protein expression were determined by monitoring bacterial growth and the levels of protein expression by Western blot analysis. Preliminary studies suggested that induction of expression of the hERG pore domain was toxic to the cell as evidenced by reduced growth rates (data not shown). Over expression of eukaryotic integral membrane proteins is widely acknowledged to be toxic in *E. coli* due to the limited membranes available for protein insertion and significant differences in protein insertion machinery (Martinez Molina *et al.*, 2008; Wagner, 2008; Wagner *et al.*, 2007). In this instance however, we postulated that expression of the function pore domain from hERG would contribute to the toxicity increasing the permeability of the bacterial membrane to K^+ ions. Accordingly, expression was optimised across a range of conditions including reduced temperatures and IPTG levels thereby reducing rates of protein expression potentially allowing greater time for insertion of the membrane protein, and through the addition of sub lethal levels of K^+ channel-blockers such as TEAB to mitigate the effects of hERG pore domain over expression. Finally, optimal bacterial densities and levels of protein expression were obtained following expression for 4 hours at 37 °C in the presence of 1 mM IPTG and 10 mM TEAB as demonstrated by the presence of a

band at approximately 15 kDa, close to the predicted monomeric protein, in the Western blot of the bacterial lysate (Figures 6.2A-B, Lane 2).

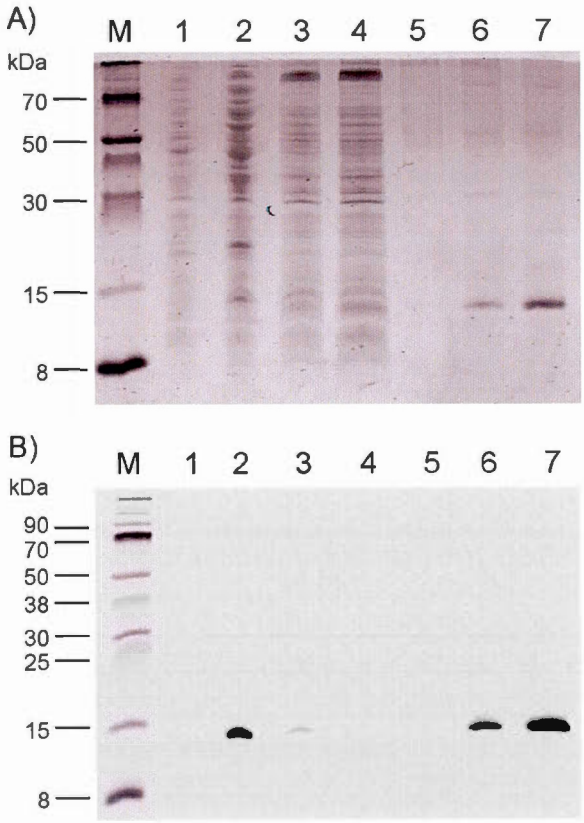

Figure 6.2 Coomassie stained (A) and Western (B) detected SDS-PAGE showing expression and purification of the hERG pore domain. Markers (M); whole cell (pre-induction), lane 1; whole cell (post-induction), lane 2; solubilized membrane fraction, lane 3; Flow through, Lane 4; Column wash, Lane 5; Elution fractions 1 and 2, Lanes 6 and 7 respectively.

Following the solubilisation of the crude membrane fraction in sarkosyl (Figure 6.2A-B, Lane 3), the hERG pore domain is retained in the solubilized material consistent with its expression and insertion into the bacterial membrane. The His tagged hERG pore domain binds with high affinity to the Ni affinity column, with little/no solubilised material apparent in either the Commassie stained gel or the Western blot

of the flow through or column wash. Elution with 600 mM imidazole resulted in strong bands at approximately 15 kDa close to the predicted molecular weight of a subunit from the hERG pore domain (Figure 6.2A-B, Lane 6-7). Typically, 2.5 mg of hERG pore domain were obtained from 1L of *E. coli* culture.

6.3.2 Mass Spectrometry

To confirm the nature of the purified hERG pore domain and ascertain that it was free of any modification we determined the molecular weight by electrospray mass-spectrometry. The predicted mass of the hERG pore domain with a hexahistidine tag preceding the N-terminus is 18,238 kDa (Expasy Protparam (Gasteiger *et al.*, 2003)). The electrospray mass spectrum of the hERG pore domain is shown in Figure 6.3A. Charged species are detected with m/z ratios ranging from +10 to +19. Deconvolution of this spectrum with MaxEnt (Figure 6.3B) (Ferrige *et al.*, 1991) gives rise to two species the first corresponding to a protein with molecular weight 18,106 Da and the second 36,211 Da. The first of these is consistent with the molecular weight predicted for the hERG pore domain and associated affinity tags after the removal of the first methionine during expression. The second of these peaks correspond to the dimeric form of the protein highlighting that even under the harsh conditions under which the mass spectrometry has been conducted there is still a tight association between the hERG subunits. This dimeric peak is not a harmonic artefact of the maximum entropy deconvolution because peaks corresponding to the odd-numbered charge states of the dimer can be seen in the multiply-charged spectrum (Figure 6.3A). These results indicate that the hERG pore domain run anomalously on SDS-PAGE appearing with a molecular weight 3-4 kDa lower than expected.

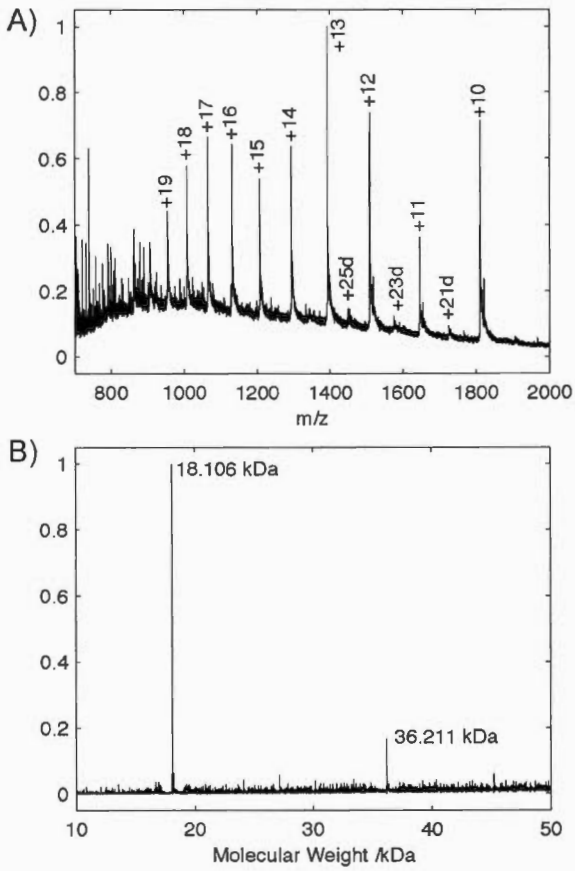

Figure 6.3 Electrospray mass spectrum of $hERG_{S5\text{-}S6}$. (A) Spectrum showing the mass to charge ratios of the species after electrospray mass spectrometry. The labelled peaks indicate the multiply charged states of $hERG_{S5\text{-}S6}$. Charge states labelled 'd' represent those arising from the dimer. Data has been normalised to the value obtained for the largest peak. (B) The deconvoluted spectrum shows two peaks, one at 18.106 kDa corresponding to the molecular weight of the $hERG_{S5\text{-}S6}$ without one methionine and the second one at 36.211 kDa corresponding to the dimer without one methionine per monomer.

6.3.3 Circular dichroism Spectroscopy

CD was used to determine the secondary structure of hERG pore domain in sarkosyl micelles. The spectrum of the hERG pore domain in sarkosyl possesses two minima

at 208 and 220 nm and a maximum at 195 nm consistent with the formation of a predominantly helical structure (Figure 6.4). Secondary structure analysis with the ContinLL with Basis Set 7 in the Dichroweb analysis webserver (Whitmore & Wallace, 2008) returned helical contributions of 48.8%, strands of 6%, turns of 17.4% and unordered of 27.5%. Such an analysis is consistent with the annotation predicted in the UniProt database, suggesting that within the sarkosyl micelles the protein adopts a well-folded conformation.

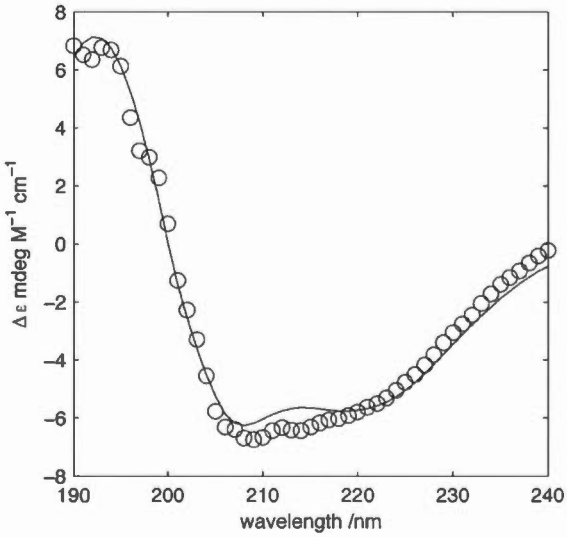

Figure 6.4 CD spectrum of $hERG_{S5\text{-}S6}$ (0.45 $mg.mL^{-1}$) into 0.15% sarkosyl revealing the expected α-helical conformation for the two transmembrane domains of hERG pore domain in detergent. Experimental data (o), with Dichroweb fit of data using basis set 7 (solid line).

6.3.4 Functional Analysis of the hERG Pore Domain

To assess whether the hERG pore domain formed a functional channel, the purified protein was reconstituted into lipid bilayers composed of DOPC/POPG that were fused with a supported lipid bilayer composed on POPG. A representative single

channel recording of the hERG pore domain is shown in Figure 6.5A. The single channel recording shows multiple channel stable opening events, whose duration is in the order of seconds. Histogram analysis of the channel opening shows that the currents are of the order of 20 pA at 150 mV applied potential, with a ±2 pA variation according to half height histogram analysis (Figure 6.5B).

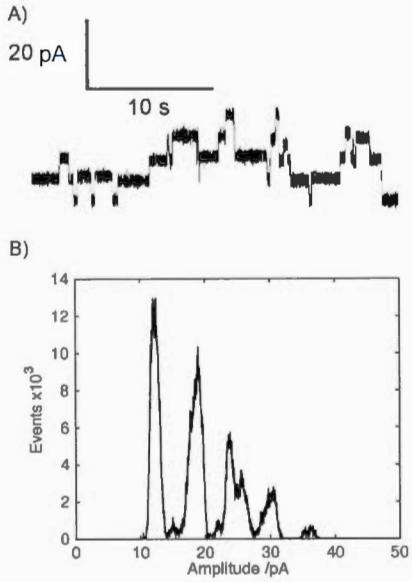

Figure 6.5 Representative single channel recording of the hERG pore domain reconstituted into aperture-suspended POPG bilayers, measurement buffer 150 mM KCl, 10 mM HEPES, pH 7.4, applied voltage 150 mV, low-pass filter 50 Hz (A). Histogram analysis of the conduction events, after applying a 20 Hz low-pass filter, for the pore domain of hERG reconstituted into POPG bilayers (B).

Comparison with single channel patch clamp data of full-length hERG heterologously expressed in *Xenopus* oocyte membranes indicates a slighter high conductance than the full-length channel, although the open state persisted for a similar time window (Kiehn *et al.*, 1996; Liu *et al.*, 2004). As expected, in contrast to the full-length channel possessing the voltage-sensing domain, pronounced rectification was not observed (data not shown).

6.4 Conclusion

A major obstacle to understanding the function and pharmacology of the hERG K+ channel at the molecular level has been the absence of a suitable expression and purification strategy with which to obtain functional channels in quantities sufficient to support biophysical studies. Here we describe, a readily scalable protocol for the expression and purification of the hERG pore domain that allows the extraction of milligrams of protein per litre of culture. Preliminary biophysical characterisation indicates that upon isolation the pore domain retains its native fold. Furthermore, upon reconstitution into lipid bilayers, single channel recordings demonstrate that the pore domain exibits single-channel gating characteristics typical of potassium channels with a conductance similar to the single-channel conductance of full-length hERG as measured by oocyte patch-clamp electrophysiology (Kiehn *et al.*, 1999, 1996). We therefore postulate that the expression system described, despite the absence of the voltage-sensing and extra-membranous domains, will permit further biophysical studies, including hERG pore modulation by a range of pharmaceuticals, providing valuable insights in the structure, function and off-target drug modulation of full-length hERG.

Acknowledgments

The authors would like to thank Alvin Shrier (McGill University) for kindly providing the full-length hERG plasmid. I. M. gratefully acknowledges funding from the Natural Sciences and Engineering Research Council (NSERC) of Canada and M. P. from the Engineering and Physical Sciences Research Council (EPSRC grant EP/I029036/1). M. B. wishes to thank the Faculté des Sciences of the Université du Québec à Montréal, the NSERC Bionanomachines training program, the Canadian

Institutes of Health Research Strategic Training Initiative in Chemical Biology, the Centre Québécois sur les Matériaux Fonctionnels (CQMF), the Ministère de l'Éducation, du Loisir et du Sport du Québec, and Fonds de Recherche du Québec - Nature et Technologies (FRQNT) for the award of scholarships. I.M. is member of the CQMF, the Bionano program and the Groupe de Recherche Axé sur la Structure des Protéines (GRASP).

CHAPTER VII

CONCLUSION AND OUTLOOK

The results of this thesis brought techniques to improve the steps of expression, solubilization and reconstitution of membrane proteins. The methods developed can be splitted into two categories: the development and characterization of model membranes and the elaboration of a protocol to express the pore domain of an important eukaryotic potassium channel. After the discussion of these two methods, a section on the limits of the model membranes, and the promising whole cell system will be discussed.

7.1 Development and Characterization of Model Membranes

Two model membranes were used for developing methods to improve the steps of solubilization and reconstitution: DMPC/DHPC bicelles, and phospholipid/ MAPCHO bicelles.

7.1.1 DMPC and DHPC Bicelles

Bicelles made of DMPC/DHPC are often used at low molar ratio q (less or equal to 0.5) and at concentrations below 150 mM (Bocharov *et al.*, 2008; Chartrand *et al.*,

2010; Faham *et al.*, 2009; Gravel *et al.*, 2013; Mineev *et al.*, 2011; Surya *et al.*, 2013; Vold *et al.*, 1997), assuming that they are still bilayers. In this thesis, by using NMR, FTIR and molecular dynamic simulations, we were able to define the limits of the use of isotropic bicelles to maintain this bilayer. From the results, it is recommended to work at molar ratio q greater or equal to 1 and ideally, at concentrations greater than 150 mM. These concentrations are well above the CBC of ~6 mM determined by NMR spectroscopy.

An attempt to go further with this project would be to add a membrane peptide or protein to DMPC/DHPC bicelles. This might affect the thresholds of molar ratio q and concentration, since it would add a substantial hydrophobic portion. For example, the bilayer section could be disrupted and changed into mixed micelles following the addition of a peptide, or contrarily, the proteic segment could trigger the adoption of a bilayer around it. A similar study with several different membrane peptides should help refine these boundaries, although the insertion of membrane peptides can lead to different results from one to another.

However, there is a limitation to the DMPC/DHPC bicelle system. It does not seem to be suitable for large membrane proteins since most of the studies in the literature were done with peptides or small membrane proteins (De Angelis *et al.*, 2004; Howard & Opella, 1996; Marcotte & Auger, 2005; Sanders & Landis, 1995; Triba, Zoonens, *et al.*, 2006). Moreover, some membrane proteins might be insoluble in DHPC micelle such as TM0026 (Columbus et al., 2009).

7.1.2 Phospholipid and MAPCHO Bicelles

To improve the solubilisation of membrane proteins and allow their study in bicellar system, DHPC was replaced by detergents from the MAPCHO family of which DPC

is known for its ability to solubilize membrane proteins. We developed MAPCHO-based bicelles continuing on from what has been done by Lu *et al.*, 2012; Nolandt *et al.*, 2012.

The low CMCs of MAPCHO detergents (1.5 mM for DPC12 and 0.12 mM for TPC14 (Sanders & Sönnichsen, 2006)) are attractive to overcome the issues associated with the dilution of DMPC and DHPC bicelles. During this thesis we were able to obtain lower CBCs with MAPCHO-based bicelles compared to classical bicelles. The CBC with DPC12 and TPC14 were ~0.8 and ~0.07 mM, respectively.

Magnetically-oriented bicelles were formed for temperatures from 12 to 77°C, molar ratio q from 1.2 to 3.4, detergent chain-length from 12 to 16 carbons and phospholipid chain-length from 12 to 18 carbons. These bicelles can be flipped with lanthanides and dopped with anionic lipids (bicelles with DMPC/DMPS/DPC).

This systematic study could allow establishment of an empirical criterion which could predict whether a given surfactant-phospholipid pair will form bicelles. For this purpose, we calculated the ratio of hydrophilic-to-hydrophobic volume ratios. For example, this ratio was ~1 for bicelles of lipids and MAPCHO detergents and ~0.4 for long- and short-chain phospholipids bicelles.

The reconstitution of proteins into lipid systems is usually preceded by the removal of the solubilizing detergent from the medium. To assess the feasibility of this system as a direct model membrane system for reconstitution, we solubilized water-insoluble pore helices peptides of potassium channels into DPC micelles, followed by the addition of DMPC. The co-solubilization of the pore helices peptides with DMPC into chloroform, methanol and trifluoroethanol was partial, since particles remained in suspension. In comparison, the samples of the peptide with DPC micelles and bicelles were transparent without visible particles. This project allowed data to be obtained on the structure of these peptides and their interaction with membranes.

Altogether, these results provide a better understanding of the behavior of the bicelles and their boundaries. MAPCHO bicelles have the potential to be suitable for the study of membrane proteins, such as hERG. Indeed, the MAPCHO detergents will be used alone first, to well solubilise the membrane proteins and then the phospholipids will be added to form the bicelles. However, this hypothesis needs to be verified.

7.1.3 Pore Helices of hERG and $K_V1.5$

By testing the potential of the MAPCHO bicelles with the pore helices peptides, interesting results were obtained. This comparative study identified a difference of behavior between the membrane interaction of the hERG and $K_V1.5$ peptides. The $K_V1.5$ pore helix interacts more strongly with zwitterionic bicelles while the hERG interacts more extensively with the negative charged lipid bilayers.

The hERG peptide has a stronger effect on anionic bicelles compared to vesicles, which highlights a potential partial solubilisation of the pore helix of hERG directly in vesicles. The solubilisation by DPC or its presence might facilitate the interaction of the hERG with the bicelles.

The interaction of the hERG peptide with the anionic bilayer might be associated with its positive KDK motif. This binding may induce a perturbation of the structure of the hERG pore helix, altering the stability of the selectivity filter, and thus lead to a regulation of the gating.

7.2 Elaboration of a Protocol to Express the HERG Pore Domain

Despite the challenges that may constitute the expression of a eukaryotic membrane protein in a prokaryotic system, a protocol was developed. This protocol leads to 2.5 mg of hERG pore domain per liter of LB. The molecular weight of the hERG segment was verified by mass spectrometry, the α-helical secondary structure by circular dichroism, and the activity was shown by the observation of gating events. From this protocol, an expression of the full transmembrane domain (S1-S6) and/or the full-length hERG channel could be tested and optimized.

The quantities of protein obtained for the hERG pore domain are sufficient to support structural studies, either by NMR with ^{13}C-^{15}N labelled sample or by X-ray crystallography. It will also permit further biophysical studies, including hERG pore effects induced by a range of pharmaceuticals, providing valuable insights in the function and off-target drug modulation of the hERG channel. The interactions of the isotopically labelled hERG pore domain with LQTS-prone drugs could be studied by monitoring changes in ^{13}C chemical shifts using 2D ^{13}C-^{13}C-NMR experiments for example. Moreover, the affinity of the hERG channel with anionic lipids could be verified similarly to what is described in Chapter V.

A relevant progression from the results obtained in this thesis will be to reconstitute the hERG pore domain either in MAPCHO-bicelles by extracting and solubilizing the protein with DPC or TPC followed by phospholipid addition, or in sarkosyl-based bicelles by adding phospholipid to the mixture of hERG pore domain and sarkosyl after the purification process. Unpublished results in our laboratory have shown the feasibility of sarkosyl/PC bicelles.

7.3 Model Membrane Limitations and Prospects

Model membranes, simplified mimetics of the native membranes, are useful to obtain structural and functional information on membrane proteins and peptides. However, the lipid and protein diversity, dynamic interactions with other constituents of the membrane and the asymmetry of the membrane are not represented. It could be interesting to introduce such complexity in membrane protein studies. With increased understanding of membrane systems, it might be possible to use specialized model membranes that encompass all essential molecules (lipid and other protein partners) needed for the structure and the function of the molecule of interest.

Another relevant approach will be to get information on the molecule(s) of interest directly in the cellular membrane. Thus, steps of extraction, solubilization and reconstitution would not be needed. However, *in situ* or even *in vivo* investigation of the whole cell is confronted by the complexity and dynamics of the natural biomembrane, which will lead to an overload of information. For clarity, *in vivo* is used for molecules studied within its organism (unicellular) while *in situ* refers to molecules studied in a unicellular host. *In situ* or *in vivo* investigations are becoming possible with solid-state NMR combined with labelling techniques to study lipids, carbohydrates and membrane proteins (Arnold *et al.*, 2014; Baldus, 2015; Miao *et al.*, 2012; Renault *et al.*, 2012; Tardy-Laporte *et al.*, 2013; Ward *et al.*, 2015). As an example, the seven transmembrane helical microbial photosensor *Anabaena* sensory rhodopsin was assigned at 40% by NMR in the inner membrane of *E. coli* (Baldus, 2015). Even if most of the studies are restricted to bacteria, other intact membranes were analyzed, such as microalgae cell membranes (Arnold *et al.*, 2014) and plant cell walls (Wang *et al.*, 2013).

Despite the complexity of *in situ* investigation of whole cells due to the overload of information, it is an appealing idea. This technique will allow omission of

reconstitution and solubilisation steps. Future improvements of labelling protocols and *in vivo* solid-state NMR techniques have great potential to help better understand the native conformation and function of membrane proteins. As ever in the structural and functional studies of biological molecules new methodologies often start from bacteria (i.e. *E. coli*) then extend to other simple systems such as yeast before reaching mammal and human cells. Although the study of a molecule in a cell from a multicellular organism remains an *in vitro* investigation, it is nevertheless a step in a more complex and representative direction compared to studies in model membranes. Experiments on molecules in intact cells – which take into account the presence of all constituents - will certainly provide insights on their structures and functions which are not yet attainable since most studies are done in model systems. Information obtained using intact cells could also provide a better understanding of diseases such as the LQTS. For example exposition of human cardiac cell lines overexpressing the full-length hERG channel in their membrane to LQTS-prone drugs in the culture medium would give valuable data on drug-protein interactions in a native-like environment. This would be a step forward in the development of new and safer treatments.

REFERENCES

Abel, S., Dupradeau, F.-Y., & Marchi, M. (2012). Molecular dynamics simulations of a characteristic DPC micelle in water. *Journal of Chemical Theory and Computation*, *8*, 4610–4623.

Adaixo, R., Harley, C. A., Castro-Rodrigues, A. F., & Morais-Cabral, J. H. (2013). Structural properties of PAS domains from the KCNH potassium channels. *PLOS ONE*, *8*(3-e59265), 1–9.

Alvis, S. J., Williamson, I. M., East, J. M., & Lee, A. G. (2003). Interactions of anionic phospholipids and phosphatidylethanolamine with the potassium channel KcsA. *Biophysical Journal*, *85*, 3828–3838.

Anderluh, G., Razpotnik, A., Podlesek, Z., Macek, P., Separovic, F., & Norton, R. S. (2005). Interaction of the eukaryotic pore-forming cytolysin equinatoxin II with model membranes: 19F NMR studies. *Journal of Molecular Biology*, *347*, 27–39.

Andersson, A., Almqvist, J., Hagn, F., & Mäler, L. (2004). Diffusion and dynamics of penetratin in different membrane mimicking media. *Biochimica et Biophysica Acta*, *1661*, 18–25.

Andersson, A., & Mäler, L. (2002). NMR solution structure and dynamics of motilin in isotropic phospholipid bicellar solution. *Journal of Biomolecular NMR*, *24*, 103–112.

Andersson, A., & Mäler, L. (2005). Magnetic resonance investigations of lipid motion in isotropic bicelles. *Langmuir*, *21*(17), 7702–7709.

Andersson, A., & Mäler, L. (2006). Size and shape of fast-tumbling bicelles as determined by translational diffusion. *Langmuir*, *22*, 2447–2449.

Armen, R. S., Uitto, O. D., & Feller, S. E. (1998). Phospholipid component volumes: determination and application to bilayer structure calculations. *Biophysical Journal*, *75*, 734–744.

Arnold, A. A., Genard, B., Zito, F., Tremblay, R., Warschawski, D. E., & Marcotte, I. (2014). Identification of lipid and saccharide constituents of whole microalgal cells by 13C solid-state NMR. *Biochimica et Biophysica Acta*, *1848*(1), 369–377.

Arnold, A. A., Labrot, T., Oda, R., & Dufourc, E. J. (2002). Cation modulation of bicelle size and magnetic alignment as revealed by solid-state NMR and electron microscopy. *Biophysical Journal*, *83*, 2667–2680.

Aronov, A. M. (2005). Predictive in silico modeling for hERG channel blockers. *Drug Discovery Today*, *10*(2), 149–155.

Arora, A., Abildgaard, F., Bushweller, J. H., & Tamm, L. K. (2001). Structure of outer membrane protein A transmembrane domain by NMR spectroscopy. *Nature Structural & Molecular Biology*, *8*, 334–338.

Arvind, S., Arivazhagan, A., Santosh, V., & Chandramouli, B. A. (2012). Differential expression of a novel voltage gated potassium channel – Kv 1.5 in astrocytomas and its impact on prognosis in glioblastoma. *British Journal of Neurosurgery*, *26*(1), 16–20.

Atkins, P., & de Paula, J. (2010). *Physical Chemistry*. New York: Oxford University Press.

Aussenac, F., Lavigne, B., & Dufourc, E. J. (2005). Toward bicelle stability with ether-linked phospholipids : temperature, composition, and hydration diagrams by 2H and 31P solid-state NMR. *Langmuir*, *21*, 7129–7135.

Bagatolli, L. A., Ipsen, J. H., Simonsen, A. C., & Mouritsen, O. G. (2010). An outlook on organization of lipids in membranes: searching for a realistic connection with the organization of biological membranes. *Progress in Lipid Research*, *49*, 378–389.

Baldus, M. (2006). Molecular interactions investigated by multi-dimensional solid-state NMR. *Current Opinion in Structural Biology*, *16*, 618–623.

Baldus, M. (2015). A solid view of membrane proteins in situ. *Biophysical Journal*, *108*(7), 1585–1586.

Barbosa-Barros, L., Barba, C., Cócera, M., Coderch, L., López-Iglesias, C., de la Maza, A., & López, O. (2008). Effect of bicellar systems on skin properties. *International Journal of Pharmaceutics*, *352*, 263–272.

Barbosa-Barros, L., Rodríguez, G., Cócera, M., Rubio, L., López-Iglesias, C., De La Maza, A., & López, O. (2011). Structural versatility of bicellar systems and their possibilities as colloidal carriers. *Pharmaceutics*, *3*, 636–664.

Beaugrand, M., Arnold, A. A., Hénin, J., Warschawski, D. E., Williamson, P. T. F., & Marcotte, I. (2014). Lipid concentration and molar ratio boundaries for the use of isotropic bicelles. *Langmuir*, *30*, 6162–6170.

Bengt, F., & Ding, X. (2009). The ins and outs of phospholipid asymmetry in the plasma membranes: roles in health and disease. *Critical Reviews in Biochemistry and Molecular Biology*, *44*(5), 264–277.

Benhorin, J., & Medina, A. (1997). Images in Clinical Medicine. *New England Journal of Medicine*, *336*(22), 1568.

Benz, R. (1994). Permeation of hydrophilic solutes through mitochondrial outer membranes`review on mitochondrial porins. *Biochimica et Biophysica Acta*, *1197*, 167–196.

Bhuiyan, Z. A. (2009). Clinical and genetic spectrum of hereditary cardiac arrhythmia syndromes. *Amsterdan University*, (September).

Biverståhl, H., Lind, J., Bodor, A., & Mäler, L. (2009). Biophysical studies of the membrane location of the voltage-gated sensors in the HsapBK and KvAP K(+) channels. *Biochimica et Biophysica Acta*, *1788*, 1976–1986.

Bloch, F. (1946). Nuclear induction. *Physical Review*, *70*(7-8), 460–474.

Blume, A. (1993). Dynamic Properties. In *Phospholipids Handbook* (pp. 455–509). New York: Cevc, G, Ed; Marcel Dekker Inc.

Bocharov, E. V, Mayzel, M. L., Volynsky, P. E., Goncharuk, M. V, Ermolyuk, Y. S., Schulga, A. A., Artemenko, E. O., Efremov, R. G., & Arseniev, A. S. (2008). Spatial structure and pH-dependent conformational diversity of dimeric transmembrane domain of the receptor tyrosine kinase EphA1. *Journal of Biological Chemistry*, *283*(43), 29385–29395.

Boroske, E., & Helfrich, W. (1978). Magnetic anisotropy of egg lecithin membranes. *Biophysical Journal*, *24*, 863–868.

Bowie, J. U. (2004). Membrane proteins: a new method enters the fold. *Proceedings of the National Academy of Sciences*, *101*(12), 3995–3996.

Brown, M. F., Ribeiro, A. A., & Williams, G. D. (1983). New view of lipid bilayer dynamics from 2H and 13C NMR relaxation time measurements. *Proceedings of the National Academy of Sciences*, *80*, 4325–4329.

Burgess, R. R. (1996). Purification of overproduced Escherichia coli RNA polymerase sigma factors by solubilizing inclusion bodies and refolding from sarkosyl. *Methods in Enzymology*, *273*, 145–149.

Burgess, R. R. (2009). *Refolding solubilized inclusion body proteins. Methods in Enzymology* (1st ed., Vol. 463). Elsevier Inc.

Cady, S. D., Schmidt-Rohr, K., Wang, J., Soto, C. S., Degrado, W. F., & Hong, M. (2010). Structure of the amantadine binding site of influenza M2 proton channels in lipid bilayers. *Nature*, *463*, 689–693.

Camacho, J. (2006). Ether à go-go potassium channels and cancer. *Cancer Letters*, *233*, 1–9.

Capener, C. E., Kim, H. J., Arinaminpathy, Y., & Sansom, M. S. P. (2002). Ion channels: structural bioinformatics and modelling. *Human Molecular Genetics*, *11*(20), 2425–33.

Carsten, M., & Unger, V. M. (2012). Membrane curvature and its generation by BAR proteins. *Trends in Biochemical Sciences*, *37*(12), 526–533.

Ceccarini, L., Masetti, M., Cavalli, A., & Recanatini, M. (2012). Ion conduction through the hERG potassium channel. *PLOS ONE*, *7*(11), 1–11.

Chapman, D. J., De-Felice, J., & Barber, J. (1983). Growth temperature effects on thylakoid membrane lipid and protein content of pea chloroplasts. *Plant Physiology*, *72*, 225–228.

Chartrand, E., Arnold, A. A., Gravel, A., Jenna, S., & Marcotte, I. (2010). Potential role of the membrane in hERG channel functioning and drug-induced long QT syndrome. *Biochimica et Biophysica Acta*, *1798*(9), 1651–62.

Chou, J. J., Baber, J. L., & Bax, A. (2004). Characterization of phospholipid mixed micelles by translational diffusion. *Journal of Biomolecular NMR*, *29*, 299–308.

Chou, J. J., Kaufman, J. D., Stahl, S. J., Wingfield, P. T., & Bax, A. (2002). Micelle-induced curvature in a water-insoluble HIV-1 Env peptide revealed by NMR

dipolar coupling measurement in stretched polyacrylamide gel. *Journal of the American Chemical Society*, *124*(11), 2450–2451.

Clunes, M. T., & Boucher, R. C. (2007). Cystic fibrosis: the mechanisms of pathogenesis of an inherited lung disorder. *Drug Discovery Today*, *4*(2), 63–72.

Columbus, L., Lipfert, J., Jambunathan, K., Fox, D. A, Sim, A. Y. L., Doniach, S., & Lesley, S. A. (2009). Mixing and matching detergents for membrane protein NMR structure determination. *Journal of the American Chemical Society*, *131*(21), 7320–6.

Cooper, G. M. (2000). *Structure of the Plasma Membrane. The Cell: A Molecular Approach. 2nd edition*. Sunderland: Sinauer Associates.

Cregg, J. M., Tolstorukov, I., Kusari, A., Sunga, J., Madden, K., & Chappell, T. (2009). *Expression in the yeast Pichia pastoris. Methods in Enzymology* (1st ed., Vol. 463). Elsevier Inc.

Cross, T. A., Sharma, M., Yi, M., & Zhou, H.-X. (2011). Influence of solubilizing environments on membrane protein structures. *Trends in Biochemical Sciences*, *36*(2), 117–125.

Cuello, L. G., Romero, J. G., Cortes, D. M., & Perozo, E. (1998). pH-Dependent Gating in the Streptomyces lividans K+ Channel. *Biochemistry*, *37*(10), 3229–3236.

Cullis, P. R., & De Kruijff, B. (1979). Lipid polymorphism and the functional roles of lipids in biological membranes. *Biochimica et Biophysica Acta*, *559*, 399–420.

Cullis, P. R., Fenske, D. B., & Hope, M. J. (1996). Physical properties and functional roles of lipids in membranes. In *Biochemistry of Lipids, Lipoproteins and Membranes* (D.E. Vance, pp. 1–33). Amsterdam: Elsevier.

Cunningham, F., & Deber, C. M. (2007). Optimizing synthesis and expression of transmembrane peptides and proteins. *Methods*, *41*, 370–380.

Curran, A. R., Templer, R. H., & Booth, P. J. (1999). Modulation of folding and assembly of the membrane protein bacteriorhodopsin by intermolecular forces within the lipid bilayer. *Biochemistry*, *38*, 9328–9236.

Curran, M. E., Splawski, I., Timothy, K. W., Vincent, G. M., Green, E. D., & Keating, M. T. (1995). A molecular basis for cardiac arrhythmia: HERG mutations cause long QT syndrome. *Cell*, *80*, 795–803.

Daleke, D. L. (2003). Regulation of transbilayer plasma membrane phospholipid asymmetry. *Journal of Lipid Research*, *44*, 233–242.

Damberg, P., Jarvet, J., & Gräslund, A. (2001). Micellar systems as solvents in peptide and protein structure determination. *Methods in Enzymology*, *339*, 271–285.

Davis, J. H., Jeffrey, K. R., Bloom, M., Valic, M. I., & Higgs, T. P. (1976). Quadrupolar echo deuteron magnetic resonance spectroscopy in ordered hydrocarbon chains. *Chemical Physics Letters*, *42*, 390–394.

De Angelis, A. A., Nevzorov, A. A., Park, S. H., Howell, S. C., Mrse, A. A., & Opella, S. J. (2004). High-resolution NMR spectroscopy of membrane proteins in aligned bicelles. *Journal of the American Chemical Society*, *126*, 15340–15351.

De Angelis, A. A., & Opella, S. J. (2007). Bicelle samples for solid-state NMR of membrane proteins. *Nature Protocols*, *2*(10), 2332–2338.

Dennis, E. A., & Plückthun, A. (1984). Phosphorus-31 NMR of phospholipids in micelles. In *Phosphorus-31 NMR: Principles and Applications* (pp. 423–446).

Dhillon, M. S., Cockcroft, C. J., Munsey, T., Smith, K. J., Powell, A. J., Carter, P., Wrighton D. C., Rong H., Yusaf S. P., & Sivaprasadarao, A. (2014). A functional Kv1.2-hERG chimaeric channel expressed in Pichia pastoris. *Scientific Reports*, *4*(4201), 1–10.

Diller, A., Loudet, C., Aussenac, F., Raffard, G., Fournier, S., Laguerre, M., Grélard A., Opella, S. J., Marassi, F. M., & Dufourc, E. J. (2009). Bicelles: a natural "molecular goniometer" for structural, dynamical and topological studies of molecules in membranes. *Biochimie*, *91*, 744–751.

Dolainsky, C., Möps, A., & Bayerl, T. M. (1993). Transverse relaxation in supported and nonsupported phospholipids model membranes and the influence of ultraslow motions: a 31P-NMR study. *Journal of Chemical Physics*, *98*, 1712–1720.

Doyle, D. A., Morais Cabral, J., Pfuetzner, R. A., Kuo, A., Gulbis, J. M., Cohen, S. L., Chait B. T., & MacKinnon, R. (1998). The structure of the potassium channel: molecular basis of K+ conduction and selectivity. *Science*, *280*, 69–77.

Dürr, U. H. N., Soong, R., & Ramamoorthy, A. (2013). When detergent meets bilayer: birth and coming of age of lipid bicelles. *Progress in NMR Spectroscopy*, *69*, 1–22.

Eisenberg, D., Weiss, R. M., & Terwilliger, T. C. (1982). The helical hydrophobic moment: a measure of the amphiphilicity of a helix. *Nature*, *299*, 371–374.

Epand, R. M., D'Souza, K., Berno, B., & Schlame, M. (2014). Membrane curvature modulation of protein activity determined by NMR. *Biochimica et Biophysica Acta*, *1848*(1), 1–9.

Ernst, R. R., & Anderson, W. A. (1966). Application of Fourier transform spectroscopy to magnetic resonance. *Review of Scientific Instruments*, *37*, 93–102.

Etezady-Esfarjani, T., Hiller, S., Villalba, C., & Wüthrich, K. (2007). Cell-free protein synthesis of perdeuterated proteins for NMR studies. *Journal of Biomolecular NMR*, *39*, 229–238.

Faham, S., & Bowie, J. U. (2002). Bicelle crystallization: a new method for crystallizing membrane proteins yields a monomeric bacteriorhodopsin structure. *Journal of Molecular Biology*, *316*, 1–6.

Faham, S., Ujwal, R., Abramson, J., & Bowie, J. U. (2009). Chapter 5 Practical aspects of membrane proteins crystallization in bicelles. *Current Topics in Membranes*, *63*, 109–125.

Fan, Y., Shi, L., Ladizhansky, V., & Brown, L. S. (2011). Uniform isotope labeling of a eukaryotic seven-transmembrane helical protein in yeast enables high-resolution solid-state NMR studies in the lipid environment. *Journal of Biomolecular NMR*, *49*(2), 151–61.

Fauchère, J., & Pliska, V. (1983). Hydrophobic parameters {pi} of amino-acid side chains from the partitioning of N-acetyl-amino-acid amides. *European Journal of Medicinal Chemistry*, *8*, 369–375.

Ferrige, A. G., Seddon, M. J., & Jarvis, S. (1991). Maximum-Entropy Deconvolution in Electrospray Mass-Spectrometry. *Rapid Communications in Mass Spectrometry*, *5*(8), 374–377.

Foo, A. C. Y., Harvey, B. G. R., Metz, J. J., & Goto, N. K. (2014). Influence of hydrophobic mismatch on the catalytic activity of Escherichia coli GlpG rhomboid protease. *Protein Society*, *00*, 1–10.

Food and Drug Administration guidelines. (2005). Guidance for industry - S7B nonclinical evaluation of the potential for delayed ventricular repolarization (QT interval prolongation) by human pharmaceuticals. Retrieved from www.fda.gov/downloads/Drugs/GuidanceComplianceRegulatoryInformation/Guidances/ucm074963.pdf

Ford, J. W., & Milnes, J. T. (2008). New drugs targeting the cardiac ultra-rapid delayed-rectifier current (IKur): rationale, pharmacology and evidence for potential therapeutic value. *Journal of Cardiovascular Pharmacology*, *52*(2), 105–120.

Friddin, M. S., Smithers, N. P., Beaugrand, M., Marcotte, I., Williamson, P. T. F., Morgan, H., & de Planque, M. R. R. (2013). Single-channel electrophysiology of cell-free expressed ion channels by direct incorporation in lipid bilayers. *Analyst*, *138*, 7294–7298.

Gasteiger, E., Gattiker, A., Hoogland, C., Ivanyi, I., Appel, R. D., & Bairoch, A. (2003). ExPASy: the proteomics server for in-depth protein knowledge and analysis. *Nucleic Acids Research*, *31*, 3784–3788.

Glover, K. J., Whiles, J. A., Wu, G., Yu, N.-J., Deems, R., Struppe, J. O., Stark, R. E., Komives, E. A., & Vold, R. R. (2001). Structural evaluation of phospholipid bicelles for solution-state studies of membrane-associated biomolecules. *Biophysical Journal*, *81*, 2163–2171.

Gong, Q., Anderson, C. L., January, C. T., & Zhou, Z. (2002). Role of glycosylation in cell surface expression and stability of HERG potassium channels. *American Journal of Physiology - Heart and Circulatory Physiology*, *283*, H77–H84.

Gorenstein, D. G. (1984). Phosphorus-31 chemical shifts: principles and empirical observations. In *Phosphorus-31 NMR: Principles and Applications* (pp. 7–36).

Gravel, A. E., Arnold, A. A., Dufourc, E. J., & Marcotte, I. (2013). An NMR investigation of the structure, function and role of the hERG channel selectivity

filter in the long QT syndrome. *Biochimica et Biophysica Acta*, *1828*, 1494–1502.

Greenfield, N. (1969). Computed circular dichroism spectra for the evaluation of protein conformation. *Biochemistry*, *8*, 4108–4116.

Gruner, S. M., Cullis, P. R., Hope, J. H., & Tilcock, C. P. S. (1985). Lipid polymorphism : the molecular basis of nonbilayer phases. *Annual Review of Biophysics and Biophysical Chemistry*, *14*, 211–238.

Gurrola, G. B., Rosati, B., Rocchetti, M., Pimienta, G., Zaza, A., Arcangeli, A., Olivotto, M., Possani, L. D., & Wanke, E. (1999). A toxin to nervous, cardiac, and endocrine ERG K+ channels isolated from Centruroides noxius scorpion venom. *Federation of American Societies for Experimental Biology Journal*, *13*, 953–962.

Haitin, Y., Carlson, A. E., & Zagotta, W. N. (2013). The structural mechanism of KCNH-channel regulation by the eag domain. *Nature*, *501*, 444–448.

Han, X., & Gross, R. W. (2005). Shotgun lipidomics: electrospray ionization mass spectrometric analysis and quantitation of cellular lipidomes directly from crude extracts of biological samples. *Mass Spectrometry Reviews*, *24*, 367–412.

Haney, E. F., Hunter, H. N., Matsuzaki, K., & Vogel, H. J. (2009). Solution NMR studies of amphibian antimicrobial peptides: linking structure to function? *Biochimica et Biophysica Acta*, *1788*, 1639–1655.

He, Y., Wang, K., & Yan, N. (2014). The recombinant expression systems for structure determination of eukaryotic membrane proteins. *Protein & Cell*, *5*(9), 658–672.

Helenius, A., & Simons, K. (1975). Solubilization of membranes by detergents. *Biochimica et Biophysica Acta*, *415*, 29–79.

Hénin, J., Shinoda, W., & Klein, M. L. (2008). United-atom acyl chains for CHARMM phospholipids. *Journal of Physical Chemistry B*, *112*, 7008–7015.

Hille, B. (2001). *Ion Channels of Excitable Membranes. 3rd edition. Sinauer Associates, Sunderland.*

Hite, R. K., Butterwick, J. a, & MacKinnon, R. (2014). Phosphatidic acid modulation of Kv channel voltage sensor function. *eLife*, *3*, 1–13.

Ho, W.-K., Kim, I., Lee, C. O., Youm, J. B., Lee, S. H., & Earm, Y. E. (1999). Blockade of HERG channels expressed in Xenopus laevis oocytes by external divalent cations. *Biophysical Journal*, *76*, 1959–1971.

Holland, P. M., & Rubingh, D. N. (1983). Nonideal multicomponent mixed micelle model. *Journal of Physical Chemistry*, *87*(11), 1984–1990.

Holzwarth, G., & Doty, P. (1965). The ultraviolet circular dichroism of polypeptides. *Journal of the American Chemical Society*, *87*(2), 218–228.

Hong, H., & Tamm, L. K. (2004). Elastic coupling of integral membrane protein stability to lipid bilayer forces. *Proceedings of the National Academy of Sciences*, *101*(12), 4065–4070.

Hoshi, T., Zagotta, W. N., & Aldrich, R. W. (1990). Biophysical and molecular mechanisms of Shaker potassium channel inactivation. *Science*, *250*(4980), 533–538.

Howard, K. P., & Opella, S. J. (1996). High-resolution solid-state NMR spectra of integral membrane proteins reconstituted into magnetically oriented phospholipid bilayers. *Journal of Magnetic Resonance B*, *112*(1), 91–4.

Hu, F., Luo, W., Cady, S. D., & Hong, M. (2011). Conformational plasticity of the influenza A M2 transmembrane helix in lipid bilayers under varying pH, drug binding, and membrane thickness. *Biochimica et Biophysica Acta*, *1808*, 415–423.

Israelachvili, J. N. (2011). *Intermolecular and Surface Forces: Revised Third Edition* (Third edi). San Diego: Academic Press.

Jahnig, F. (1984). Lipid exchange between membranes. *Biophysical Journal*, *46*, 687–694.

Jeener, J. (1971). Lecture at International Ampere Summer School II (p. Basko Polje, Yugoslavia).

Jiang, M., Zhang, M., Maslennikov, I. V, Liu, J., Wu, D.-M., Korolkova, Y. V, Arseniev, A. S., Grishin, E. V., & Tseng, G.-N. (2005). Dynamic conformational changes of extracellular S5-P linkers in the hERG channel. *Journal of Physiology*, *569*(1), 75–89.

Jones, D. H., Hodges, R. S., Barber, K. R., & Grant, C. W. M. (1997). Pilin C-terminal peptide binds asialo-GM1 in liposomes: a 2H-NMR study. *Protein Science*, *6*, 2459–2461.

Kallick, D. A., Tessmer, M. R., Watts, C. R., & Li, C.-Y. (1995). The use of dodecylphosphocholine micelles in solution NMR. *Journal of Magnetic Resonance B*, *109*, 60–65.

Kalsi, S., Powl, A. M., Wallace, B. A., Morgan, H., & De Planque, M. R. R. (2014). Shaped apertures in photoresist films enhance the lifetime and mechanical stability of suspended lipid bilayers. *Biophysical Journal*, *106*(8), 1650–1659.

Kamiya, K., Niwa, R., Mitcheson, J. S., & Sanguinetti, M. C. (2006). Molecular determinants of hERG channel block. *Molecular Pharmacology*, *69*(5), 1709–1716.

Kang, C., & Li, Q. (2011). Solution NMR study of integral membrane proteins. *Current Opinion in Chemical Biology*, *15*, 560–569.

Kaplan, W. D., & Trout, W. E. (1969). The behavior of four neurological mutants of Drosophila. *Genetics*, *61*, 399–409.

Katsaras, J. (1998). Alignable biomimetic membranes. *Physica B*, *241-243*, 1178–1180.

Katsaras, J., Donaberger, R. L., Swainson, I. P., Tennant, D. C., Tun, Z., Vold, R. R., & Prosser, R. S. (1997). Rarely observed phase transitions in a novel lyotropic liquid crystal system. *Physical Review Letters*, *78*(5), 899–902.

Kelly, S. M., Jess, T. J., & Price, N. C. (2005). How to study proteins by circular dichroism. *Biochimica et Biophysica Acta*, *1751*(2), 119–39.

Kelly, S. M., & Price, N. (2000). The use of circular dichroism in the investigation of protein structure and function. *Current Protein & Peptide Science*, *1*, 349–384.

Kiehn, J., Lacerda, A. E., & Brown, A. M. (1999). Pathway of hERG inactivation. *American Journal of Physiology - Heart and Circulatory Physiology*, *277*(1), H199–H210.

Kiehn, J., Lacerda, A. E., Wible, B., & Brown, A. M. B. (1996). Molecular physiology and pharmacology of HERG. Single-channel currents and block by dofetilide. *Circulation*, *94*, 2572–2579.

Killian, J. A. (1998). Hydrophobic mismatch between proteins and lipids in membranes. *Biochimica et Biophysica Acta*, *1376*, 401–415.

Kimble-Hill, A. C. (2013). A review of factors affecting the success of membrane protein crystallization using bicelles. *Frontiers in Biology*, *8*(3), 261–272.

Klauda, J. B., Venable, R. M., Freites, J. A., O'Connor, J. W., Tobias, D. J., Mondragon-Ramirez, C., Vorobyov, I., MacKerell, A. D., & Pastor, R. W. (2010). Update of the CHARMM all-atom additive force field for lipids: validation on six lipid types. *Journal of Physical Chemistry B*, *114*, 7830–7843.

Knight, W. D. (1949). Nuclear magnetic resonance shift in metals. *Physical Review*, *76*(8), 1259–1260.

Koehler, J., Sulistijo, E. S., Sakakura, M., Kim, H. J., Ellis, C. D., & Sanders, C. R. (2010). Lyso-phospholipid micelles sustain the stability and catalytic activity of diacylglycerol kinase in the absence of lipids. *Biochemistry*, *49*(33), 7089–7099.

Koolman, J., & Roehm, K.-H. (2013). Membranes - Structure and Components. In *Color Atlas of Biochemistry. 3rd edition*. Flexibook - Thieme.

Korn, E. D., & Wright, W. L. (1973). Macromolecular Composition of an Amoeba Plasma Membrane. *Journal of Biological Chemistry*, *248*(2), 439–447.

Korn, S. J., & Trapani, J. G. (2005). Potassium channels. *Institute of Electrical and Electronics Engineers Transactions on NanoBioscience*, *4*(1), 21–33.

Korolkova, Y. V, Kozlov, S. A., Lipkin, A. V, Pluzhnikov, K. A., Hadley, J. K., Filippov, A. K., Brown, D. A., Angelo, K., Strøbaek, D., Jespersen, T., Olsen, S.-P., Jensen, B. S., & Grishin, E. V. (2001). An ERG channel inhibitor from the scorpion Buthus eupeus. *Journal of Biological Chemistry*, *276*, 9868–9876.

Kutteh, R., Vandenberg, J. I., & Kuyucak, S. (2007). Molecular Dynamics and Continuum Electrostatics Studies of Inactivation in the HERG Potassium Channel. *Journal of Physical Chemistry B*, *111*, 1090–1098.

Landau, E. M., & Rosenbusch, J. P. (1996). Lipidic cubic phases: A novel concept for the crystallization of membrane proteins. *Proceedings of the National Academy of Sciences*, *93*, 14532–14535.

Lasic, D. D. (1998). Novel applications of liposomes. *Trends in Biotechnology*, *16*(7), 307–321.

Lauterwein, J., Bösch, C., Brown, L. R., & Wüthrich, K. (1979). Physicochemical studies of the protein-lipid interactions in melittin-containing micelles. *Biochimica et Biophysica Acta*, *556*, 244–264.

Laverty, H. G., Benson, C., Cartwright, E. J., Cross, M. J., Garland, C., Hammond, T., Holloway, C., McMahon, N., Milligan, J., Park, B. K., Pirmohamed, M., Pollard, C., Radford, J., Roome, N., Sager, P., Singh, S., Suter, T., Suter, W., Trafford, A., Volders, P. G. A., Wallis, R., Weaver, R., Work, M., & Valentin, J. P. (2011). How can we improve our understanding of cardiovascular safety liabilities to develop safer medicines? *British Journal of Pharmacology*, *163*, 675–93.

Le Maire, M., Champeil, P., & Moller, J. V. (2000). Interaction of membrane proteins and lipids with solubilizing detergents. *Biochimica et Biophysica Acta*, *1508*, 86–111.

Lee, A. G. (2003). *Lipid-protein interactions in biological membranes: a structural perspective. Biochimica et Biophysica Acta* (Vol. 1612).

Lee, A. G. (2004). How lipids affect the activities of integral membrane proteins. *Biochimica et Biophysica Acta*, *1666*, 62–87.

Lee, D. C., & Chapman, D. (1986). Infrared spectroscopic studies of biomembranes and model membranes. *Bioscience Reports*, *6*(3), 235–256.

Levitt, M. H. (2001). *Spin dynamics - Basics of nuclear magnetic resonance*. Chichester: John Wiley & Sons, Ltd.

Levitt, M. H. (2005). Nuclear isotopes and their properties. In *Spin Dynamics: Basics of Nuclear Magnetic Resonance* (p. 14). Wiley.

Lewis, R. N. A. H., & McElhaney, R. N. (1998). The structure and organization of phospholipid bilayers as revealed by infrared spectroscopy. *Chemistry and Physics of Lipids*, *96*, 9–21.

Li, Q., Gayen, S., Chen, A. S., Huang, Q., Raida, M., & Kang, C. (2010). NMR solution structure of the N-terminal domain of hERG and its interaction with the S4-S5 linker. *Biochemical and Biophysical Research Communications*, *403*(1), 126–132.

Lichtenberg, D., Robson, R. J., & Dennis, E. A. (1983). Solubilization of phospholipids by detergents. *Biochimica et Biophysica Acta*, *737*, 285–304.

Linke, D. (2009). Detergents: an overview. In *Methods in Enzymology* (1st ed., Vol. 463, pp. 603–617). Elsevier Inc.

Liu, G. X., Zhou, J., Nattel, S., & Koren, G. (2004). Single-channel recordings of a rapid delayed rectifier current in adult mouse ventricular myocytes: basic properties and effects of divalent cations. *Journal of Physiology*, *556*, 401–413.

Lorigan, G. A. (2006). Chapter 10. Solid-State Nuclear Magnetic Resonance Spectroscopy Studies of Magnetically Aligned Phospholipid Bilayers. In A. Ramamoorthy (Ed.), *NMR Spectroscopy of Biological Solids* (pp. 237–259). Boca Raton: Tayler & Francis Group.

Loudet, C., Manet, S., Gineste, S., Oda, R., Achard, M.-F., & Dufourc, E. J. (2007). Biphenyl bicelle disks align perpendicular to magnetic fields on large temperature scales: a study combining synthesis, solid-state NMR, TEM, and SAXS. *Biophysical Journal*, *92*(11), 3949–59.

Lu, Y., Mahaut-Smith, M. P., Varghese, A., Huang, C. L.-H., Kemp, P. R., & Vandenberg, J. I. (2001). Effects of premature stimulation on HERG K(+) channels. *Journal of Physiology*, *537*(3), 843–851.

Lu, Z., Horn, W. D. Van, Chen, J., Mathew, S., Zent, R., & Sanders, C. R. (2012). Bicelles at low concentrations. *Molecular Pharmaceutics*, *9*, 752–761.

Luchette, P. A., Vetman, T. N., Prosser, R. S., Hancock, R. E. W., Nieh, M.-P., Glinka, C. J., Krueger, S., & Katsaras, J. (2001). Morphology of fast-tumbling bicelles: a small angle neutron scattering and NMR study. *Biochimica et Biophysica Acta*, *1513*, 83–94.

Macdonald, P. M., Saleem, Q., Lai, A., & Morales, H. H. (2013). NMR methods for measuring lateral diffusion in membranes. *Chemistry and Physics of Lipids*, *166*, 31–44.

MacKinnon, R. (2003a). Potassium channels. *Federation of European Biochemical Societies Letters*, *555*, 62–65.

MacKinnon, R. (2003b). Potassium channels and the atomic basis of selective ion conduction. *Nobel Lecture*, 214–235.

Mackinnon, R., Aldrich, R. W., & Lee, A. W. (1993). Functional stoichiometry of Shaker potassium channel inactivation. *Science*, *262*, 757–759.

Mäler, L., & Gräslund, A. (2009). Artificial membrane models for the study of macromolecular delivery. In M. Belting (Ed.), *Methods in Molecular Biology. Macromolecular Drug Delivery. Methods and Protocols.* (Vol. 480, pp. 129–139). Lund, Sweden: Humana Press.

Mantsch, H. H., & McElhaney, R. N. (1991). Phospholipid phase transitions in model and biological membranes as studied by infrared spectroscopy. *Chemistry and Physics of Lipids*, *57*, 213–226.

Marcotte, I. (2003). *Étude de l'interaction de la méthionine-enképhaline et de peptides antibiotiques avec des membranes modèles par spectroscopies de RMN et infrarouge.*

Marcotte, I., & Auger, M. (2005). Bicelles as model membranes for solid- and solution-state NMR studies of membrane peptides and proteins. *Concepts in Magnetic Resonance A*, *24A*, 17–37.

Marcotte, I., Dufourc, E. J., Ouellet, M., & Auger, M. (2003). Interaction of the neuropeptide Met-Enkephalin with zwitterionic and negatively charged bicelles as viewed by 31P and 2H solid-state NMR. *Biophysical Journal*, *85*, 328–339.

Marcotte, I., Separovic, F., Auger, M., & Gagné, S. M. (2004). A multidimensional 1H NMR investigation of the conformation of methionine-enkephalin in fast-tumbling bicelles. *Biophysical Journal*, *86*, 1587–1600.

Marius, P., de Planque, M. R. R., & Williamson, P. T. F. (2012). Probing the interaction of lipids with the non-annular binding sites of the potassium channel KcsA by magic-angle spinning NMR. *Biochimica et Biophysica Acta*, *1818*, 90–96.

Marius, P., Zagnoni, M., Sandison, M. E., East, J. M., Morgan, H., & Lee, A. G. (2008). Binding of anionic lipids to at least three nonannular sites on the potassium channel KcsA is required for channel opening. *Biophysical Journal*, *94*, 1689–98.

Marsh, D. (2013). *Handbook of lipid bilayers* (Second edi). Boca Raton: CRC Press, Taylor & Francis Group.

Martin, D. D. (2007). Component of the normal EKG waveform. In *The Complete Study Guide to Learning the Electrocardiogram* (p. 9). Surprise, Arizona: Mind-Forge Publishing.

Martinez Molina, D., Cornvik, T., Eshaghi, S., Haeggström, J. Z., Nordlund, P., & Sabet, M. I. (2008). Engineering membrane protein overproduction in Escherichia coli. *Protein Science*, *17*(4), 673–680.

Maslennikov, I., Klammt, C., Hwang, E., Kefala, G., Okamura, M., Esquivies, L., Mörs, K., Glaubitz, C., Kwiatkowski, W., Jeon, Y. H., & Choe, S. (2010). Membrane domain structures of three classes of histidine kinase receptors by cell-free expression and rapid NMR analysis. *Proceedings of the National Academy of Sciences*, *107*(24), 10902–10907.

McCusker, E. C., Bagnéris, C., Naylor, C. E., Cole, A. R., D'Avanzo, N., Nichols, C. G., & Wallace, B. A. (2012). Structure of a bacterial voltage-gated sodium channel pore reveals mechanisms of opening and closing. *Nature Communications*, *3*(1102), 1–8.

McCusker, E. C., D'Avanzo, N., Nichols, C. G., & Wallace, B. A. (2011). Simplified bacterial "pore" channel provides insight into the assembly, stability, and structure of sodium channels. *Journal of Biological Chemistry*, *286*(18), 16386–16391.

Mendelsohn, R., & Mantsch, H. H. (1986). *Fourier transform infrared studies of lipid-protein interaction. In Progress in Protein-Lipid Interactions. Elsevier: Amsterdam.* Elsevier: Amsterdam, Watts & DePont.

Miao, Y., Qin, H., Fu, R., Sharma, M., Can, T., Hung, I., Luca, & Cross, T. A. (2012). M2 Proton channel structural validation form full length protein samples in synthetic bilayers and E. coli membranes. *Angewandte Chemie*, *51*(33), 8383–8386.

Mineev, K. S., Bocharov, E. V, Volynsky, P. E., Goncharuk, M. V, Tkach, E. N., Ermolyuk, Y. S., Schulga, A. A., Chupin, V. V., Maslennikov I. V., Efremov R. G., & Arseniev, A. S. (2011). Dimeric structure of the transmembrane domain of Glycophorin A in lipidic and detergent environments. *Acta Naturae*, *3*(2 (9)), 90–98.

Mitcheson, J. S., Chen, J., Lin, M., Culberson, C., & Sanguinetti, M. C. (2000). A structural basis for drug-induced long QT syndrome. *Proceedings of the National Academy of Sciences*, *97*(22), 12329–12333.

Mitcheson, J. S., Perry, M., Stansfeld, P., Sanguinetti, M. C., Witchel, H., & Hancox, J. (2005). Chapter 11. Structural Determinants for High-Affinity Block of hERG Potassium Channels. In D. J. Chadwick & J. Goode (Eds.), *The hERG Cardiac*

Potassium Channel: Structure, Function and Long QT Syndrome: Novartis Foundation Symposium 266 (pp. 136–154). Novartis Foundation Symposia.

Morais Cabral, J. H., Lee, A. G., Cohen, S. L., Chait, B. T., Li, M., & Mackinnon, R. (1998). Crystal structure and functional analysis of the HERG potassium channel N terminus: a eukaryotic PAS domain. *Cell*, *95*(5), 649–655.

Mouritsen, O. G. (2005). *Life - as a matter of fat. The Frontiers Collection - Springer.*

Murrell-Lagnado, R. D., & Aldrich, R. W. (1993a). Energetics of Shaker K channels block by inactivation peptides. *Journal of General Physiology*, *102*, 977–1003.

Murrell-Lagnado, R. D., & Aldrich, R. W. (1993b). Interactions of amino terminal domains of Shaker K channels with a pore blocking site studied with synthetic peptides. *Journal of General Physiology*, *102*, 949–975.

Naito, A. (2009). Structure elucidation of membrane-associated peptides and proteins in oriented bilayers by solid-state NMR spectroscopy. *Solid State Nuclear Magnetic Resonance*, *36*, 67–76.

Nicolson, G. L. (2014). The fluid-mosaic model of membrane structure: still relevant to understanding the structure, function and dynamics of biological membranes after more than 40 years. *Biochimica et Biophysica Acta*, *1838*, 1451–1466.

Nietlispach, D., & Gautier, A. (2011). Solution NMR studies of polytopic α-helical membrane proteins. *Current Opinion in Structural Biology*, *21*(4), 497–508.

Nolandt, O. V, Walther, T. H., Grage, S. L., & Ulrich, A. S. (2012). Magnetically oriented dodecylphosphocholine bicelles for solid-state NMR structure analysis. *Biochimica et Biophysica Acta*, *1818*, 1142–1147.

Nyholm, T. K. M., Özdirekcan, S., & Killian, J. A. (2007). How protein transmembrane segments sense the lipid environment. *Biochemistry*, *46*(6), 1457–1465.

Oberai, A., Ihm, Y., Kim, S., & Bowie, J. U. (2006). A limited universe of membrane protein families and folds. *Protein Science*, *15*, 1723–1734.

Olson, T. M., Alekseev, A. E., Liu, X. K., Park, S., Zingman, L. V, Bienengraeber, M., Sattiraju, S., Ballew, J. D., Jahangir, A., & Terzic, A. (2006). Kv1.5

channelopathy due to KCNA5 loss-of-function mutation causes human atrial fibrillation. *Human Molecular Genetics*, *15*(14), 2185–2191.

Ottiger, M., & Bax, A. (1998). Characterization of magnetically oriented phospholipid micelles for measurement of dipolar couplings in macromolecules. *Journal of Biomolecular NMR*, *12*, 361–372.

Ouellet, M. (2007). *Étude des mécanismes de perturbation membranaire de peptides amphiphiles par spectroscopies de RMN à l'état solide et infrarouge*.

Oxenoid, K., Sönnichsen, F. D., & Sanders, C. R. (2002). Topology and secondary structure of the N-terminal domain of diacylglycerol kinase. *Biochemistry*, *41*, 12876–12882.

Pages, G., Torres, A. M., Ju, P., Bansal, P. S., Alewood, P. F., Kuchel, P. W., & Vandenberg, J. I. (2009). Structure of the pore-helix of the hERG K(+) channel. *European Biophysics Journal*, *39*, 111–120.

Pardo-Lopez, L., Zhang, M., Liu, J., Jiang, M., Possani, L. D., & Tseng, G.-N. (2002). Mapping the binding site of a human ether-a-go-go-related gene-specific peptide toxin (ErgTx) to the channel's outer vestibule. *Journal of Biological Chemistry*, *277*, 16403–16411.

Park, S. H., & Opella, S. J. (2010). Triton X-100 as the "short-chain lipid" improves the magnetic alignment and stability of membrane proteins in phosphatidylcholine bilayers for oriented-sample solid-state NMR spectroscopy. *Journal of the American Chemical Society*, *132*(36), 12552–3.

Parker, M. A., King, V., & Howard, K. P. (2001). Nuclear magnetic resonance study of doxorubicin binding to cardiolipin containing magnetically oriented phospholipid bilayers. *Biochimica et Biophysica Acta*, *1514*, 206–216.

Pearlstein, R. A., Vaz, R., & Rampe, D. (2003). Understanding the structure-activity relationship of the human ether-a-go-go-related gene cardiac K+ channel. A model for bad behavior. *Journal of Medicinal Chemistry*, *46*(11), 2017–2022.

Perozo, E., Kloda, A., Cortes, D. M., & Martinac, B. (2002). Physical principles underlying the transduction of bilayer deformation forces during mechanosensitive channel gating. *Nature Structural Biology*, *9*, 696–703.

Phillips, J. C., Braun, R., Wang, W., Gumbart, J., Tajkhorshid, E., Villa, E., Chipot, C., Skeel, R. D., Kalé, L., & Schulten, K. (2005). Scalable molecular dynamics with NAMD. *Journal of Computational Chemistry*, *26*, 1781–1802.

Pickford, A. R., & O'Leary, J. M. (2004). Isotopic labeling of recombinant proteins from the methylotrophic yeast Pichia pastoris. *Methods in Molecular Biology*, *278*, 17–33.

Pires, J. M., de Moura, A. F., & Freitas, L. C. G. (2012). Investigating the spontaneous formation of SDS micelle in aqueous solution using a coarse-grained force field. *Química Nova*, *35*(5), 978–981.

Post, J. A., Verkleij, A. J., & Langer, G. A. (1995). Organization and function of sarcolemmal phospholipids in control and ischemic / reperfused cardiomyocytes. *Journal of Molecular and Cellular Cardiology*, *760*, 749–760.

Preußat, K., Beetz, C., Schrey, M., Kraft, R., Wölfl, S., Kalff, R., & Patt, S. (2003). Expression of voltage-gated potassium channels Kv1.3 and Kv1.5 in human gliomas. *Neuroscience Letters*, *346*, 33–36.

Prevarskaya, N., Zhang, L., & Barritt, G. (2007). TRP channels in cancer. *Biochimica et Biophysica Acta*, *1772*, 937–946.

Pronk, S., Páll, S., Schulz, R., Larsson, P., Bjelkmar, P., Apostolov, R., Shirts, M. R., Smith, J. C., Kasson P. M., van der Spoel, D., Hess, B., & Lindahl, E. (2013). GROMACS 4.5: a high-throughput and highly parallel open source molecular simulation toolkit. *Bioinformatics*, *29*(7), 845–854.

Prosser, R. S., Evanics, F., Kitevski, J. L., & Al-Abdul-Wahid, M. S. (2006). Current Applications of Bicelles in NMR Studies of Membrane-Associated Amphiphiles and Proteins. *Biochemistry*, *45*(28), 8453–8465.

Prosser, R. S., Hunt, S. A., Dinatale, J. A., & Vold, R. R. (1996). Magnetically aligned membrane model systems with positive order parameter : switching the sign of Szz with paramagnetic ions. *Journal of the American Chemical Society*, *118*, 269–270.

Prosser, R. S., Hwang, J. S., & Vold, R. R. (1998). Magnetically aligned phospholipid bilayers with positive ordering: a new model membrane system. *Biophysical Journal*, *74*, 2405–2418.

Rakotomanga, M., Loiseau, P. M., & Saint-Pierre-Chazelet, M. (2004). Hexadecylphosphocholine interaction with lipid monolayers. *Biochimica et Biophysica Acta*, *1661*, 212–218.

Ram, P., & Prestegard, J. H. (1988). Magnetic field induced ordering of bile salt/phospholipid micelles: new media for NMR investigations. *Biochimica et Biophysica Acta*, *940*, 289–294.

Ramirez, B. E., Voloshin, O. N., Camerini-Otero, R. D., & Bax, A. D. (2000). Solution structure of DinI provides insight into its mode of RecA inactivation. *Protein Science*, *9*, 2161–2169.

Ramu, Y., Xu, Y., & Lu, Z. (2006). Enzymatic activation of voltage-gated potassium channels. *Nature*, *442*, 696–699.

Rance, M., & Byrd, R. A. (1983). Obtaining high-fidelity spin-1/2 powder spectra in anisotropic media: phase-cycled Hahn echo spectroscopy. *Journal of Magnetic Resonance*, *52*, 221–240.

Raschle, T., Hiller, S., Etzkorn, M., & Wagner, G. (2010). Non-micellar systems for solution NMR spectroscopy of membrane proteins. *Current Opinion in Structural Biology*, *20*(4), 471–479.

Ravens, U., & Cerbai, E. (2008). Role of potassium currents in cardiac arrhythmias. *Europace*, *10*(10), 1133–1137.

Recanatini, M., Poluzzi, E., Masetti, M., Cavalli, A., & De Ponti, F. (2005). QT prolongation through hERG K+ channel blockade: Current knowledge and strategies for the early prediction during drug development. *Medicinal Research Reviews*, *25*(2), 133–166.

Redfern, W. S., Carlsson, L., Davis, a. S., Lynch, W. G., MacKenzie, I., Palethorpe, S., Siegl, P. K. S., Strang, I., Sullivan A. T., Wallis, R., Camm, A. J., & Hammond, T. G. (2003). Relationships between preclinical cardiac electrophysiology, clinical QT interval prolongation and torsade de pointes for a broad range of drugs: evidence for a provisional safety margin in drug development. *Cardiovascular Research*, *58*(1), 32–45.

Renault, M., Tommassen-van Boxtel, R., Bos, M. P., Post, J. A., Tommassen, J., & Baldus, M. (2012). Cellular solid-state nuclear magnetic resonance spectroscopy. *Proceedings of the National Academy of Sciences*, *109*(13), 4863–4868.

Roden, D. M., & Temple, R. (2005). The US food and drug administration cardiorenal advisory panel and the drug approval process. *Circulation*, *111*, 1697–1702.

Rodríguez, G., Rubio, L., Cócera, M., Estelrich, J., Pons, R., de la Maza, A., & López, O. (2010). Application of bicellar systems on skin: diffusion and molecular organization effects. *Langmuir*, *26*(13), 10578–10584.

Rodriguez, N., Amarouch, M. Y., Montnach, J., Piron, J., Labro, A. J., Charpentier, F., Mérot, J., Baro I, & Loussouarn, G. (2010). Phosphatidylinositol-4,5-bisphosphate (PIP2) stabilizes the open pore conformation of the Kv11.1 (hERG) channel. *Biophysical Journal*, *99*, 1110–1118.

Romo, T. D., & Grossfield, A. (2009). LOOS: an extensible platform for the structural analysis of simulations. In *31st Annual International Conference of the IEEE EMBS* (pp. 2332–2335).

Rosano, G. L., & Ceccarelli, E. A. (2014). Recombinant protein expression in Escherichia coli: advances and challenges. *Frontiers in Microbiology*, *5*(172), 1–17.

Rubio, L., Alonso, C., Rodríguez, G., Barbosa-Barros, L., Coderch, L., De la Maza, A., Parra J. L., & López, O. (2010). Bicellar systems for in vitro percutaneous absorption of diclofenac. *International Journal of Pharmaceutics*, *386*, 108–113.

Sakuma, Y., Taniguchi, T., & Imai, M. (2010). Pore formation in a binary giant vesicle induced by cone-shaped lipids. *Biophysical Journal*, *99*, 472–479.

Sakurai, I., Kawamura, Y., Ikegami, A., & Iwayanagi, S. (1980). Magneto-orientation of lecithin crystals. *Proceedings of the National Academy of Sciences*, *77*, 7232–7236.

Sanders, C. R., Hare, B. J., Howard, K. P., & Prestegard, J. H. (1994). Magnetically-oriented phospholipid micelles as a tool for the study of membrane-associated molecules. *Progress in NMR Spectroscopy*, *26*, 421–444.

Sanders, C. R., & Landis, G. C. (1994). Facile acquisition and assignment of oriented sample NMR spectra for bilayer surface-associated proteins. *Journal of the American Chemical Society*, *116*, 6470–6471.

Sanders, C. R., & Landis, G. C. (1995). Reconstitution of membrane proteins into lipid-rich bilayered mixed micelles for NMR studied. *Biochemistry*, *34*, 4030–4040.

Sanders, C. R., & Prestegard, J. H. (1990). Magnetically orientable phospholipid bilayers containing small amounts of a bile salt analogue, CHAPSO. *Biophysical Journal*, *58*, 447–460.

Sanders, C. R., & Prosser, R. S. (1998). Bicelles: a model membrane system for all seasons? *Structure*, *6*(10), 1227–1234.

Sanders, C. R., & Schwonek, J. P. (1992). Characterization of magnetically orientable bilayers in mixtures of dihexanoylphosphatidylcholine and dimyristoylphosphatidylcholine by solid-state NMR. *Biochemistry*, *31*, 8898–8905.

Sanders, C. R., & Sönnichsen, F. D. (2006). Solution NMR of membrane proteins: practice and challenges. *Magnetic Resonance in Chemistry*, *44*, S24–S40.

Sanguinetti, M. C., Jiang, C., Curran, M. E., & Keating, M. T. (1995). A mechanistic link between an inherited and an acquired cardiac arrhythmia: HERG encodes the IKr potassium channel. *Cell*, *81*, 299–307.

Sanguinetti, M. C., & Mitcheson, J. S. (2005). Predicting drug-hERG channel interactions that cause acquired long QT syndrome. *Trends in Pharmacological Sciences*, *26*(3), 119–24.

Sanguinetti, M. C., & Tristani-Firouzi, M. (2006). hERG potassium channels and cardiac arrhythmia. *Nature*, *440*(7083), 463–469.

Sastry, K. V., & Tomer, B. S. (2008). *Cell Biology* (Ninth edi). New Dehli: Rastogi Publications.

Schechter, E. (1990). *Biochimie et Biophysique des Membranes: Aspects Structuraux et Fonctionnels*. Paris: Masson.

Schmidt-Rohr, K., & Spiess, H. W. (1994). *Multidimensional solid-sate NMR and polymers*. London: Academis Press.

Schnell, J. R., & Chou, J. J. (2008). Structure and mechanism of the M2 proton channel of influenza A virus. *Nature*, *451*(7178), 591–595.

Seddon, A. M., Curnow, P., & Booth, P. J. (2004). Membrane proteins, lipids and detergents: not just a soap opera. *Biochimica et Biophysica Acta*, *1666*, 105–117.

Seelig, J. (1978). 31P nuclear magnetic resonance and the head group structure of phospholipids in membranes. *Biochimica et Biophysica Acta*, *515*, 105–140.

Seelig, J., Borle, F., & Cross, T. A. (1985). Magnetic ordering of phospholipid membranes. *Biochimica et Biophysica Acta*, *814*, 195–198.

Semchyschyn, D. J., & Macdonald, P. M. (2004). Conformational response of the phosphatidylcholine headgroup to bilayer surface charge: torsion angle constraints from dipolar and quadrupolar couplings in bicelles. *Magnetic Resonance in Chemistry*, *42*, 89–104.

Sezonov, G., Joseleau-Petit, D., & D'Ari, R. (2007). Escherichia coli physiology in Luria-Bertani broth. *Journal of Bacteriology*, *189*(23), 8746–8749.

Shah, R. R. (2008). If a drug deemed "safe" in nonclinical tests subsequently prolongs QT in phase 1 studies, how can its sponsor convince regulators to allow development to proceed? *Pharmacology & Therapeutics*, *119*, 215–221.

Shaya, D., Kreir, M., Robbins, R. A, Wong, S., Hammon, J., Brüggemann, A., & Minor, D. L. (2011). Voltage-gated sodium channel (NaV) protein dissection creates a set of functional pore-only proteins. *Proceedings of the National Academy of Sciences*, *108*(30), 12313–12318.

Shrivastava, I. H., Tieleman, D. P., Biggin, P. C., & Sansom, M. S. P. (2002). K(+) versus Na(+) ions in a K channel selectivity filter: a simulation study. *Biophysical Journal*, *83*, 633–645.

Silvius, J. R., & Gagné, J. (1984). Calcium-induced fusion and lateral phase separations in phosphatidylcholine-phosphatidylserine vesicles. Correlation by calorimetric and fusion measurements. *Biochemistry*, *23*, 3241– 3247.

Singer, S. J., & Nicolson, G. L. (1972). The fluid mosaic model of the structure of cell membranes. *Science*, *175*(4023), 720–731.

Singh, S. M., & Panda, A. K. (2005). Solubilization and refolding of bacterial inclusion body proteins. *Journal of Bioscience and Bioengineering*, *99*(4), 303–310.

Smith, I. C. P., & Magid, A. D. (1984). Phosphorus-31 NMR of phospholipids in membranes. In *Phosphorus-31 NMR: Principles and Applications* (pp. 447–475). London: Gorenstein, DG, Ed; Academic Press Inc.

Sobhanifar, S., Reckel, S., Junge, F., Schwarz, D., Kai, L., Karbyshev, M., Löhr, F., Bernhard, F., & Dötsch, V. (2010). Cell-free expression and stable isotope labelling strategies for membrane proteins. *Journal of Biomolecular NMR*, *46*, 33–43.

Son, W. S., Park, S. H., Nothnagel, H. J., Lu, G. J., Wang, Y., Zhang, H., Cook, G. A., Howell, S. C., & Opella, S. J. (2012). "q-Titration" of long-chain and short-chain lipids differentiates between structured and mobile residues of membrane proteins studied in bicelles by solution NMR spectroscopy. *Journal of Magnetic Resonance*, *214*, 111–118.

Sreerama, N., & Woody, R. W. (2000). Estimation of protein secondary structure from circular dichroism spectra: comparison of CONTIN, SELCON, and CDSSTR methods with an expanded reference set. *Analytical Biochemistry*, *287*(2), 252–260.

Stansfeld, P. J., Gedeck, P., Gosling, M., Cox, B., Mitcheson, J. S., & Sutcliffe, M. J. (2007). Drug Block of the hERG Potassium Channel : Insight From Modeling. *Proteins: Structure, Function and Bioinformatics*, *68*, 568–580.

Sternin, E., Nizza, D., & Gawrisch, K. (2001). Temperature dependence of DMPC / DHPC mixing in a bicellar solution and its structural implications. *Langmuir*, *17*, 2610–2616.

Stevens, T. J., & Arkin, I. T. (2000). Do more complex organisms have a greater proportion of membrane proteins in their genomes? *Proteins: Structure, Function and Genetics*, *39*, 417–420.

Strandberg, E., Ozdirekcan, S., Rijkers, D. T. S., van der Wel, P. C. A., Koeppe II, R. E., Liskamp, R. M. J., & Killian, J. A. (2004). Tilt angles of transmembrane model peptides in oriented and non-oriented lipid bilayers as determined by 2H solid-state NMR. *Biophysical Journal*, *86*, 3709–3721.

Struppe, J., & Vold, R. R. (1998). Dilute bicellar solutions for structural NMR work. *Journal of Magnetic Resonance*, *135*, 541–546.

Stummann, T. C., Beilmann, M., Duker, G., Dumotier, B., Fredriksson, J. M., Jones, R. L., Hasiwa, M., Kang, Y. J., Mandenius, C.-F., Meyer, T., Minotti, G.,

Valentin Y. J.-P., Zünkler, B. J., & Bremer, S. (2009). Report and recommendations of the workshop of the European centre for the validation of alternative methods for drug-induced cardiotoxicity. *Cardiovascular Toxicology*, *9*, 107–125.

Subbiah, R. N., Clarke, C. E., Smith, D. J., Zhao, J., Campbell, T. J., & Vandenberg, J. I. (2004). Molecular basis of slow activation of the human ether-a-go-go related gene potassium channel. *Journal of Physiology*, *558*(2004), 417–431.

Sun, S., Han, Y., Paramasivam, S., Yan, S., Siglin, A. E., Williams, J. C., Byeon, I.-J. L., Ahn, J., Gronenborn, A. M., Polenova, T. (2012). Solid-state NMR spectroscopy of protein complexes. *Methods in Molecular Biology*, *831*, 303–331.

Surya, W., Li, Y., Millet, O., Diercks, T., & Torres, J. (2013). Transmembrane and juxtamembrane structure of αL Integrin in bicelles. *PLOS ONE*, *8*(9), e74281.

Swain, C. (2007). Open access and medicinal chemistry. *Chemistry Central Journal*, *1*, 1–2.

Swartz, K. J. (2006). Greasing the gears of potassium channels. *Nature*, *2*(8), 401–402.

Tamargo, J., Caballero, R., Gómez, R., & Delpón, E. (2009). IKur/Kv1.5 channel blockers for the treatment of atrial fibrillation. *Expert Opinion on Investigational Drugs*, *18*(4), 399–416.

Tamargo, J., Caballero, R., Gómez, R., Valenzuela, C., & Delpón, E. (2004). Pharmacology of cardiac potassium channels. *Cardiovascular Research*, *62*, 9–33.

Tardy-Laporte, C., Arnold, A. A., Genard, B., Gastineau, R., Morançais, M., Mouget, J. L., Tremblay, R., & Marcotte, I. (2013). A 2H solid-state NMR study of the effect of antimicrobial agents on intact Escherichia coli without mutating. *Biochimica et Biophysica Acta*, *1828*(2), 614–622.

Tempel, B. L., Papazian, D. M., Schwarz, T. L., Jan, Y. N., & Jan, L. Y. (1987). Sequence of a probable potassium channel component encoded at Shaker locus of Drosophila. *Science*, *237*(4816), 770–775.

Thai, K.-M., Windisch, A., Stork, D., Weinzinger, A., Schiesaro, A., Guy, R. H., Timin, E. N., Hering, S., & Ecker, G. F. (2010). The hERG potassium channel

and drug trapping: insight from docking studies with propafenone derivatives. *ChemMedChem*, *5*(3), 436–442.

Thiyagarajan, P., & Tiede, D. M. (1994). Detergent micelle structure and micelle-micelle interactions determined by small-angle neutron scattering under solution conditions used for membrane protein crystallization. *Journal of Physical Chemistry*, *98*, 10343–10351.

Torres, A. M., Bansal, P. S., Sunde, M., Clarke, C. E., Bursill, J. A., Smith, D. J., Bauskin, A., Breit, S. N., Campbell, T. J., Alewood, P. F., Kuchel, P. W., & Vandenberg, J. I. (2003). Structure of the HERG K+ channel S5P extracellular linker: Role of an amphipathic α-helix in C-type inactivation. *Journal of Biological Chemistry*, *278*(43), 42136–42148.

Triba, M. N., Devaux, P. F., & Warschawski, D. E. (2006). Effects of lipid chain length and unsaturation on bicelles stability. A phosphorus NMR study. *Biophysical Journal*, *91*, 1357–1367.

Triba, M. N., Warschawski, D. E., & Devaux, P. F. (2005). Reinvestigation by phosphorus NMR of lipid distribution in bicelles. *Biophysical Journal*, *88*, 1887–1901.

Triba, M. N., Zoonens, M., Popot, J.-L., Devaux, P. F., & Warschawski, D. E. (2006). Reconstitution and alignment by a magnetic field of a beta-barrel membrane protein in bicelles. *European Biophysics Journal*, *35*, 268–275.

Trudeau, M. C., Warmke, J. W., Ganetzky, B., & Robertson, G. A. (1995). HERG, a human inward rectifier in the voltage-gated potassium channel family. *Science*, *269*(5220), 92–5.

Tseng, G.-N., Sonawane, K. D., Korolkova, Y. V, Zhang, M., Liu, J., Grishin, E. V, & Guy, H. R. (2007). Probing the outer mouth structure of the HERG channel with peptide toxin footprinting and molecular modeling. *Biophysical Journal*, *92*, 3524–3540.

Tulumello, D. V, & Deber, C. M. (2012). Efficiency of detergents at maintaining membrane protein structures in their biologically relevant forms. *Biochimica et Biophysica Acta*, *1818*, 1351–1358.

Vácha, R., & Frenkel, D. (2014). Stability of bicelles: a simulation study. *Langmuir*, *30*(15), 4229–4235.

Van Dam, L., Karlsson, G., & Edwards, K. (2004). Direct observation and characterization of DMPC/DHPC aggregates under conditions relevant for biological solution NMR. *Biochimica et Biophysica Acta*, *1664*, 241–256.

Van der Cruijsen, E. A. W., Nand, D., Weingarth, M., Prokofyev, A., Hornig, S., Cukkemane, A. A., Bonvin, A. M. J. J., Becker, S., Hulse, R. E., Perozo, E., Pongs, O., & Baldus, M. (2013). Importance of lipid-pore loop interface for potassium channel structure and function. *Proceedings of the National Academy of Sciences*, *110*(32), 13008–13.

Van der Wel, P. C. A., Strandberg, E., Killian, J. A., & Koeppe, R. E. (2002). Geometry and intrinsic tilt of a tryptophan-anchored transmembrane alpha-helix determined by 2H NMR. *Biophysical Journal*, *83*, 1479–1488.

Vandenberg, J. I., Perry, M. D., Perrin, M. J., Mann, S. A., Ke, Y., & Hill, A. P. (2012). hERG K+ channels: structure, function, and clinical significance. *Physiological Reviews*, *92*, 1393–1478.

Vandenberg, J. I., Varghese, A., Lu, Y., Bursill, J. A., Mahaut-Smith, M. P., & Huang, C. L.-H. (2006). Temperature dependence of human ether-a-go-go-related gene K+ currents. *American Journal of Physiology. Cell Physiology*, *291*, C165–C175.

Vega, A. J. (2000). Chapter 2. Quadrupolar Nuclei in Solids. In R. E. Wasylishen, S. E. Ashbrook, & S. Wimperis (Eds.), *NMR of Quadrupolar Nuclei in Solid Materials* (pp. 17–44). Chichester, UK: Wiley.

Venyaminov, S. Y., Baikalov, I. A., Shen, Z. M., Wu, C.-S. C., & Yang, J. T. (1993). Circular Dichroic Analysis of Denatured Proteins: Inclusion of Denatured Proteins in the Reference Set. *Analytical Biochemistry*, *214*, 17–24.

Vinogradova, O., Sönnichsen, F., & Sanders, C. R. (1998). On choosing a detergent for solution NMR studies of membrane proteins. *Journal of Biomolecular NMR*, *11*(4), 381–386.

Vold, R. R., & Prosser, R. S. (1996). Magnetically oriented phospholipid bilayered micelles for structural studies of polypeptides. Does the ideal bicelle exist? *Journal of Magnetic Resonance B*, *113*, 267–271.

Vold, R. R., Prosser, R. S., & Deese, A. J. (1997). Isotropic solutions of phospholipid bicelles: a new membrane mimetic for high-resolution NMR studies of polypeptides. *Journal of Biomolecular NMR*, *9*, 329–335.

Von Heijne, G. (1999). A day in the life of Dr K. or How I learned to stop worrying and love lysozyme: a tragedy in six acts. *Journal of Molecular Biology, 293*, 367–379.

Wagner, S. (2008). *From biogenesis to over-expression of membrane proteins in Escherichia coli.*

Wagner, S., Baars, L., Ytterberg, a J., Klussmeier, A., Wagner, C. S., Nord, O., Nygren, P.-A., van Wijk, K. J., & de Gier, J.-W. (2007). Consequences of membrane protein overexpression in Escherichia coli. *Molecular & Cellular Proteomics, 6*(9), 1527–1550.

Wallin, E., & von Heijne, G. (1998). Genome-wide analysis of integral membrane proteins from eubacterial, archaean, and eukaryotic organisms. *Protein Science, 7*, 1029–1038.

Wang, S., Liu, S., Morales, M. J., Strauss, H. C., & Rasmusson, R. L. (1997). A quantitative analysis of the activation and inactivation kinetics of HERG expressed in Xenopus oocytes. *Journal of Physiology, 502.1*, 45–60.

Ward, M. E., Wang, S., Munro, R., Ritz, E., Hung, I., Gor'kov, P. L., Jiang, Y., Liang, H., Brown, L. S., & Ladizhansky, V. (2015). In situ structural studies of Anabaena sensory rhodopsin in the E. coli membrane. *Biophysical Journal, 108*(7), 1683–1696.

Warschawski, D. E., Arnold, A. A., Beaugrand, M., Gravel, A., Chartrand, É., & Marcotte, I. (2011). Choosing membrane mimetics for NMR structural studies of transmembrane proteins. *Biochimica et Biophysica Acta, 1808*, 1957–1974.

Watkins, P. A. (2005). Physical Properties of Fatty Acids. In B. Caballero, L. Allen, & A. Prentice (Eds.), *Encyclopedia of Human Nutrition. 2nd edition* (p. 187). Elsevier Academic Press.

Watts, A., Burnett, I. J., Glaubitz, C., Gröbner, G., Middleton, D. A., Spooner, P. J. R., & Williamson, P. T. F. (1998). Structural descriptions of ligands in their binding site of integral membrane proteins at near physiological conditions using solid-state NMR. *European Biophysics Journal, 28*, 84–90.

Whiles, J. A., Deems, R., Vold, R. R., & Dennis, E. A. (2002). Bicelles in structure–function studies of membrane-associated proteins. *Bioorganic Chemistry, 30*, 431–442.

Whitmore, L., & Wallace, B. A. (2008). Protein secondary structure analyses from circular dichroism spectroscopy: Methods and reference databases. *Biopolymers*, *89*(5), 392–400.

Whittaker, J. W. (2007). Selective isotopic labeling of recombinant proteins using amino acid auxotroph strains. *Methods in Molecular Biology*, *389*, 175–187.

Williamson, I. M., Alvis, S. J., East, J. M., & Lee, A. G. (2003). The potassium channel KcsA and its interaction with the lipid bilayer. *Cellular and Molecular Life Sciences*, *60*, 1581–1590.

Wulff, H., Castle, N. A., & Pardo, L. A. (2010). Voltage-gated potassium channels as therapeutic drug targets. *Nature Reviews. Drug Discovery*, *8*(12), 982–1001.

Wüthrich, K. (1987). *NMR of Proteins and Nucleic Acids*. Wiley.

Yamamoto, K., Pearcy, P., & Ramamoorthy, A. (2014). Bicelles exhibiting magnetic alignment for a broader range of temperatures: a solid-state NMR study. *Langmuir*, *30*, 1622–1629.

Yamamoto, K., Soong, R., & Ramamoorthy, A. (2009). Comprehensive analysis of lipid dynamics variation with lipid composition and hydration of bicelles using nuclear magnetic resonance (NMR) spectroscopy. *Langmuir*, *25*(12), 7010–7018.

Yellen, G. (2002). The voltage-gated potassium channels and their relatives. *Nature*, *419*, 35–42.

Yokoyama, H., Ikeda, K., Wakabayashi, M., Ishihama, Y., & Nakano, M. (2013). Effects of lipid membrane curvature on lipid packing state evaluated by isothermal titration calorimetry. *Langmuir*, *29*, 857–860.

Yokoyama, J., Matsuda, T., Koshiba, S., Tochio, N., & Kigawa, T. (2011). A practical method for cell-free protein synthesis to avoid stable isotope scrambling and dilution. *Analytical Biochemistry*, *411*, 223–229.

Zachariae, U., Giordanetto, F., & Leach, A. G. (2009). Side chain flexibilities in the human ether-a-go-go related gene potassium channel (hERG) together with matched-pair binding studies suggest a new binding mode for channel blockers. *Journal of Medicinal Chemistry*, *52*(14), 4266–76.

Zandomeneghi, G., Tomaselli, M., Williamson, P. T. F., & Meier, B. H. (2003). NMR of bicelles: orientation and mosaic spread of the liquid-crystal director under sample rotation. *Journal of Biomolecular NMR*, *25*(2), 113–123.

Zaydman, M. A., & Cui, J. (2014). PIP2 regulation of KCNQ channels: biophysical and molecular mechanisms for lipid modulation of voltage-dependent gating. *Frontiers in Physiology*, *5*(195), 1–11.

Zaydman, M. A., Silva, J. R., Delaloye, K., Li, Y., Liang, H., Larsson, H. P., Shi, J., & Cui, J. (2013). Kv7.1 ion channels require a lipid to couple voltage sensing to pore opening. *Proceedings of the National Academy of Sciences*, *110*(32), 13180–5.